ANALYSIS OF EDM PARAMETERS WITH TOOL ROTATION

by

MUKESH KUMAR

2K12 / PhD / ME / 02

Supervisor

Prof. Vipin

DEPARTMENT OF MECHANICAL ENGINEERING
DELHI TECHNOLOGICAL UNIVERSITY
(FORMERLY DELHI COLLEGE OF ENGINEERING)
Bawana Road, Delhi-110042, India

2019

Dedicated to

My

Guru's

and

Beloved Parents

DECLARATION

I declare that the work presented in this thesis entitled "*Analysis of EDM Parameters with Tool Rotation*", is submitted to the Department of Mechanical Engineering, Delhi Technological University, Delhi, India, for the award of the ***Doctor of Philosophy*** degree in ***Mechanical Engineering***, is my original research work carried out by me. The work presented in this thesis has not been submitted to any other university or institution for the award of any degree or diploma.

Mukesh Kumar

CERTIFICATE

This is to certify that the Ph.D. thesis entitled **"Analysis of EDM Parameters with Tool Rotation"** being submitted by Mr. MUKESH KUMAR for the award of degree, Doctor of Philosophy in Mechanical Engineering, Delhi Technological University, Delhi, India, is a bonafide record of original research work carried out by him under my guidance and supervision. The work presented in this thesis has not been submitted to any other university or institution for the award of any degree or diploma.

Dated:

Prof. VIPIN

Professor & Head
Department of Mechanical Engineering,
Delhi Technological University,
Delhi.

Acknowledgement

First and foremost I am thankful to the almighty for keeping me fit, healthy and energetic during the entire course of my Ph.D. work.

I would like to express my gratitude to Prof. Yogesh Singh, Vice-chancellor, Delhi Technological University, Delhi for providing this opportunity to carry out this work in this prestigious institute.

I would like to thank Prof. R.S Mishra, DRC Chairman, Department of Mechanical, Production, Industrial, and Automobile Engineering, Delhi Technological University, Delhi for his support to finish this work.

With pleasure, I would like to express my greatest gratitude to my supervisor Prof. Vipin, Professor& Head of the department, Department of Mechanical, Production, Industrial and Automobile Engineering, Delhi Technological University, Delhi for his proficient guidance, intelligent approach, constructive critique, wholehearted and ever available help, which has been the primary impetus behind the research. He is not only the supervisor and also my guardian, without the wise advice and able guidance, it would have been impossible to complete. He is always on the stand by to bring me to positivity, hope and smiles when things didn't seem to favor. It has been an honor to be a Ph.D. scholar. I respect all his contributions of time and ideas to make my Ph.D. productive. I am also thankful for the excellent example he has provided as a successful professor.

I would like to specially thank to Dr. S.C. Vettivel for helping and encouraging me throughout my research.

Special mention is deserved for, who I am greatly indebted to my parents, my brother and sisters and in-laws for their love and blessings to see me scaling greater heights of life. One who matters most in my Ph.D. work is my wife Mrs. Suresh Kumari, without whose motivation and encouragement, the pursuit of this Ph.D. work would have never been possible. I thank her for care and encouraging me throughout my research work. Last, but not the least I am thankful to my son Chaitanya and daughter Saanvi whose single smile could remove all the tiredness of my work.

Above all, I would thank the Almighty for blessing such an affectionate & efficient people playing great asset for me.

September, 2019 Mukesh Kumar

ABSTRACT

In advanced manufacturing process, the Electric Discharge Machining (EDM) plays a vital role in precision tool room of manufacturing industries such as automobile, aerospace and defence. The manufacturing industries require unique and exact methodology for EDM machining with maximum machining rate, low tool wear rate and high surface finish. EDM with tool rotation facilitates to get maximum material removal rate (MRR), low tool wear rate (TWR) and low surface roughness (R_a) for AISI D3 and EN-31 Steel.

Researchers have tried to investigate and improve the responses i.e. MRR, TWR and R_a of different materials by different EDM processes. The literature reveals that less research has been conducted to maximize MRR and minimize R_a. It is noted that the MRR is very low for significant surface characteristics of the material. It is a well-known fact that good surface quality and high MRR may not be achieved simultaneously.

The present research work involves experimental investigation of the MRR, TWR and R_a for AISI D3 and EN-31 steel with copper tool and input parameters viz. peak current, pulse-on-time and tool rotation. The Central Composite Design (CCD) method of Response Surface Methodology (RSM) was effectively used to develop and analyze the parameters of the model. It is used to reduce the number of experiments. The second-order mathematical model is developed through the regression analysis to predict better performance characteristics.

The ANOVA predicts I_p is competent variable for MRR having participation of 56.024%, T_{on} for TWR having participation of 44.95%, T_R for R_a having participation of 43.43% for AISI D3 steel. The T_R is competent variable for MRR having participation of 44.32%, T_{on} for TWR having participation of 31.68%, I_p for R_a having participation of 49.72% for EN-31 steel.

The Characterization of the surface is done by Scanning Electron Microscopy (SEM), Energy Dispersive X-Ray Spectroscopy (EDS) and its spectra mapping. The morphology shows the presence of tungsten carbide and iron carbide on the machined surface, which is responsible for high hardness and providing resistance against hot corrosion and high temperature. Residual stresses are present in tensile (25 MPa to 257 MPa) and compressive (11826 MPa) for AISI D3 steel and tensile (207 MPa to 380 MPa) and compressive (2008 MPa) for EN-31 steel. The discharge pulse formation verified with a Digital Storage Oscilloscope (DSO) and found that current and voltage have fluctuation/disturbance due to the high frequency of charging and discharging. The model adequacy is established by the correlation of predicted and actual values of the MRR, TWR and R_a.

Table of Contents

List of Figures

List of Tables

Abbreviations and Symbols

EDM	Electrical Discharge Machining
MRR	Material Removal Rate
TWR	Tool Wear Rate
T_R	Tool Rotation
IEG	Inter Electrode Gap
I_p	Peak Current
T_{on}	Pulse-on-Time
R_a	Surface Roughness
RPM	Rotation Per Minute
HAZ	Heat Affected Zone
RLT	Recast Layer Thickness
CCD	Central Composite Design
RSM	Response Surface Methodology
R	Resistance
RC	Resistance-Capacitance
VI	Voltage-Current
XRD	X-ray Diffraction
CNC	Computer Numerical Control
BCC	Body-centered cubic
FCC	Face-centered cubic
CAD	Computer Aided Design

CAM	Computer-Aided manufacture.
Q	Discharge Energy Per Pulse
θ	Theta
σ	Stress
Tau	Shear Stress

CHAPTER 1

INTRODUCTION

1.1 Overview

The inventor of Electric Discharge Machining (EDM) was Joseph Priestley. The scientist, in 1770, came to know the eroding impact of electrical spark generated. But the control of spark generation is difficult, due to this, the process will not become famous for a long duration. Two Russian scientists were doing experiments for the avoidance of electrical sparks on tungsten electrodes by contacting, in 1943. Although, Lazarenko and Lazarenko scientists, not able to perform experiment successfully. But these, scientists discovered control of spark erosion. This can be controlled strictly in between electrodes if they submerged in a dielectric medium i.e. non-conductor of electricity. This controlled spark erosion discovered EDM. It is used for machining irrespective of its strength and geometry but respective to electrical conductivity. The machining of high toughness, good strength, electrically conductive material and alloys or superalloys can be performed by EDM. This process is well known for absolute reproduction or geometry mirroring of tool on the work material. Thus the EDM process having a specific tool or electrode for a specific operation. The hard materials like high-speed steel, tungsten carbides, thermic treated components, composites materials, advanced-alloys, etc. can be machined easily. Nowadays, EDM process having specific applications in tool, die and mould manufacturing, aero-industries and nuclear power plant. EDM operation is also having applications in medical and surgical instruments as well as implants. The EDM process becomes well famous in industries, in the middle of the 1980s after the controller controlled by computer i.e. known as Computer Numerical Control (CNC). The time has elapsed and continuous operational advancement in the process, the process become more capable, it can work continuously round the clock under the control of an electronic adaptive control system. The EDM emergent advantages were highly seen by the manufacturing industries in terms of huge cost-effective gains and creating interest in research.

The EDM is a non-conventional machining process, the machining takes place without any contact in between electrode (tool) and work material. This process is used to produce complex geometry parts within very close tolerances, this feature makes the process unique within the non-traditional machining process. The advantages of EDM to perform an operation on hard-to-machine materials and manufacture problematic part shapes in very close tolerances limits. This makes the process unique amongst the other non-conventional machining process.

Nowadays, EDM is a well-established and known technology and used in approximately all precision manufacturing work to produce intricate part geometry. However, it has low machining rate, it is major drawback for the tool engineering. Therefore, research for improvement in machining efficiency is still in progress.

1.2 EDM Working Principle

EDM works on the principle of thermoelectric behavior. The tool and workpiece both are electrically conductive and submerged in a dielectric fluid. The inter-electrode-gap (IEG) experiences the formation of short discharge by a distinct series of repeated spark pulse discharge in between both electrodes. The tool moves downwards (it is mounted on vertical z-axis) towards the workpiece, the electric field applied and increases within IEG which resultsin the breakup of dielectric fluid. This results in heating the metal for melting and vaporization. The resistance and capacitance circuit is used to discharge the energy in between the electrodes. During machining, voltage drops and current rises sharply in RC-type circuit for short duration of time, the dielectric fluid ionization takes place and form electrons and ions. The ionization of dielectric fluid and formation bubble of ionized zone taken place in inter electrodes. The transfer of ions and electrons continuously takes place in IEG, due to this plasma channel gets broaden. The outcome of this occurrence is constant heating on the workpiece surface and raising the localized temperature in order of 8000 ^{0}C to 12000 ^{0}C (Boothroyd and Winston, 1989). A little pool of molten metal is created by melting metal. The molten metal evaporates from the pool and also flushed away continuously by dielectric fluid in the form of debris and a small cavity of craters is created on the workpiece. A number of spark emits and strike on the surface of workpiece and reproduction of mirror image of tool is generated on the surface of workpiece.

1.2.1 Ignition

The electric field induced by voltage gradient, the transfer of electrons takes place i.e. known as primary electrons are emitted from cathode to anode through the dielectric fluid. It plays an important role to maximize the gradient, shown in figure 1.1. These electrons get attracted towards the anode and start moving through a dielectric medium. The collision between metal atoms in the dielectric takes place. This is known as secondary electrons and positive ions, shown in figure 1.2.

1.2.2 Plasma Channel Formation

A number of electrons released by hitting positive ions on the cathode. The electron emission by hitting is known as the secondary electron emission. The emission of neutral atoms from dielectric takes place due to the movement of the electrons. The current generated instantly as electrons and ions movement takes place in the ionization zone and the heating of dielectric starts locally. This decreases electric resistance and a further increase in current. The dielectric fluid continuously heated and plasma channel is formed, it is characterized by high temperature and pressure. The plasma channel is induced, this is also known as breakdown phase voltage. The duration of delay in the application of voltage and voltage breakdown is known as ignition delay time. This is shown in figure 1.3.

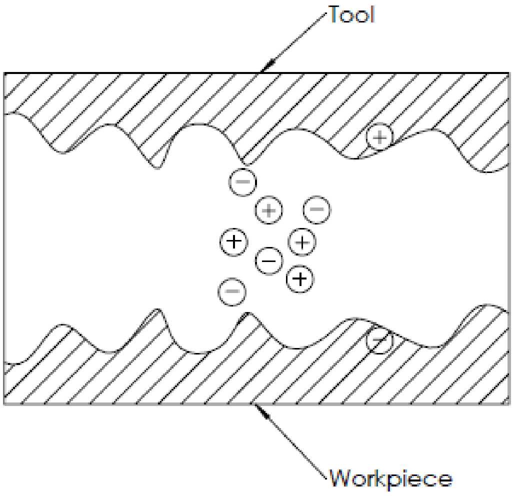

Figure 1.1: Formation of primary electrons

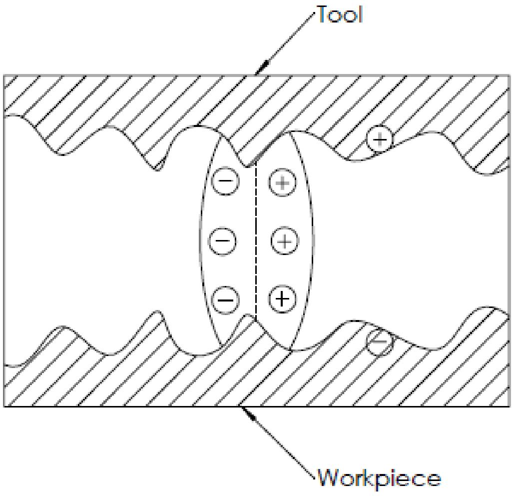

Figure 1.2: Formation of secondary electrons

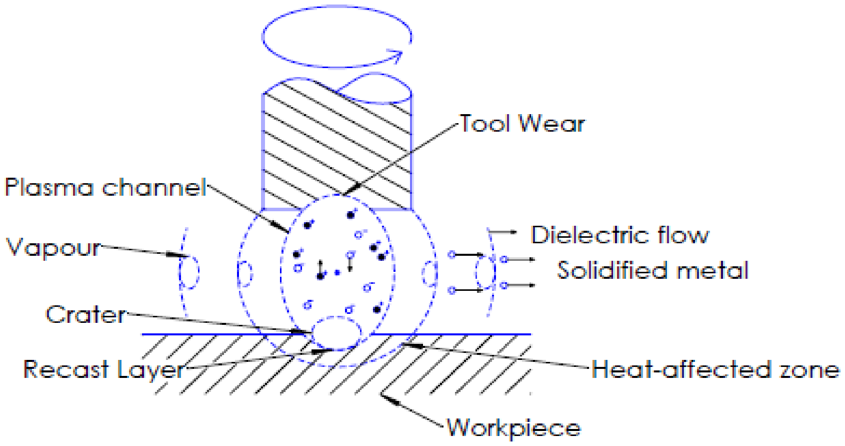

Figure 1.3: Plasma channel formation

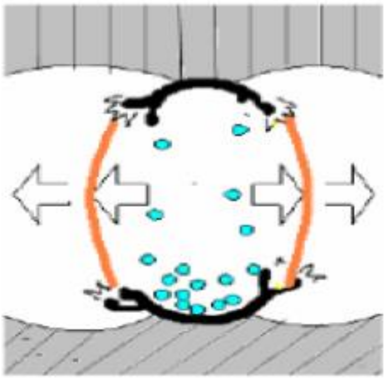

Figure 1.4: Melting and evaporation (Boothroyd and Winston, 1989)

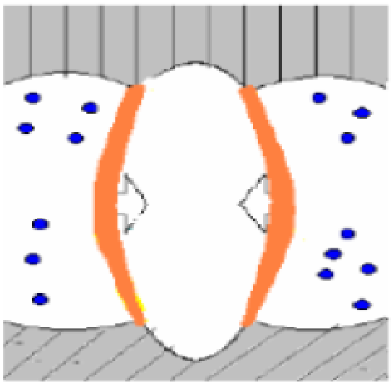

Figure 1.5: Ejection of molten metal (Boothroyd and Winston, 1989)

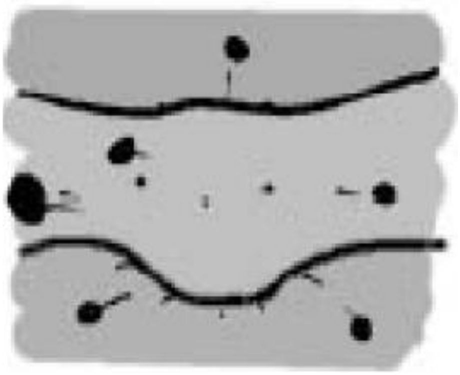

Figure 1.6: Solidification and flushing of eroded particles (Boothroyd and Winston, 1989)

1.2.3 Melting and Evaporation

The kinetic energy is converted into heat energy as the electron or ion strikes with the workpiece surface. This generated heat causes melting and partial evaporation from workpiece face. The volume of molten metal depends upon the amount of available heat. The number of atoms striking per discharge depends upon the discharge energy.

When ions strike with cathode for a small duration of discharge then electron generates a high amount of heat due to the difference in mass. The kinetic energy of ions develop a large amount of heat and melting the cathode surface. This is shown in figure 1.4.

1.2.4 Molten Material Ejection

At the end of discharge duration, the supply of current is instantly stopped by the electronic circuit of the EDM machine. The sudden breakdown of the plasma channel creates pressure drop on the molten cathode and anode surfaces. This produces the molten material at both ends i.e. electrode and workpiece and metal debris flushed away from the pool of molten metal. This is shown in figure 1.5.

1.2.5 Solidification and Flushing of Eroded Particles

The supply of discharge current and voltage interrupted in pulse-off-time, i. e. zero discharge energy and the molten metal pool is flushed away by dielectric fluid in the form of tiny particles. The rotation of electrode in EDM enhances the flushing of molten material due to whirling effect. This is shown in figure 1.6

1.3 Categorization of EDM

The classification of EDM on the basis of industrial requirements/ applications are represented in figure 1.7 as:

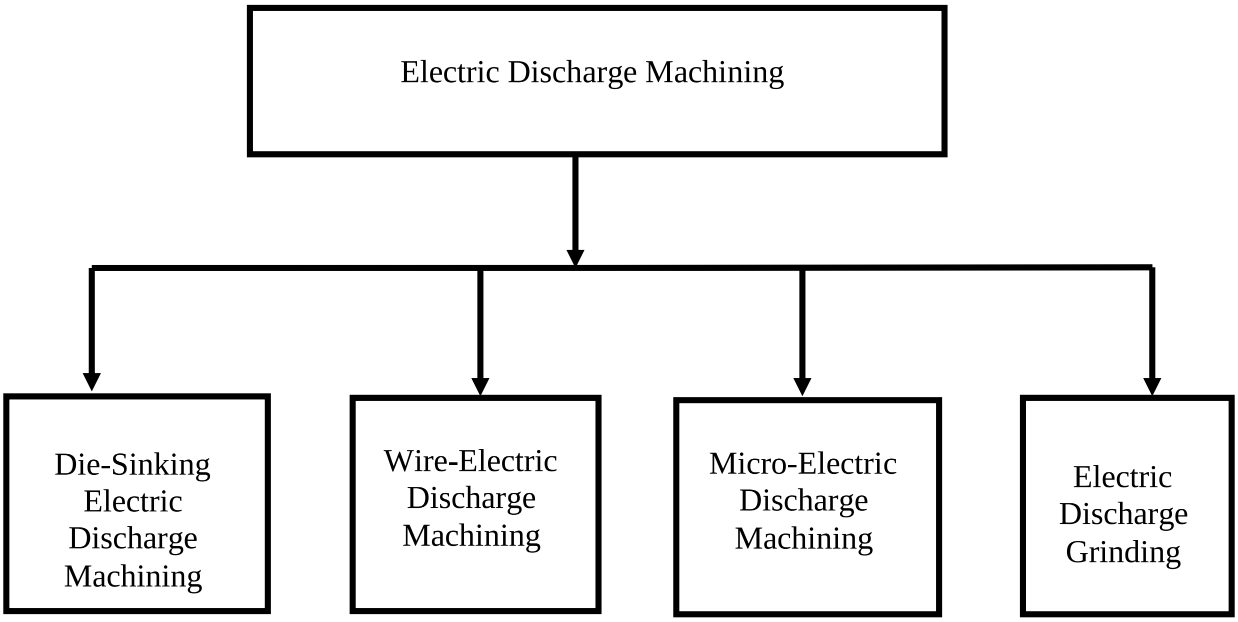

Figure 1.7: Classification of Electric Discharge Machining

(a) Die-sink Electric Discharge Machining

The die-sink EDM is shown in figure 1.8. The tool and workpiece are immerged in the dielectric fluid. The pulse discharge energy is produced by a separate power supply unit i.e. known as pulse generator. The discharge energy generated between both conductive electrodes that form a pair of the electrode. Most of the machines working on the R-C type circuit (Pradhan, M. K. 2010). The movement of Z-axis is controlled by a servo motor with a controller. It maintains the ionization gap between the tool and workpiece during machining. The flushing function is completed by the flow of dielectric fluid from the ionization gap of electrodes.

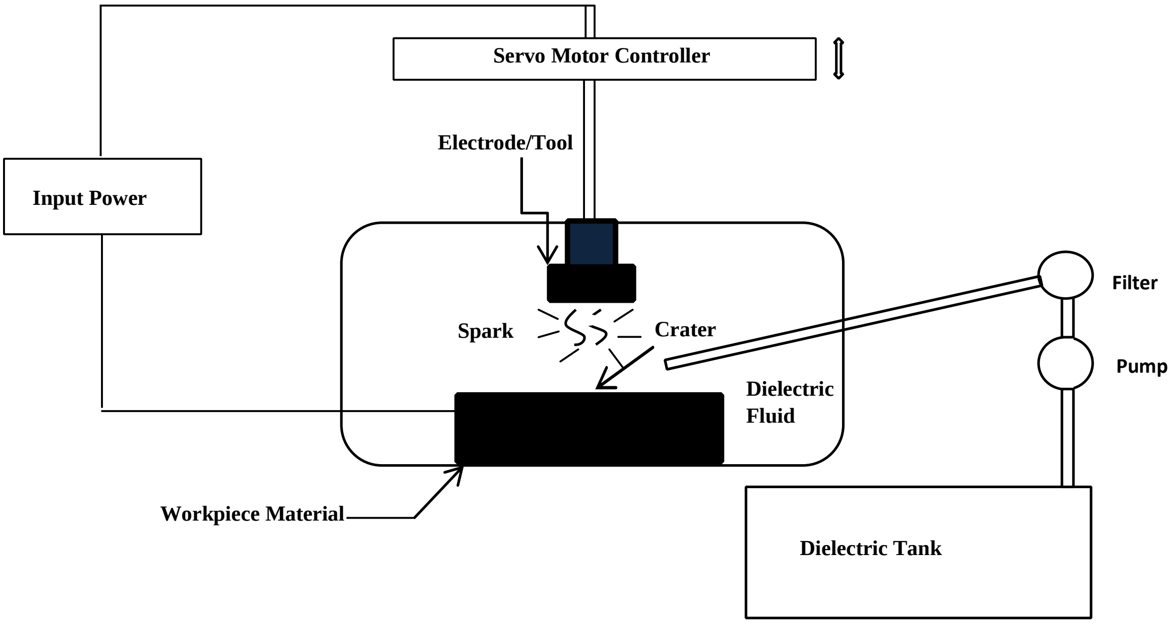

Figure 1.8: Die sink Electric Discharge Machining

(b) Wire Electric Discharge Machining

The wire is used as an electrode in the machine having diameter 0.02 to 0.40 mm. The wire should be continuous and conductive. The wire is wrapped around the pulley. Generally, copper or brass wire is used for the operation. The machine has accuracy up to ± 0.0025 mm. Deionized water directly supplied around the wire and it is used as dielectric fluid.

(c) Micro-Electric Discharge Machining

The Micro-electric discharge machining process used for micro-machining. The electrode diameter from 5 microns to 10 microns was used to generate micro-holes in workpiece material. This process is fully efficient for generating at micro-level complicated 3D geometries and micro-injection moulding.

(d) Electrical Discharge Grinding (EDG)

The traditional electrode is exchanged by a rotating grinding wheel in electrical discharge grinding. The Electrical Discharge Grinding (EDG) and EDM functioning on same principle. The grinding wheel is electrically conductive and used as an electrode in EDG. This process is fairly good for machining electrically conductive material irrespective of physical property.

1.4 Electric Discharge Machining with Tool Rotation

The Tool Rotation Electric Discharge Machining performed by heating, melting and vaporization action with the rotary tool electrode setup as shown in figure 1.9. It is fabricated and mounted on Z-axis head of die sink EDM (Model: Sparkonix SN35). The rotary tool electrode setup is powered by a servo motor with digital rotation control per minute display from 0 - 5000 RPM. The Z-axis is powered by up-down and rotary motion. The servo motor controller sensor will provide the up-down motion as per the IEG sensor. The rotation is provided by another servo motor.

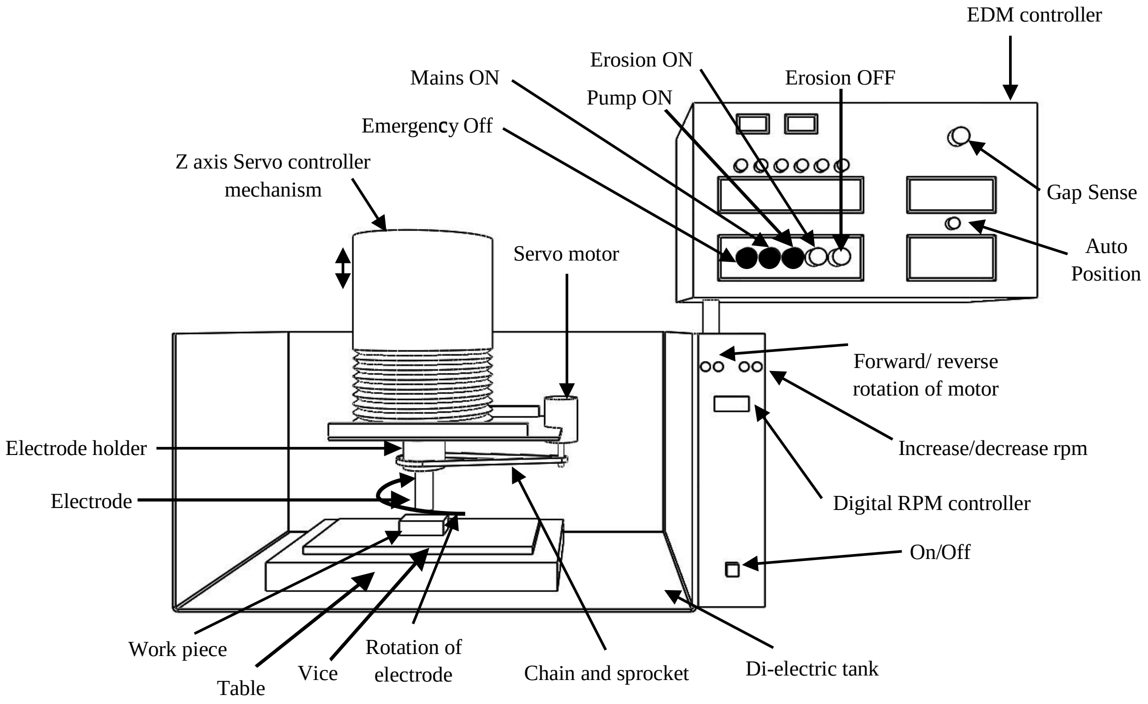

Figure 1.9: EDM line sketch with tool rotation attachment.

1.5 Organization of Thesis

The each chapter is emphasized as the title. The main focus is given to the data collection and result discussion. The chapters of the thesis are arranged as per the schematic block diagram. It is shown in figure 1.10.

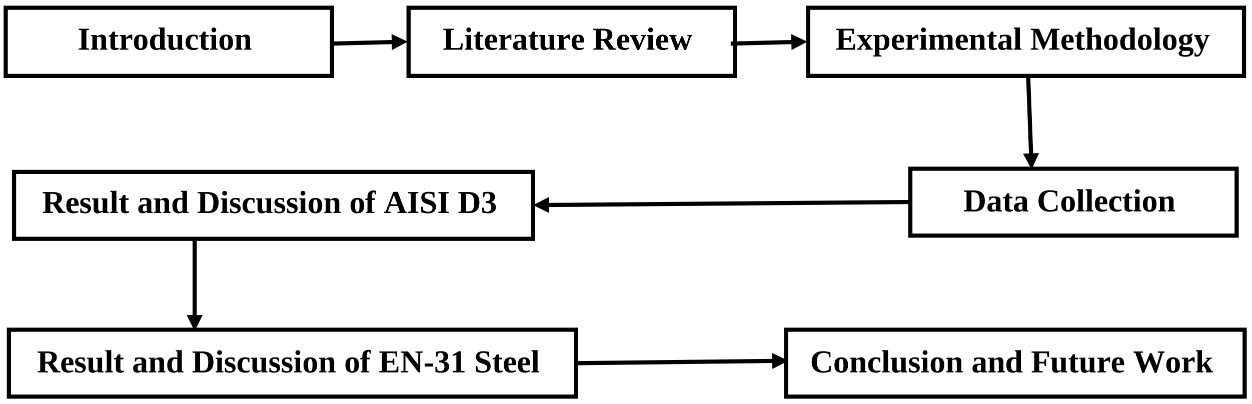

Figure 1.10: Organization of thesis

CHAPTER 2

LITERATURE REVIEW

2.1 Introduction

Electrical Discharge Machining (EDM) with tool rotation from its basic mechanism to its future applications is presented in detail. A literature review of surface characteristics and morphology of surface also presented, along with a description of its fundamental principles. This can be addressed through exhaustive experimentation or development of model obtained from the experimental analysis. This chapter provides details of the various research activities reported in the field.

2.2 Electrical Discharge Machining Process

Robert *et al* [1994] discussed open circuit refers to a situation where the tool distance of separation between the tool and the workpiece is more than the maximum gap required for sparking to occur. There is no potential difference between the tool and the workpiece. As a result, there is no sparking in this case and this should be avoided since it leads to more machining time. A short circuit occurs when the workpiece and tool is in ionization gap. Arcing is an I_p that is brief, strong and highly luminous. An arc is the luminous I_p discharge which is produced when strong I_p leaps across the gap between the tool and the workpiece.

Takahisa [1997] discussed the EDM process by thermal eroding material in the path of electrical discharges that form an arc between a tool and workpiece. The sparking phenomenon utilizes the widely accepted non-contact technique of material removal process. Die sink EDM process is used with tool made up of graphite, copper tungsten or pure copper which is machined into the desired shape. The entire machining operation for die sink EDM is performed while submerged in a dielectric fluid. The fluid serves to flush the machined material away, acts as a coolant to minimize the heat-affected zone (thereby preventing potential damage to the workpiece) and when it deionizes, it acts as a conductor for the I_p to pass between the tool and the workpiece.

Tarng *et al* [1997] developed a fuzzy pulse discriminating system for EDM. The development used fuzzy set theory to construct a new pulse discriminator. The classification of various discharge pulses in EDM was based on the features of the measured gap voltage and gap I_p. To obtain optimal classification performance, a machine learning method based on a simulated annealing algorithm was adopted to automatically synthesize the membership functions of the fuzzy pulse discriminator. Experimental results showed that EDM discharge pulses could be correctly and quickly classified under varying cutting conditions using this approach.

Karthikeyan *et al* [1999] have presented the mathematical modeling of EDM with aluminum-silicon carbide particulate composites. A mathematical equation is $Y = f(V, I_p, T_{on})$ and the effect of material removal rate (MRR), tool wear rate (TWR) and surface roughness (R_a) with process parameters taken into consideration were ($I_{p)}$, pulse-on-time (T_{on}) and percent volume fraction of SiC (25 µm size). A three-level full factorial design was taken and the models were checked using the Analysis of Variance (ANOVA). The MRR was found to decrease with an increase in the percent volume of SiC, whereas the TWR and the R_a increase with an increase in the volume of SiC.it showed the graph between the interactive effect of the percent volume of SiC and the I_p on MRR figure 2.1.

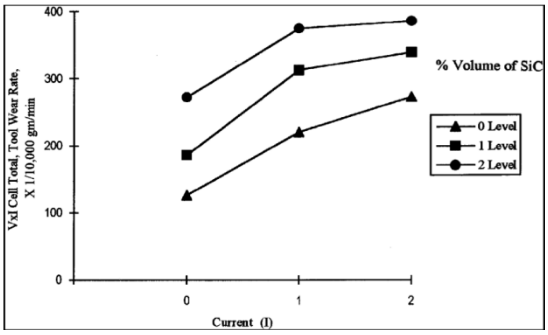

Figure 2.1: Effect of I_p on the tool wear rate (Karthikeyan et al, 1999)

Lee and Li [2001] studied the effect of the machining parameter in EDM of tungsten carbide on the machining characteristics. The EDM process with tungsten carbide better machining performance is obtained generally with the tool as the cathode and the workpiece is an anode. The tool with negative polarity gives the higher MRR, lower TWR and better surface finish. High open-circuit voltage is necessary for tungsten carbide due to its high melting point and high hardness value and copper-tungsten as the tool material with negative polarity. This study confirms that there exists an optimum condition for precision machining of tungsten carbide although the condition may vary with the composition of the material.

Cogun and Akaslan [2002] studied about electrode wear on machining of 2080 die steel with central hole on a cylindrical copper electrode which resulted that the inner radii were found to be increasing with pulse time, discharge current and Di-electric fluid pressure.

Mohan *et al* [2002] discussed the effect of EDM peak current (I_p), tool material polarity, pulse duration and rotation of tool on MRR, TWR, R_a and the EDM of Al-SiC with 20-25 vol. % SiC, the polarity of the tool and volume present of SiC, the MRR increased with an increase in discharge I_p and specific I_p decreased with an increase in pulse duration. Increasing the speed of the rotation tool resulted in a positive effect with MRR, TWR and better R_a than stationary.

The electric motor can be used to rotate the tool. A v-belt was used to transmit the power from the motor to the tool. The parameters optimization for EDM drilling were also developed to summarize the effect of machining characteristics such as MRR, TWR and R_a.

Simao *et al* [2003] modified the surface using EDM, details of operations are given. The powder metallurgy (PM) tool and the use of powders suspended in the dielectric fluid, typically aluminum, nickel, titanium, etc. experimental results are presented on the surface alloying of AISI H13 hot work tool steel during a die-sink operation using partially sintered WC / Co tools operating in a hydrocarbon oil dielectric. An L_8 factorial Taguchi experiment was used to identify the effect of key operating factors on output measures (tool wear, workpiece surface hardness, etc.). With respect to micro-hardness, the Percentage Contribution Ratios (PCR) for I_p, tool polarity and T_{on}. Even so, the very low error PCR value (for micro-hardness ~6%) implies that all the major effects were taken into account.

Tsai *et al* [2003] have worked the material of graphite, copper and copper alloys using EDM because these materials have high melting temperature and excellent electrical and thermal conductivity. The tools made by using powder metallurgy technology from special powders have been used to modify EDM surfaces in recent years to improve wear and corrosion resistance. Tools are made at low pressure (20 MPa) and temperature (200 °C) in a hot mounting machine According to the experimental results, a mixing ratio of Cu–0wt%Cr and a sinter pressure of 20 MPa obtained an excellent MRR. Moreover, this work also revealed that the composite tools obtained a higher MRR than Cu metal tools. The recast layer was thinner and fewer cracks were present on the machined surface.

Puertas and Luis [2004] has defined the optimization of machining parameter for EDM of boron carbide of conductive ceramic materials. It is the conditions that determine such important characteristics as R_a, TWR and MRR. In this article, a review of the state of art of the die-sinking EDM processes for conductive ceramic materials, as well as a description of the equipment used for carrying out the experiments are presented. Also, a series of mathematical models will be devised using the design of experiments techniques combined with multiple linear regression, which will only perform a small number of experiments, to select the optimal machining conditions for the finishing stage of the EDM process.

Singh *et al* [2004] discuss the evolution of EDM and effect of I_p and flushing pressure (F) on MRR, TWR, Taper (T), ROC and R_a of machining cast Al-MMC with 10% SiC_2 and use of metal matrix composites. ELEKTRAPULS spark erosion machine was used for the purpose and jet flushing of the dielectric fluid, kerosene, was employed. The brass tool of diameter 2.7 mm was chosen to drill the specimens. An L_{27} OA, for the three machining parameters at three levels each, was opted to conduct the experiments. ANOVA was performed and the optimal levels for maximizing the responses were established. Scanning Electron Microscopy (SEM) analysis was done to study the surface characteristics.

Hewidy *et al* [2005] investigated the super alloy material and concluded that the I_p, duty factor and T_R influence MRR, whereas the I_p and duty factors alone strongly influence the R_a.

Kun *et al* [2005] conducted a study on improvement of R_a on SKD steel using EDM with aluminium and surfactant added dielectric. In the study, the effect of surfactant and Aluminium powders added in the dielectric on the surface status of the workpiece after EDM was investigated. It was observed that the best distribution effect was found when the concentrations of the aluminium powder and surfactant in the dielectric are 0.1 and 0.25 gm/Lt, respectively. An optimal R_a value of 0.172 µm was achieved with the parameters being, positive polarity, I_p of 0.3 A, T_{on} of 1.5 µsec, open circuit potential of 140 V, gap voltage of 90 V and surfactant concentration of 0.25 gm/Lt. The Ra status of the workpiece was improved up to 60% as compared to that machined under pure dielectric with high R_a of 0.434 µm.

Shabgard *et al* [2006] conducted experimental studies to investigate the influence of EDM input parameters on the output characteristics of the EDM process. The process characteristics including machining features, i.e., MRR, TWR, arithmetical mean roughness, and surface integrity characteristics significantly comprising of the thickness of the white layer and the depth of heat-affected zone in the machining of AISI H13 tool steel were investigated. The experiments that were performed considered EDM input parameters that included T_{on} and I_p. It was found that, when machining AISI H13 tool steel, increase in T_{on} lead to increase in MRR, R_a, as well the white layer thickness and depth of heat-affected zone. The research also found that an increase in I_p leads to a sharp increase in the material removal rate and surface roughness. It was thus concluded that maintaining a constant level of discharge energy, high I_p and low T_{on} lead to a reduction in the white layer thickness and depth of heat affected zone on the surface of the machined workpiece.

Lin *et al* [2006] investigated the effects of the machining parameters (MRR, TWR and R_a) of EDM on the machining characteristics of SKH 57 high-speed steel. The experimental design was used to reduce the total number of experiments. Parts of the experiment were conducted with the L18 orthogonal array based on the Taguchi method. Moreover, the signal-to-noise ratios associated with the observed values in the experiments were analysed by ANOVA and F-test. The relationship of MRR and R_a with pulse duration graph in different I_p is as shown in figure 2.2. During the experiment, MRR increases with I_p. MRR initially increased to a T_{on} 100 µsec, and then decreases.

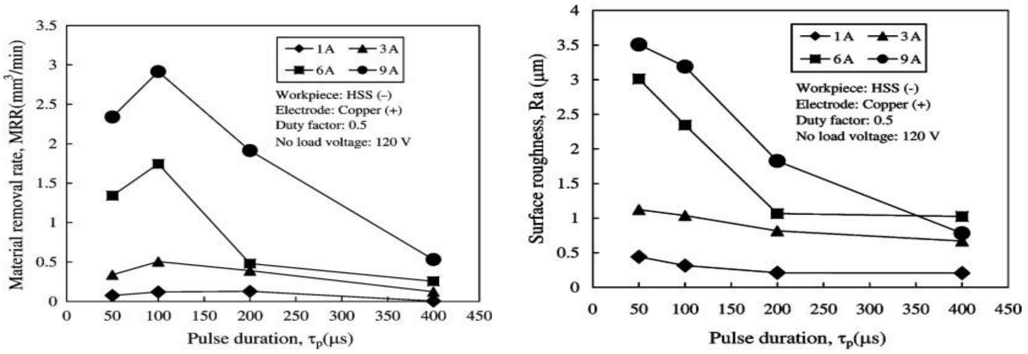

Figure 2.2: MRR and surface roughness with pulse duration graph (Lin et al, 2006)

Bulent *et al* [2006] used a semi-empirical approach to model residual stresses in EDM. Layer removal method was used to measure the residual stress profile as a function of depth beneath the surface caused by die sink type EDM. Cracking and its consequences on residual stresses were also studied on samples machined at long pulse durations. A modified empirical equation was developed for scaling residual stresses in machined surfaces with respect to operating conditions. In the model, a unit amplitude shape function that represented a change in curvature with respect to removal depth was proposed. The proposed form was a special form of a Gauss distribution. It was the sum of two Gaussian peaks, with the same amplitude and pulse width, but opposite centre location. The form could also be represented by three constant coefficients, which depended on the energy released by a power function.

Zhang *et al* [2006] conducted an investigation on ultrasonic-assisted EDM in gas. The study focused on using ultrasonic waves to improve the efficiency of EDM in the gas medium. In this case, the tool was a thin-walled pipe and the high-pressure gas medium was applied from inside, while the ultrasonic actuation was applied onto the workpiece. The workpiece material used in the experiment was AISI 1045 steel while that of the tool was copper. The experimental results showed that the MRR increased with increase in open voltage, pulse duration, the amplitude of ultrasonic actuation, I_p. MRR also increased with a decrease in wall thickness of tool pipe. Finally, the experimental results showed that the R_a increased with increase in open voltage, pulse duration, and I_p. Based on experimental results, a theoretical model to estimate the MRR and the R_a was developed.

Nizar *et al* [2006] numerically studied thermal aspects of the EDM process. The numerical results concerning the temperature distribution due to the EDM process were presented. From these thermal results, the MRR and the total roughness were reduced and compared with experimental observations. The comparison showed that taking into account the temperature variation of conductivity was importance and gave better correlations with experimental data.

Dhar *et al* [2007] evaluated the effect of I_p, T_{on} and air gap voltage (v) on MRR, TWR, Radial over cut (ROC) of EDM with Al–4Cu–6Si alloy–10 wt. % SiC composites. This experiment did by using the PS LEADER ZNC EDM machine and a cylindrical brass tool of 30 mm diameter three factors, three levels of the full factorial design was using and analysing the results. A second-order, a non-linear mathematical model has been developed for establishing the relationship among machining parameters. The significant of the models were checked using technique ANOVA and finding the MRR, TWR and ROC increase significantly in a non-linear fashion with an increase in I_p.

Kao *et al* [2007] investigated the near dry EDM process in this process liquid-gas mixture used as a two-phase dielectric fluid. This had the benefit that, the concentration of the liquid and properties of the dielectric medium could be tailored to meet desired performance targets. A dispenser for minimum quantity lubrication was used to supply a certain amount of liquid droplets at a controlled rate to the gap between the workpiece and the tool. Wire EDM cutting and EDM drilling were investigated under the wet, dry, and near dry conditions. The mixture of water and air was the dielectric fluid used for near dry EDM. The near dry EDM showed advantages over the dry EDM in higher MRR, sharper cutting edge, and less debris deposition. Compared to wet EDM, the near dry EDM had a higher MRR low discharge energy. However, the near dry EDM placed a higher thermal load on the tool, which leads to wire breakage in wire EDM and increased tool wear in EDM drilling. A mathematical model was also developed to quantitatively correlate the water-air mixture dielectric strength and viscosity to the gap distance. In the model, it was assumed that the gap distance consisted of the discharge distance and material removal depth. The model was able to predict the dielectric strengths of various water-air mixtures.

Carlo *et al* [2008] investigated the effects of the tools metallic materials (Ag, Ni, Ti, W) on EDM responses. Linear mixed-effects models were fitted to the experimental data using the restricted maximum likelihood method. The main conclusion drawn was that the I_p and V as defined and measured in the framework depending on the tool material even when keeping all the other machining conditions unchanged.

Lin *et al* [2008] have reported that EDM machining of Cemented Tungsten Carbide using an electrolytic copper tool. The machining parameters of EDM were varied to explore the effects of electrical discharge energy on the machining characteristics, such as MRR, TWR, and R_a. Moreover, the effects of the electrical discharge energy on heat-affected layers, surface cracks and machining debris were also determined. The experimental results show that the MRR increased with the density of the electrical discharge energy. The TWR and diameter of the machining debris were also related to the density of the electrical discharge energy. When the amount of electrical discharge energy was set to a high level, serious surface cracks on the machined surface of the cemented tungsten carbides caused by EDM were evident.

Payal *et al* [2008] analysed EN-31 tool steel machined by using copper, brass and graphite as tool electrodes and concluded that three specimens showed different pattern of heat affected zones. Among the three electrodes the graphite electrode has a deeper heat affected zone than others.

Soveja *et al* [2008] have defined the experimental study of the surface layer texturing of TA6V alloy. The influence of the operating factors on the layer texturing process has been studied using two experimental approaches: Taguchi methodology and Response Surface Methodology (RSM). Empirical models have been developed and discussed the correlation between process operating factors and performance indicators, such as surface roughness and MRR. Results analysis shows that the laser pulse energy and frequency are the most important operating factors. Mathematical models, that have been developed, can be used for the selection of operating factors proper values in order to obtain the desired values of the objective functions.

Zhou [2009] worked on servo system for EDM, adaptive control of with self-tuning regulator a new EDM adaptive control system which directly and automatically regulates tool downtime has been developed. Based on the real-time-estimated parameters of the EDM process model, by using the minimum-variance control strategy, the process controller, a self-tuning regulator, was designed to control the machining process, this adaptive system improves the machining rate by, approximately, 100% and in the meantime achieves more robust and stable machining than the normal machining without adaptive control. This adaptive control system helps to gain the expected goal of optimal machining performance.

Sohani *et al* [2009] discussed die-sink EDM process effect of tool shape and size factor were considered in the process by using RSM process parameters like I_p, T_{on}, pulse off-time (T_{off}), and tool area. The RSM-based mathematical models of MRR and TWR have been developed using the data obtained through Central Composite Design (CCD). The analysis of variance was applied to verify the lack of fit and adequacy of the developed models. The investigations revealed that the best tool shape for higher MRR and lower TWR is circular, followed by triangular, rectangular, and square cross-sections. From the parametric analysis, it is also observed that the interaction effect of I_p and T_{on} is highly significant on MRR and TWR, whereas the main factors such as T_{off} and tool area are statistically significant on MRR and TWR.

Habib [2009] Studied parameter in EDM by using the RSM, the parameter like MRR, TWR, gap size and R_a and relevant experimental data were obtained through experimentation. They are using Al/SiC composites material and shown the correlations between the cutting rates, the R_a and the physical material parameters of this process. Optimal combination of these parameters was obtained for achieving controlled EDM of the workpiece and finding the MRR increases with an increase of T_{on}, I_p and V. MRR decrease with increasing of SiC%.

Sourabh [2009] studied the different EDM processes. Wire EDM is used primarily for shapes cut through a selected part or assembly. With a wire EDM machine, if a cut-out needs to be created, an initial hole must first be drilled in the material, then the wire can be fed through the hole to complete the machining. Die sinking EDMs are generally used for complex geometries.

In this case, the EDM machine uses a machined tool, it uses an tool to erode the desired shape into the part or assembly. Die sink EDM cut a hole into the part without having a hole pre-drilled for the tool.

Jin *et al* [2012] to investigated the debris and bubble movements during EDM, due to the fact that debris accumulation in the discharge gap causes poor machining stability and low production efficiency They established a series of experimental devices using transparent materials to observe debris and bubble movements. Based on the observations, the mechanism of debris and bubble exclusion during consecutive pulse discharges was analysed, and the effects of the tool jump height and speed on the debris and bubble movements investigated. It was found that during an tool down-time, the bubble expansion was the main factor that excluded the debris from space/gap between the tool and the workpiece. At the beginning of consecutive pulse discharges, the bubbles rapidly excluded the debris from the gap. As the discharge continued, the bubbles ability to exclude the debris became weak, resulting in a debris aggregation in the gap and thus, unstable machining. Finally, the results showed that the tool jump speed affected the mixing degree of the debris and oil.

Rajesha *et al* [2012] described, the alteration in surface characteristics of the machined surface takes place. The white layer (recast layer) caused by the EDM process increases surface roughness, decreases wear resistance and fatigue strength of the material. The thickness of the recast layer is dictated mainly by T_{on}, T_{off}, I_p and spark gap set voltage.

Donald [2013] concluded that material removal in EDM is by the production of a rapid series of repetitive electrical discharges. These electrical discharges are passed between a tool and the piece of metal being machined (workpiece). The small amount of material that is removed from the workpiece is flushed away with a continuously flowing fluid. The repetitive discharges create a set of successively deeper craters in the workpiece until the final shape is produced. The workpiece material must be electrically conductive.

Gopalakannan *et al* [2013] analysed the EDM parameters on machining of aluminium metal matrix composite, using Taguchi based grey analysis and reported that pulse current and T_{on} are primary factors that affect the quality of metal matrix composite and T_{on} is considered as primary factor.

Hasan [2014] studied the EDM process with many input parameters that include I_p, T_{on}, tool speed (T_R) and flushing. The processes that occur during EDM are sparking, open circuit, short circuit and arcing. The electric sparks are generated between two tools when a high potential difference is applied across them while they are separated by a narrow gap in a dielectric medium. Localized regions of high temperatures are formed due to the sparks occurring between the two tool surfaces. Workpiece material in this zone heats, melts and vaporizes. Most of the molten and vaporized material is carried away from the inter-electrode gap by the dielectric flow in the form of debris particles.

Muthuramalingam and Mohan [2015] reviewed the electrical process parameters to improve the thermal energy produced in the EDM process. It is mainly due to the applied electrical energy. The input electrical variables pulse shape and discharge energy on performance measures such as MRR, R_a and TWR. Also discussed that the electrical process parameters and empirical relationships between process parameters and optimization of process parameters in the EDM process.

Sarand *et al* [2015] studied the effect of thermal diffusivity coefficient of tool material on electrode-tool wear in the EDM process. Experiments were conducted on AISI H13 using copper alloy, copper-iron alloy, aluminum alloy and graphite as tools. A decreasing trend in the tool wear rate was observed with increase in the thermal diffusivity of the electrode material. It was also reported that, by using the tool materials with low thermal diffusivity, the tool wear rated was intensified with increase in the current and the pulse on time.

Younis *et al* [2015] studied the effect of the two types of electrodes i.e. Dura graphite 11 and Poco graphite EDMC-3 electrode material on electrode discharge machining of tool steel to avoid the residual stresses, the surface roughness and cracks. It was found that POCO Graphite EDMC-3 electrode results higher residual stresses compared with Dura Graphite 11 electrode. Also Soft EDM machining exhibits higher residual stresses as a result of higher pulse on duration time.

Mathan *et al* (2015) conducted the EDM experiments on Al 2618 alloy reinforced with Si3N4, AlN and ZrB2 composites using copper electrode. The performance in terms of MRR and tool wear rate was studied by varying the current, pulse on time and the pulse off time. Improved mechanical properties were observed in the work piece with reduction in the MRR and the tool wear rate.

Beri *et al* [2015] investigated the micro hardness and XRD analysis on the machined surface at the best parameter setting and compared with the surface machined using conventional copper electrode.

Dewangan *et al* [2015] conducted the EDM experiments in the AISI P20 tool steel using 12 mm diameter cylindrical copper tool and analyzed the surface integrity characteristics such as the white layer thickness, surface crack density and the surface roughness. Pulse on time was found as the most significant factor followed by the discharge current affecting the surface integrity characteristics.

Mandaloi *et al* [2016] investigated the crystalline structure of AISI M2 steel by using tungsten–thorium tool in the EDM process. The MRR, TWR and R_a of tool steel material depending upon three input process parameters. Subsequently, the surface topography of the processed material was examined through different characterization techniques like SEM, Optical Surface Profiler (OSP) and Atomic Force Microscopy (AFM), respectively. An X-Ray Diffraction (XRD) study, broadening of the peak was observed which confirmed the change in material properties due to the homogeneous dispersion of the particles inside the matrix. Lowest R_a and MRR of 0.001208 mg/min were obtained. Minimum R_a was obtained 1.12 µm and 2.18427 nm by OSP and AFM study, respectively. Also, minimum TWR was found as 0.013986 mg/min.

Soundhar [2019] described the EDM parameters by CCD and optimized the datasets by RSM technique. When less I_p and V applied to the EDM machining was lesser, it reduces the output discharge energy and MRR. In reverse increase the V and I_p it produces higher the value of discharge energy so, high MRR. It can be observed that the T_{on} increases, the MRR value is also increased. When the I_p increases, the value of TWR also increases. The Effect of process parameters on R_a, the high electrical discharge between tool and workpiece produces crater wear on workpiece surface which introduces poor surface finish. So optimum parameters to be needed to control the R_a. When the value of T_{on} and I_p rising simultaneously the R_a value also increases, and further raising the input voltage the value increases. Thus increasing or decreasing the value of pulse off time does not affect the R_a. So, pulse off time is insignificant parameters for the R_a.

Bahgat *et al* [2019] specified the significance of EDM process parameters on H13 die steel. The I_p is the most important factor affecting both TWR% (using Cu tool) and MRR, the type of tool material and the T_{on} have a negligible effect on the MRR. While the T_{on} is the most important factor affecting the R_a using brass tool, the type of tool material and the I_p has a negligible effect on the R_a. The optimal process parameters are copper tool with 14 amp I_p and 150 µsec T_{on}, for the highest MRR; copper tool with 2 amp I_p and 150 µsec T_{on}, for the lowest TWR%; brass tool with 2 amp I_p and 50 µsec T_{on} to produces the high surface quality.

2.3 Tool Rotation EDM

Koshy *et al* [1993] investigated, the provision of holes in the tool is impracticable, and flushing of the working gap poses a major problem. Use of a rotating disk tool is proposed as a more productive and accurate technique than the use of a conventional tool. MRR, TWR, relative tool wear, corner reproduction accuracy, and R_a aspects of a rotary tool are compared with those of a stationary one. The effective flushing of the working gap brought about by the rotation of the tool remarkably improves MRR and machines surfaces with a better finish.

Yan *et al* [2000] have discussed the investigation of the feasibility and optimization of a rotary EDM with ball burnishing for inspecting the machinability of Al_2O_3/6061Al composite using the Taguchi method. Three ZrO_2 balls attached as additional components behind the tool offer immediate burnishing following EDM. Three observed values MRR, R_a and improvement of R_a are adopted to verify the optimization of the machining technique. Design of tool is copper ring-shaped used in EDM with ball burnishing (BEDM) as shown in figure 2.3. This B-EDM process approaches both a higher machining rate and a finer surface roughness. Furthermore, the B-EDM process can achieve an approximately constant machining rate.

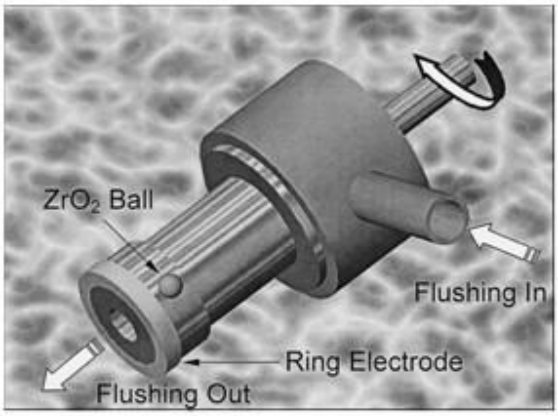

Figure 2.3: Design of Cu-ring tool shaped B-EDM (Yan et al, 2000)

Wei and Lee [2002] have patent about EDM with multiple holes in the tool and electrically conductive workpiece, includes an EDM for rotatable mounting for first tool and at least one electrical discharge unit for the rotatable mounting second tool. The EDM includes a driver and a controller, the driver is desirably coupled to the EDM and the electrical discharge unit for rotating the first tool and the at least one second tool, and the controller is desirably coupled to the EDM and the at least one electrical discharge unit for controlling a supply of electrical energy from the first tool and second tool to the workpiece.

Fujun *et al* [2004] introduced the shaping principle of machining non-sphere with the rotary tool, analyses in greater detail the functions of machining non-sphere system with the rotary tool and the motion laws of machining rotary work-pieces. On the basis of those works, the general laws of forming non-sphere through rotary tool bevelling circle are studied and establishes mathematical models. This lays a foundation of mathematics for computer simulation, virtual machining and establishment of the real machining system of machining non-sphere by rotary EDM. This lays a solid foundation of mathematics for the study on the virtual machining and for the establishment of the CAD, CAPP and CAM integration systems of machining non-sphere by rotary EDM.

Chattopadhyay *et al* [2009] investigated the machining characteristics of EN-8 steel with copper as a tool during the rotary EDM process. The empirical models for prediction of output parameters have been developed using linear regression analysis by applying logarithmic data transformation of the non-linear equation. Three input parameters viz. I_p, T_{on} and rotational speed of tool are chosen as variables for evaluating the output parameters such as MRR, TWR and R_a. The I_p and T_{on} are the most significant parameters for MRR and TWR, respectively. But I_p and tool rotation become the most significant for MRR and significant parameters for R_a, respectively. Experimental results further revealed that maximizing the MRR while minimizing TWR and improving the R_a, cannot be achieved simultaneously at a particular combination of control parameters setting.

Han *et al* [2009] proposed high-speed EDM milling method using moving electric arcs with the copper tool. Electric arc takes place in the gap between the tools move rapidly as a result of the high-speed rotation of the tools. Material on the workpiece can be eroded by moving electric arc continuously without discharge intervals by moving electric arcs. The discharge pulse duration time can be considered as infinite, and this results in an extremely low or zero tool wear when the machining is carried out in dielectric oil and have thinner heat-affected layers.

Wang and Lin [2009] discussed the optimization of W/Cu composite material by the Taguchi method. W/Cu composites are a type of cooling material highly resistant to heat corrosion produced through PM. The Taguchi method and L_{18} orthogonal array to obtain the polarity, I_p, pulse duration, duty factor, T_R rotational speed, and V in order to explore the MRR, TWR, and R_a. The influenced of each variable and optimal processing parameter will be obtained through ANOVA analysis through experimentation to improve the process.

Izquierdo *et al* [2009] studied the EDM process. The workpiece was generated by the superposition of multiple discharges, as it happens during an actual EDM operation, by the diameter of the discharge channel and MRR efficiency can be estimated using inverse identification from the results of the numerical model. An original numerical model for simulation of the EDM process has been presented. The model generates EDM surfaces by calculating temperature fields inside the workpiece using a finite difference-based approach and taking into account the effect of successive discharges.

Kung *et al* [2009] discussed the effect of MRR and TWR study on the powder mixed EDM of cobalt-bonded tungsten carbide (WC-Co) has been carried out. In the PM EDM process, the aluminium powder particle suspended in the dielectric fluid disperses and makes the discharging energy dispersion uniform; it displays multiple discharging effects within a single input pulse. This study was made only for the finishing stages and has been carried out taking into account the four processing parameters: I_p, T_{on}, grain size, and concentration of aluminium powder particle for the machinability evaluation of MRR and TWR. The RSM has been used to plan and analyse the experiments. Notice that the residuals generally fall on a straight line implying that the errors are normally distributed. Furthermore, this supports the adequacy of the least-squares fit. The MRR generally increases with an increase of aluminium powder concentration.

Kunieda and Kameyama [2010] described the method to reduce TWR in EDM by applying the relative sliding motion between electrodes. Experimentally, it was found that the cathode spot is more likely to slide on the tool surface than the anode spot. Heat conduction analysis showed that MRR increases once with the moving speed of the heat source when the moving speed is low. The tungsten anode rod was machined by a copper cathode disc rotating at a high circumferential speed. It represents the TWR ratio decreases with increasing rotational speed.

Teimouri and Baseri [2012] studied the effects of tool rotation and various intensities of external magnetic field on EDM. The influences of process parameters were investigated on the main outputs of MRR and R_a. The influence of input parameters and output responses by the mathematical model were developed to predict the MRR and R_a according to variations of discharge energy, magnetic field intensity and tool rotational speed. Results indicated that applying a rotational magnetic field around the machining gap improves the MRR and R_a. Combination of the rotational magnetic field and rotary tool increases the machining performance due to better flushing debris from the machining gap.

Dwivedi and Choudhry [2016a] discussed the surface integrity the AISI D3 Tool Steel using the tool rotation in EDM process. R_a, Micro-Cracks and recast layers have been studied as the output parameters. The results show that the machined workpiece has a finer surface, improvement in the surface quality of the workpiece with rotary tool EDM is around 9-10%; micro-cracks are significantly less with rotary tool EDM as compared with the stationary tool EDM process and recast layer thickness using rotary tool EDM in the range of 2 to 25 µm, which is almost half of that which is obtained using stationary tool EDM. The rotation of tool enables uniform workpiece machining, because of the fact that the tool rotation provides a better passage for the clearance of the debris from the machining cavity, therefore, very less molten material gets re-deposited.

Dwivedi and Choudhry [2016b] analysed that the tool rotation methodology increases the MRR by increasing the spark efficiency and effective debris clearing. That shows the tool rotation phenomenon significantly improves the average MRR and R_a by 41% and 12% respectively. Moreover, the final surface is more uniform in structure with less number of micro-cracks and thinner recast layer as compared to the stationary tool EDM.

Li *et al* [2015] analysed hybrid machining process (HMP) based on EDM end milling for AISI 1045 steel. It combines cutting action and an electrical thermal process. A tungsten carbide end mill was used as a tool to machine the workpiece with different electric energy pulses. The machining mechanism was investigated, and a mathematical model of EDM-end milling is presented. Simulated and experimental cutting results were compared to validate the model. The EDM-end milling has 14.4 times higher processing efficiency than traditional EDM. HMP has better performance than conventional milling when machining difficult-to-cut materials.

Dwivedi and Choudhry [2017] described the measurement of the recast layer thickness of AISI-D3 tool steel using the rotary tool EDM process. The recast layer is an undesirable property of the material and a demerit of this process. The rotary tool EDM helps to reduce the thickness of this layer significantly. The average recast layer thickness (RLT) obtained with the rotary tool EDM process is 40.26 μm whereas it comes out to be 69.03 μm for the stationary tool EDM. Due to improved passage for debris clearance from the machined cavity. Hence, the amount of molten material re-deposited on the machined surface is very less. So, the final workpiece has a very thin recast layer which is almost half of the stationary tool EDM.

Nakagawa *et al* [2017] investigated high-speed electrical discharge machining (EDM) milling with working gap control. T_R improves the MRR, but the rotation causes a periodic change in the working voltage. As a consequence, the periodic change causes a disturbance that decreases the control performance. The proposed controller introduces a notch filter, which eliminates the frequency component due to the rotation of the tool. It also has a fed forward compensator to eliminate the steady offset. The controller for each machining condition is derived from a coordinate transformation and the least-squares approximation. It is confirmed that the proposed controller achieves machining speeds that are 2–6 times faster in a straight line and greater than 30% higher in the profile machining than in the conventional one.

Tanjilul *et al* [2018] studied the EDM process. It removes the material through spark erosion and is often used for drilling holes in difficult-to-cut materials such as Nickel-based super alloys. The flushing pressure becomes inefficient for the effective evacuation of process debris leading to secondary discharges and resulting in increased machining time. The vacuum-assisted debris removal system used for better flushing. Experimentally measured particle size data of full-length scale act as a reference for the proposed numerical model. The analysis provides significant insight into the sizes of the debris particles in different machining conditions. Improved R_a was observed in the case of suction-assisted drilling. Machining I_p significantly influences the size of the debris particles, and particles size increases with increasing I_p

2.4 Summary of Literature Review

This review brings about systematic studies on the machinability and surface texture property of AISI D3 and EN-31 Steel using tool rotation EDM. In this study, an attempt was made to machine AISI D3 and EN-31 steel using tool rotation EDM with a copper tool to study the effects of process parameters such as I_p (amp.), T_{on} and T_R on MRR, TWR and R_a. AISI D3 and EN-31 steel is used for engineering applications such as manufacturing of dies and punches, press tools, bushes, blanking and forming dies; gauges, swaging dies, ejector pins, ball and roller bearing. ANOVA was carried out to obtain the optimal levels of process parameters for effective machining of AISI D3 and EN-31 Steel.

Most of the previous studies on EDM and T_R reveal that productivity aspects such as MRR as well as accuracy measures namely surface roughness, dimensional deviation, kerf are mainly decided by pulse on time, pulse off time, I_p, spark gap set voltage. Tool rotation EDM is capable of machining hard materials with intricate shapes and profiles. However, alteration in surface characteristics of the machined surface takes place. The workpiece has finer surface quality with rotary tool EDM is around 9-10%; micro-cracks are significantly less with rotary tool EDM as compared with the stationary tool EDM process and recast layer thickness using rotary tool EDM in the range of 2 to 25 µm, which is almost half of that which is obtained using stationary tool EDM. The thickness of the recast layer is dictated mainly by pulse on time, pulse off time, I_p and spark gap set voltage.

2.5 Identified Literature Review Gaps

The comprehensive study of the existing literature review, a number of gaps have been observed in tool rotation EDM. Although a literature search revealed very fewer studies in the machining of AISI D3 and EN-31 steel, most of it has investigated a limited number of process parameters on the performance measures of EDM.

- Many researchers had investigated only selected process parameters on the output responses.

- Very limited work had been done on AISI D3 steel and EN-31.
- Only few researchers applied RSM using Central Composite Design approach.
- Researchers have not concentrated much to study about the Residual Stresses on tool rotation EDM machined surfaces.
- Only few researchers had done Surface roughness analysis by stylus.
- Very limited work had been analysed pulse discharge analysis with digital storage oscilloscope (DSO).

2.6 Research objective

The major performance measure of the EDM process is material removal rate (MRR), tool wear rate (TWR), surface roughness and re-cast/white layer of the machined surface. For cost-effective machining, it is essential to identify and estimate the changes that are taking place within tool materials with respect to the material removal rate. The tool material life plays an important role in increasing productivity and subsequently, is an important economic aspect of the process. The high wear rate of tool material leads to interruption during machining which in turn increases machining time and declines productivity of the process by increasing the machining cost. Therefore, it is utmost important to have higher material removal and minimal tool wear to enhance the productivity of the process and also better surface characteristics during machining. To understand the effect of important parameters on the performance measures, modeling of the process is vital.

The objectives of this dissertation rest on study of the effect of control parameters during machining of AISI D3 and EN-31 steel in EDM with tool rotation process. The study will help the tool engineers to reduce the experimental cost and errors associated with the process and optimize the process by setting the requisite parameters. To this end, the following objectives are set for this research work.

1. To assess the influence of I_p on the performance of the EDM process with tool rotation.
2. To study the effect of tool rotation (T_R) in the EDM process responses.
3. To analyse the significance of pulse-on-time.
4. To study the effect of parameters on Surface Roughness (R_a).
5. To study the effect of process parameters on Residual Stresses.

CHAPTER 3

EXPERIMENTAL METHODOLOGY

3.1 Electric Discharge Machine with Tool Rotation

The experiments were performed on EDM die-sink machine (SN35, Sparkonix (India) Pvt. Ltd, Pune) shown in fiure 3.1. The tool rotation arrangement installed on the Z-axis of EDM die-sink machine in the Mechanical Engineering Department, DTU, Delhi, India. The detailed specification of the machine is listed in table 3.1.

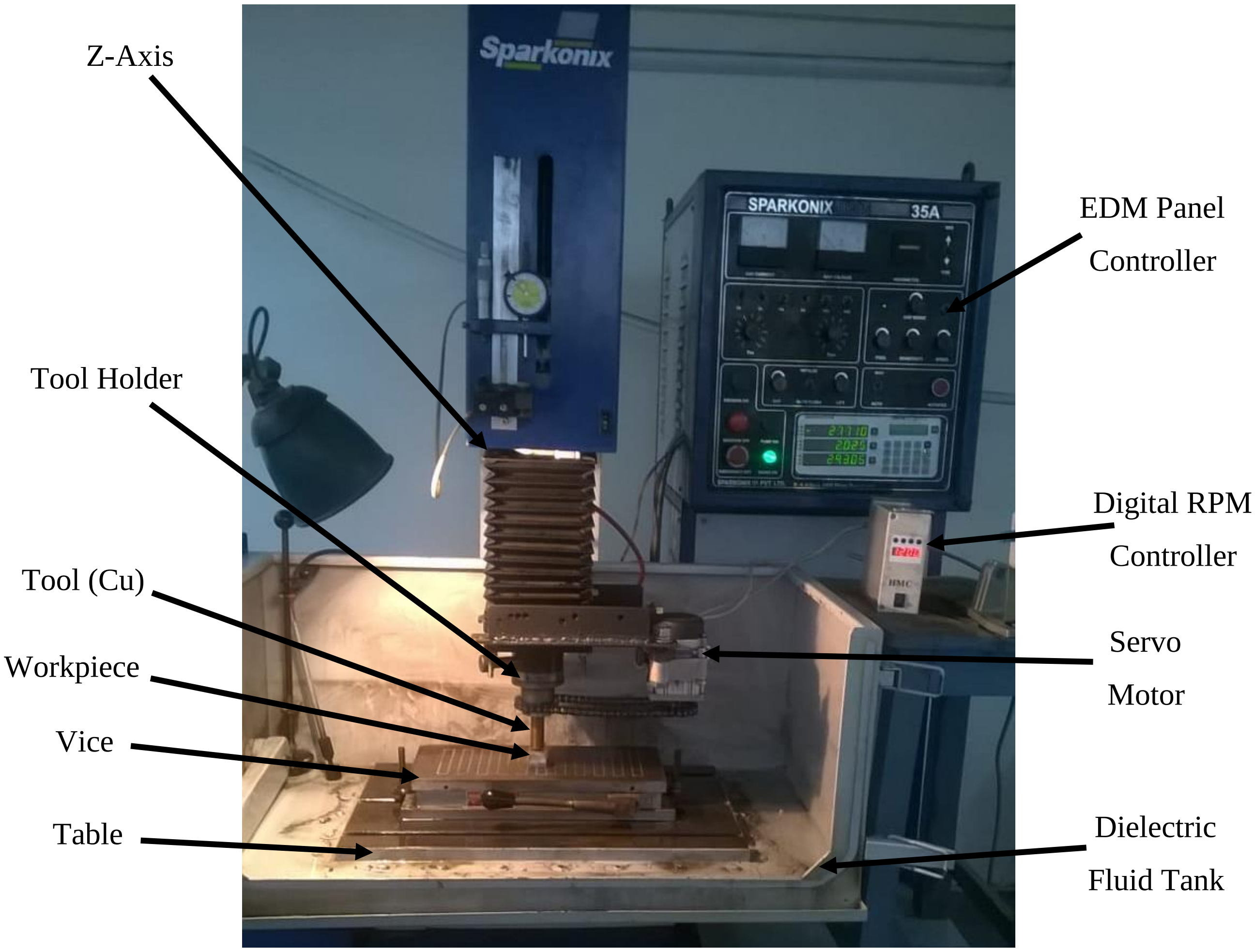

Figure 3.1: Schematic view of EDM with Tool Rotation

Tool rotation die with servo motor was assembled on the z-axis of EDM. The tool holder rotation was provided by servo motor. The servo motor output shaft is connected to the tool die attachment by chain and sprocket arrangement. The servo motor is connected to the digital RPM controller, which provides 0 to 5000 rpm to tool, so z-axis having two types of motions i.e. Tool rotation, upward and downward. The upward and downward motion is controlled by switch (manually) as well as automatic (auto position) push button.

3.1.1 EDM machine specification

The machine specifications are shown as:

Table 3.1 Machine specification

Current range	1 to 35 amps
Pulse range	1 to 10 nodes
Work tank size	775 x 450 x 325 mm
Worktable size	550 x 350 mm
Longitudinal travel (X)	200 mm
Transverse travel (Y)	200 mm
Quill travel (Z)	200 mm
Dielectric capacity	260 liters
Height of work piece (Maximum)	300 mm
Weight of work piece (Maximum)	400 Kg
Tool weight (Maximum)	35 Kg
Motor for pump (Maximum)	1 HP

3.2 Fabrication of Tool Rotation Die

The tool rotation die is essential to mount the tool and provide the rotation with servo motor for machining EN-31 and AISI D3 steel workpiece.

The tool rotation die consist of following elements:

(i) Hub with bearing housing

(ii) Bearing

(iii) Rotary die

(iv) Sprocket with chain

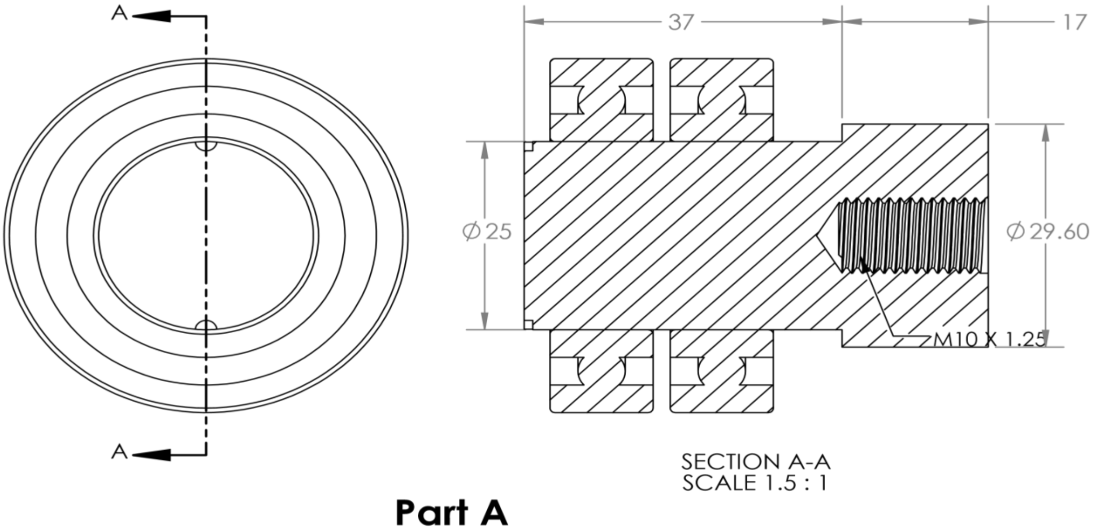

Figure 3.2: Hub die with two bearing

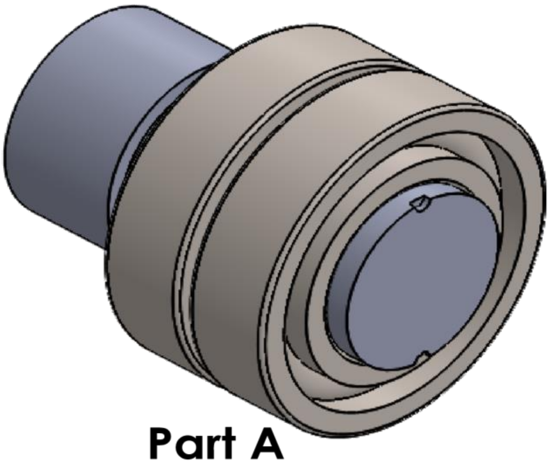

Figure 3.3: 3D Modelling of hub die with two bearing

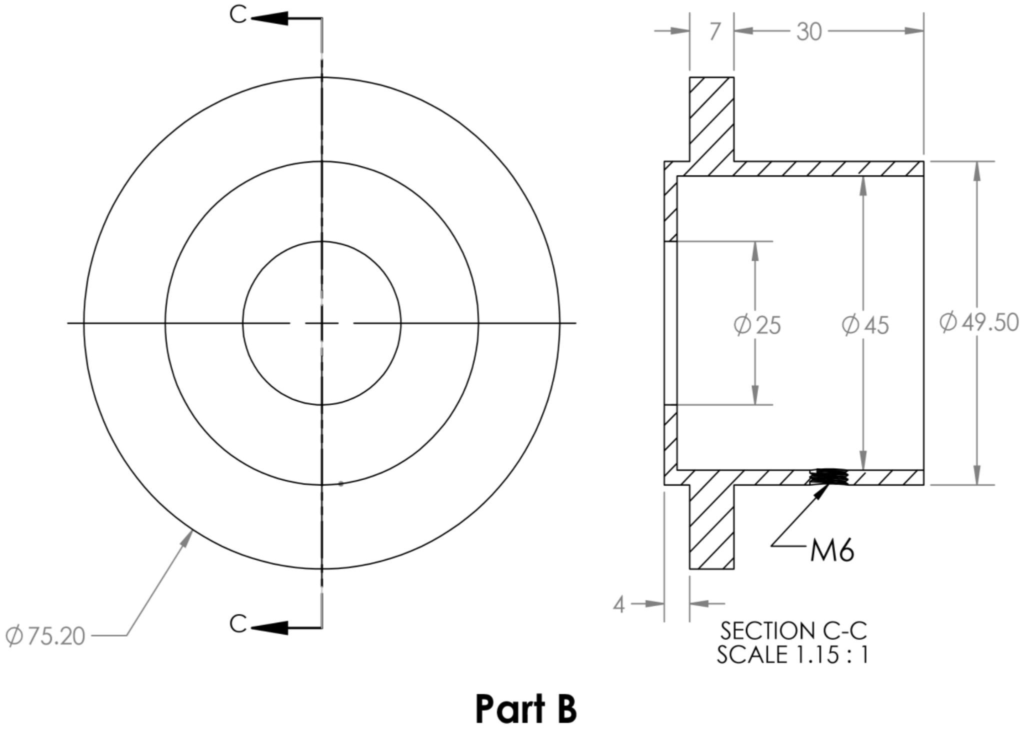

Figure 3.4: Flange diagram

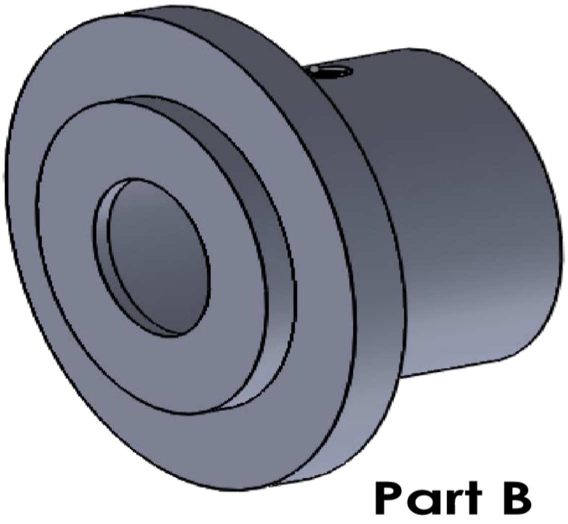

Figure 3.5: Flange modelling

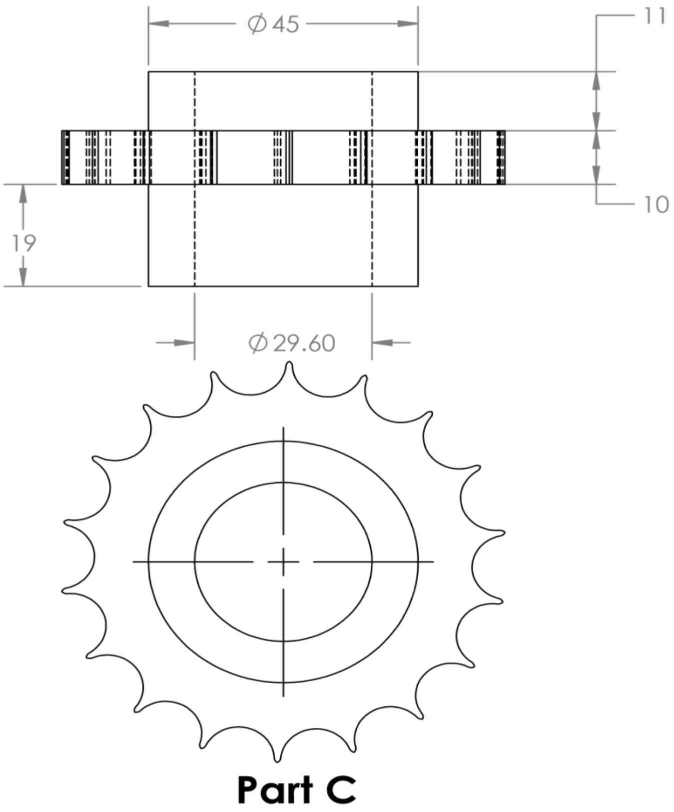

Figure 3.6: Sprocket

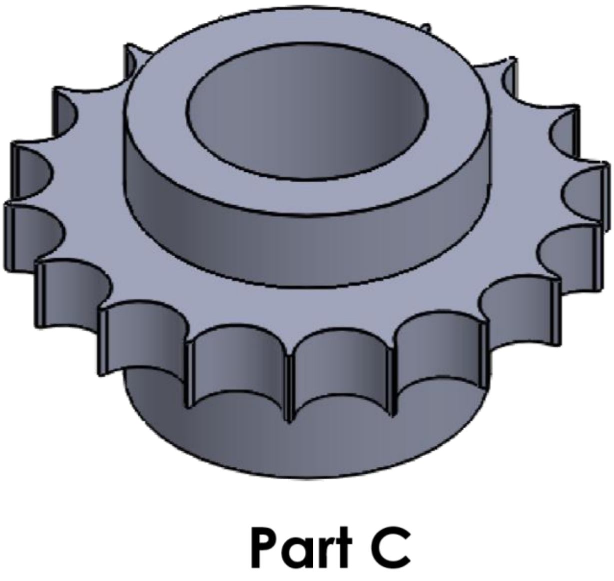

Figure 3.7: Sprocket Modelling

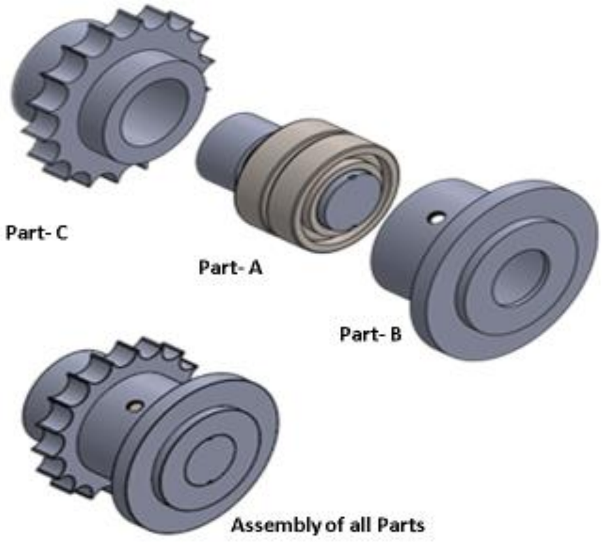

Figure 3.8: Part C-A-B CAD Model Assembly

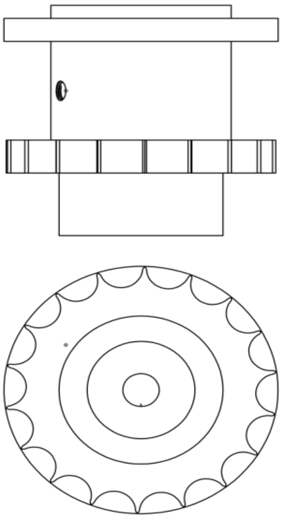

Figure 3.9: Part C-A-B Assembly

The hub with bearing housing, sprocket and assembly was shown in figure 3.2 to 3.9. This tool rotation die attachment was mounted on the z-axis of EDM. The tool rotation die was powered by servo motor from 0-5000 rpm in either clockwise or counter clock-wise direction. The rotation per minute and direction of tool rotation is controlled by servo motor controller shown in figure 3.10.

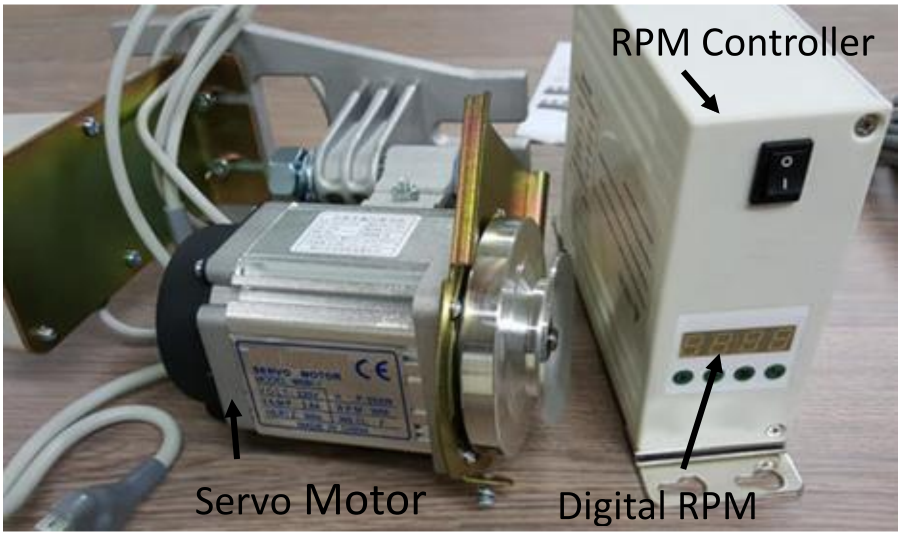

Figure 3.10: Servo motor with controller

3.3 Workpiece Material

The detailed chemical composition of EN31 and AISI D3 steel is furnished in Tables 3.2 and 3.3

Table 3.2 Elemental Composition of EN-31 Steel

C	Mn	Si	P	S	Cr	Fe
0.90 - 1.2 %	0.3 - 0.75 %	0.10 - 0.35 %	max 0.05 %	max 0.05 %	1.00 - 1.60 %	Remaining %

Table 3.3 Elemental Composition of AISI D3 Steel

C	Cr	Mn	Ni	Si	Fe
2.1 %	12 %	0.35 %	0.5 %	0.3 %	Remaining %

3.4 Process Parameters

The process parameters of tool rotation EDM machining may be classified as electrical and non-electrical. Considering both electrical and non-electrical parameters, the following were selected for this research as input parameters for machining EN31 and AISI D3 steel workpieces.

(i) I_p- Current (amp.)

(ii) T_{on}-Pulse-on Time (µsec)

(iii) T_R-Tool Rotation (rpm)

(iv) Pulse-off-time (const.) (µsec)

(v) Tool Material (Electrolyte Copper ϕ 20mm) (const.)

(i) Current (amp.)

It is the measure of current supplied to the discharged gap, measured in units of amp. If this current value increases, higher pulse energy is generated and deep craters are formed. High amount of current is used in cavities and rough machining. During EDM process, the measurement of average current over a complete cycle considered. It is measured in current meter during operation. A large amount of current is not applied because it leads to destroy the workpiece surface and produce a large quantity of recast layer. The machined material (vapour/liquid phase) was not washed entirely from surface and re-solidify on its surface. It is known as recast layer or white layer. The acute temperature developed around the machining areas of workpiece called the heat treatment of material.

(ii) Pulse-on-time (µsec.)

It is the time period for one succession to discharge current. Material removal is linearly related to the amount of discharge energy per cycle. The arc gap is bridged and flow of current from tool to the workpiece and the metal removal take place and work is completed. The spark sustained for a higher period of time then high metal removal takes place. Due to the presence of high energy, the impression will be wider and acute. Hence, the surface will be rough. This proves that in a small duration of sparking the surface finish will be fine.

(iii) Pulse-off-time (µsec.)

It is the duration of a time period not allowed to flow current for one succession. Metal removal does not take place during this period. During pulse rests time, deionization of the dielectric fluid will take place. The pulse-off time increases the machining time. The stability of arcing in EDM process based on pulse-off time. It is an integral part of the EDM process and must exist. An inappropriate pulse-off-time can lead to irregular succession. This is called pulse interval time.

(iv) Tool Rotation (rpm)

Tool rotation was provided to facilitate the flushing of material removed during machining in the form of debris or tiny particles. Flushing is important for increasing the performance of machining, since it carries away the debris of the materials from the work surface, while machining (kuruvila and Ravindra, 2011). Flushing increases with tool rotation as well as the energy distribution is uniform.

(v) Tool Material

In this research, non-ferrous tools viz. oxygen-free high thermal conductivity (OFHC) solid cylindrical copper is used for the experiment of diameter 20 mm. The contour of the machined surface is the replica of the tool size and geometry. Circular tools are preferred over triangular and rectangular sizes.

3.5 Fabrication of Tool

Electrolyte solid cylindrical copper rod is used for experimentation by turning the rod to diameter 20 mm. The tool material from raw to finished tool, shown in figure 3.11 - 3.13. The specification of electrolyte solid cylindrical copper material is shown in table 3.4.

Figure 3.11: Raw copper rod

Figure 3.12: Copper tool with threading

Figure 3.13: Copper tool with facing

Table 3.4 Specification of the tool material.

Tool	Electrolytic Copper rod
Diameter	20 mm
Height	100 mm
Purity	99.99%
Conductivity (Electrical)	100% IACS (International Annealed Copper Standard
Conductivity (Thermal)	391.1 (W/m-K) on 100°C
Temperature of melting	1083 °C

3.6 Dielectric Fluid

In EDM, the localized spot heating, melting and evaporation of the material from the surface of tool and workpiece takes place. As thermic treatment is performed in the unavailability of oxygen so that the operation can be in control and the oxidation can be prevented. The excessive heat of plasma damages the machined surface integrity and tool geometry. The oxidation repeatedly brings to bad conductivity to the workpiece and further obstructs in machining. Therefore, the dielectric fluid must provide oxygen-less atmosphere. The dielectric fluid does not breakdown electrically due to strong dielectric resistance. It ionized during the striking of electrons with its molecules in the inter-elcetrode gap. Moreover, during arcing, it must be well heat resistant. The dielectric fluid should possess a high flash point, low viscosity and cheap in cost (McGeough and Rasmussen, 1997).

The dielectric fluid should perform the following functions:

(a) It initiates discharge when adequate voltage is built-up in the IEG. The cold emission of electrons caused by electrostatic field from the cathode. The micro-irregularities on the tool surfaces originating towards anode surface. The free electrons liberated from cathode will be accelerated towards anode by an electric field. The electrons strike with molecules of dielectric fluid, after gaining the sufficient velocity. Then it breaks into electrons and positive ions. Two electrodes connected in a narrow ionized column of dielectric fluid molecules.

(b) It assists to interrupt the sparking.

(c) It flushes debris aside from machined surface by an uninterrupted flow of dielectric fluid.

(d) It functions as a quenching agent.

The commonly used dielectric fluid is transformer oil, silicon oil, EDM oil, kerosene oil and de-ionized water. Dielectric fluid is flushed in between the IEG (spark zone). It is flushed through the jet to obtain efficient flushing of eroded material. The experimentation was performed with EDM–

30 dielectric fluid. EDM fluid has low viscosity, high flash point which reduces the fire. It also exhibits high dielectric strength, which acts as insulation of tool, workpiece and also to control the electric discharge. In this study, EDM-30 dielectric was used.

3.7 Method of Flushing

Flushing method is also an important function in EDM machining operation because eroded particles must be removed from the gap for efficient cutting. Flushing is the process of supplying dielectric fluid into the spark gap and reduce the temperature of tool and workpiece upto dielectric fluid or room temperature. Deeper the cavity, the greater the struggle for proper flushing. Improper flushing causes abnormal cutting. This increases the machining time. The debris under some machining conditions attaches themselves to the workpiece. This prevents the tool from machining efficiently, it is then necessary to remove the attached particles by cleaning the workpiece. The danger of arcing in the IEG also exists when the eroded particles have not been successfully removed. Arcing occur when the IEG contains too many eroded particles and then electric current passed through the accumulated particles. The arcing causes an unwanted cavity or cavities which may damage the workpiece. Arcing is most probable to occur during the finishing operation because of the small gap that is needed for finishing. There are numerous methods for flushing out from which pulse flushing with a combined vertical and rotary flushing system is used and efficient one shown in figure 3.14.

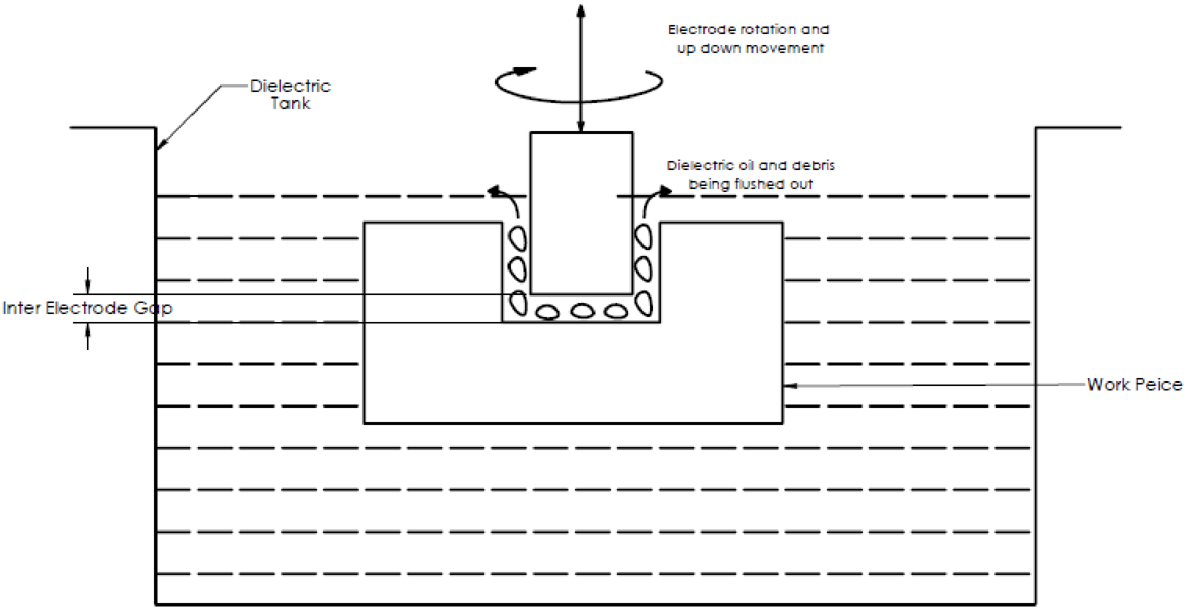

Figure 3.14: Pulse flushing with a combined vertical and rotary flushing system

3.8 Measurement of Output Responses

EDM with tool rotation is mainly used for removing the material from the workpiece as per the requirements of industries like aerospace and medical. While machining the workpieces, tool also subjected to wear, which is called tool wear. This leads to changes in the surface finishes of the workpiece and tool also. Considering the above concept the important output responses are MRR, TWR and R_a.

3.8.1 Weighing Machine

The weighing machine BSA224S-CW Sartorius BSA electronic analytical balance has been used to weight the workpiece and tool, shown in figure 3.15 and 3.16. The weight machine has readability 0.1 mg Repeatability ≤ ± 0.1 mg.

Figure 3.15: Weighing scale for tool

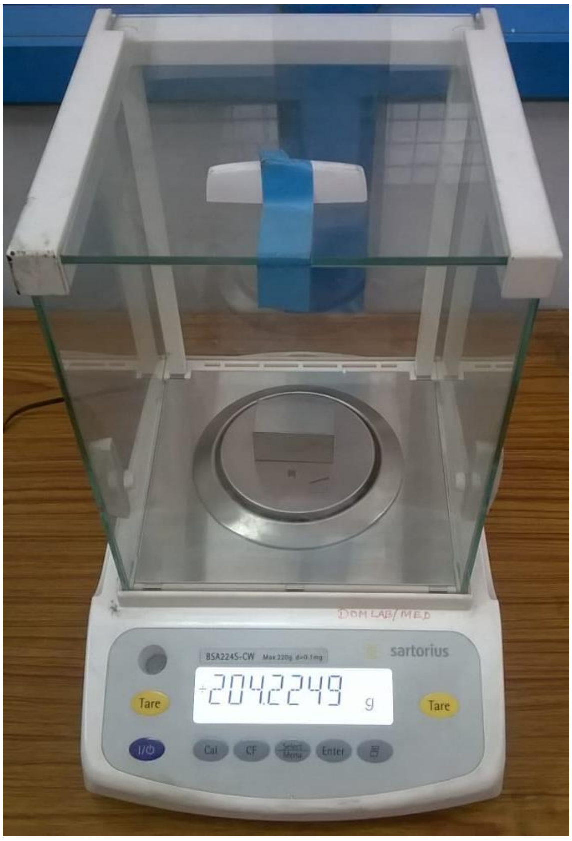

Figure 3.16: Weighing scale for workpiece

3.8.2 Material Removal Rate (MRR)

MRR evaluated by work material weight difference prior and later of machining, using a digital weighing scale and recorded.

$$MRR = (W_{bm} - W_{am})/T \qquad \text{(gm/min)} \qquad (3.1)$$

Where:

W_{bm} = Workpiece weight prior to machining in grams

W_{am} = Workpiece weight later of machining in grams

T = Machining time in minutes.

3.8.3 Tool Wear Rate (TWR)

Tool wear rate was determined by the difference of tool material weight prior and later of operation, using digital weighing scale and recorded.

$$TWR = (T_{bm} - T_{am})/T \qquad (gm/min) \tag{3.2}$$

Where:

T_{bm} = Tool weight prior to machining in grams

T_{am} = Tool weight later of machining in grams

T = Machining time in minutes.

3.8.4 Assessment of Surface Characteristics

Surface characteristics are the measure of surface roughness (R_a) and the integrity of the work surface. R_a is the deviation of actual surface of workpiece from its ideal nature. If the abnormalities are high, then R_a is rough, but abnormalities are very small, then R_a is less i.e. smooth surface. Generally, surface roughness is characterized by R_a (Rahman et al., 2011). It estimates average roughness by evaluating peak and valley with the mean line and average value has been taken over the surface texture on machined length. The profilometer stylus was dragged across the machined surface length. A shorter machined length gives less accurate while larger machined length gives more accurate. In this study, the machined diameter is selected as 20 mm. The surface roughness values have been measured by a stylus-based profilometer, illustrated in figure 3.17

Figure 3.17: Surface Roughness Profilometer Tester

3.9 Selection of Process Parameters

In industries for advance materials, the time for machining the components has to be reduced to obtain high profit. In EDM with tool rotation process, it is essential to obtain high MRR, minimum TWR and minimum R_a i.e. high surface finish. It is very essential to find out the significant parameters for machining the workpiece. There is a number of input parameters in EDM with tool rotation process, out of which pulse-on-time, current and tool rotation are found significant input parameters, shown in figure 3.18.

If current increases, pulse discharge energy also increase, which lead to enhancement in MRR, TWR and R_a. Furthermore, material removal is linearly related to the amount of discharge energy during that particular time period, it is called pulse-on-time. Tool rotation is an essential parameter because it performs a significant role in uniform distribution of discharge energy and flushing away debris or tiny particles from the IEG in-between tool and workpiece during machining. The contour of the machined area is the replica of tool geometry. Considering the above, the input parameters for the analysis are current (I_p), pulse-on-time (T_{on}), tool rotation (T_R).

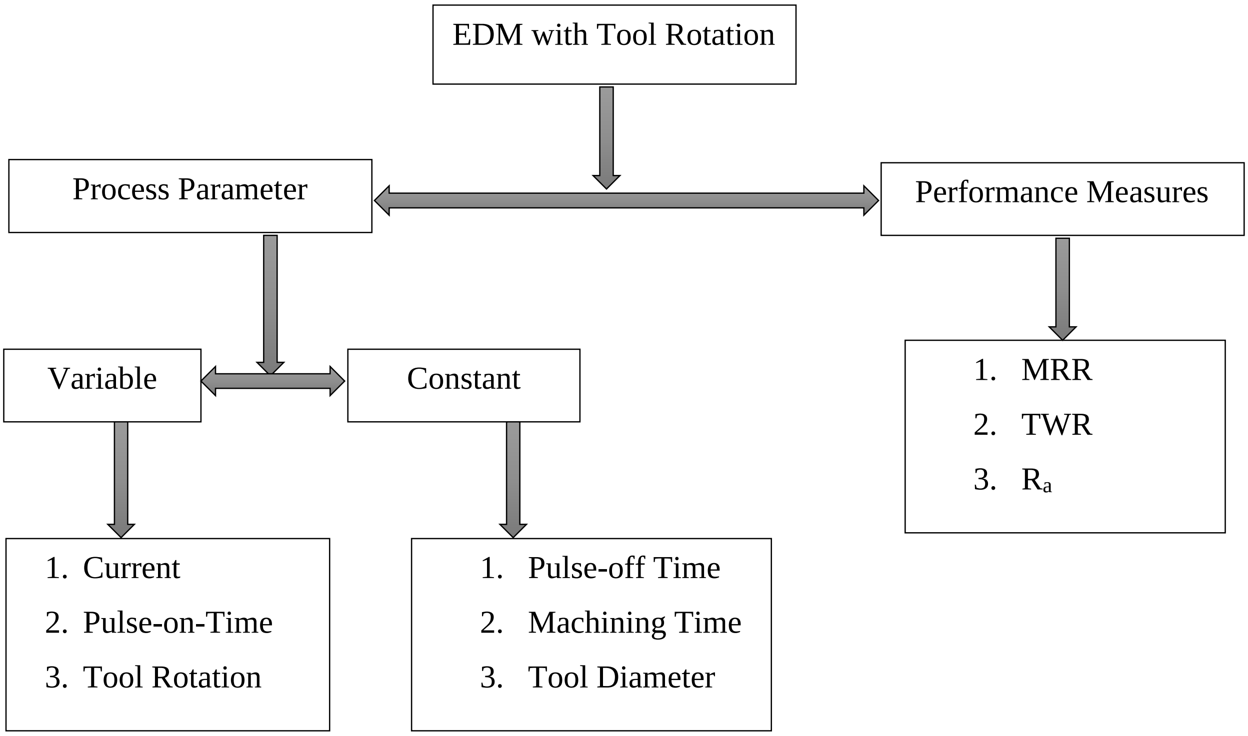

Figure 3.18: Selection of process parameter

CHAPTER 4

COLLECTION OF DATA

4.1 Introduction

In this chapter, the numerical model of the responses was developed with respect to input parameters. Design matrix is formed by using the statistical software package Design Expert Software- 12 version, (Stat Ease, Inc., and Minneapolis, USA) with considering the input parameter such as Current (I_p), Pulse-on-time (T_{on}) and Tool Rotation (T_R) parameters with 3 levels, other machining parameters kept constant.

RSM with the Central Composite Design method was used for analyzing the parameters. In this study, 20 experiments as per DOE were performed to examine effect of input variables over the output solutions i.e. MRR, TWR and R_a.

RSM is a set of mathematical and statistical information useful for the modelling and analysis of problems in which a response of interest is influenced by several input variables called independent variables and the objective is to optimize this response (Montgomery 2005).

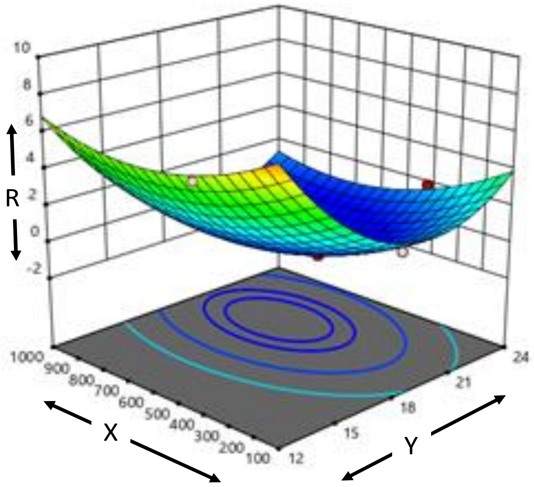

Figure 4.1: Theoretical Response Surface, representing the relationship between Response "R" and variable "X" and "Y"

Figure 4.1 represents the correlation of response variable (R) and two process variables “X” and “Y”. Each value of X and Y have a corresponding value of yield as a surface laying above the X-Y plane. It shows a graphical perspective of the problem environment that has lead to term RSM.

Most of the application of RSM is iterative and sequential in nature. A screening experiment is designed and executed to understand the nature of the process and eliminate the non-significant variables from the process and focus on the important variables. The iterative experiments are performed along with observation of trend and response behaviour. The direction of steepest ascent or decent is determined by considering the area of interest (i.e. maximization or minimization). RSM designs are applied for:

1. Find improved or optimal settings.
2. Troubleshoot process problems and weak points.
3. Prepare a robust process against external and non-controllable influences.

4.2 Iterative Response Surface Methodology

It is the process of sequential experimentation with rapidly and efficiently along with the path of improvement towards general vicinity of the optimum. Figure 4.2 depicts the procedure where first two-level full factorial experiments are executed to understand the behavior of the process and to eliminate the insignificant factors, this is known as screening experiments. After, screening experiment the full factorial design with centre point is designed using only significant factors from the screening experiments. After each design, the phases were changed and the first-order model is determined for the response. The experiments were executed in the path of steepest descent for the minimization of response. At some point in this iterative process, the response reaches the minimum value after which it starts increasing. At that stage, the central composite design is executed to get the exact behavior of the optimal level of the factors involved in the experiment. The eventual objective of RSM is to determine the optimum operating conditions for the system or to determine a region of the factor space in which operating requirements are satisfied.

RSM is a mathematical modelling technic applied to forecast the outcome correlation for multi-combinational parameters. The numerical interpretation for the outcome responses can be achieved w.r.t. input value. The model anticipates the value of the unknown parameters for any desirable input. The outcome can be correlated among experimental values found for the same. The degree of proximity for forecasted and experimental evaluation will show the perfect fit of the model, for the particular experiment. The RSM is an optimization method that works on approximation technic. response surface is based on functional parameters that approaches to the problem with design parameters. It states about the size of volume using several analytic or experimental responses. The design of experiments is used for the analysis of experiments by point parameter setting and the least square approach is used for function approximation. This chapter is mainly developed to discuss the mathematical modelling technique using the RSM for AISI D3 and EN-31 Steel.

4.3 Types of Experimental Design

The CCD and Box-Behnken are best experimental strategies for analysis of input variable. Hence, it is important to categorize the parameters and their levels. The input parameter known as factor i.e. regulated by the examiner to change the response. It is also sometimes called independent variables. The components that could affect machining parameters are I_p, T_{on} and T_R. These are important for output conditions or dependent variables called response.

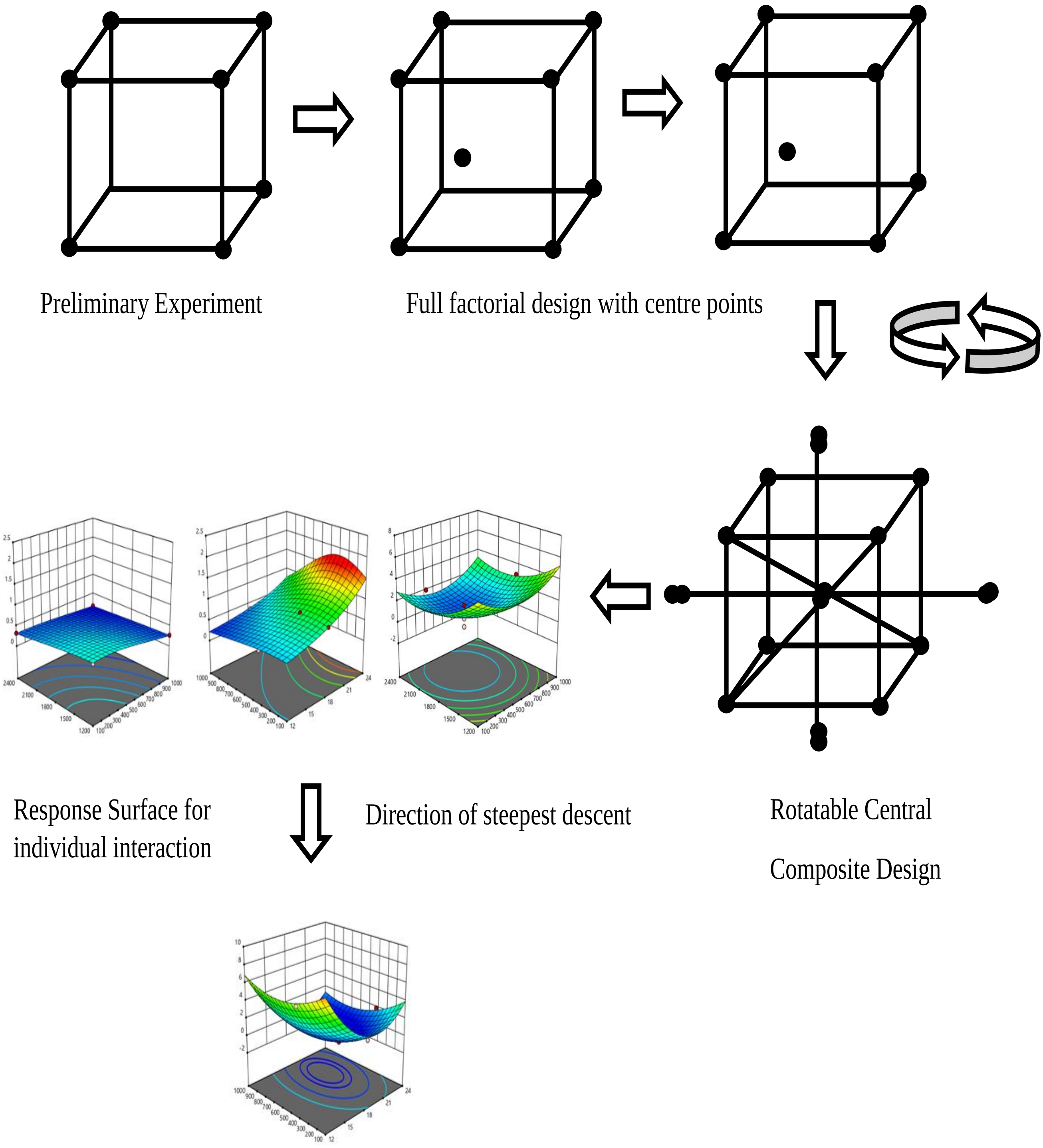

Figure 4.2: Iterative Response Surface Methodology

In the CCD, the input variables like I_p, T_{on} and T_R have referred variables. CCD experiment of RSM has been elected to find the correlation of the response functions and input variables.

It is a factorial design of three-level. The combination of analysis are the midpoints of edges factor and the centre points. The analysis of design points require three levels of each factor. These points are rotatable (or nearly rotatable). The CCD can fit well with quadric response surface models and offers advantages over other response surface designs.

The RSM primarily considered for the interdependency between the variables of the ANOVA analysis. The excellence of fit for this model is identified by the coefficient of determination R^2, adj. R^2 and predicted $R^{2.}$ The CCD and Box-Behnken are the most widespread applications of RSM. The input variables potentially affect the measures of implementation process or quality characteristic. The quality characteristic of performance measure is called response. The field of response methodology consists of an experimental approach for exploring the space of the process or independent variables, parametric statistical modelling to establish an appropriate relationship between the input and output parameters.

The proposal of the examination was carried out in the following manner as indicated in figure 4.3 to establish the parametric correlation and forecast MRR, TWR and R_a.

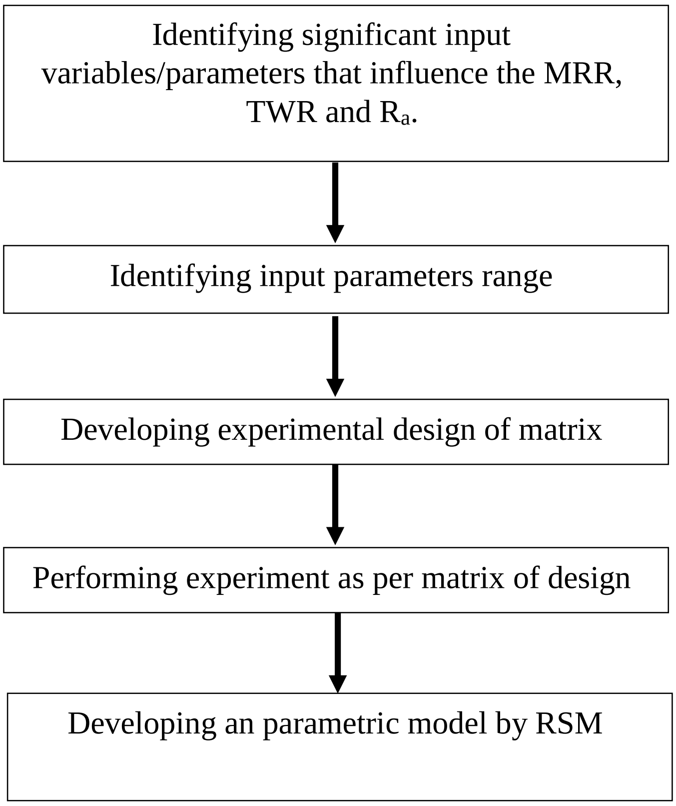

Figure 4.3: The investigation scheme for RSM

4.4 Machining Parameters

The parameters used on the machine are shown in table 4.1 as:

Table 4.1 Machine Parameters

S. No	Machine Parameters	Fixed Value
1	Open circuit voltage	100 V
2	Polarity	Reverse
3	Pulse-off-time	30 µsec
4	Machining time	2 min.
5	Type of di-electric fluid	EDM 30
6	Flushing pressure	0.4 kg/cm^3
7	Workpiece material	AISI D3 and EN-31 steel
8	Tool material	Electrolyte Copper (Dia. 20 mm)

4.5 Design of Experiment for AISI D3 and EN-31 steel

The experimental design (DOE) is designed for the collection of information where dissimilarities present in data. The variation is under the full control of the experimenter or not. However, in statistics, these terms are usually used for controlling the experiments.

- DOE is the most economical and efficient technic for identifying the key input factors and correlating the relationship between input factors and response.
- DOE examines a number of input factors with relatively less number of tests.
- DOE helps to recognize the important/critical characteristics of a process improvement effort.

The important parameters for the MRR, TWR and R_a were identified. They mainly depend on the I_p, T_{on} and T_R. According to the selected process parameters of three factors of three levels, units and notations are done by the central composite design model of response surface methodology as per the data are given in table 4.2

Table 4.2 Input Parameters and their levels

S. No	Input Parameters		Units	Level		
				-1	0	+1
1	Current	I_p	amp	12	18	24
2	Pulse-on-time	T_{on}	µsec	100	400	1000
3	Tool rotation	T_R	rpm	1200	1800	2400

4.5.1 Central Composite Design and Machined Samples of AISI D3 Steel

The AISI D3 Steel samples have been machined as per the central composite design and shown in table 4.3

Table 4.3 CCD table along with performance measures of AISI D-3 steel

Run No.	**Factor Level**			**MRR (gm/min)**	**TWR (gm/min)**	**R_a (μm)**
	I_p	**T_{on}**	**T_R**			
1	24	100	2400	1.14	0.429	1.59
2	18	400	1800	0.83	0.099	1.15
3	12	100	1200	0.598	0.125	6.7
4	18	400	1800	0.83	0.099	1.25
5	12	400	1800	0.5891	0.045	2.45
6	18	400	2400	0.67	0.15	1.4
7	18	400	1800	0.88	0.099	1.25
8	24	400	1800	1.26	0.25	1.1
9	12	1000	1200	0.2923	0.045	4.95
10	18	400	1200	0.928	0.123	4.2
11	24	100	1200	1.56	0.41	4.96
12	18	100	1800	0.792	0.2	2.48
13	18	400	1800	0.83	0.099	1.25
14	12	100	2400	0.27	0.15	5.1
15	18	400	1800	0.83	0.099	1.23
16	18	1000	1800	0.39	0.0039	2.55
17	24	1000	2400	0.6507	0.13	3.59
18	12	1000	2400	0.29	0.062	2.87
19	24	1000	1200	0.714	0.093	6.96
20	18	400	1800	0.85	0.099	1.24

4.5.2 Machined Samples of AISI D3 Steel

Machined samples are arranged as per the design of experiments (20 samples) of AISI D3 with respective parameters, shown in figure 4.4.

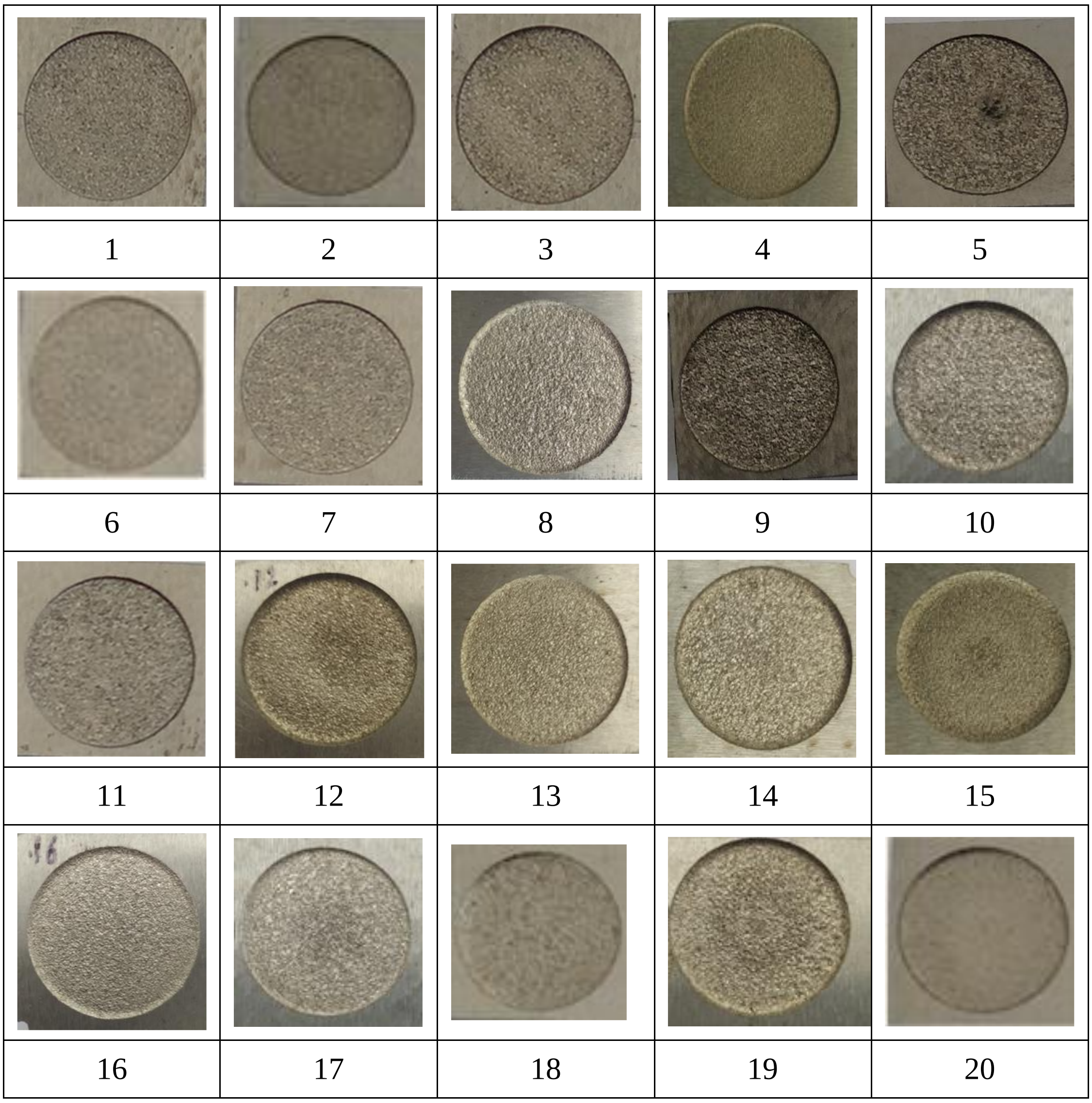

Figure 4.4: AISI D3 steel machined samples

4.5.3 CCD and Machined Samples of EN-31 Steel

The EN-31 Steel samples have been machined as per the central composite design and shown in table 4.4

Table 4.4 CCD table along with performance measures of EN-31 steel

Run No.	**Factor Level**			**MRR (gm/min)**	**TWR (gm/min)**	**R_a (μm)**
	I_p	**T_{on}**	**T_R**			
1	18	400	1200	0.7800	0.064	0.5000
2	12	400	1800	0.4330	0.01	6.45
3	24	1000	2400	0.5100	0.06	2.15
4	18	400	1800	0.6064	0.0847	0.0234
5	24	100	2400	0.4736	0.1847	4.85
6	18	400	1800	0.6064	0.0847	0.0234
7	18	400	1800	0.6064	0.0847	0.0234
8	18	400	1800	0.6064	0.0847	0.0234
9	12	1000	2400	0.1785	0.009	7.08
10	18	400	2400	0.4200	0.004	0.3800
11	12	1000	1200	0.4950	0.0358	8.00
12	18	400	1800	0.6064	0.0847	0.0234
13	18	1000	1800	0.5229	0.132	0.0500
14	18	400	1800	0.6064	0.0847	0.0234
15	18	100	1800	0.6700	0.256	2.05
16	12	100	1200	0.8600	0.1575	9.31
17	24	1000	1200	0.4300	0.078	1.18
18	12	100	2400	0.1590	0.067	8.19
19	24	100	1200	0.7443	0.251	3.90
20	24	400	1800	0.5600	0.1	1.82

4.5.4 Machined Samples of EN-31

Machined samples are arranged as per the design of experiments (20 samples) of EN-31 with respective parameters, shown in figure 4.5.

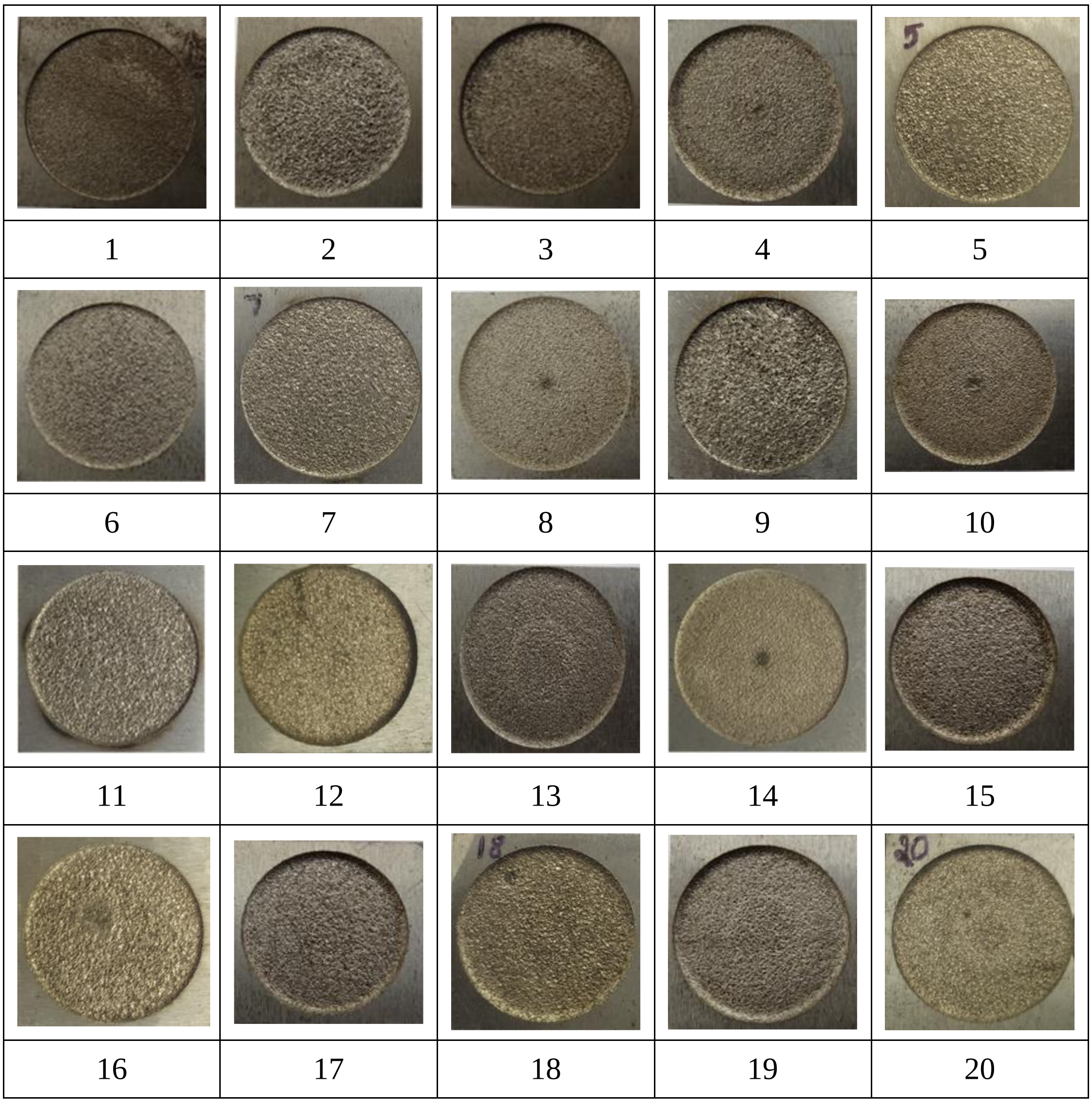

1 2 3 4 5
6 7 8 9 10
11 12 13 14 15
16 17 18 19 20

Figure 4.5: EN-31steel machined samples

CHAPTER 5

RESULT AND DISCUSSION OF AISI D3 STEEL

5.1 Analysis and Discussion of AISI D3 steel

The machining process parameters were investigated by EDM with tool rotation process. The machining parameters I_p, T_{on} and T_R investigated on MRR, TWR and R_a. Appropriate planning and execution of experiments are utmost important for developing clear and authentic findings from the experimental observations. DOE is one of the most valuable strategies to accomplish a relationship between appropriate methods, gathering experimental data and deriving inferences from observations that are subjected to variation. It helps to identify the most important controlling variables of the process and improving the performance of the process by significantly reducing the number of trials to be performed. The optimal set of significant machining parameters were developed. The experimental errors are controlled, the minimization of which will increase the performance of the process. The present investigation uses RSM central composite design of experiment technique, which is simple and cost-effective as it uses a minimum number of experimental runs to understand the effect of various machining process parameters on response variables.

The ANOVA fitted model for MRR, TWR and R_a for AISI-D3 and Electrolyte copper tool is given in table 5.1, 5.2 and 5.3. The tables shows that the model selected for experimentation is significant and also represent the contribution of each parameters.

Table 5.1 ANOVA fitted model for MRR on AISI-D3-Electrolyte copper tool

Source	**SS**	**df**	**MS**	**FV**	**PV**		**% contribution**
Model	1.83	9	0.2031	1211.81	< 0.0001	significant	
I_p-Current	0.9493	1	0.9493	5664.58	< 0.0001		56.93636
T_{on}-Pulse-on Time	0.3667	1	0.3667	2188.33	< 0.0001		21.99364
T_R-Tool Rotation	0.0844	1	0.0844	503.53	< 0.0001		5.062076
I_p T_{on}	0.1196	1	0.1196	713.44	< 0.0001		7.173274
I_p T_R	0.0013	1	0.0013	7.61	0.0202		0.07797
T_{on} T_R	0.0398	1	0.0398	237.54	< 0.0001		2.387093
I_p^2	0.0288	1	0.0288	171.89	< 0.0001		1.727344
T_{on}^2	0.0733	1	0.0733	437.31	< 0.0001		4.396329
T_R^2	0.0024	1	0.0024	14.33	0.0036		0.143945
Residual	0.0017	10	0.0002				0.101961
Lack of Fit	0.0017	5	0.0003				
Pure Error	0.0000	5	0.0000				
Cor Total	1.83	19					
R^2	0. 9551	Adjusted R^2		0.9332	Predicted R^2		0. 9297

Table 5.2 ANOVA fitted model for TWR on AISI-D3-Electrolyte copper tool

Source	**SS**	**df**	**MS**	**FV**	**PV**		**% contribution**
Model	0.2082	9	0.0231	2634.3	< 0.0001	significant	
I_p-Current	0.0679	1	0.0679	7728.2	< 0.0001		35.6972
T_{on}-Pulse-on Time	0.0855	1	0.0855	9731.8	< 0.0001		44.95008
T_R-Tool Rotation	0.0015	1	0.0015	170.24	< 0.0001		0.788598
I_p T_{on}	0.0251	1	0.0251	2854.7	< 0.0001		13.19587
I_p T_R	8.00E-06	1	8.00E-06	0.9109	0.3624		0.004206
T_{on} T_R	2.82E-06	1	2.82E-06	0.3208	0.5836		0.001481
I_p^2	0.0053	1	0.0053	604.95	< 0.0001		2.786379
T_{on}^2	0.0018	1	0.0018	205.73	< 0.0001		0.946318
T_R^2	0.003	1	0.003	340.05	< 0.0001		1.577196
Residual	0.0001	10	8.78E-06				0.052573
Lack of Fit	0.0001	5	0				
Pure Error	0	5	0				
Cor Total	0.2083	19					
R^2	0.9463	Adjusted R^2		0.9192	Predicted R^2		0.9176

Table 5.3 ANOVA fitted model for R_a on AISI-D3-Electrolyte copper tool

Source	SS	df	MS	FV	PV		% contribution
Model	70.7	9	7.86	2057.3	< 0.0001	significant	
I_p-Current	1.02	1	1.02	267.38	< 0.0001		2.615364
T_{on}-Pulse-on Time	4E-04	1	4E-04	0.0943	0.7651		0.001026
T_R-Tool Rotation	16.94	1	16.94	4435.9	< 0.0001		43.43556
I_p T_{on}	8.17	1	8.17	2138.8	< 0.0001		20.94856
I_p T_R	1.17	1	1.17	306.55	< 0.0001		2.999977
T_{on} T_R	0.029	1	0.029	7.5	0.0209		0.073333
I_p^2	0.923	1	0.923	241.76	< 0.0001		2.366905
T_{on}^2	4.53	1	4.53	1185.4	< 0.0001		11.6153
T_R^2	6.18	1	6.18	1619.2	< 0.0001		15.84603
Residual	0.038	10	0.004				0.097948
Lack of Fit	0.032	5	0.006	4.68	0.0577	not significant	
Pure Error	0.007	5	0.001				
Cor Total	70.73	19					
R^2	0.9318	Adjusted R^2		0.9260		Predicted R^2	0.9188

*** SS = Sum of Squares, MS = Mean Square, FV = F-value, PV = p-value**

5.2 Mathematical Model and Diagnostic

5.2.1 The Mathematical model expressing the response variables and process parameters which were developed for minimizing the number of experiments of tool rotation EDM. The developed mathematical model for AISI D3 Steel responses through analysis of regression using Design Expert CCD are given below:

$$
\begin{aligned}
MRR = 0.442131 &- (0.019913 * Ip) + (0.000928 * Ton) + (0.000063 * TR) \\
&- (0.000045 * Ip * Ton) - \{(3.50694 * 10^{-6})Ip * TR)\} \\
&+ \{(2.58406 * 10^{-7}) * Ton * TR\} + (0.002843 * Ip^{2}) \\
&- \{(9.20673 * 10^{-7}) * Ton^{2}\} - \{(8.20960 * 10^{-8}) * TR^{2}\}
\end{aligned}
\tag{5.1}
$$

$$
\begin{aligned}
TWR = 0.434873 &- (0.019407 * Ip) + (8.58052 * 10^{-6} * Ton) \\
&- (0.000313 * TR) - (0.000021 * Ip * Ton) \\
&+ \{(2.77778 * 10^{-7}) * Ip * TR\} - \{(2.17391 * 10^{-9}) * Ton * TR\} \\
&+ (0.001221 * Ip^{2}) + \{(1.44562 * 10^{-7}) * Ton^{2}\} \\
&+ \{(9.15404 * 10^{-8}) * TR^{2}\}
\end{aligned}
\tag{5.2}
$$

$$
\begin{aligned}
Ra = 26.81431 &- (0.645070 * Ip) - (0.014213 * Ton) - (0.015135 * TR) \\
&+ (0.000370 * Ip * Ton) - (0.000106 * Ip * TR) \\
&- \{(2.19203 * 10^{-7}) * Ton * TR\} + (0.016093 * Ip^{2}) \\
&+ \{(7.23535 * 10^{-6}) * Ton^{2}\} + \{(4.16490 * 10^{-6}) * TR^{2}\}
\end{aligned}
\tag{5.3}
$$

5.2.2 Diagnostics of Predicted and Actual Parameters

The predicted and actual values have been diagnosed through the regression analysis. The residual of predicted and actual values are in good agreement. The predicted and actual values are given in the table 5.4

Table 5.4 Predicted and actual values of AISI D3 Steel for MRR, TWR and R_a

Run No.	MRR		TWR		R_a	
	Actual Value	Predicted Value	Actual Value	Predicted Value	Actual Value	Predicted Value
1	1.14	1.12	0.429	0.4172	1.59	1.63
2	0.83	0.8262	0.099	0.1008	1.15	1.2
3	0.598	0.5804	0.125	0.1156	6.7	6.76
4	0.83	0.8262	0.099	0.1008	1.25	1.2
5	0.5891	0.5793	0.045	0.0437	2.45	2.44
6	0.67	0.6813	0.15	0.1462	1.4	1.42
7	0.88	0.8262	0.099	0.1008	1.25	1.2
8	1.26	1.28	0.25	0.2458	1.1	1.13
9	0.2923	0.2996	0.045	0.0426	4.95	4.9
10	0.928	0.912	0.123	0.1213	4.2	3.99
11	1.56	1.47	0.41	0.3895	4.96	4.89
12	0.792	0.7882	0.2	0.1885	2.48	2.5
13	0.83	0.8262	0.099	0.1008	1.25	1.2
14	0.27	0.2819	0.15	0.1393	5.1	5.04
15	0.83	0.8262	0.099	0.1008	1.23	1.2
16	0.39	0.4052	0.0039	0.0036	2.55	2.52
17	0.6507	0.631	0.13	0.1204	3.59	3.53
18	0.29	0.2802	0.062	0.0639	2.87	2.93
19	0.714	0.7009	0.093	0.095	6.96	7.02
20	0.85	0.8262	0.099	0.1008	1.24	1.2

5.3 ANOVA Significant Factors on Responses

The ANOVA significant factors on MRR, TWR and R_a are as:

5.3.1 Material Removal Rate

Table 4.3 (in the last chapter) represents CCD as well as performance measure on every experiment. The collection and analysis of experimental data to set up significance for several parametric responses using statistical analysis “ANOVA” at a significant level of 0.05 performed. Table 5.1 represents statistical analysis for MRR having percentage of participation for every variable along with their dominance. The parameters such as I_p, T_{on} and T_R, their square terms and inter-relationship terms: $I_p \times T_{on}$, I_p x T_R and T_{on} x T_R. The I_p is more dominant variable for MRR with 56.93 % contribution, followed by T_{on} 22 % and T_R 5.06 % respectively. This shows the model is significant with F-value of 1211.81. This indicates the model is significant because P-values is less than 0.0500. In this case, model terms I_p, T_{on}, T_R, I_p T_{on}, T_R T_{on}, I_p^2, T_{on}^2 and T_R^2 are significant. If values greater than 0.1000 shows model terms are not significant. The determination coefficient (R^2), adjusted (R^2) and Predicted (R^2) values are identified as 95.51 %, 93.32 % and 92.97 % respectively.

5.3.2 Tool Wear Rate

The TWR ANOVA table 5.2 represents the percentage of participation for every variable along with the relationship. I_p, T_{on} and T_R; their squares and correlation term: $I_p \times T_{on}$, I_p x T_R and T_{on} x T_R are important terms. It represents that T_{on} is considered to the more dominant parameter for TWR having a percentage of participation of 44.95 % succeeded by I_p and T_R having percentage participation of 35.7 %, 0.8 % respectively. This shows the model is significant with F-value of 2634.3. This indicates the model is significant because P-values **is** less than 0.0500. In this case, model terms I_p, T_{on}, T_R, $I_p T_{on}$, I_p^2, T_{on}^2 and T_R^2 are significant. Values greater than 0.1000 shows model terms are not significant. Coefficient of R^2, adj. R^2 and predicted (R^2) values are obtained 94.63 %, 91.92 %, 91.76 % respectively.

5.3.3 Surface Roughness

The ANOVA table 5.3 for R_a having participation percentage for every variable with their dominance. The I_p, T_{on} and T_R, their square-terms and interrelation terms: $I_p \times T_{on}$, I_p x T_R and T_{on} x T_R are important terms. It represents that T_R is considered to the stronger parameter for R_a having the greatest percentage of participation of 43.43 % succeeded by I_p having percentage of participation of 2.6 %. The T_{on} is considered to inconsequential process parameters for R_a. Model F-value of 2057.3 implies the model is significant. There is only a 0.01 % chance that an F-value could large occur due to noise. P-values (Values of "Prob > F") less than 0.0500 represents model terms are considerable. In this case model terms I_p, T_R, $I_p T_{on}$, $I_p T_R$, I_p^2, T_{on}^2 and T_R^2 are significant. The values are higher than 0.1000 means the model terms are not significant. The coefficient of R^2, adj. R^2 and Predicted (R^2) terms are obtained 93.18 %, 92.60 %, 91.88 % respectively.

5.4 Effect of Factors on Responses

The impact of input variables on MRR, TWR and R_a have been studied as:

5.4.1 Effect of Tool Rotation

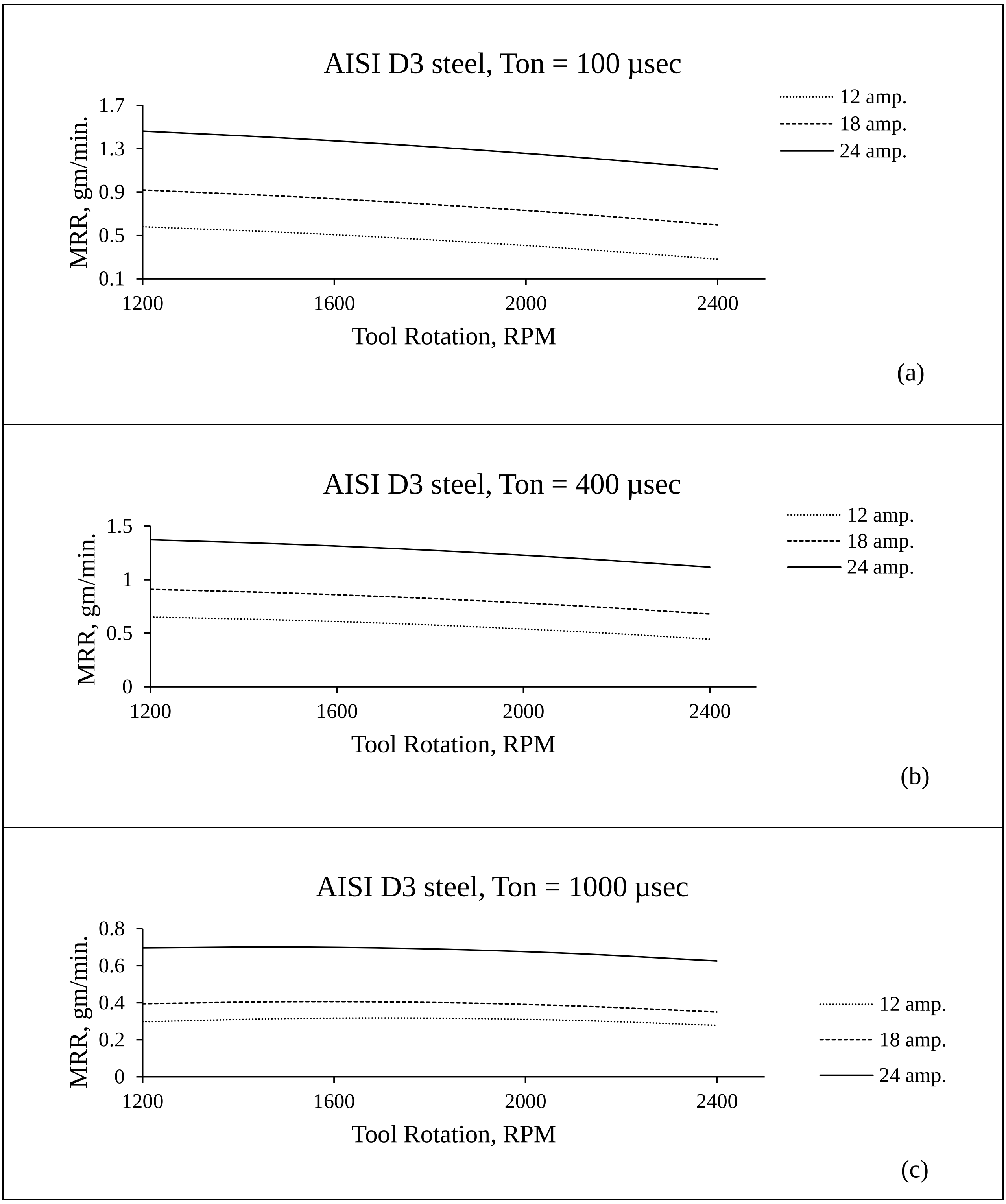

Figure 5.1: Effect of tool rotation on MRR at 100, 400 and 1000 µsec

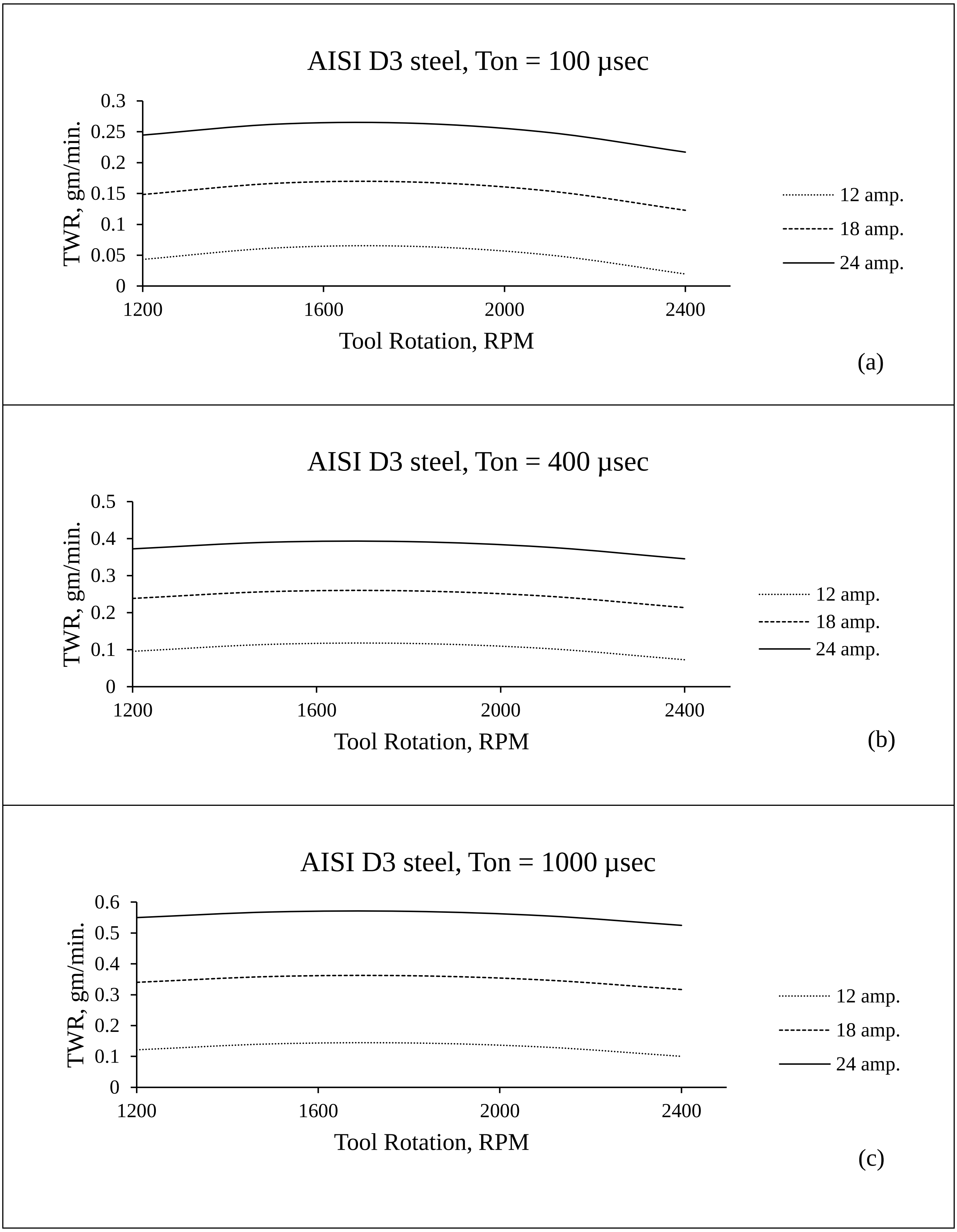

Figure 5.2: Effect of tool rotation on TWR at 100, 400 and 1000 µsec

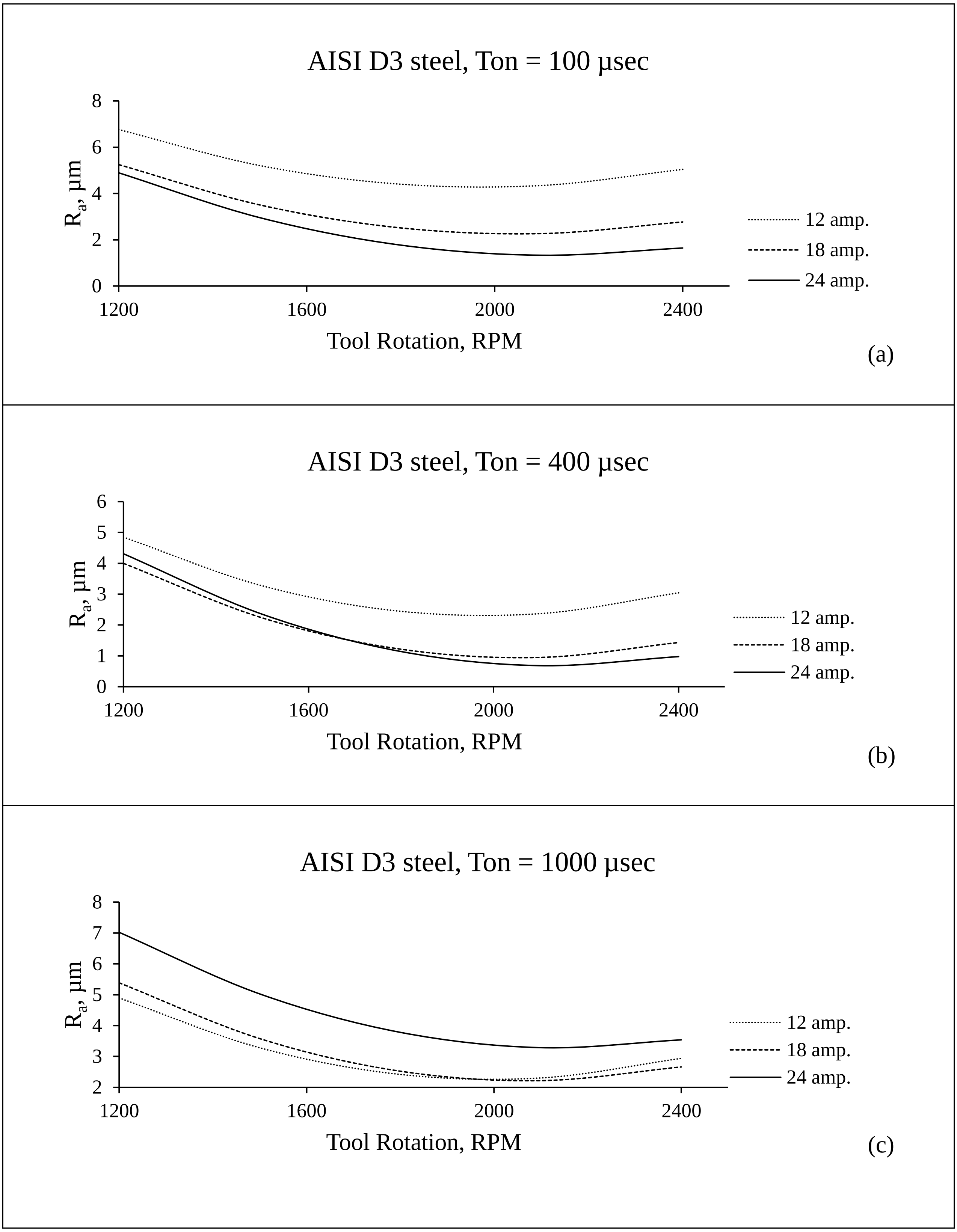

Figure 5.3: Effect of tool rotation on R_a at 100, 400 and 1000 µsec

Figure 5.1 (a-c) shows the plot between MRR and T_R on 100, 400 and 1000 T_{on}. It shows that MRR increases as I_p increases from 12 amp. to 24 amp. The figure clearly shows that MRR decreases for higher values of T_R, due to the thermal effect on the workpiece through IEG decreases.

Figure 5.2 (a-c) shows plot between TWR and T_R on 100, 400 and 1000 T_{on}. It shows that TWR increases as T_R increases from 1200 rpm to 1800 rpm and than it starts decreasing from 1800 to 2400 rpm for all value of currents. At the highest T_R the TWR is 0.099 gm/min. at 400 μsec. The TWR is higher for high value of currents, due to the availability of high discharge energy.

Figure 5.3 (a-c) shows plot between R_a and T_R on 100, 400 and 1000 T_{on}. It shows that the value of R_a decreases as T_R increases upto a certain value and than it starts increasing for all value of currents. The distribution of pulse discharge energy throughout was uniform. Further increment in T_R deteriorates the thermic effect significantly. The flow rate dielectric fluid increases due to the whirling effect. The spark produced move towards the outskirt of whirling. This increases flushing between workpiece and tool, but at higher rpm thermic effect significantly decrease.

5.4.2 Effect of Current

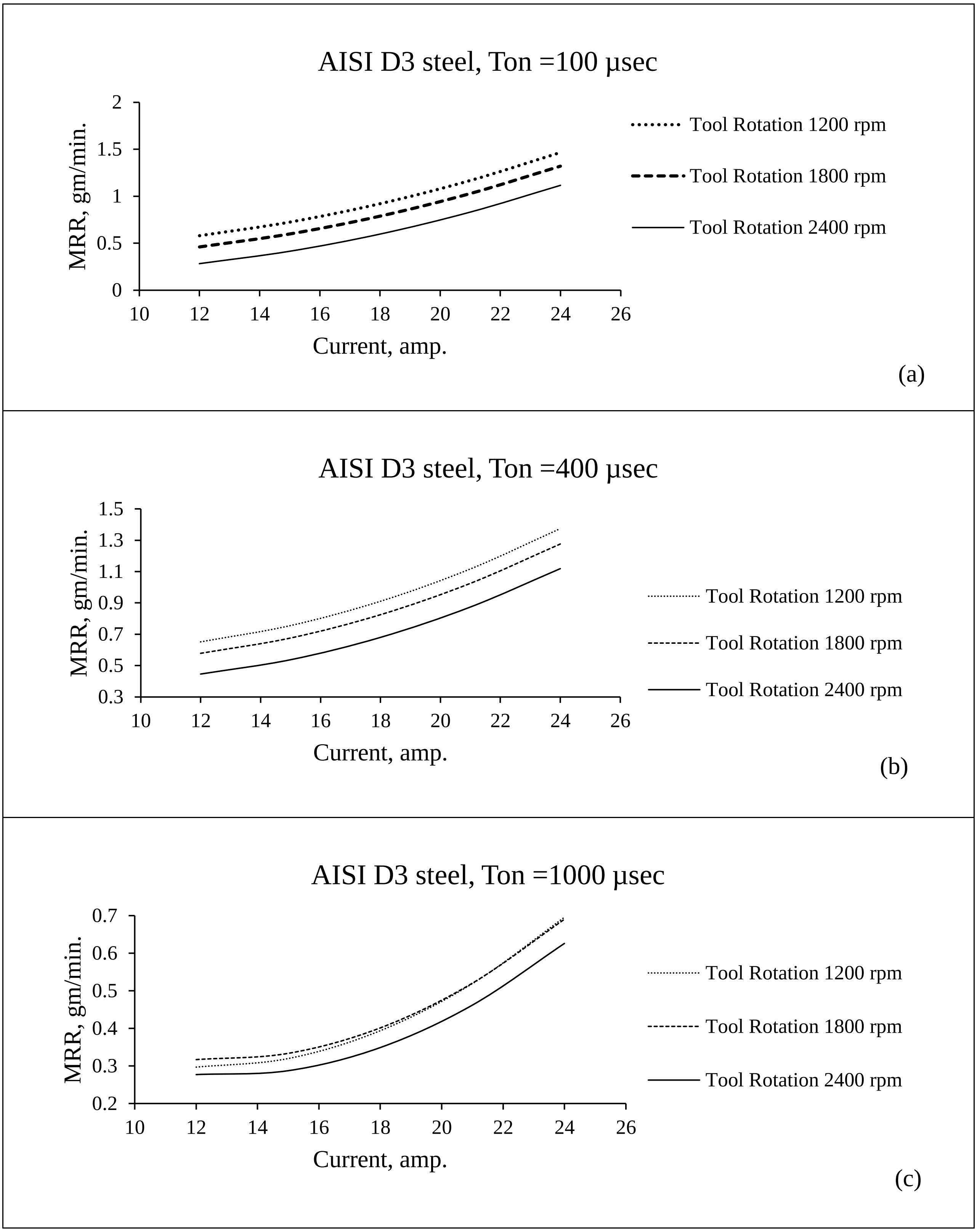

Figure 5.4: Effect of Current on MRR at 100, 400 and 1000 µsec

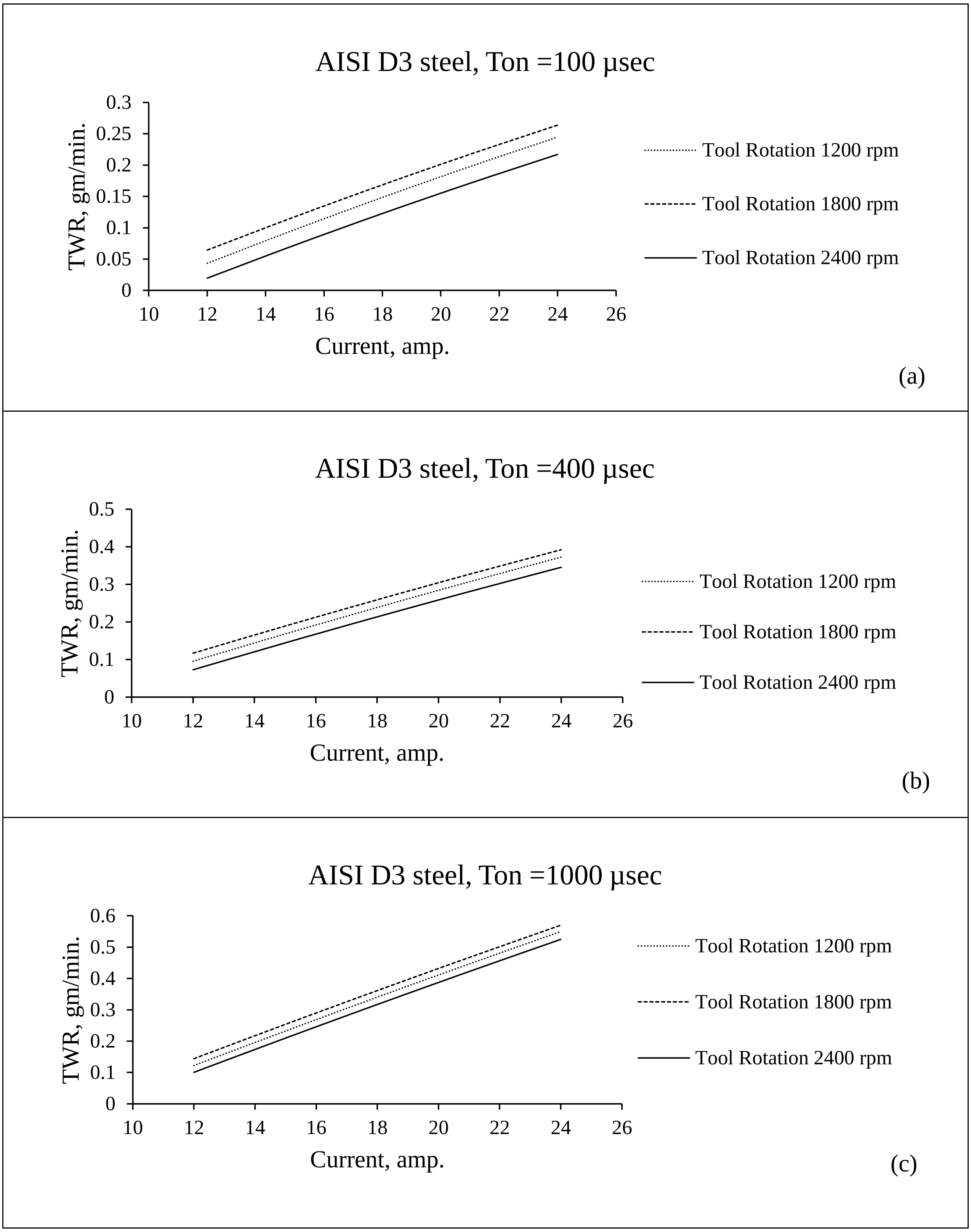

Figure 5.5: Effect of Current on TWR at 100, 400 and 1000 µsec

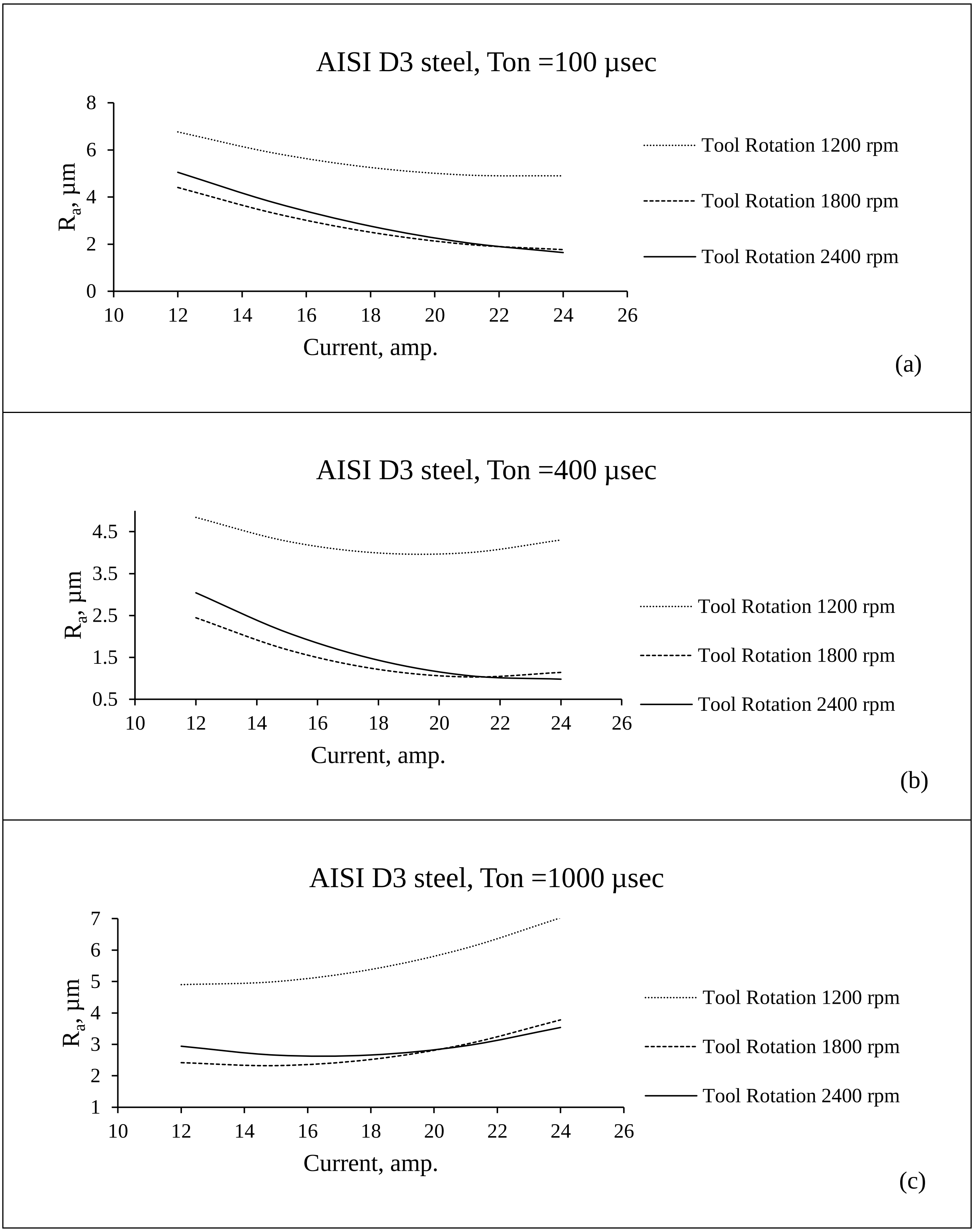

Figure 5.6: Effect of current on R_a at 100, 400 and 1000 µsec

Figure 5.4 (a-c) shows the plot between MRR and I_p on 100, 400 and 1000 T_{on}. It shows that MRR increases as I_p increases (12 amp. to 24 amp.). The figure clearly shows that MRR decreases as tool rotation increases.

Figure 5.5 (a-c) shows the plot between TWR and I_p on 100, 400 and 1000 µsec T_{on}. It shows that TWR increase as T_{on} increases form 100 µsec to 1000 µsec for all value of currents. TWR is higher for low value of $T_{R.}$

Figure 5.6 (a-c) shows plot between R_a and I_p on 100, 400 and 1000 T_{on}. . It shows that the value of R_a decreases as T_R increases upto a certain value and than it starts increasing for all value of currents.

The concentric effect of heat is decreased by increase in T_R w.r.t. I_p. While it enhances the removal of tinny particles produced during machining in ionization zone of both electrodes. Due to high amount of heat, more melting will take place that results white cast layers.

5.4.3 Effect of Pulse-on-Time

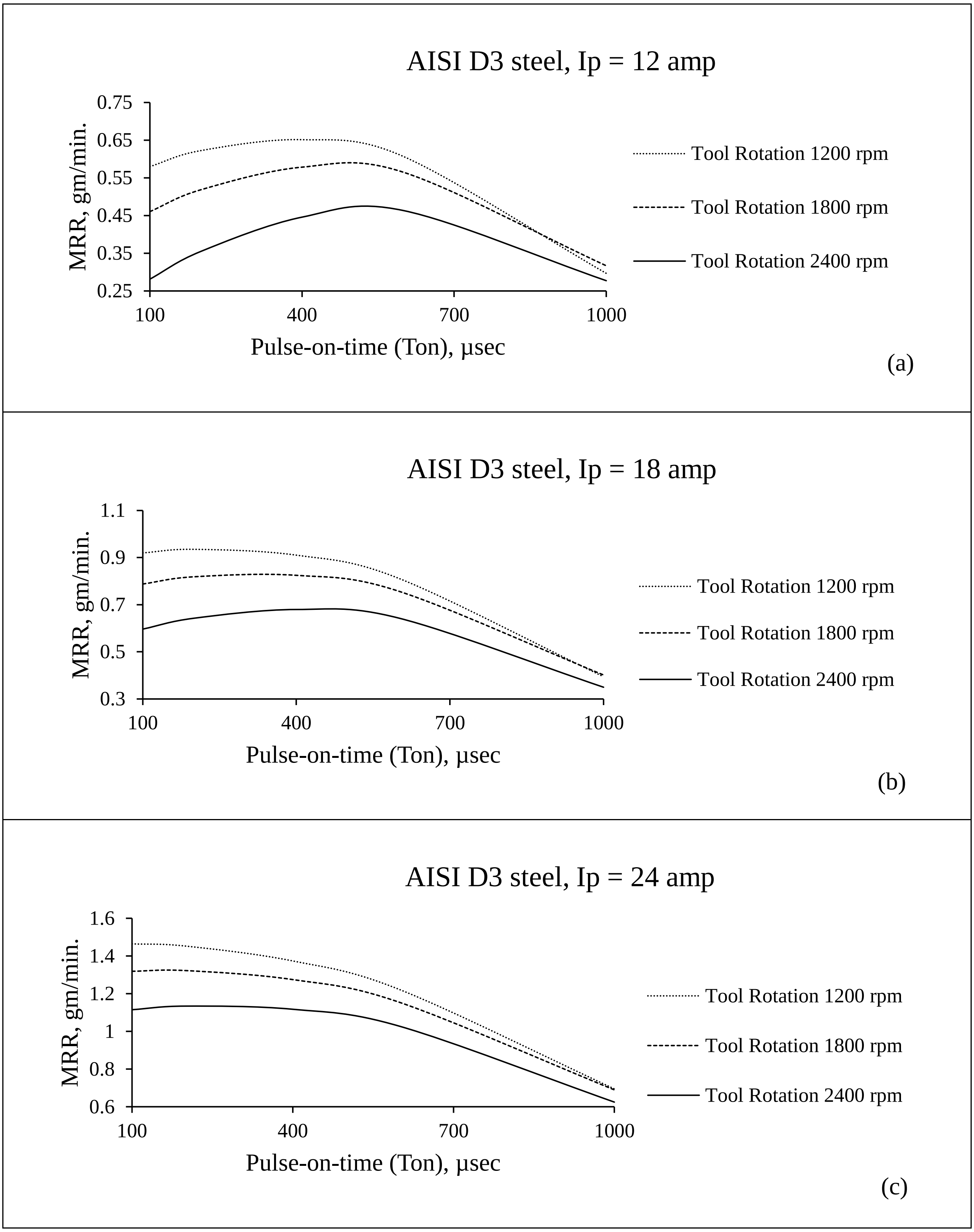

Figure 5.7: Effect of pulse-on-time on MRR at 100, 400 and 1000 µsec

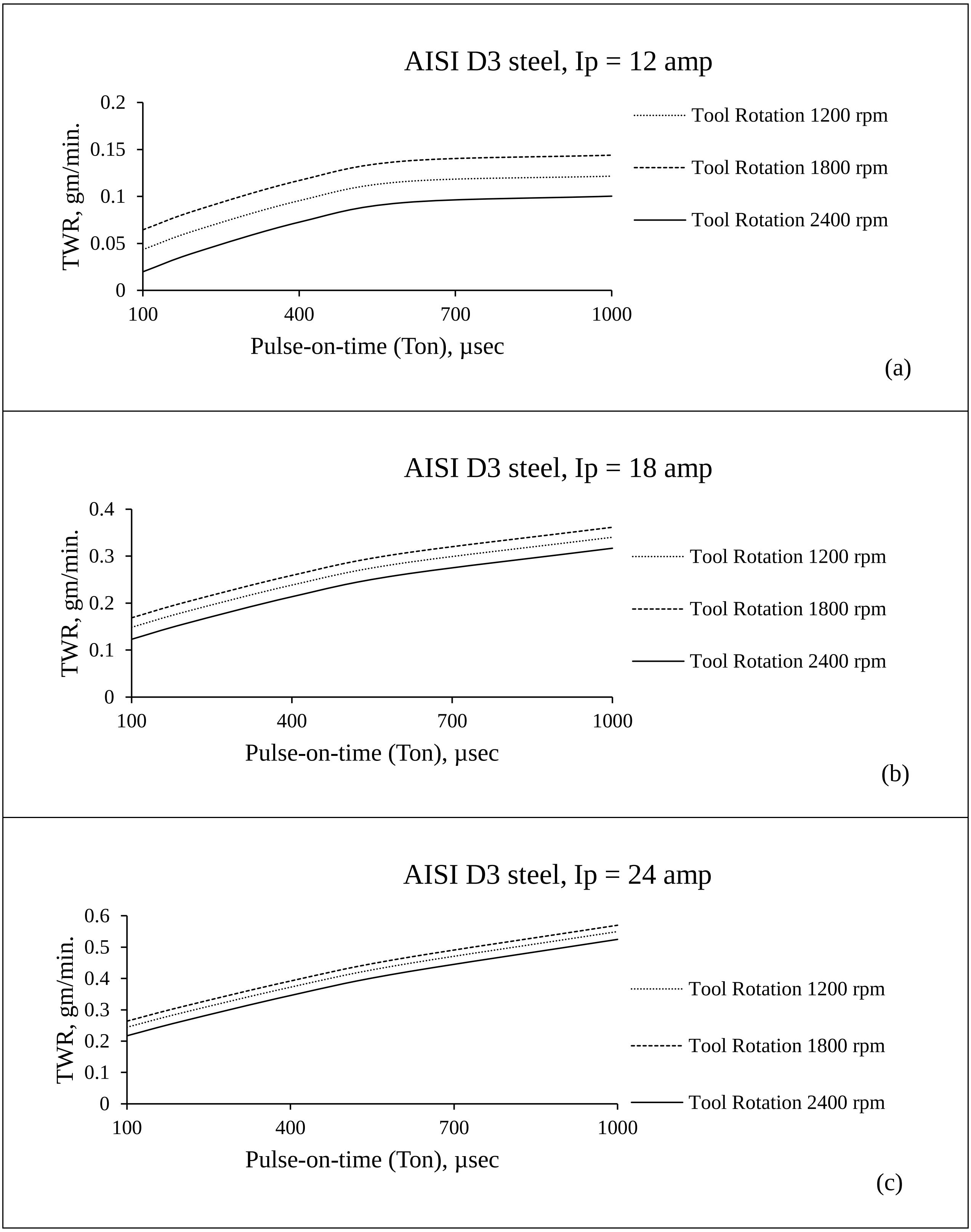

Figure 5.8: Effect of pulse-on-time on TWR at 100, 400 and 1000 µsec

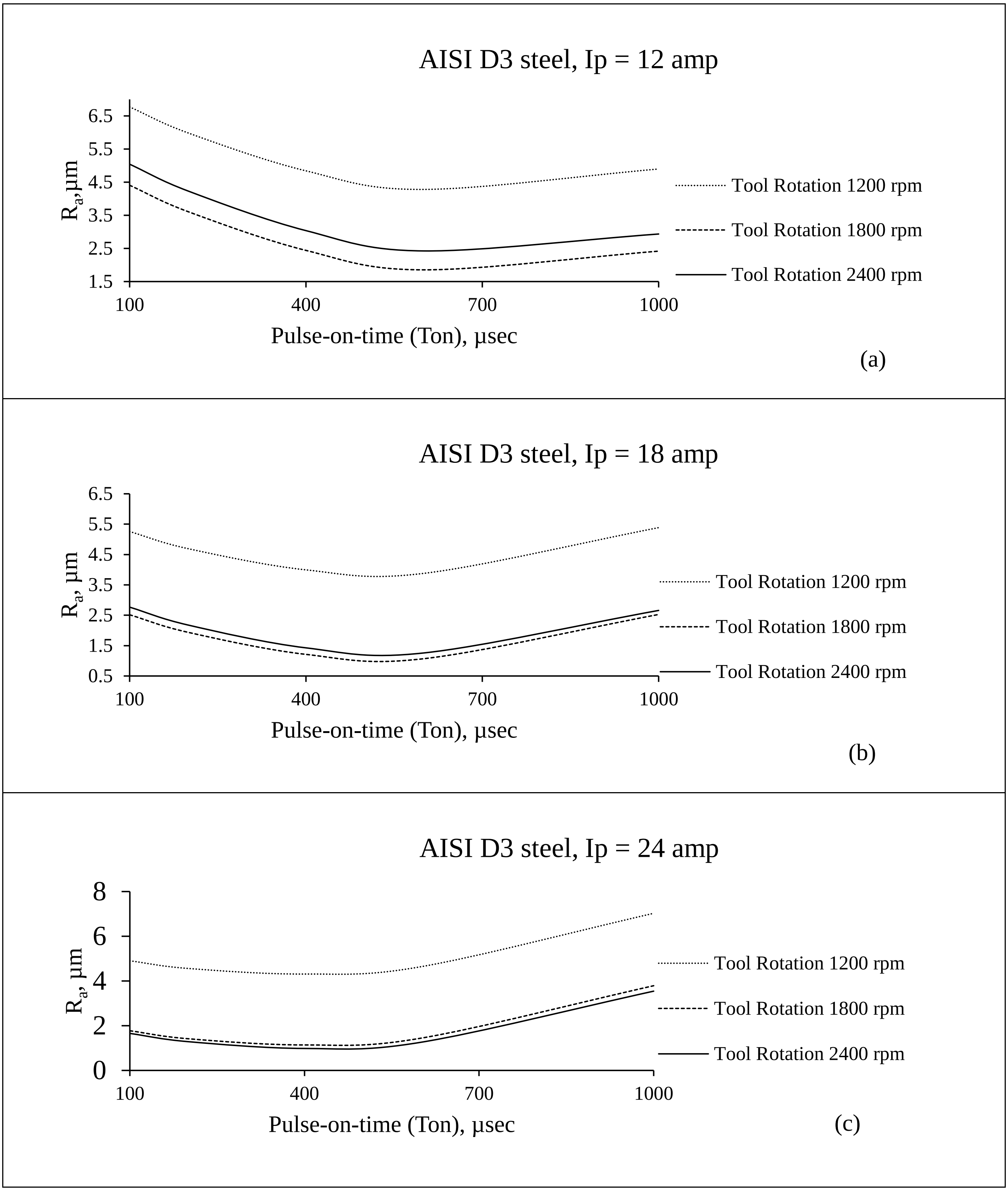

Figure 5.9: Effect of pulse-on-time on R_a at 100, 400 and 1000 µsec

Figure 5.7 (a-c) shows an interaction plot between MRR and T_{on} for 12, 18 and 24 amp. I_p. It shows that MRR increases as I_p increases from 12 amp. to 24 amp. MRR increases as T_{on} increases upto to a particular value and then decreases for all values of I_p.

Figure 5.8 (a-c) shows an plot between TWR and T_{on} for 12, 18 and 24 amp I_p. It shows that TWR increases as T_{on} increases for all value of currents. This can be easily identified form figures of TWR lower for higher values of T_R.

Figure 5.9 (a-c) shows interaction plot between R_a and T_{on} for 12, 18 and 24 amp $I_{p.}$ It represents that the R_a value decreases upto the certain value of T_{on} and then increases for all values of T_R.

The results of effective concentration of spark is the rough surfaces. The surface finish is enhanced by providing the effect of T_R. This facilates the removal of debries as well as reduces the recast layers and prevent from thermal stresses.

5.5 Interaction Plots Analysis

The interaction plot for MRR, TWR and R_a of AISI D3 steel is as:

(i) Material Removal Rate

Figure 5.10 (a) shows interaction plot of MRR w.r.t. I_p (12 amp. to 24 amp.) and T_{on} (100 µsec to 1000 µsec indicated in black and red colour lines respectively). The figure clearly shows that MRR increases as the increase in I_p for all values of current, at current 12 amp., the figure clearly indicates that, MRR is less than 0.5 gm/min., but as the current increase from 12 amp. to 24 amp. the rate of MRR slightly higher, due to increase in T_{on} i.e. I_p duration is high that reveals the high amount of discharge energy. The optimal MRR obtained at 18 amp. current. Figure 5.10 (b) indicates that the effect of pulse duration decreased due to the T_R. It provides uniform distribution of discharge energy. Figure 5.10 (c) shows that MRR initially increases from 100 µsec to 400 µsec but after that, it decreases. The optimal T_{on} is 400 µsec**.**

(ii) Tool Wear Rate

Figure 5.11 represents plot for variation of TWR. The figure represents, TWR rise as current rise for particular value of T_{on}. This rise in TWR is lower at contants tool rotation. While the value of TWR decreased for all value of T_{on} w.r.t. T_R. But due to polarity, the tool wear rate is less. The effect of current significantly reduced by tool rotation.

(iii) Surface Roughness

Figure 5.12 represents that R_a initially decreases but after a point it enhances as I_p w.r.t.T_{on} increases. This effect was decreased as T_R increases. Due to the whirling effect, the distribution of discharge energy is uniform. The interaction plot has been taken at parametric conditions as A: I_p = 18 amp., B: T_{on} = 400 µsec and C: T_R = 1800 rpm

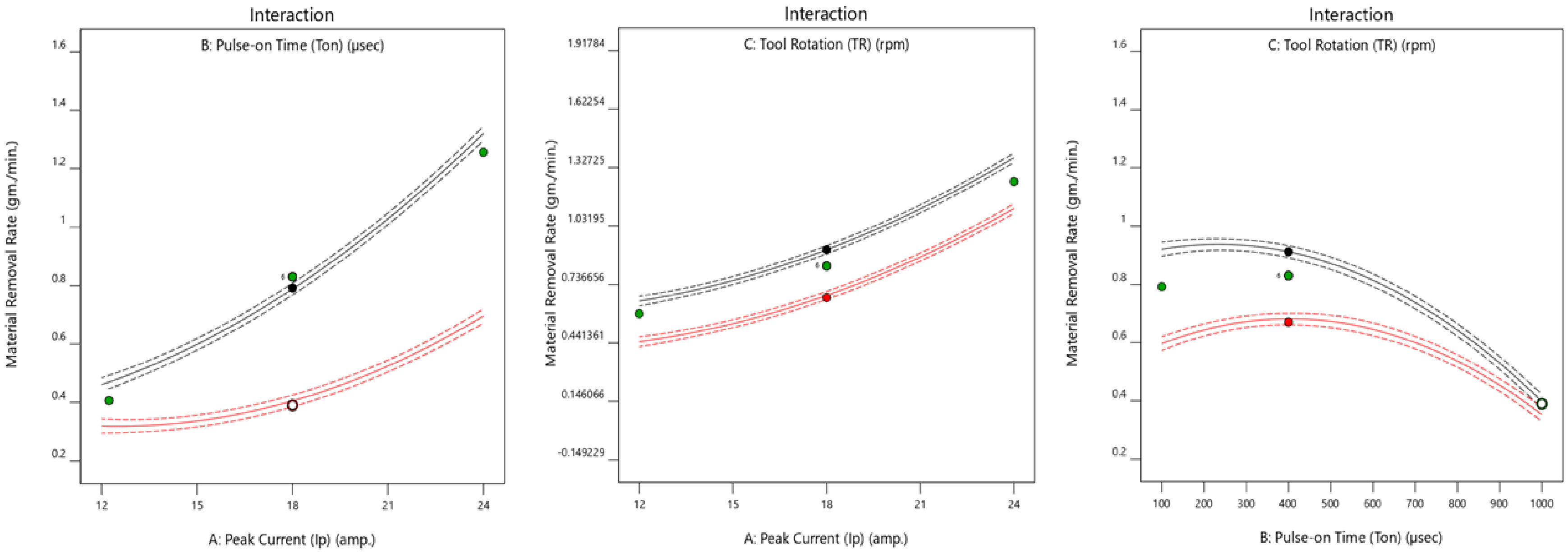

(a) Interaction plot of AB

(b) Interaction plot of AC

(c) Interaction plot of BC

Figure 5.10: Interaction plot of AB, AC and BC for MRR. The actual factor A: I_p = 18 amp., B: T_{on} = 400 μsec and C: T_R = 1800 rpm

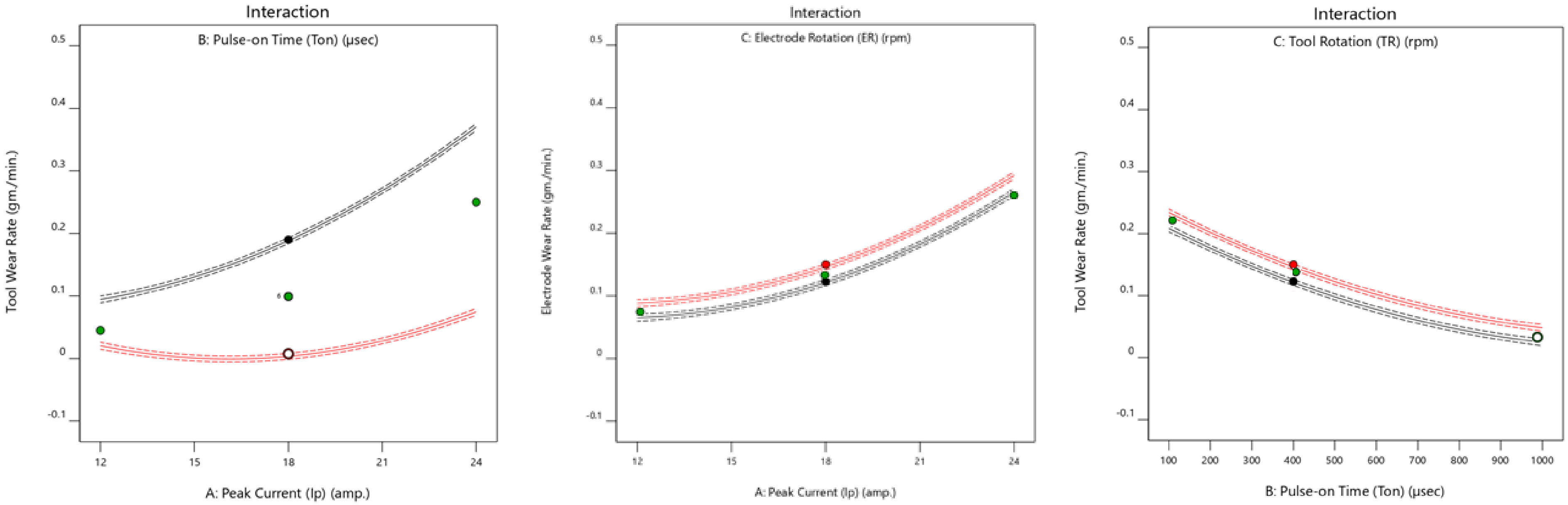

Interaction plot of AB

Interaction plot of AC

Interaction plot of BC

Figure 5.11: Interaction plot of AB, AC and BC for TWR. The actual factor A: I_p = 18 amp., B: T_{on} = 400 μsec and C: T_R = 1800 rpm

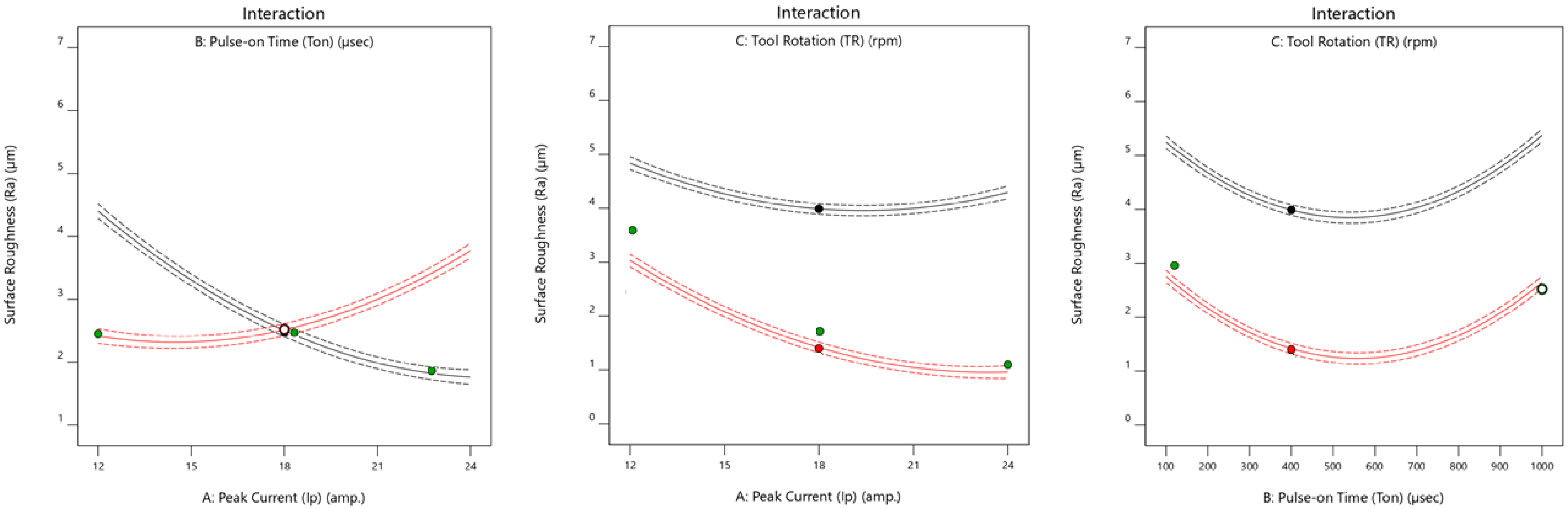

(a) Interaction plot of AB

(b) Interaction plot of AC

(c) Interaction plot of BC

Figure 5.12: Interaction plot of AB, AC and BC for Surface Roughness (R_a). The actual factor A: I_p = 18 amp., B: T_{on} = 400 µsec and C: T_R = 1800 rpm

5.6 Influence of Input Parameters on Responses by 2D Contour and 3D Surface Interaction plot

The Input Parameters Influence on Responses by 3D surface interaction plot is as:

(i) Material Removal Rate

Figure 5.13 (a-b) represents 2D contour-plot and 3D-surface-plot for change in MRR by I_p and T_{on}. This represents that MRR increases along with I_p for all terms of current. The discharge energy gets affected linearly by current along with T_{on} duration which results in more crater dimension i.e. high MRR. The design points and predicted points are laying on the 3D-surface plot between blue to red colour. The blue, green and red colour represents the low, optimum and high value of MRR. The actual parameters of MRR at I_p, T_{on} and T_R were 18 amp, 400 μsec and 1800 rpm represented in figures. Figure 5.13 (c-d) indicate the 2D contour and 3D- surface plot for varying MRR along with I_p, T_R. The MRR increases as I_p for all values of current. It represents MRR increases as increase of I_p. The maximum MRR aat high I_p and low T_R. At high I_p and T_R, MRR slightly decreased. The design points and predicted points are laying on the 3D-surface plot between blue to red colour. Figure 5.13 (e-f) represents the 3D-surface plot for varying MRR with T_{on} and T_R. The design points for all interactions are laying on the surfaces. The design points range are 0.27 to 1.46.

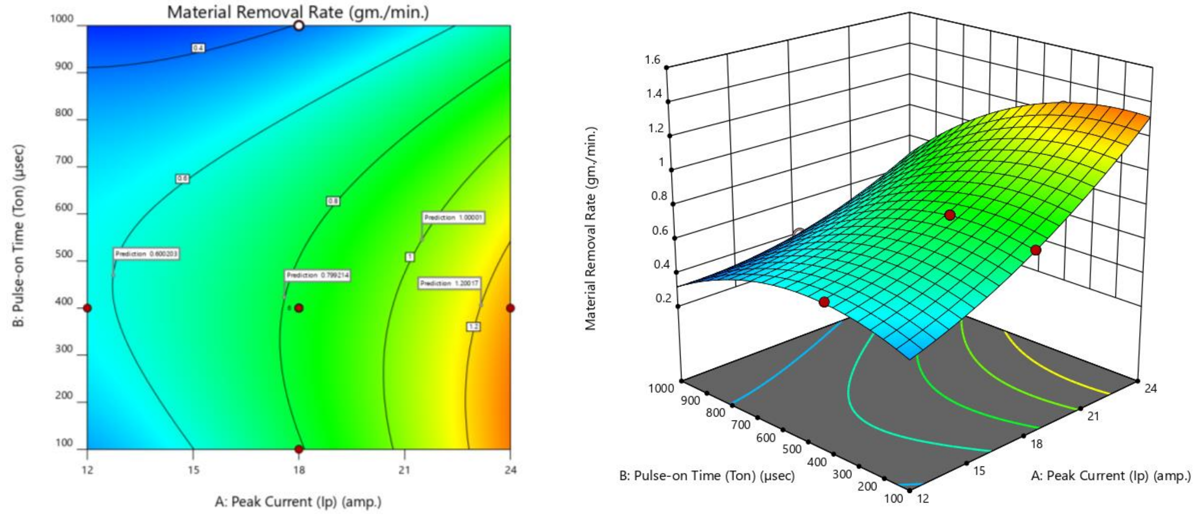

(a) 2-D Contour Plot of AB (b) 3-D Surface interaction Plot of AB

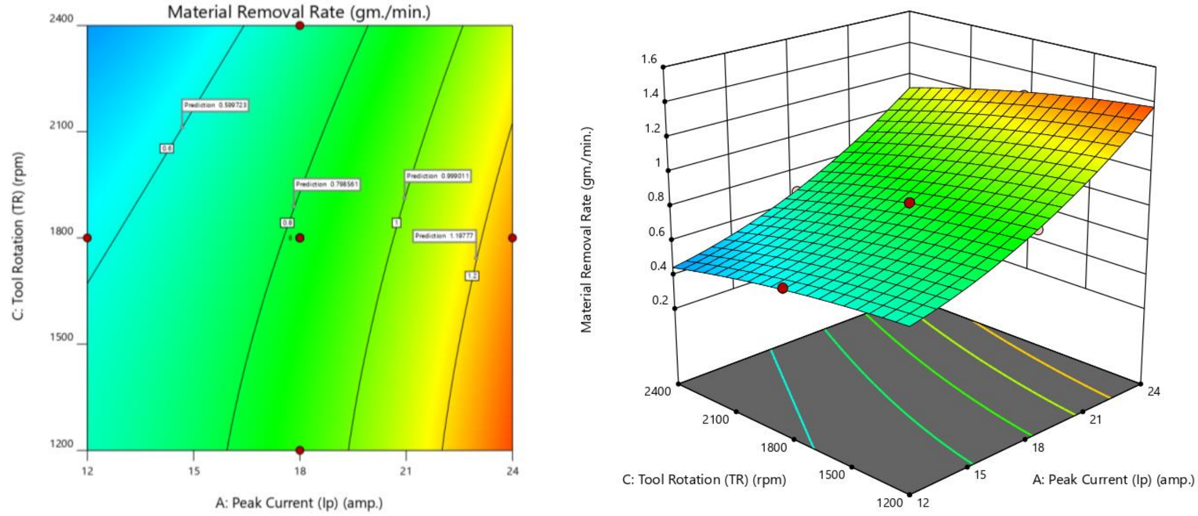

(c) 2-D Contour Plot of AC (d) 3-D Surface interaction Plot of AC

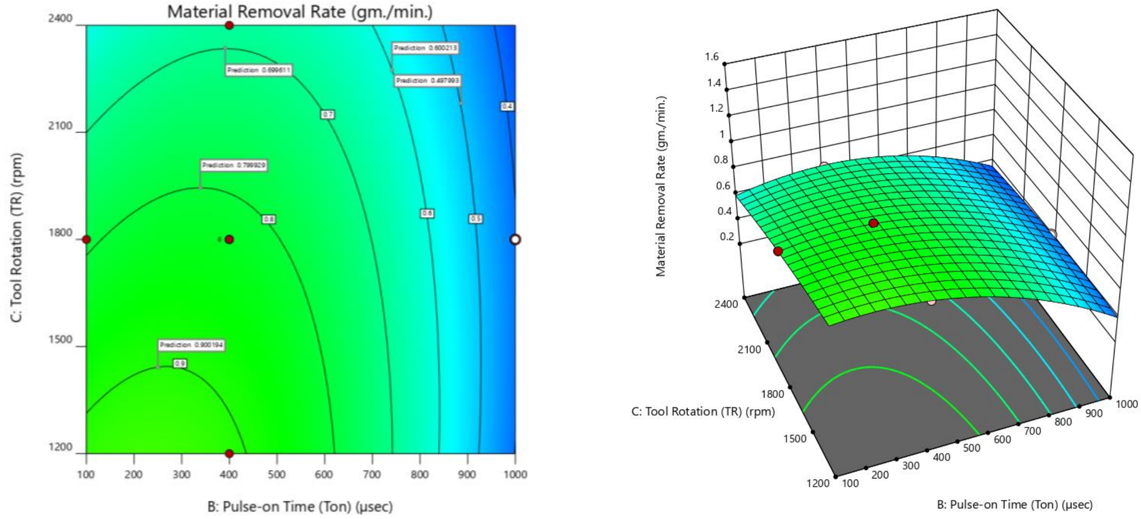

(e) 2-D Contour Plot of BC (f) 3-D Surface interaction Plot of BC

Figure 5.13: 2-D Contour and 3-D Surface plot with interaction AB, AC and BC for MRR.

The actual factor A: I_p = 18 amp., B: T_{on} = 400 µsec and C: T_R = 1800 rpm

(ii) Tool Wear Rate

TWR is extensive machining characteristic in EDM with tool rotation method using the copper electrode, it exactly causes the machining cost of the operation. The carbon particles from the dielectric fluid may be deposited on the surface of the tool, which protects further erosion of the tool. If the I_p increased, the TWR also increased but relatively small with high-speed T_R, due to the uniform distribution of discharge energy. The response graph for TWR with the interaction of I_p, T_{on} and T_R are shown in Figure 5.14.

Figure 5.14 (a-b) shows the 2D contour and 3D surface plot for TWR w.r.t. I_p and T_{on}. The TWR increase as an increase in I_p that increases arc energy, which results to increase in melting metal quantity from both electrodes thereby increase of TWR. This represents, that TWR increases along with T_{on}, but this effect is minimized by T_R. This is because reduced in arc/spark energy density in IEG as diameter of plasma channel broaden with an increase in T_{on}. This expansion is enhanced by T_R. The formation of the carbonic layer on the tip of tool that increases in wear resistance of tool and reducing TWR. The actual parameters of TWR at I_p, T_{on} and T_R were 18 amp, 400 µsec and 1800 rpm represented in figures. Figure 5.14 (c-d) the 2D contour and 3D surface plot of TWR with I_p, T_R, it is found that increase in TWR is less as increase in I_p due to the uniform distribution of discharge energy by T_R. Similarly, Figure 5.14 (e-f) the 2D contour and 3D surface graph of TWR with T_{on} and T_R, it is identified that TWR decreased slightly as increase in T_{on} due to expansion in the plasma channel. The design points for all interactions are laying on the surfaces. The design points range are 0.0075 to 0.415.

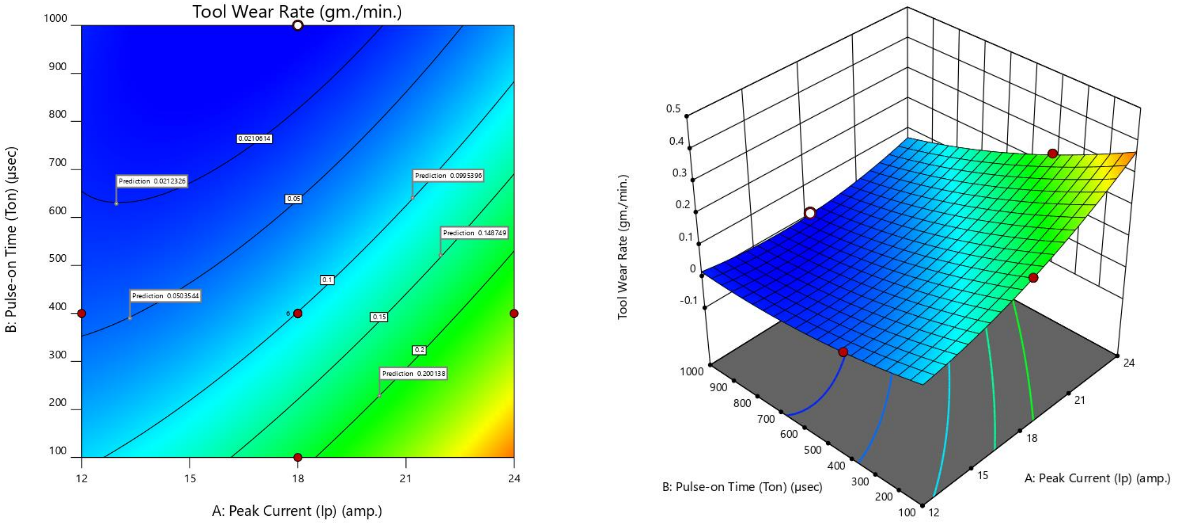

(a) 2-D Contour Plot of AB (b) 3-D Surface interaction Plot of AB

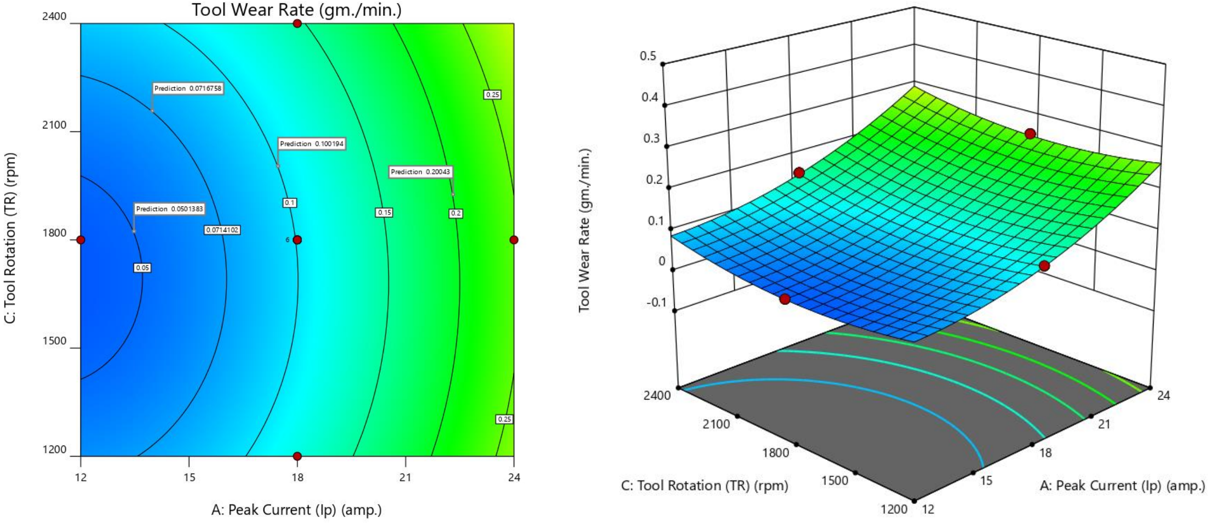

(c) 2-D Contour Plot of AC (d) 3-D Surface interaction Plot of AC

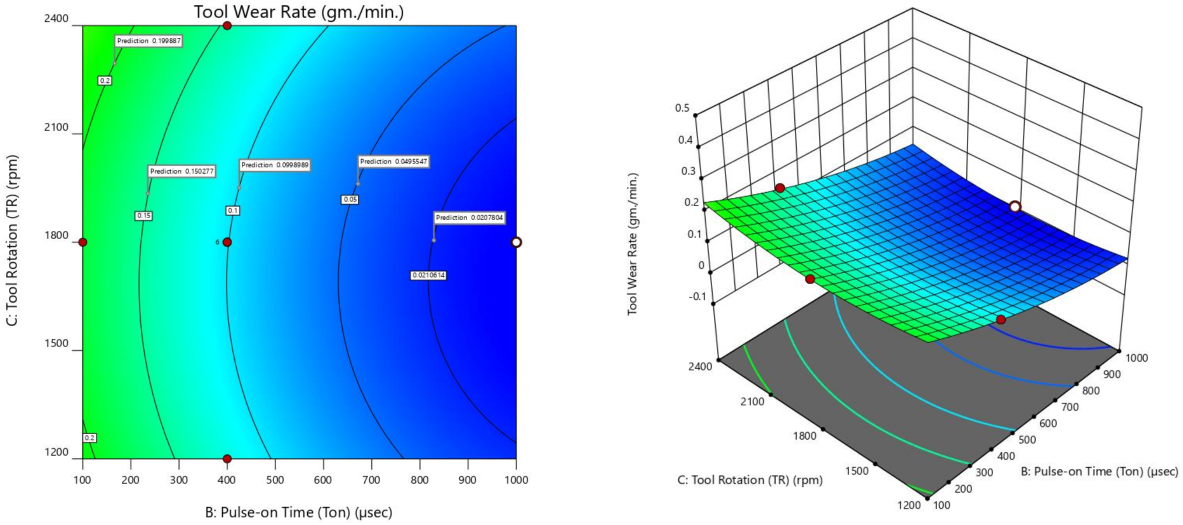

(e) 2-D Contour Plot of BC (f) 3-D Surface interaction Plot of BC

Figure 5.14: 2-D Contour and 3-D Surface plot with interaction AB, AC and BC for TWR. The actual factor A: I_p = 18 amp., B: T_{on} = 400 µsec and C: T_R = 1800 rpm

(iii) Surface Roughness

Figure 5.15 represents the change in R_a with I_p, T_{on} and T_R. It represents, surface characteristics deteriorate as enhancement in I_p as well as T_{on}. The increment in spark discharge energy along with I_p. Thus, thermal energy generated at a high amount and more crater on of workpiece material. It lower the surface characteristics of the machining surface. The high amount of melting and vaporisation results recasting of melted material, if flushing is not efficient, surface cracks, pores, carbon deposition and pitting may appear. The copper tool at lower amount of discharge current generates the enhanced surface.

Figure 5.15 (a-b) represents the R_a rises along T_{on}. The Increase in T_{on} to maximum reveals R_a value to the maximum even at a low value of I_p. Furthermore, whenever the T_{on} is at a minimum with a low value of I_p, the R_a value is minimum. The actual parameters of R_a at I_p, T_{on} and T_R were 18 amp, 400 µsec and 1800 rpm represented in figures. Figure 5.15 (c-d) shows the, R_a increases with I_p due to high energy is produced, leaves craters on the machined surface and leads to poor surface finish. Similarly, figure 5.15 (e-f) R_a increases with T_{on}, which results in high surface roughness. The design points for all interactions are laying on the surfaces. The design points range are 1.1 to 1.96.

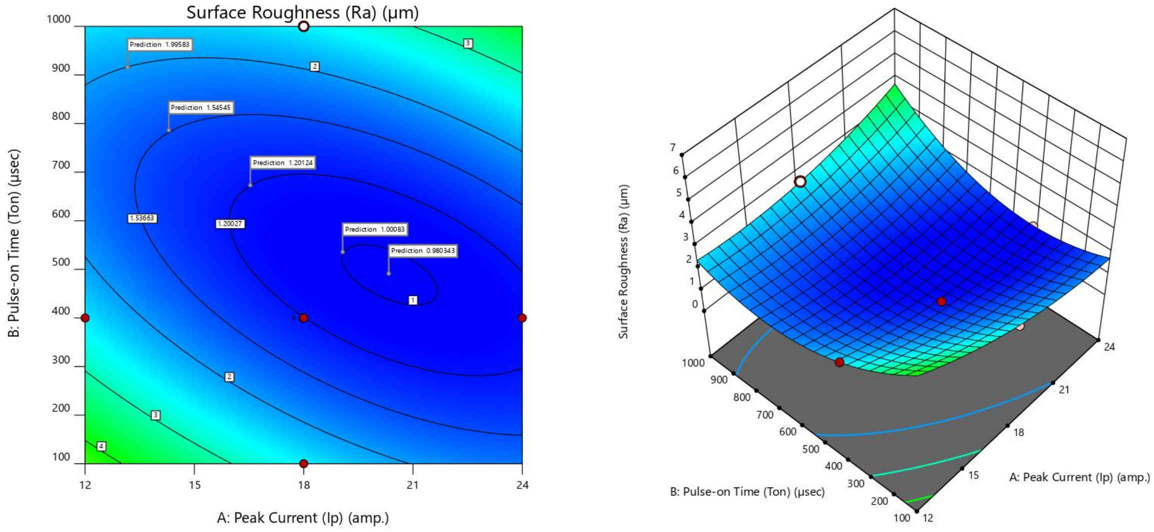

(a) 2-D Contour Plot of AB (b) 3-D Surface interaction Plot of AB

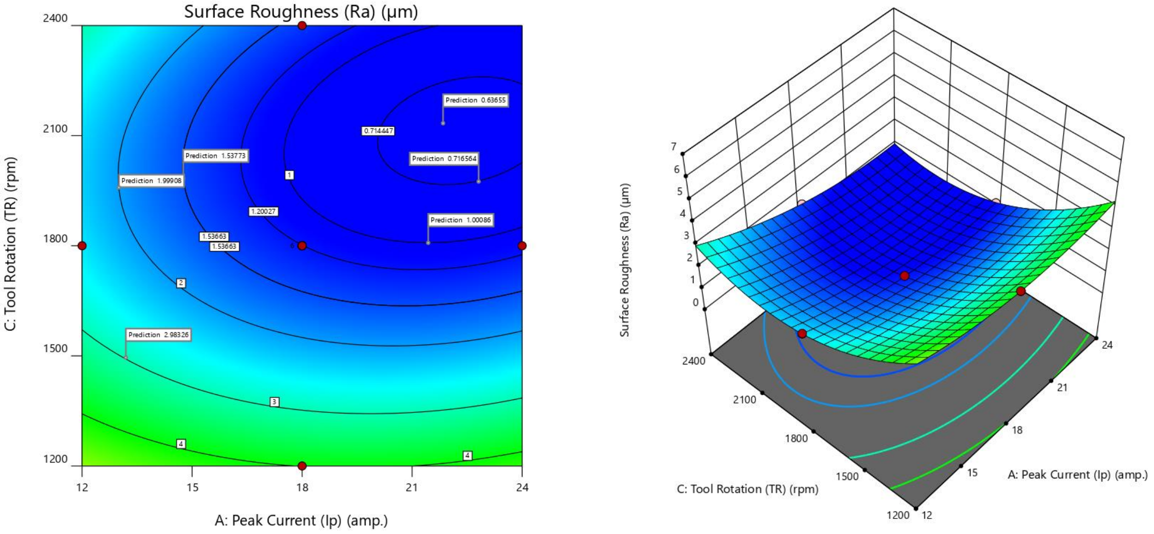

(c) 2-D Contour Plot of AC (d) 3-D Surface interaction Plot of AC

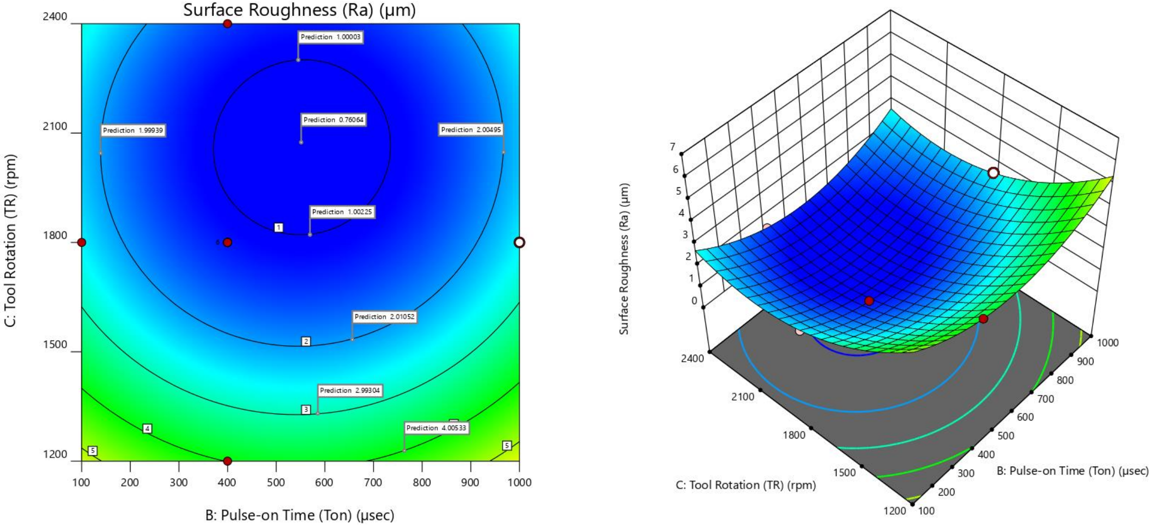

(e) 2-D Contour Plot of BC (f) 3-D Surface interaction Plot of BC

Figure 5.15: 2-D Contour and 3-D Surface plot with interaction AB, AC and BC for R_a. The actual factor A: I_p = 18 amp., B: T_{on} = 400 µsec and C: T_R = 1800 rpm

5.7 Stylus Based Surface Roughness Analysis

Roughness (R_a) was assessed to evaluate the variations in surface peak and trough. The aim of surface roughness analysis is to improve the properties of the surface using tool rotation EDM. The effect of process variables on the response of R_a was analysed.

R_a, Roughness is universally recognized by the R_a parameter. The arithmetical average of absolute departures from peak to valley of unevenness contour from the mean line.

Table 5.5 Taylor Hobson (Surtronic 3+) instrument settings

Function	**Value**
Parameter	R_a
Cut-off	0.8 mm
Evaluation length	4.0 mm
Range	100 µm
Data dump evaluation length	4.0 mm
Data dump range	100 µm
Filter Gaussian	

After machining the experimental run was measured using Taylor Hobson Surtronic 3+ surface roughness profilometer. The surface was measured 3 times on each experimental run as shown in figure 4.4 (Chapter 4). The measurement was done and profile was obtained which was the replicate of the surface on which the stylus moved. The evaluation length (i.e. the distance travelled by the stylus during each measurement) was 4 mm, which was kept constant for all the runs. The profile obtained as shown the following figure 5.16 to 5.18 was used to analyse the surface.

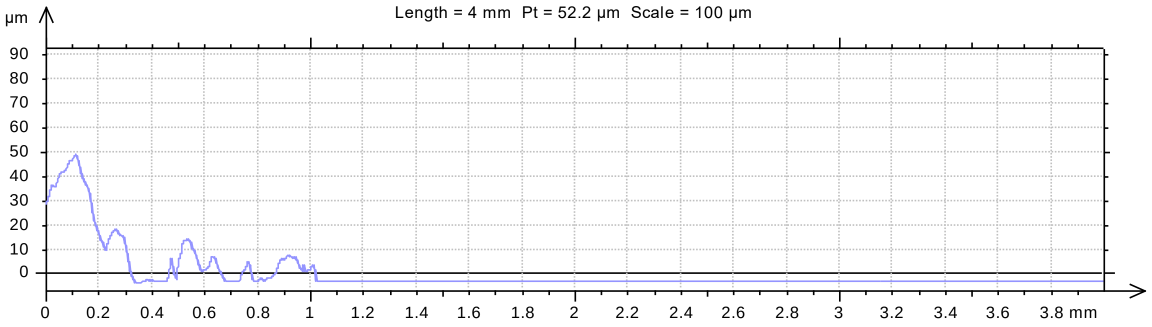

Figure 5.16: Peak and valley profile for surface after EDM machining, $R_a = 1.25$ µm

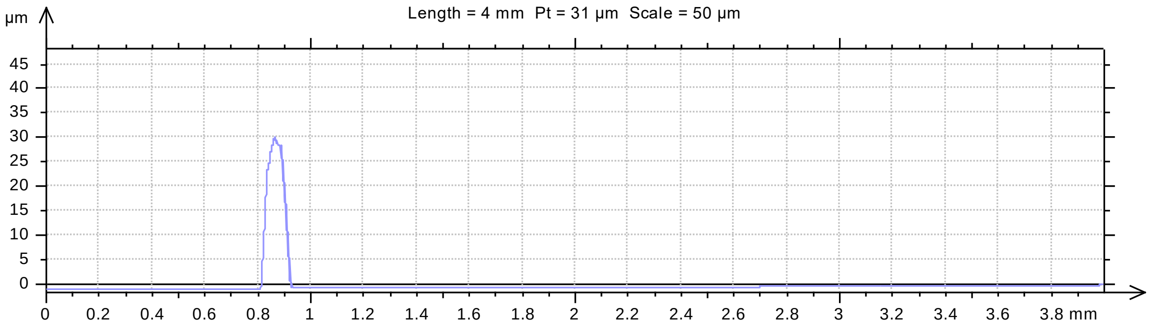

Figure 5.17: Peak and valley profile for surface after EDM machining, $R_a = 1.4$ µm

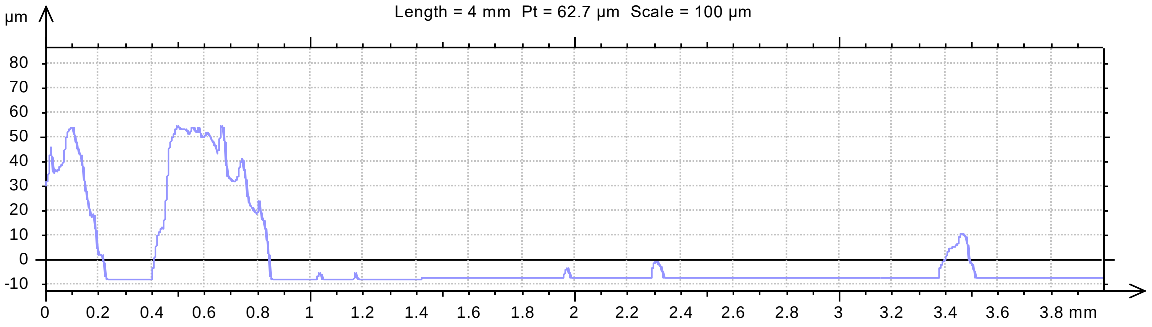

Figure 5.18: Peak and valley profile for surface after EDM machining, $R_a = 4.2$ µm

Figure 5.16, 5.17 and 5.18 represents the profiles of machined surfaces for T_{on} 400 µsec. The machining area has high frequency and the peaks and troughs of less magnitude as compared from 100 µsec to 1000 µsec T_{on} on machined surface. Figure 5.16 represents the R_a peak value is 49 µm from 0 to 0.22 mm region, 0.22 mm to 1.1 mm the variation is very less and rest surface after 1.1 mm is uniform. The high amplitude of peak and valley from 0 to 0.22 mm due to the resolidification of metal. It reveals to formation of recast layer in this zone. Figure 5.17 and 5.18 shows the more peak and valleys, the average value of R_a is 4.2 µm, because the high amount of discharge energy, the melting rate is high. The maximal peak crest was considerably reduced after tool rotation EDM. This was also indicated by the reduction of R_a parameter from the 1200 rpm to 1800 rpm on the samples from 4.2 µm to 1.25 µm i.e. 70 % reduction in R_a by tool rotation. Tool rotation facilitates to remove debris from the inter-electrode gap, due to the presence of whirling of debris. That prevents solidification of the recast layer and plays an important role in the formation of a martensitic structure.

5.8 Morphology of AISI D3 Steel

Scanning Electron Micrograph (SEM) is used to analyse the closed spaced specimen at higher magnification since electromagnets are used instead of lenses (Prabhu and Vinayagam, 2011). The plasma channel causes from high value of I_p causes the temperature or cool surface to rise above the liquid temp, which lead to vaporize (Panda and Bhoi, 2005)

At a low value of I_p, the surface is very smooth, the formation of craters are shallow in nature. In high I_p, more sparks are created and lead to the formation of craters on the face of the tool. Mahardika et al., (2008) reported similar findings while carrying out on EDM. The craters are wider and also deeper. For every pulse at single location where the electrode materials are evaporated in molten phase lead to the formation of crater on workpiece and tool. At the high value of current the size of surface crack increases. The surface characteristics show the formation of pores, pitting, rough surface with carbon deposition on the material surface. Increase of I_p results in debris formation, the debris may re-solidified on the workpiece surface. This re-solidification of material reduced by tool rotation. This is due to the whirling effect.

As I_p is considered to a dominant either as a variable or in interaction with another variable for all the responses so, the effect of I_p examination is important microscopically. Figure 5.19 (a), 5.20 (a) and 5.21 (a) represents the SEM micrographs at parametric condition $I_p = 18$ amp, $T_{on} = 400$ µsec, $T_{R} = 1800$ rpm (MRR = 0.88 gm/min., TWR = 0.099 gm/min., $R_a = 1.25$ µm); $I_p = 24$ amp, $T_{on} = 1000$ µsec, $T_{R} = 2400$ rpm (MRR = 0.6507 gm/min., TWR = 0.13 gm/min., $R_a = 3.59$ µm); $I_p = 12$ amp, $T_{on} = 100$ µsec, $T_{R} = 1200$ rpm (MRR = 0.598 gm/min., TWR = 0.125 gm/min., $R_a = 6.7$ µm) with copper tool for MRR, TWR and R_a. The SEM microscopy, it was observed that micro surface cracks, material re-deposition as well as minor carbon deposition on the machining surface rise with I_p rise from 12 A to 24 A and smoothness (fineness) of the surface decrease respectively.

The re-solidified layer is available in all experiments but notably visible in the figure. 5.20 and 5.21. The dielectric fluid ionized i.e. the spark heat-generating cracks that reveals dissociation of carbon and hydrogen. The fact is known as pyrolysis. The carbon dissociated form dielectric fluid become the included in ferrous material and subsequent quenching results to a very hard martensitic coat on the surface. It is non-etchable by traditional vital etchants. This appearance of resolidified coat is defined as white cast layer or recast layer in EDM. This thick layer is prominently visible as an unetched layer. The white layer is mostly non-uniform and reveals the occurrence of pitting and cracking, it is limited to the re-solidified layer. This emphasizes the summary of spark craters characteristic.

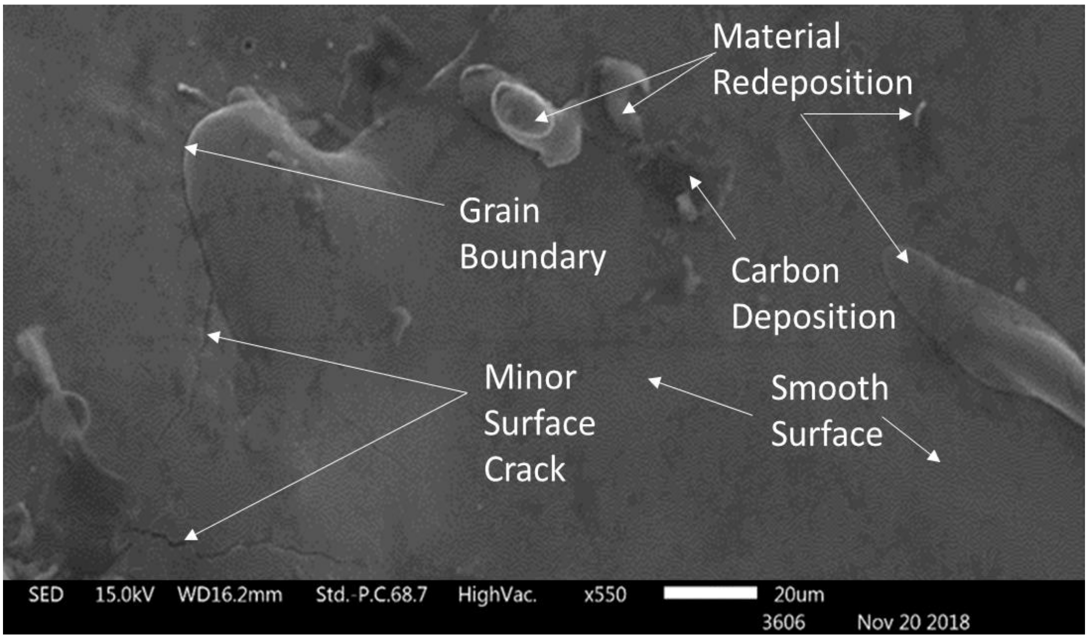

Figure 5.19 (a) Scanning Electron Microscopy representing micro-cracks and smooth surface

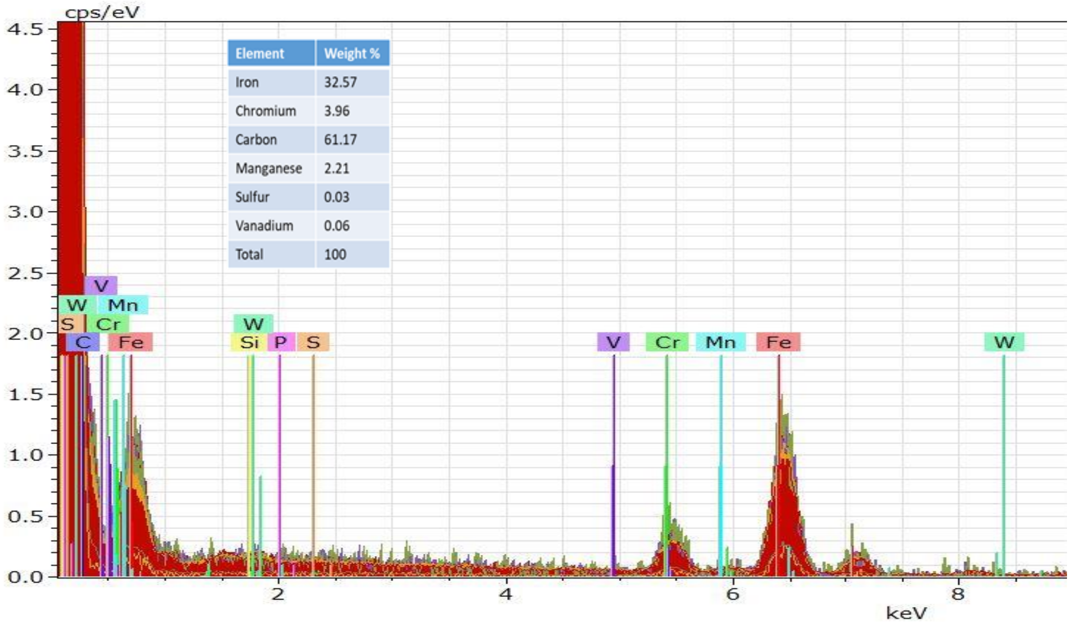

Element	Weight %
Iron	32.57
Chromium	3.96
Carbon	61.17
Manganese	2.21
Sulfur	0.03
Vanadium	0.06
Total	100

Figure 5.19 (b) EDS Spectrum

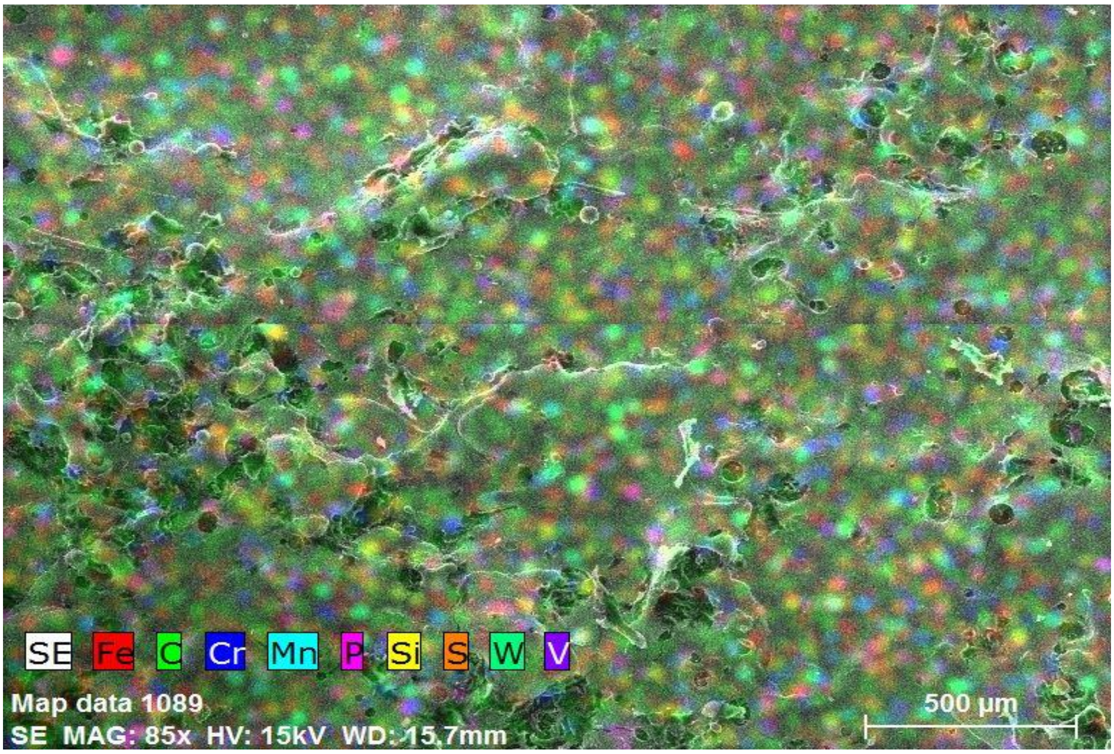

Figure 5.19 (c) EDS Mapping

Figure 5.19: SEM, EDS, EDS Mapping. At I_P = 18 amp, T_{on} = 400 µsec, T_R = 1800 rpm

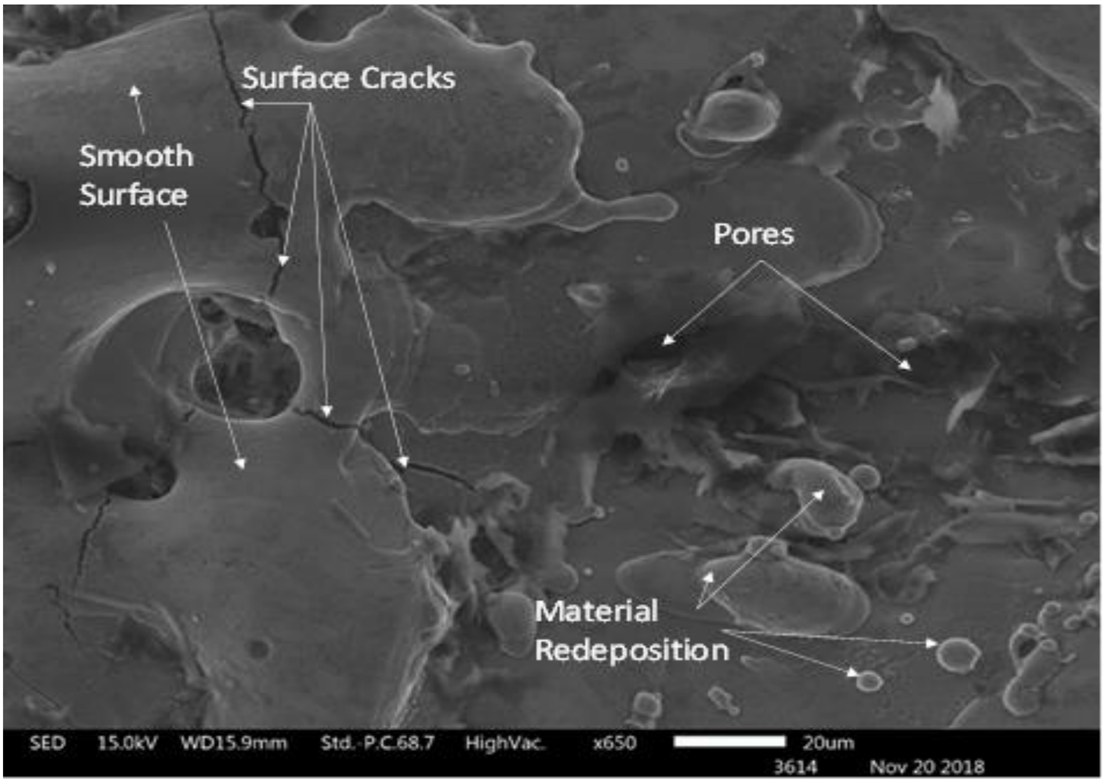

Figure 5.20 (a) Scanning Electron Microscopy representing micro-cracks and material deposition

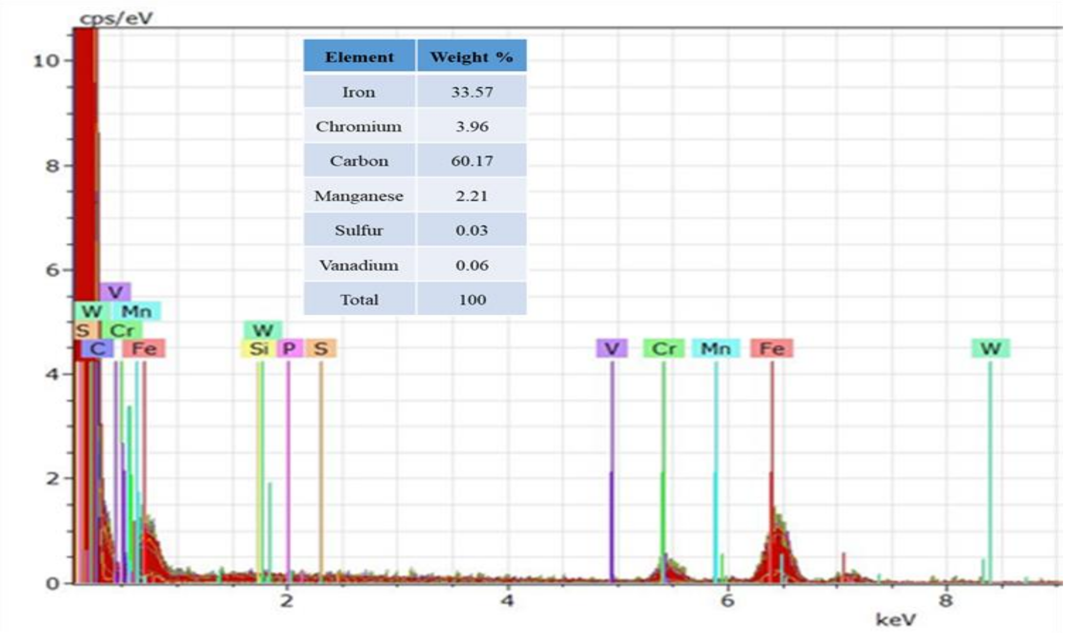

Element	Weight %
Iron	33.57
Chromium	3.96
Carbon	60.17
Manganese	2.21
Sulfur	0.03
Vanadium	0.06
Total	100

Figure 5.20 (b) EDS Spectrum

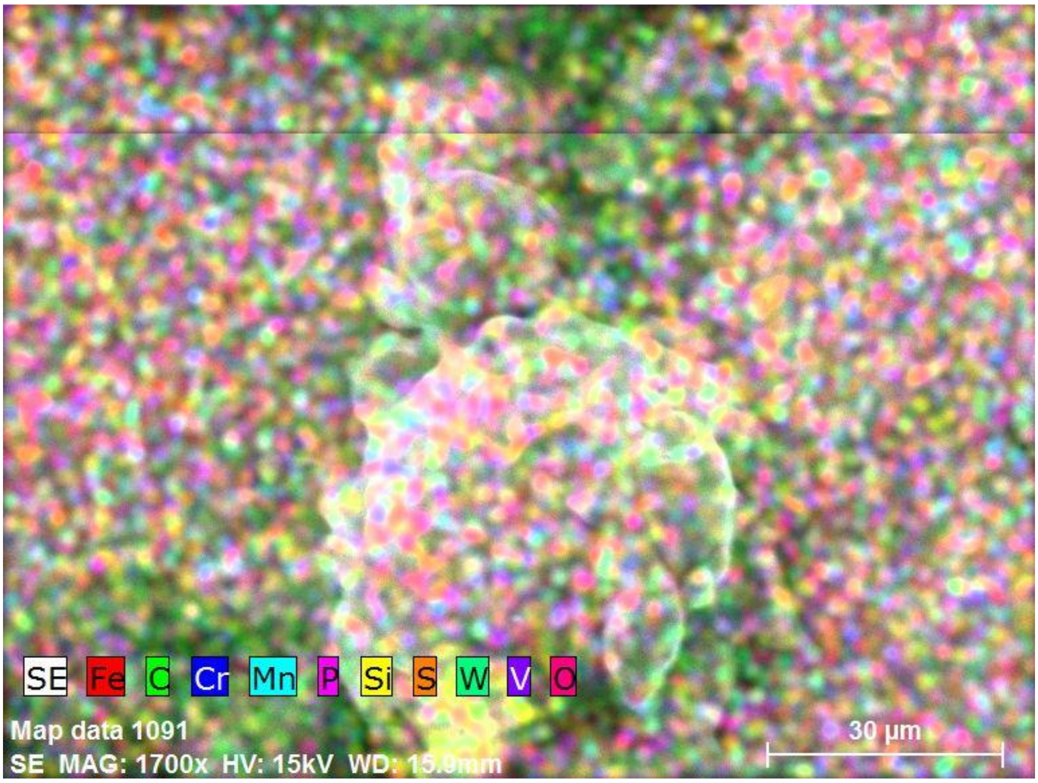

Figure 5.20 (c) EDS Mapping

Figure 5.20: SEM, EDS, EDS Mapping. At I_p = 24 amp, T_{on} = 1000 µsec, T_R = 2400 rpm

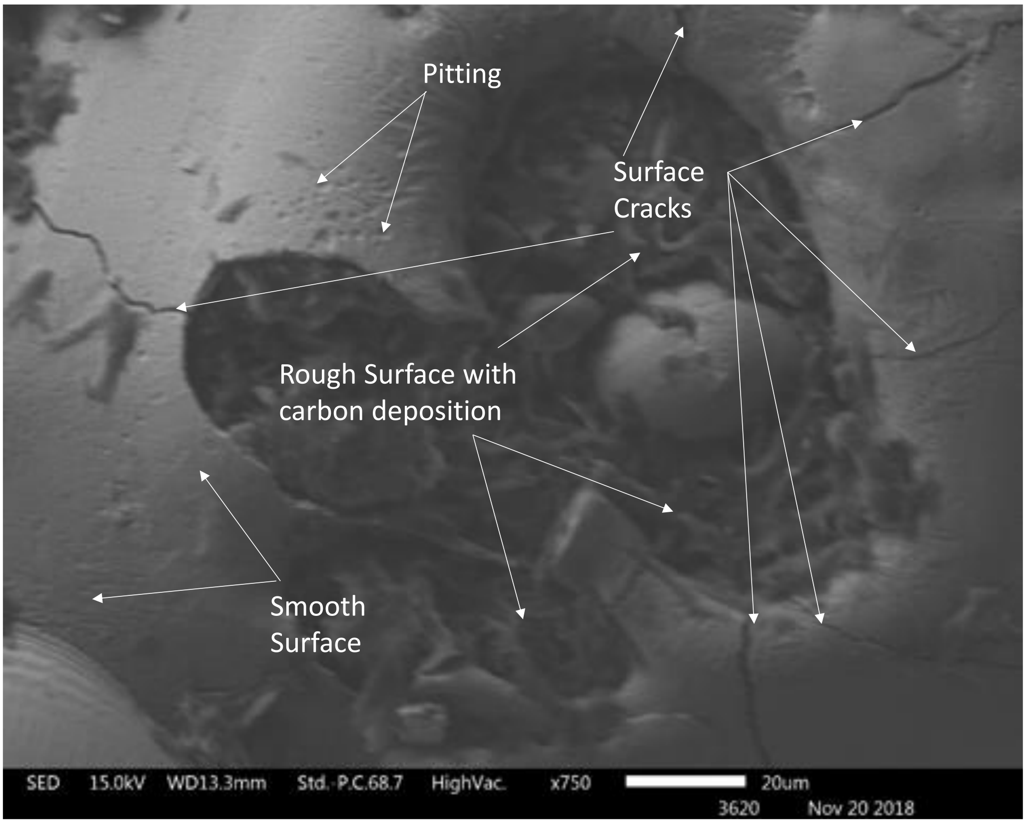

Figure 5.21 (a) Scanning Electron Microscopy representing surface cracks, pitting and rough surface with carbon deposition

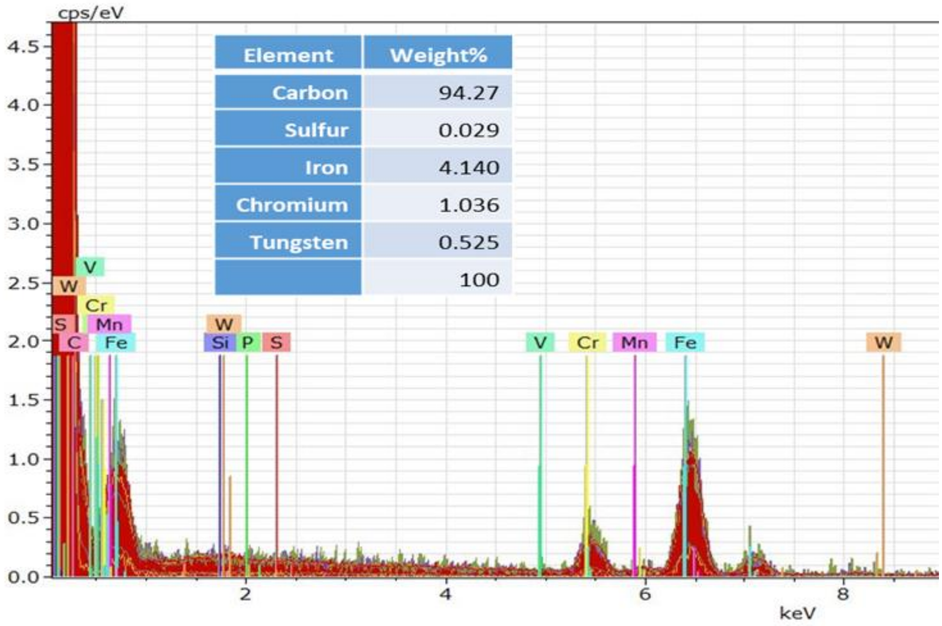

Element	Weight%
Carbon	94.27
Sulfur	0.029
Iron	4.140
Chromium	1.036
Tungsten	0.525
	100

Figure 5.21 (b) EDS Spectrum.

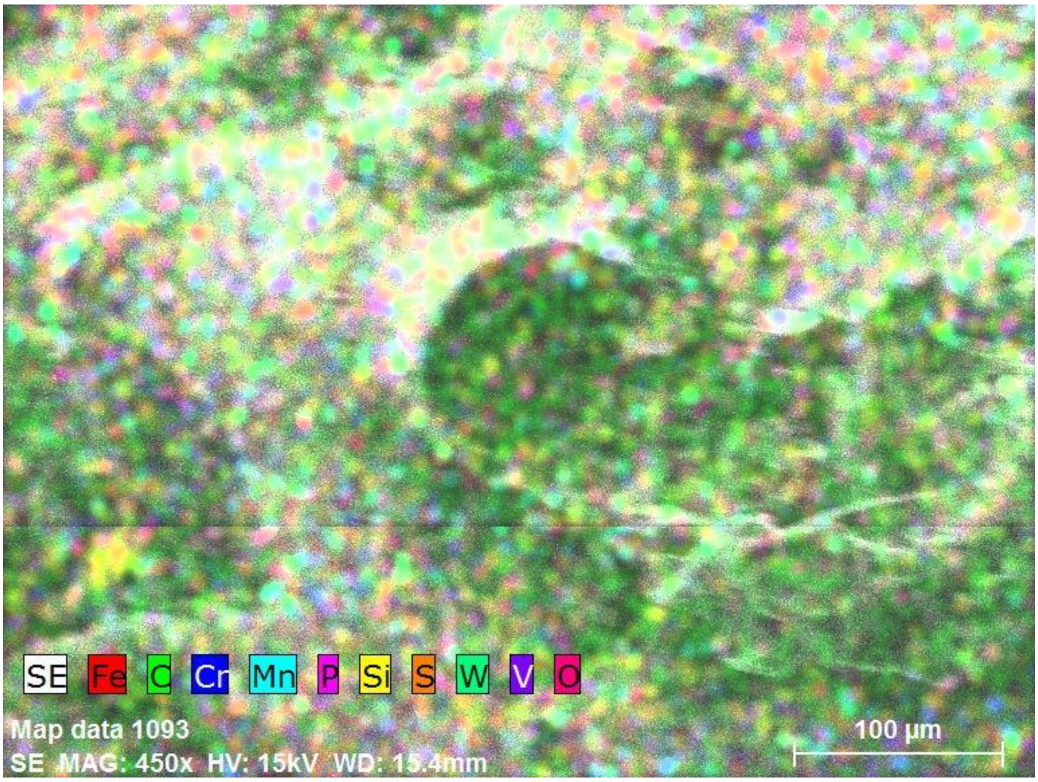

Figure 5.21 (c) EDS Mapping

Figure 5.21: SEM, EDS, EDS Mapping. At I_p = 12 amp, T_{on} = 100 µsec, T_R = 1200 rpm

Energy Dispersive X-ray Spectroscopy analysis (EDS), it is a scientific approach for examination of workpiece by elemental or chemical characterization analysis. EDS works as an integral component of SEM. During EDS operation, the electron rays bombardment to workpiece takes place and strike on the specimen atom's own electrons, knocking some of them away from the process. A location empty by an expelled inner shell electron is ultimately engaged by a higher-energy electron from an outermost shell. However, the transferred outermost electron should give up some of its energy by emitting an X-ray. This characterization is part of principle that each constituent atom has a unique atomic structure. It allows electromagnetic emission spectrum for unusual set of peaks.

Figure 5.19 (b), 5.20 (b), 5.21 (b) and 5.19 (c), 5.20 (c), 5.21 (c) represents the energy dispersive analysis of x-rays (EDS). Figure 5.19 (b), 5.20 (b), 5.21 (b) represents constituent elements by wt. % i.e. major composition of carbon i.e. 61, 60, and 94; iron i.e. 32, 33 and 4 respectively. 5.19 (c), 5.20 (c), 5.21 (c) shows its elemental distribution.

5.9 Residual Stress Analysis

The residual stresses examination and analysis of the specimen was done by non-destructive testing methods. The measurement of longitudinal and transverse stresses on the machined face was done by diffraction method of an X-ray. It is non-destructive testing of the workpiece. The examination completed with μ- X360 portable residual stress analyser, it is made by Pulsate USA, Inc. Figure 5.22, indicates the measuring device which consists of a power supply, sensor unit and height adjustment stand. Residual stresses can be evaluated with full X-Ray Debye ring in the non-stressed state. The pitch used for measurement was 50 μm for measuring each point.

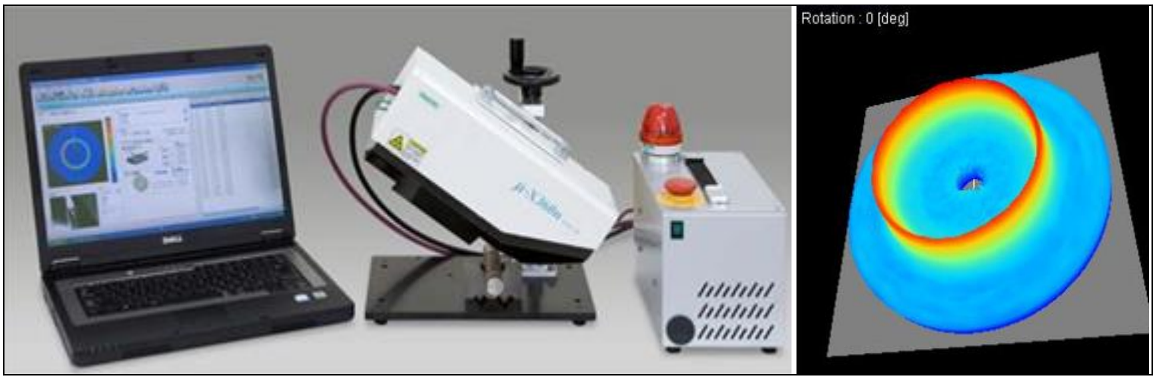

Figure 5.22: Pulstec μ- X360 portable stress analyser with Debye-ring

The primary reason of residual stress is the fact that the machined surface has been heated, melted and cooled at a high rate of metallurgical transformations [Heuvelman 1974; Yang

2013; Vishwakarma 2012]. The residual stress was produced due to thermic shrinkage by cooling, micro-structural modifications were considered in explanation. The residual stresses investigation of EDM components was tensile as well as compressive in nature represented by positive and negative value respectively. The increase in their extent is acknowledged on outer skin layers as rising pulse discharge energy. Because, the integrity of machined face is deteriorated by the unpredictable arcing which constantly appear in machining operation period, the quality of machining is estimated w.r.t. machined-face integrity, it is categorized as surface roughness, micro-cracks and residual stresses. The roughness of machined face is correlated with the allocation of craters formed by an electric arc. Some amount of melted metal redeposit on machined-face because rapid heat transfer reveals to fast cooling rate by the dielectric fluid. Due to the deposition of material, a recast layer is introduced and known as white skin because it is very complicated to remove and looks white when examined with SEM microscopy. This has been discussed already that the spark produced during machining, disintegrate the dielectric fluid. The dielectric fluid is hydrocarbon oil that results in carbon penetration into the machined surface area. The liquid metal remains over the surface due to high freezing rate of metal and shrinkage takes place. The solidified layer considerably set up the high amount of stresses on the machined area. The nature of stress changes at a certain distance below the surface over to compressive. Because the skin of work material surface machined by EDM is brittle, the work material face after operation has been discovered to the existence of micro-cracks networks, sometimes this may penetrate into the base metal. The surface damage depth depends on the discharge parameters of the machine i.e. I_p and T_{on} are decisive factors.

Tensile residual stress was discovered to approach the above tensile strength of workpiece at the consecutive surface and then drop quickly to a comparatively down value before offering a path to less residual compressive stresses in the centre of the material. Measurements of residual stress on different phases have also shown that the general stress distribution is not greatly affected. The effects of pulse duration and pulse discharge energy on the development of residual stresses. The surface finish and depth of surface skin layer affected depended on a considerable extent upon the pulse duration. The observed residual stresses support the expected formats and increased by both the pulse duration and pulse discharge energy. The stresses were supposed to develop due to the result of the thermic shrinkage of re-solidified material, which was not ejected from craters, the relatively not affected original material, inducing plastic deformation and bi-axial tensile stress.

The effect of polarity is a significant factor. The higher absorption of spark energy efficiency with positive polarity leads to higher temperatures as well as high residual stresses. The Impact of I_p and T_{on} was significant in residual stresses. The thermic load of the skin to a high temperature taken place by thermal succession of T_{on} and T_{off} in EDM process and results in heating gradually of HAZ skin. It is the first phase of thermic loading due to the generation of thermal energy by the spark. Once the interruption of spark taken place, the molten metal at that spot of spark impingement is quenched. The quenching of upper skin or outer layer is done by dielectric fluid. The flow of dielectric fluid takes heat from workpiece and results to its original temperature.

Each layer of skin has different cooling rate because web skin is quenched by its base or parent metal skin i.e. below it. The parent metal re-established its original temperature before the skin temperature. Because the heat transfer of parent metal takes place by conduction. Therefore, the parent material presents resistance to the shrinkage of skin, that leads to tensile residual stresses on skin or outer surface.

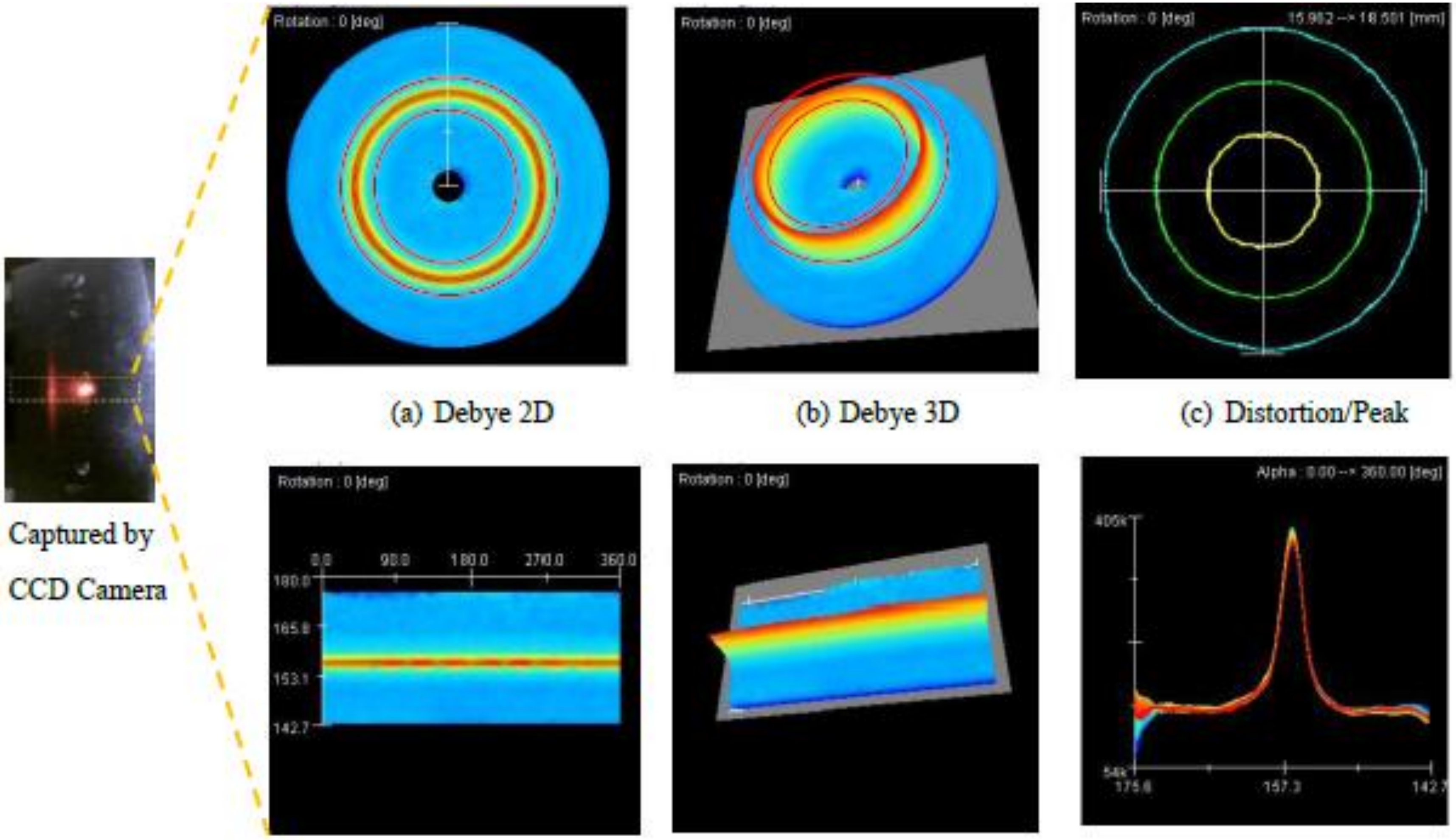

Captured by CCD Camera

(a) Debye 2D (b) Debye 3D (c) Distortion/Peak

(d) Extract 2D (e) Extract 3D (f) Profile ($\alpha = 0\text{-}360^{\circ}$)

Figure 5.23: Residual Stress Mapping of Base Metal AISI D3 Steel, σ (x) = 25 MPa

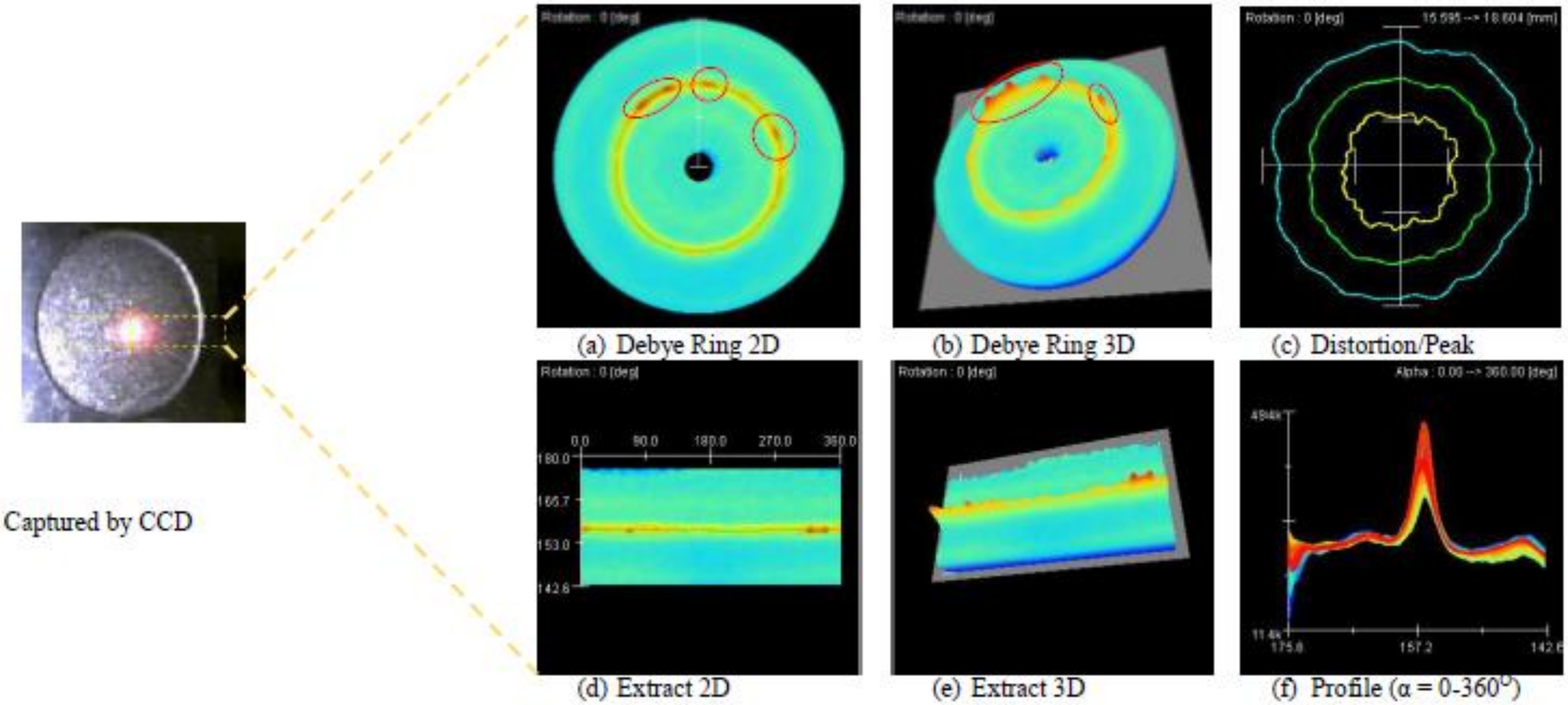

(a) Debye Ring 2D (b) Debye Ring 3D (c) Distortion/Peak

(d) Extract 2D (e) Extract 3D (f) Profile ($\alpha = 0\text{-}360^{0}$)

Figure 5.24: Residual Stress Mapping at I_p = 12 amp, T_{on} = 100 µsec, T_R = 1200 rpm, σ (x) = 208 MPa, Tau (xy) = -99 MPa

Figure 5.23 shows the residual stress mapping of base material of AISI D3 with Interplanar spacing (d) 1.170, Diffraction plane (h, k, l) 2, 1, 1 and Crystal structure B.C.C done by keeping X-ray tube current 1.00 mA, X-ray incidence angle 35°, K-alpha, X-ray wavelength is 2.29093 A°, K-Beta, X-ray wavelength is 2.08480 A° reveal average residual stress ($\sigma = 25$ MPa) profile in the subsurface are uniformly distributed and intensity of peak lying on the 157.5°.

Figure 5.24 (a–f) illustrates the Debye ring (2D and 3D), distortion/peak, surface extract (2D and 3D) profile of specimens during residual test analysis. The residual stress concentration is shown in the Debye ring by circle/ellipse (from red to blue colour) in the substrate material. Red colour indicates the concentration of residual stresses are more in that region while blue colour indicates no or less residual stress concentration. The magnitude of residual stress and strain can be accurately measured by the position of Debye rings. The distortion/peak profile represents that no or less damage i.e. no or less residual stresses are present in the machined sample.

Figure 5.24 to 5.27 illustrates the impact of I_p on average residual stress, it was represented by its profile in the subsurface. The I_p vary from 12 amp. to 24 amp. The discharge energy per pulse will increase as equation 5.4. The average higher value of the residual stress in tensile to some extent increased from 208 MPa to 269 MPa for the same T_{on} and T_R i.e. 100 µsec and 1200 rpm and compressive stresses significantly increased from 781 MPa to 11826 MPa, when T_{on} increased from 100 µsec to 400 µsec. The effect of I_p and T_{on} that represents the distortion intensity of peak lying on the 157.2°, 157.1°, 156.8° and 152.7° respectively. The residual stress ring distorted on these points and the average value of residual stresses is 208, 257, 269 MPa (tensile) and 11826 MPa (compressive). The residual shear stress varies from 99 to 2679 MPa.

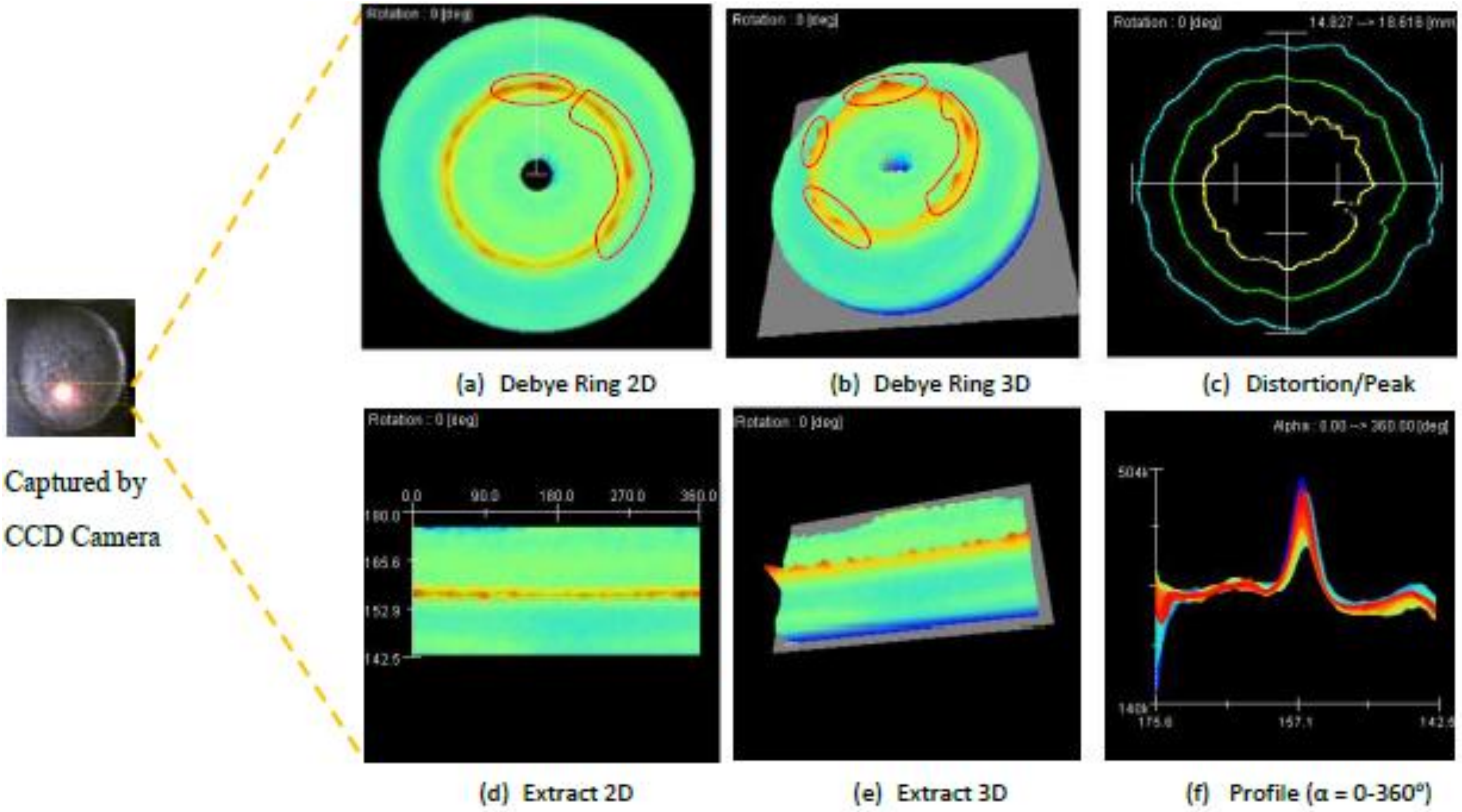

(a) Debye Ring 2D

(b) Debye Ring 3D

(c) Distortion/Peak

(d) Extract 2D

(e) Extract 3D

(f) Profile (α = 0-360°)

Figure 5.25: Residual Stress Mapping at I_p = 18 amp, T_{on} = 100 µsec, T_R = 1200 rpm, σ (x) = 257 MPa, Tau (xy) = -60 MPa

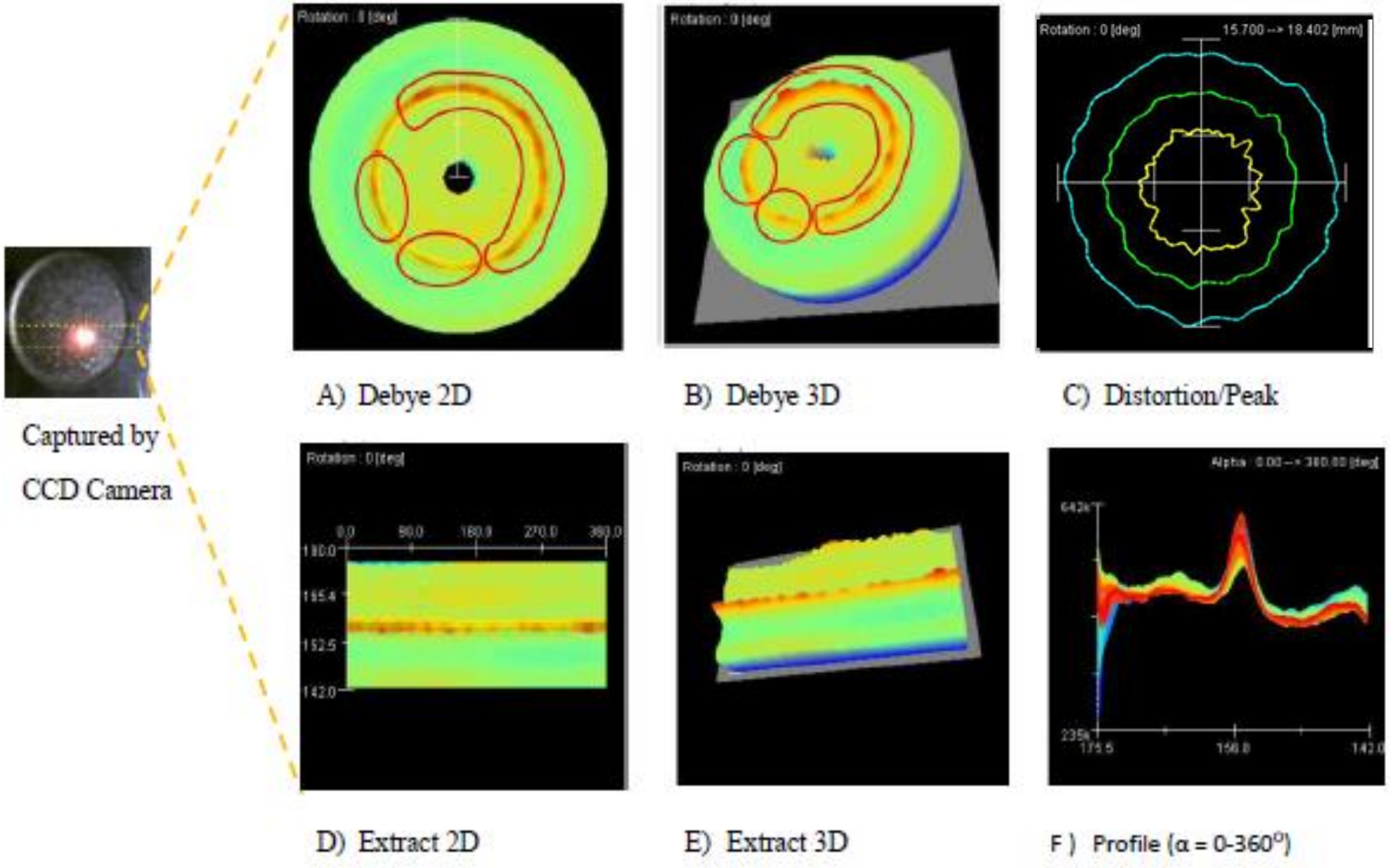

Captured by

CCD Camera

A) Debye 2D

B) Debye 3D

C) Distortion/Peak

D) Extract 2D

E) Extract 3D

F) Profile (α = 0-360°)

Figure 5.26: Residual Stress Mapping at I_p = 24, T_{on} = 100, T_R = 1200, σ (x) = 269 MPa, Tau (xy) = -22 MPa, σ (y) = -781 MPa

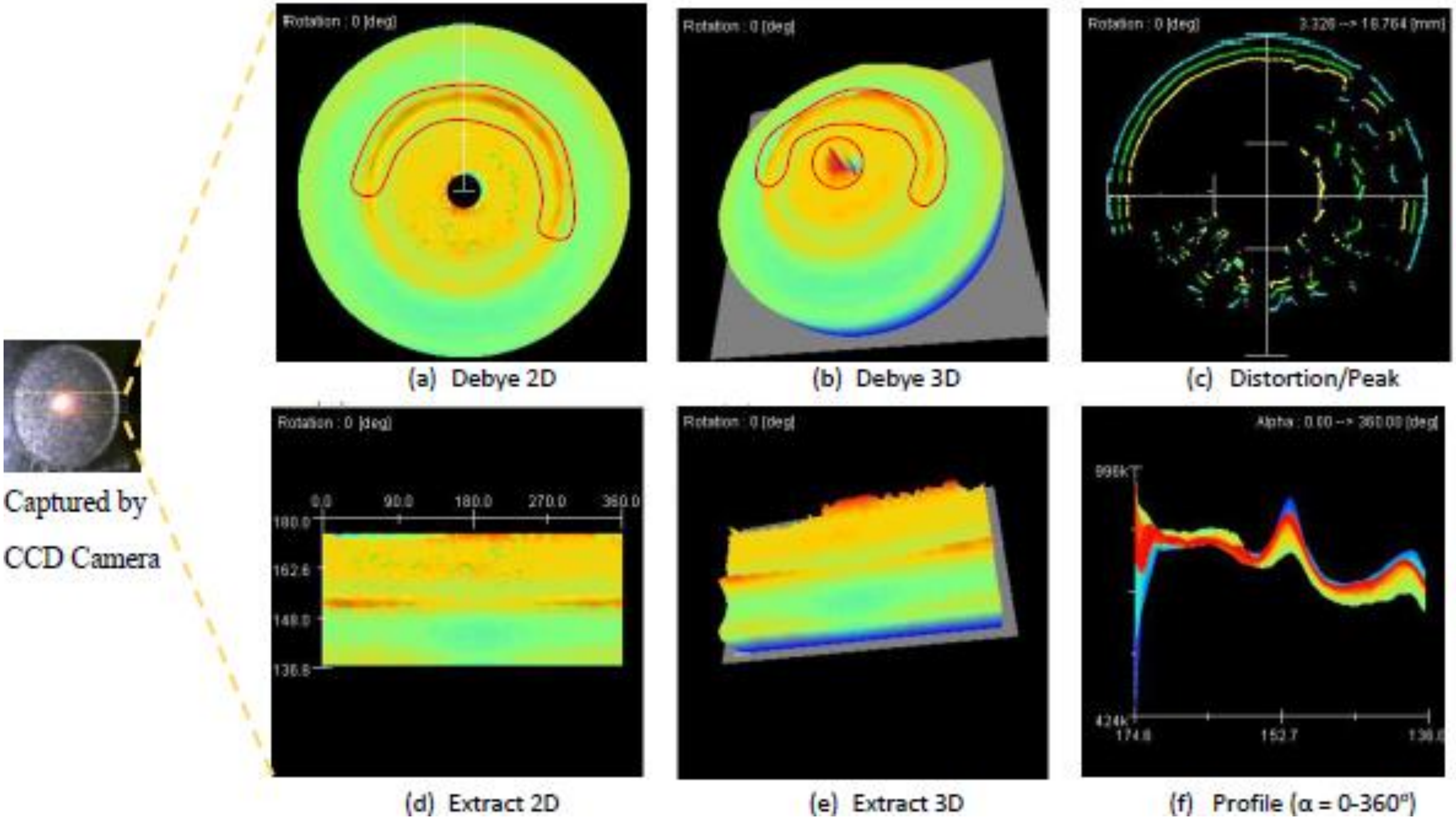

(a) Debye 2D (b) Debye 3D (c) Distortion/Peak

(d) Extract 2D (e) Extract 3D (f) Profile (α = 0-360°)

Figure 5.27: Residual Stress Mapping at I_p = 12, T_{on} = 400, T_R = 1200, σ (x) = -11826 MPa, Tau (xy) = -2679 MPa

This is mainly due to the long duration of the pulse at discharge, it is responsible for more MRR and resulted in high R_a.

Hence, less pulse discharge energy is preferred in EDM to achieve a lower tensile and compressive residual stress and also decreasing surface roughness. The discharge energy in one pulse “Q” may be determined by pulse waveforms profile for EDM process and given as:

$$Q = I_p * V * T_{on} \tag{5.4}$$

Where

I_p = discharge current,

V = discharge voltage and

T_{on} = Pulse-on-Time or discharge duration.

5.10 Pulse Discharge Energy Analysis

Pulse discharge energy analysis was done with the digital storage oscilloscope (Siglent SDS1102CML), shown in figure 5.28. Oscilloscope attached to EDM polarity terminal of tool and workpiece with interfacing devised electronic circuit (shown in Figure 5.31) for pulse discharge energy waveform. The current travel from the tool (positive terminal) to work material (negative terminal) through the medium of dielectric fluid. The IEG between tool and workpiece is reduced to constricted area approximately 10 to 50 µm Yahya (2011). The discharge of energy in-between the tool and work material transferred in the form of pulses. This energy transferred into heat energy and builds up workpiece temperature and melts the area on its surface. The pulse power plays an influential role in affecting the MRR and the properties of the machined surface Minhat (2014); Tsai (2007).

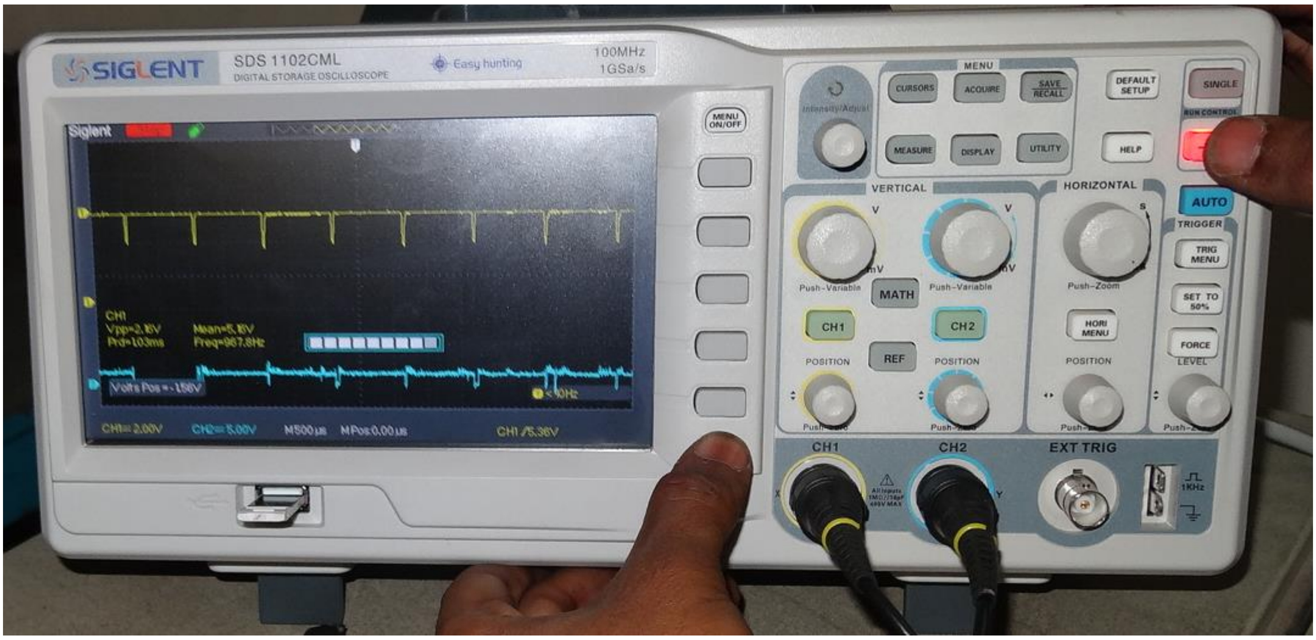

Figure 5.28: Siglent SDS1102CML, Digital Storage Oscilloscope

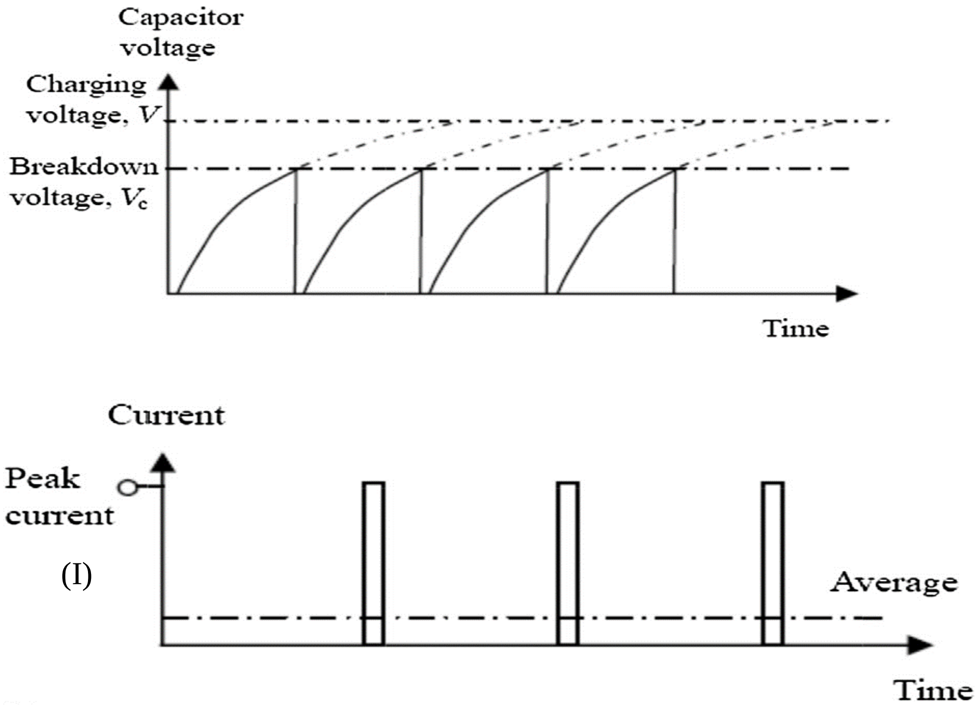

Figure 5.29: V and I characteristics for ideal conditions of Resistance-Capacitance (RC) type pulse generator

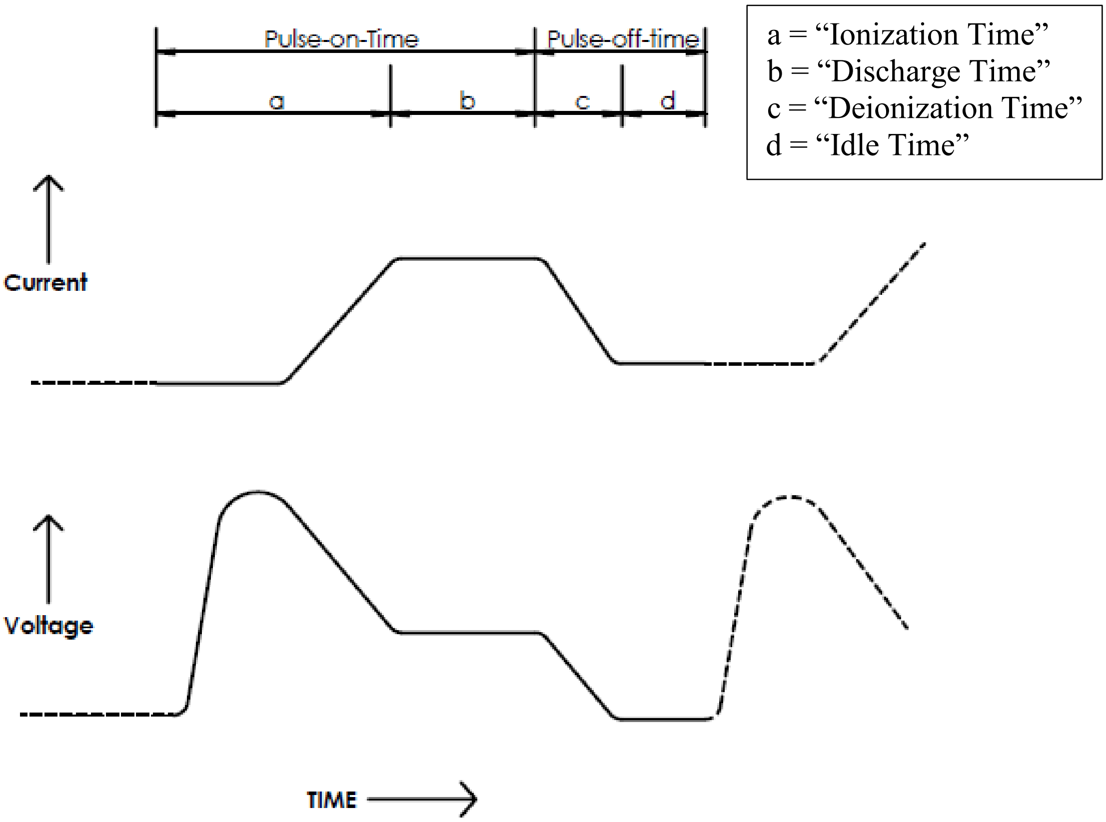

Figure 5.30: Substantive Pulse Profile of Single EDM

Figure 5.29 represents the voltage and current (V-I) characteristics of resistance-capacitance (RC-type) pulse generators for ideal conditions. The actual voltage and current characteristic curves are shown in figure 5.30. The pulse for charging and discharging was generated by RC-type pulse generator and used for EDM working in finishing and micro-machining. The circuit supply constant-pulse energy that is adequately short.

In an RC relaxation type circuit, the discharge pulse duration is dominated by the capacitance of the capacitor. The wire inductance connecting capacitor to workpiece and the tool. The frequency of discharge (discharge repetition rate) depends upon the charging time, which is decided by the resistance (R) used in the circuit. Therefore, R-value should high because at the beginning of process arcing phenomenon takes place instead of sparking and a specific resistance is desirable it should prevent arcing in between the electrodes. The applied capacitance and stray capacitance was used to determine the discharge energy. It exists in between the tool and workpiece. This signify that minimum per pulse discharge energy is considered by stray capacitance. Hence, all the charge stored in the stray capacitance is discharged to the working gap along with the charge stored in the capacitor wired to the circuit.

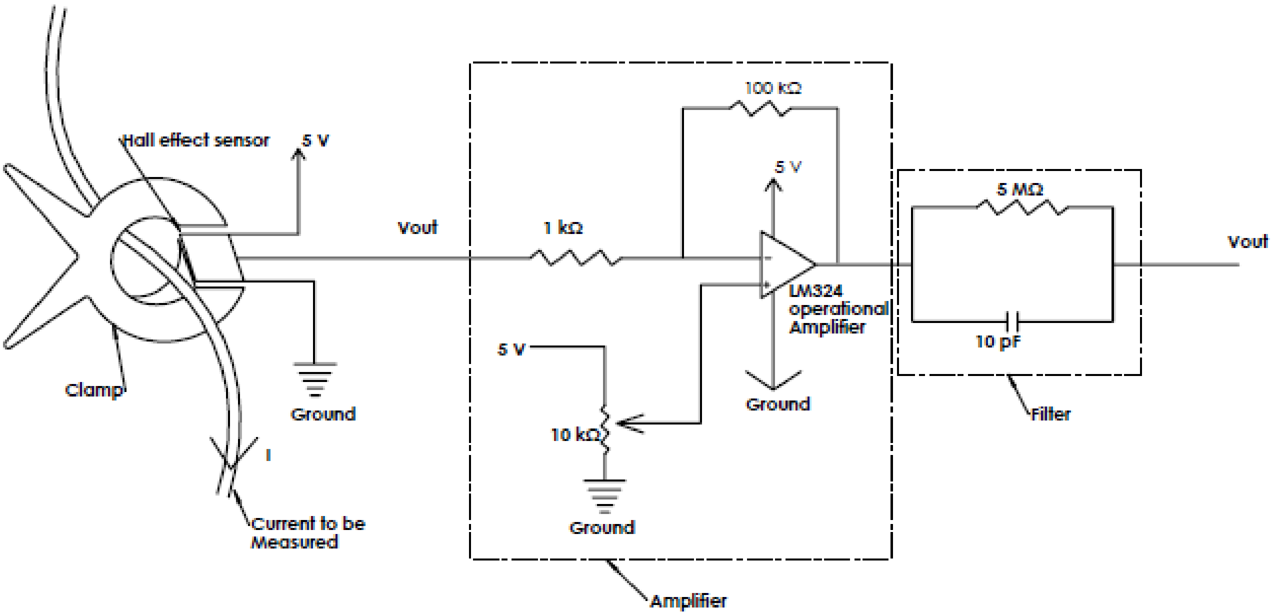

Figure 5.31: Electronic circuit for interfacing between digital oscilloscope storage and EDM with tool rotation machine

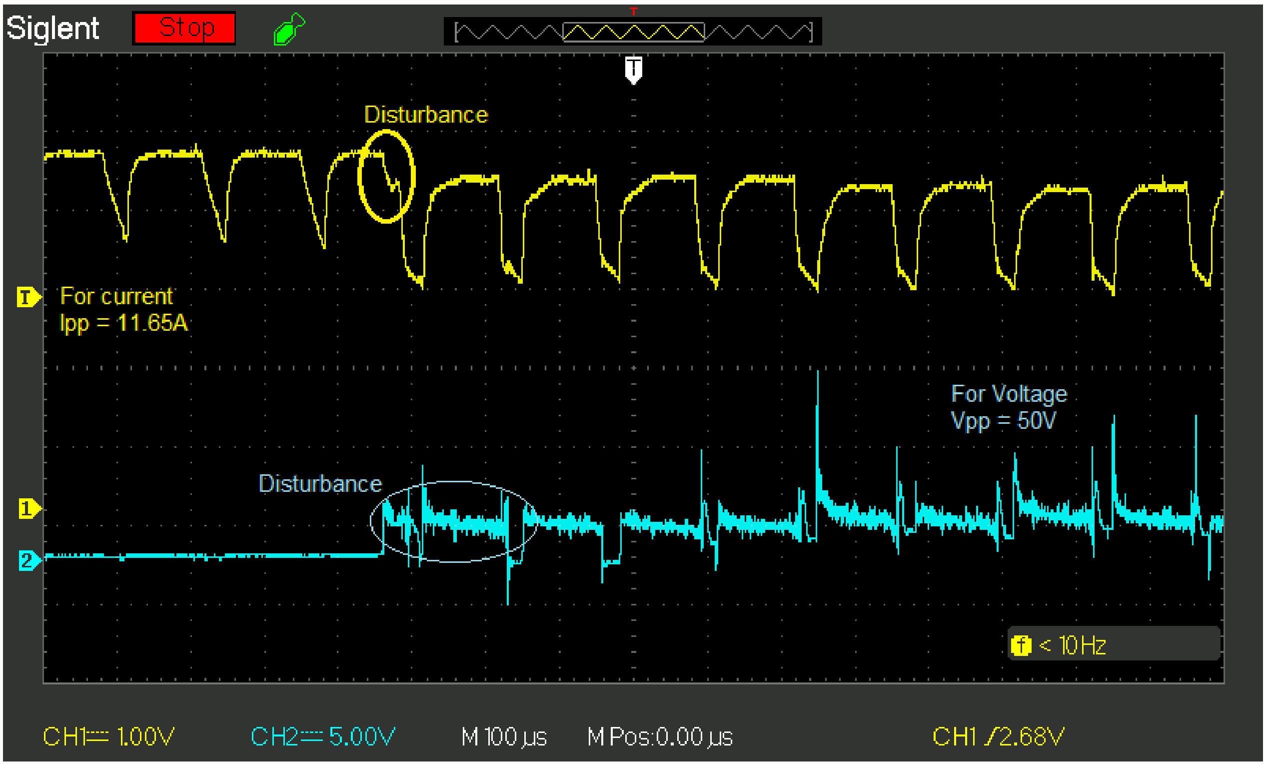

CH1⎓ 1.00V CH2⎓ 5.00V M 100 µs M Pos:0.00 µs CH1 ∕ 2.68V

Figure 5.32: Current and Voltage Waveform, I_p = 12 amp., T_{on} = 100 µsec and T_R = 1200 rpm

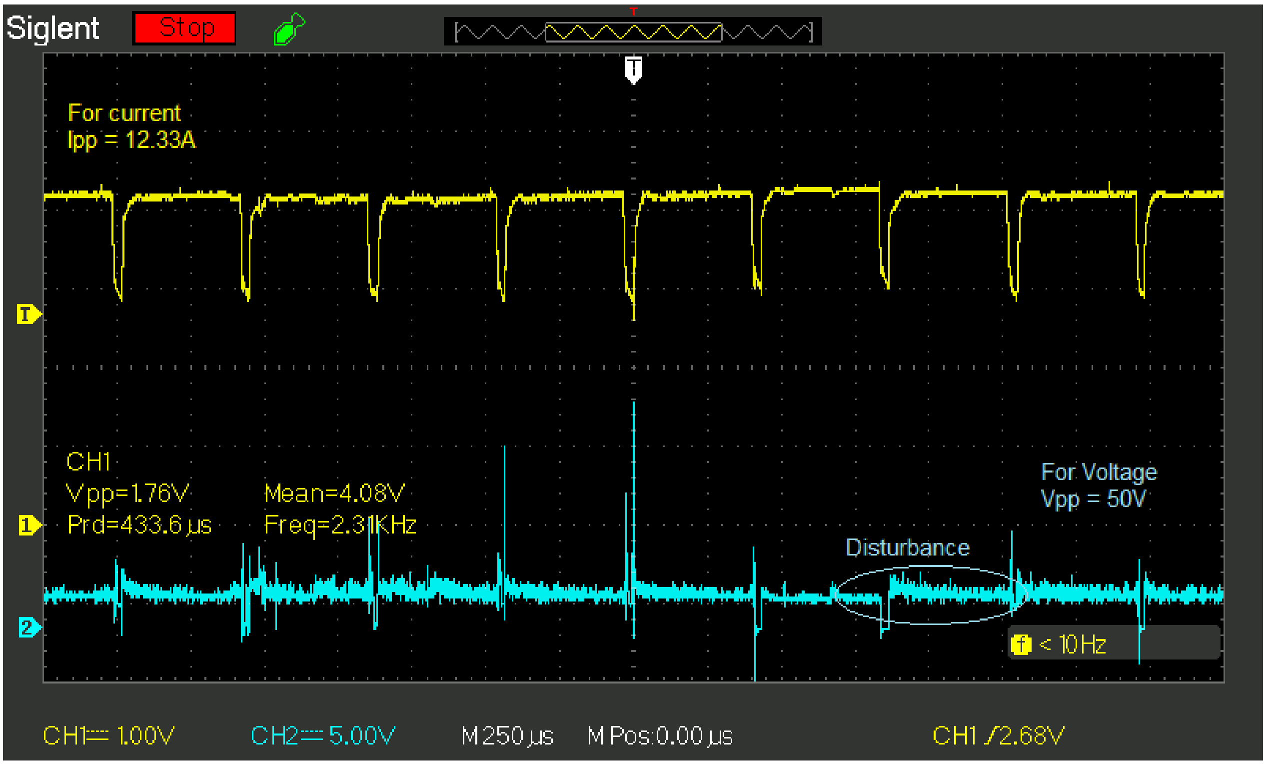

CH1
Vpp=1.76V Mean=4.08V
Prd=433.6 µs Freq=2.31KHz

CH1⎓ 1.00V CH2⎓ 5.00V M 250 µs M Pos:0.00 µs CH1 ∕ 2.68V

Figure 5.33: Current and Voltage Waveform, I_p = 12 amp., T_{on} = 400 µsec and T_R = 1200 rpm

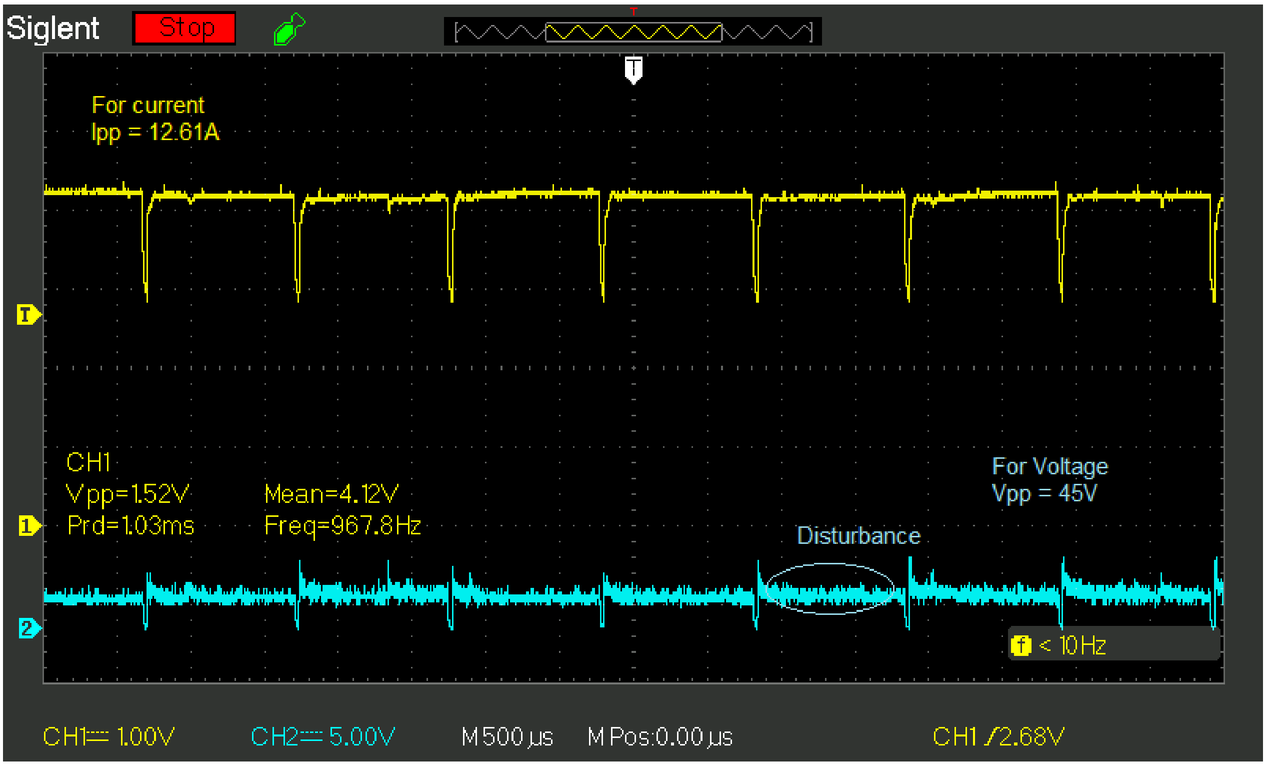

Figure 5.34: Current and Voltage Waveform, I_p = 12 amp., T_{on} = 1000 µsec and T_R = 1200 rpm

Figure 5.32 to 5.34: shows the actual waveform of current (CH1) and voltage (CH2). One block in y-axis represents 1 volt and 2.5 volts at 0 amp. for channel 1 and 5 volts for channel 2. On x-axis time in µsec. the peak-to-peak current for channel 1 is 11.65, 12.33 and 12.61 amp. and voltage of 50, 50 and 45 volt for channel 2 respectively.

Figure 5.35 to 5.37: shows the actual waveform of current (CH1) and voltage (CH2). One block in y-axis represents 2, 1 and 1 volt. At 0 amp. 2.5 volt for channel 1 and 2, 2 and 5 volt for channel 2. On x-axis time in µsec. the peak-to-peak current for channel 1 is 18.33, 18.33 and 17.5 amp. and voltage of 40, 50 and 60 volts form channel 2 respectively.

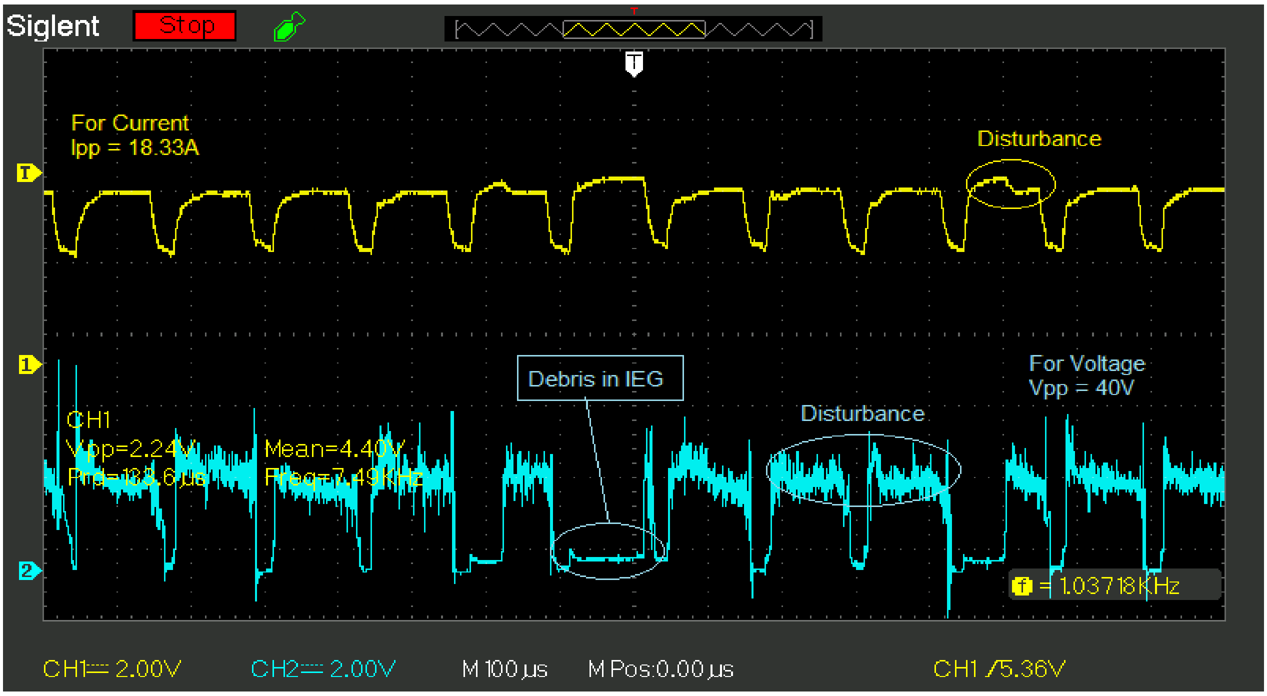

Figure 5.35: Current and Voltage Waveform, I_p = 18 amp., T_{on} = 100 µsec and T_R = 1800 rpm

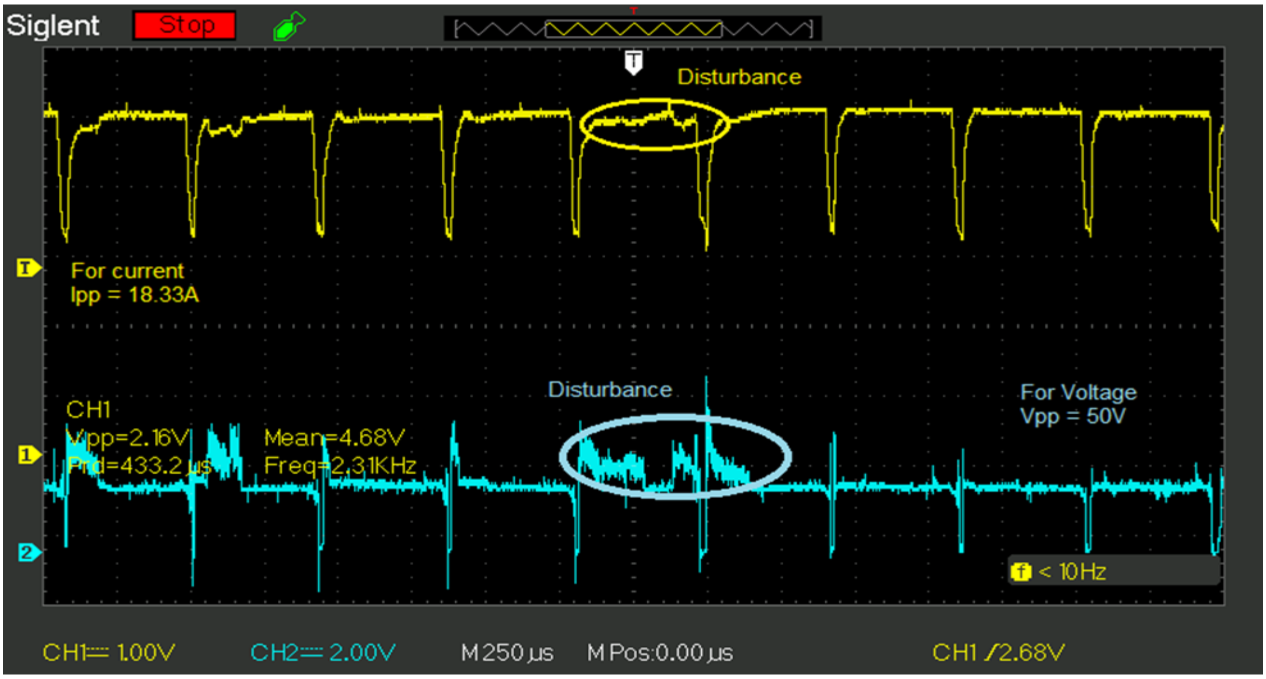

Figure 5.36: Current and Voltage Waveform, Ip = 18 amp., T_{on} = 400 µsec and T_R = 1800 rpm

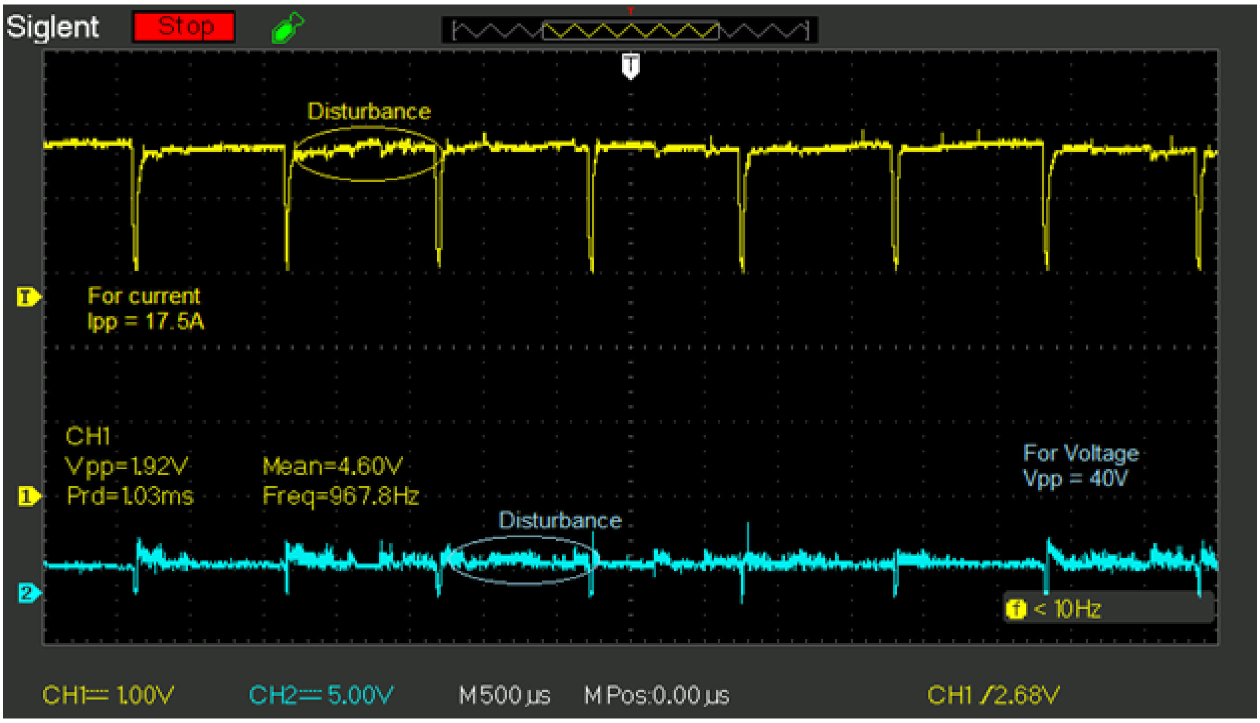

Figure 5.37: Current and Voltage Waveform, I_p = 18 amp., T_{on} = 1000 µsec and T_R = 1800 rpm

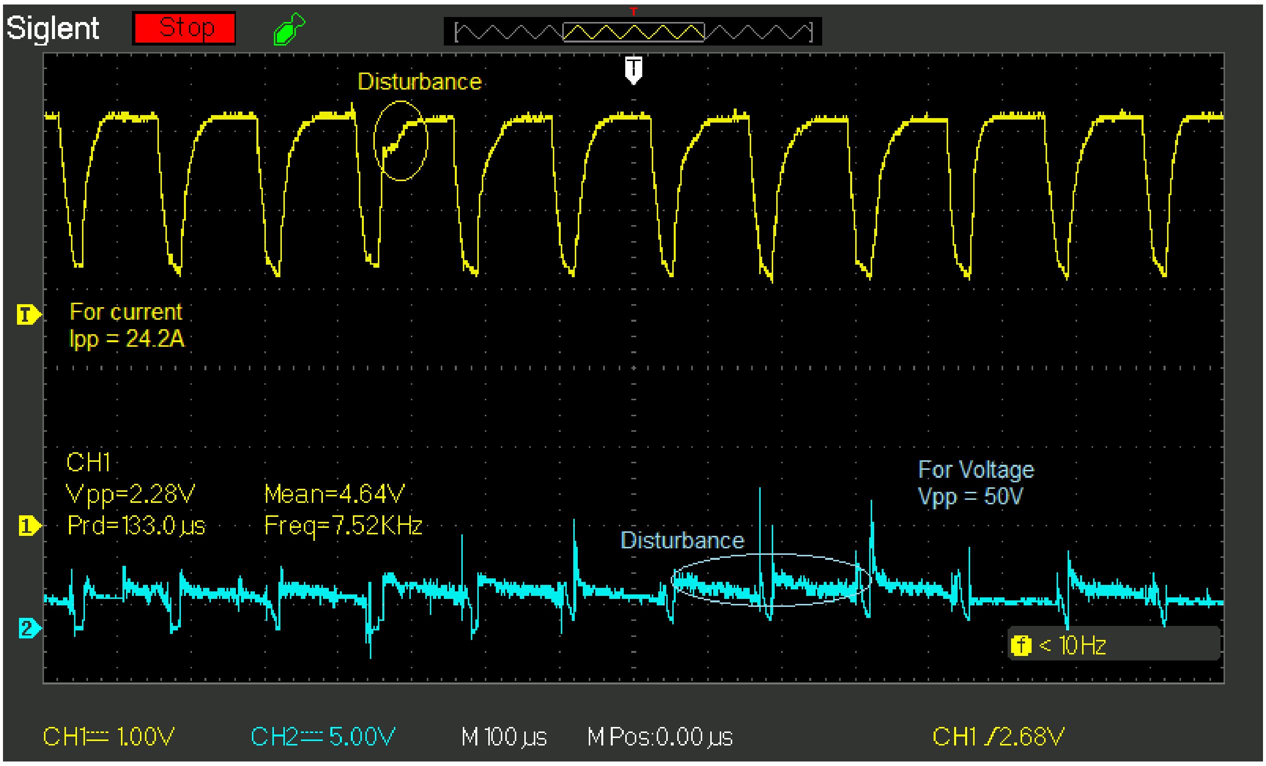

Figure 5.38: Current and Voltage Waveform, I_p = 24 amp., T_{on} = 100 µsec and T_R = 2400 rpm

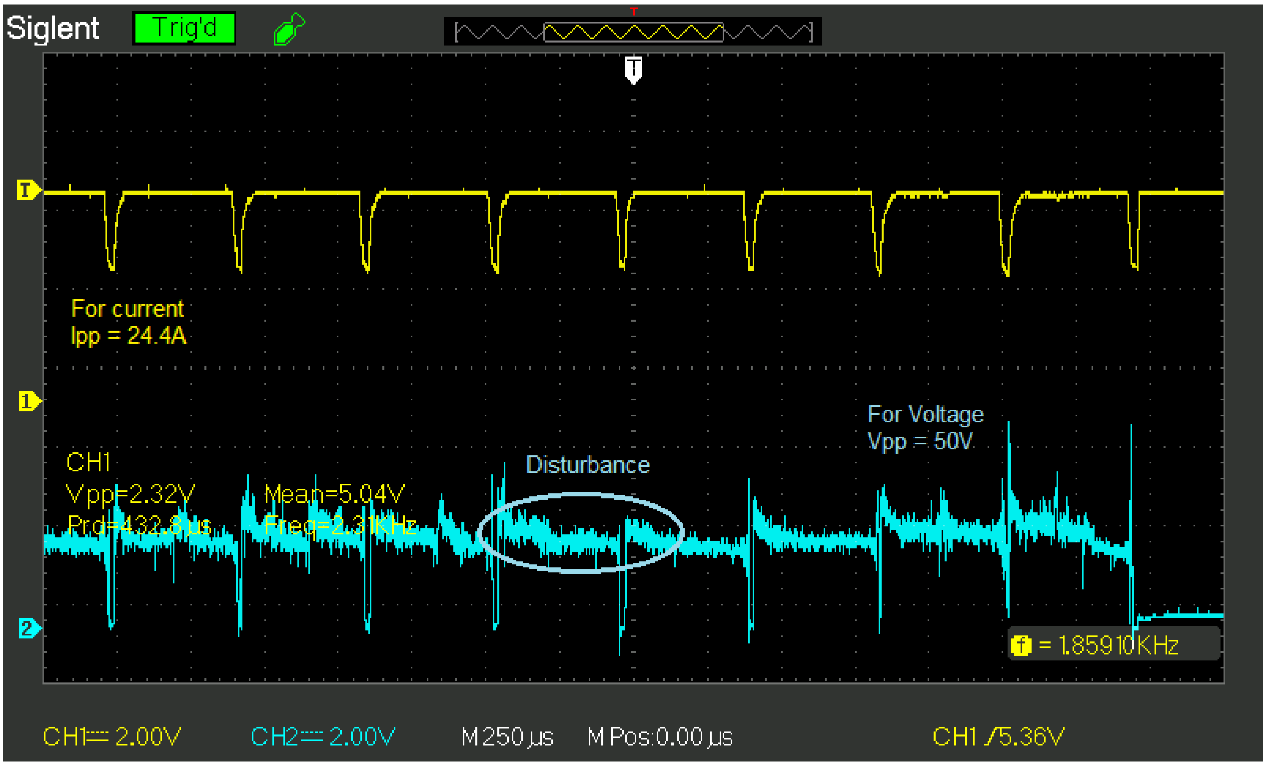

Figure 5.39: Current and Voltage Waveform, I_p = 24 amp., T_{on} = 400 µsec and T_R = 2400 rpm

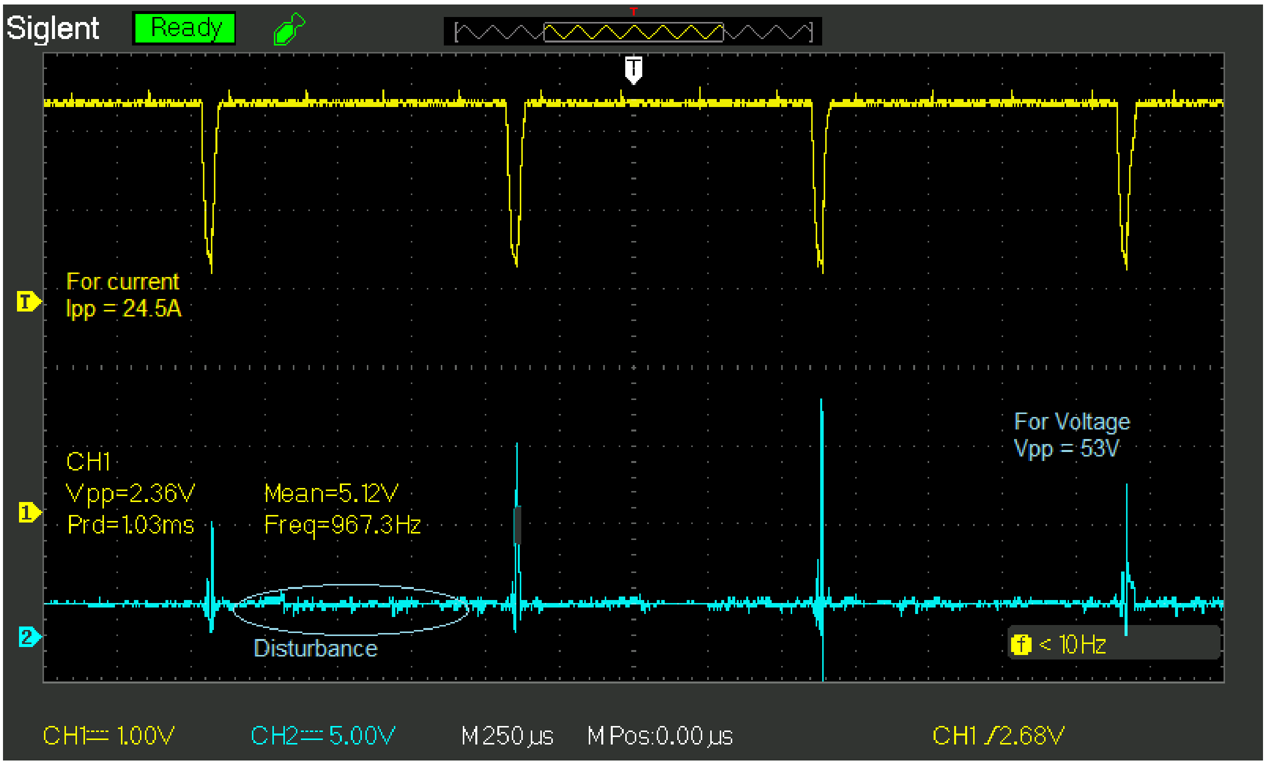

Figure 5.40: Current and Voltage Waveform, I_p = 24 amp., T_{on} = 1000 µsec and T_R = 2400 rpm

Figure 5.38 to 5.40: shows the actual waveform of current (CH1) and voltage (CH2). One block in y-axis represents 1, 2 and 1 volt. At 0 amp. 2.5 volt for channel 1 and 5, 2 and 5 volt for channel 2. On x-axis time in µsec. the peak-to-peak current for channel 1 is 24.2, 24.4 and 24.5 amp. and voltage of 50, 50 and 53 volts form channel 2 respectively

All waveform represents less disturbance in the current while more disturbance in voltage waveform. The actual current and voltage waveform differ from ideal waveform, the primary reason for the sharp peaks and fluctuation in the waveform is a high frequency of pulse charging-discharging the capacitor that results in discharge energy. The secondary reason for disturbance in the waves due to noise.

5.11 XRD Analysis

The orientation of crystal structure have been studied by a powerful material characterization technic i.e. known as X-ray diffraction (XRD) metod. It is used to identify the modification in texture arrangement of the grains in the crystal structure of specimen.

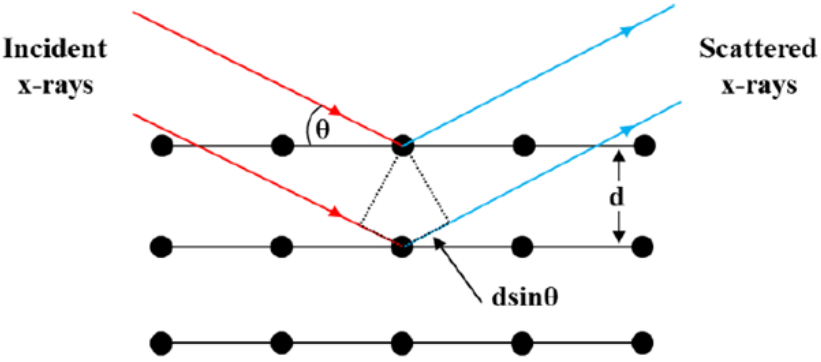

Figure 5.41: X-Ray Diffraction (Mandaloi et al, 2016)

X-rays incident on the workpiece is either transmitted with consistent direction or scattered (diffracted) by electrons from the workpiece. X-rays have good diffraction characteristics, Since the amplitude of d-spacing's and their wavelengths are of the same order in the crystal lattice.

XRD - analysis only uses effective interference of scattered X-rays. Figure 5.41 gives an exemplification of diffraction process. If the scattering of atoms is arranged uniformly in a crystal lattice, with separation d, the scattered waves are added effectively in directions of path-length difference 2dsinθ equals to a round number of X-ray wavelengths. The resulting reflection point at multiple angles of 2θ yields a diffraction pattern unique to specific crystals. Accordingly, all the phases present in the material can be easily be identified, and the ratios between their amounts can be correlated.

XRD analysis was conducted on the samples machining with tool rotation EDM using 100, 400 and 1000 µsec T_{on} with T_R i.e. as run no. 3, 7 and 17 on Bruker D8 Advance and subject to 40 kV cathode voltage and 40 mA current to observed metallurgical changes.

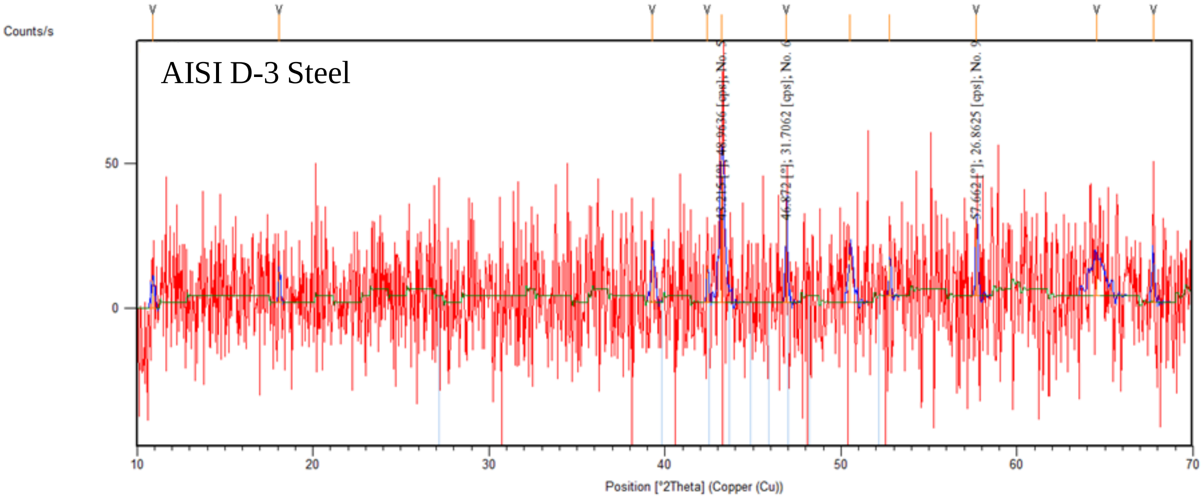

(a)

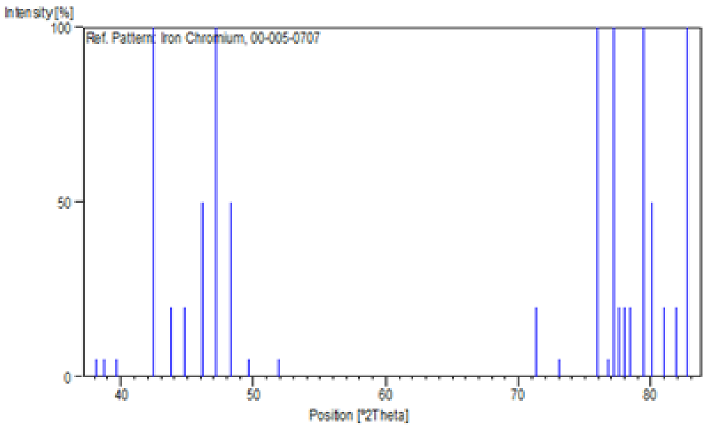

(b)

Figure 5.42: XRD investigation (a) XRD Spectra at T_{on} 100 µsec, (b) Stick Pattern of Peak no. 5

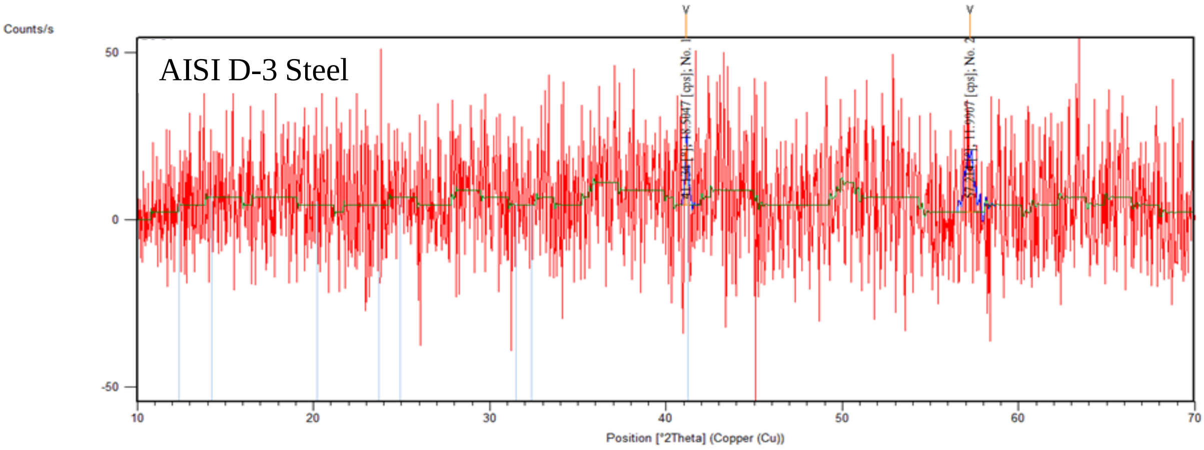

(a)

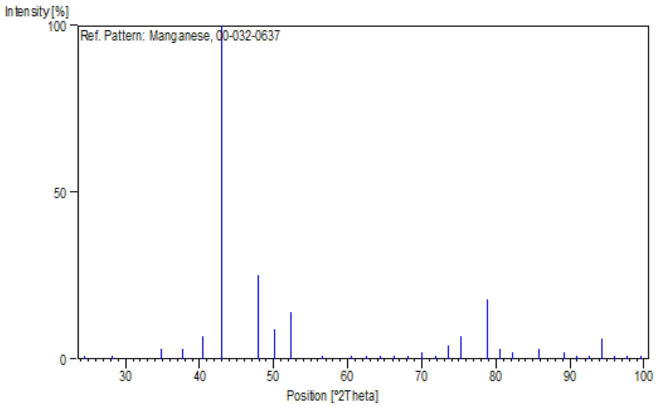

(b)

Figure 5.43: XRD investigation (a) XRD Spectra at T_{on} 400 µsec, (b) Stick Pattern of Peak no. 1

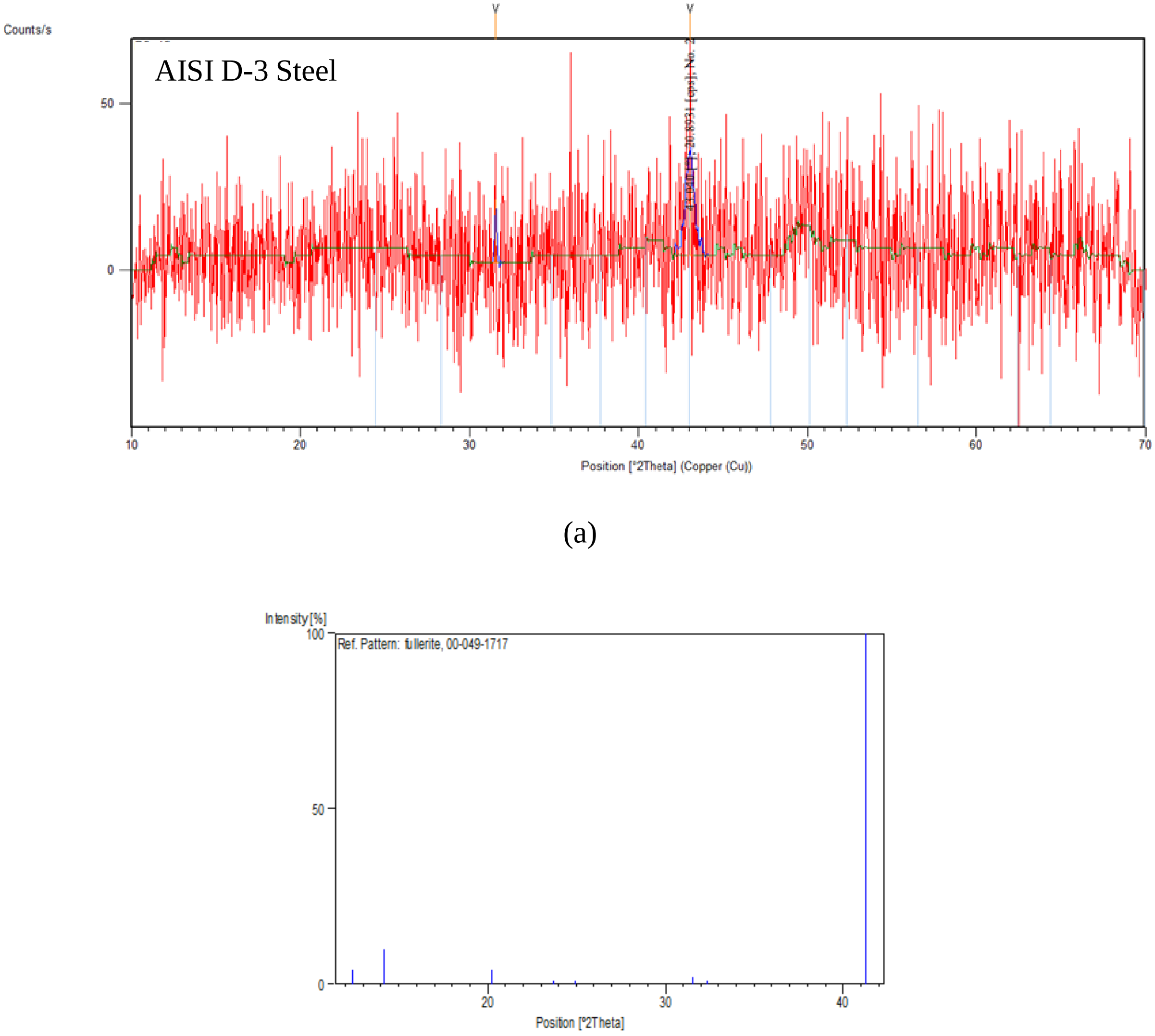

(a)

(b)

Figure 5.44: XRD investigation (a) XRD Spectra at T_{on} 1000 µsec, (b) Stick Pattern of Peak no. 2

Figure 5.42 (a) the maximum intensity of peak at position 43.215°, peak height 48.9636 [cps] at peak no. 5. At 100 µsec T_{on}. The stick pattern figure 5.42 (b) at peak no. 20 and 24 for Iron Chromium (FeCr)); d [A] is 1.20500 and 1.16600; 2 Theta at 79.472 and 82.697; I (Intensity %) is 100.0.

Figure 5.43 (a) The maximum intensity of peak at position 43.040°, peak height 20.8931 [cps] at peak no. 2. At 400 µsec T_{on}. The stick pattern figure 5.43 (b) at peak no. 6 for Manganese (Mn); h, l, k are 3, 3, 0; d [A] is 2.10100; 2 Theta at 43.016; I (Intensity %) is 100.0.

Figure 5.44 (a) the maximum intensity of peak at position 41.134°, peak height 18.5047 [cps] at peak no.1. At 1000 µsec T_{on}. The stick pattern figure 5.44 (b) at peak no. 8 for Carbon (C60) also known as fullerite; h, l, k are 4, 4, 0; d [A] is 2.18597; 2 Theta at 41.266; I (Intensity %) is 100.0. The Diffraction data was collected and the pressure-induced phase was produced due to quenching. The cubic FCC phase is always found in the samples, quenched from the temperature range 720-870 K and 13 GPa.

X-ray diffraction method is attempted to determine the relocation of material. Figure 5.42 to 5.44 represents the XRD results of the machined surface. The profile of XRD represents that the crystallography structure of the composite is modified. When the T_{on}, 1000 µsec shown in XRD spectra, then the peak is sharp, corresponding 2 theta 43.215 and intensity is 48.9636° too high; When the T_{on} is 100 µsec shown in XRD spectra, then the diffraction peak reduced, corresponding 2 theta 41.134 and intensity is 18.5047° somewhat low and peaks are broaden. This shows when T_{on} rises the intensity of peaks are sharp so that the crystallography structure of the material is modified. The chromium is insoluble and it is significant for the dense structure. The solid solution was formed by Si and C at temperature (8000–12,000 C) because Cr has good solubility with C. As Cr existing in the compound and it forms the FeCr. The presence of FeCr responsible to increase its mechanical properties such as hardness, toughness, tensile strength, and thermal wear resistance. The properties of material enhanced due to the homogeneous dispersion of the atoms inside the composites of the metal matrix due to uniform energy distribution.T_R and dielectric fluid have a significant effect on cleaning and cooling the workpiece. The recrystallization of material affected because pitting action and crack density minimized and space between the lattices are filled by another atom.

5.12 Correlation of Actual and Predicted Terms

The correlation of predicted and actual terms of the MRR, TWR and the R_a is shown in figure 5.45. The predicted models are satisfactory and the respective terms are in excellent accordance with the corresponding terms.

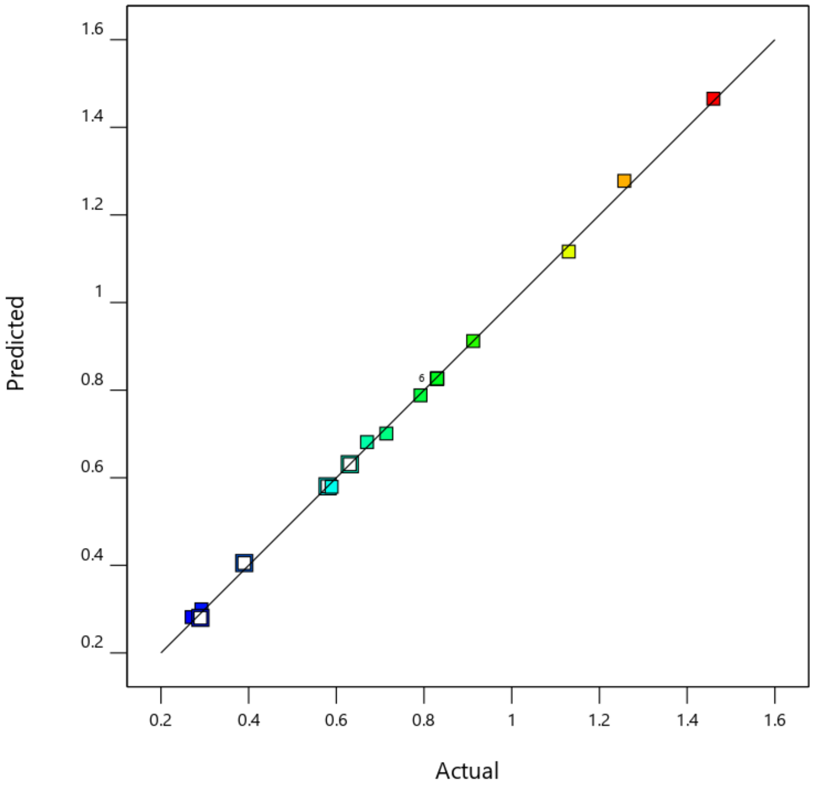

(a)

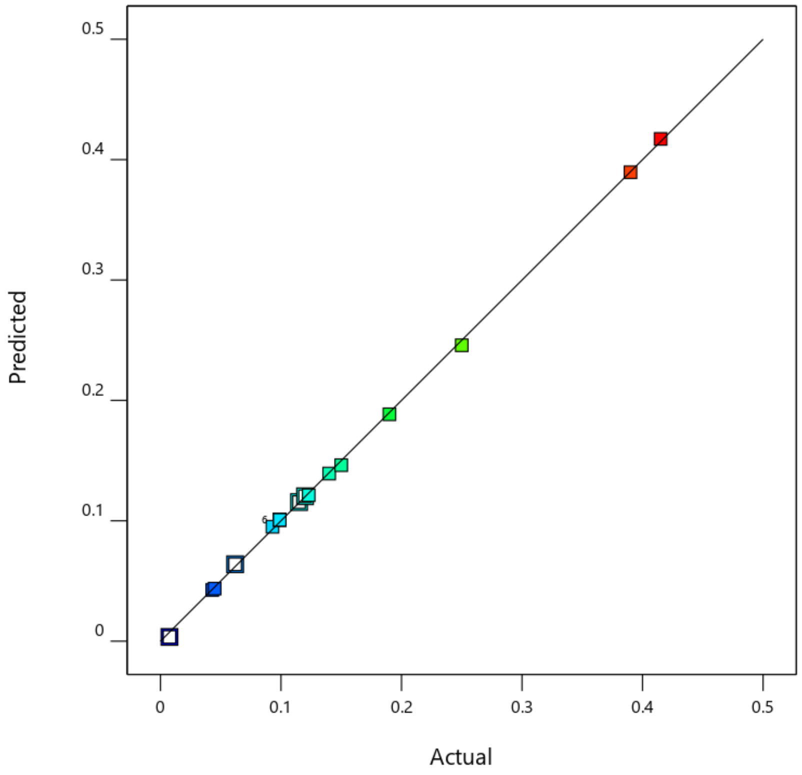

(b)

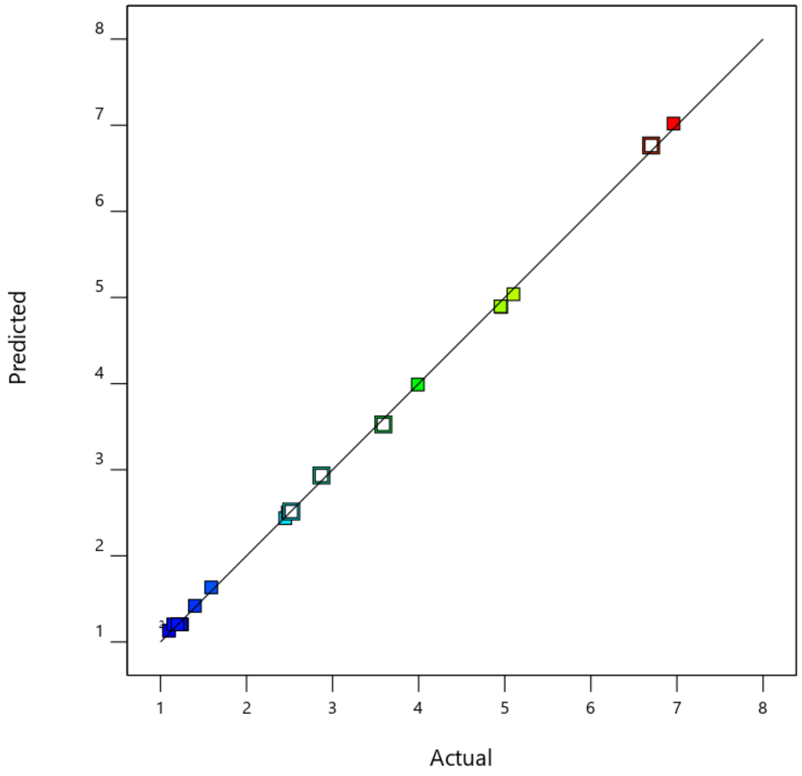

(c)

Figure 5.45: Correlation of predicted and exemplification values

(a) MRR (b) TWR (c) R_a

CHAPTER 6

RESULT AND DISCUSSION OF EN-31 STEEL

6.1 Analysis and Discussion of EN-31steel

The significance of machining process variables on responses i.e. MRR, TWR and R_a were investigated by EDM with tool rotation process for EN-31 steel. RSM is applied for analysing the parameters. DOE is one of the most significant approach to find out the relationship between appropriate methods, gathering experimental data and deriving inferences from observations that are subjected to variation. It helps to identify the most important controlling variables of the process. The optimal set of significant machining parameters were developed. The minimization of experimental errors will increase the performance of the tool rotation EDM process. The present investigation uses RSM central composite design of experimental technique which is simple and cost-effective as it uses a minimum number of experimental runs to understand the effect of various machining process parameters on response variables.

The ANOVA fitted model for MRR, TWR and R_a for EN-31 and electrolyte copper tool is given in table 6.1, 6.2 and 6.3. The tables shows that the model selected for experimentation is significant and also represent the contribution of each parameters.

Table 6.1 ANOVA fitted model for MRR on EN31 Steel-Electrolyte copper tool

Source	SS	df	MS	FV	PV		% contribution
Model	0.5663	9	0.0629	2230.97	< 0.0001	significant	
I_p-Current	0.0355	1	0.0355	1259.60	< 0.0001		6.964881
T_{on}-Pulse-on Time	0.0594	1	0.0594	2104.73	< 0.0001		11.65391
T_R-Tool Rotation	0.2259	1	0.2259	8008.05	< 0.0001		44.32019
I_p T_{on}	0.0005	1	0.0005	18.18	0.0017		0.098097
I_p T_R	0.0854	1	0.0854	3029.44	< 0.0001		16.75495
T_{on} T_R	0.0689	1	0.0689	2442.84	< 0.0001		13.51776
I_p^2	0.0330	1	0.0330	1168.61	< 0.0001		6.474397
T_{on}^2	0.0007	1	0.0007	24.68	0.0006		0.137336
T_R^2	0.0001	1	0.0001	3.49	0.0913		0.019619
Residual	0.0003	10	0.0000				0.058858
Lack of Fit	0.0003	5	0.0001				
Pure Error	0.0000	5	0.0000				
Cor Total	0.5666	19					
R^2	0.9367	Adjusted R^2		0.9290	Predicted R^2		0.9210

Table 6.2 ANOVA fitted model for TWR on EN31 Steel-Electrolyte copper tool

Source	SS	df	MS	FV	PV		% contribution
Model	0.0927	9	0.0103	1007.74	< 0.0001	significant	
I_p-Current	0.0145	1	0.0145	1413.69	< 0.0001		12.83186
T_{on}-Pulse-on Time	0.0358	1	0.0358	3502.23	< 0.0001		31.68142
T_R-Tool Rotation	0.0060	1	0.0060	588.99	< 0.0001		5.309735
$I_p\ T_{on}$	0.0019	1	0.0019	186.59	< 0.0001		1.681416
$I_p\ T_R$	0.0001	1	0.0001	11.00	0.0078		0.088496
$T_{on}\ T_R$	0.0017	1	0.0017	163.61	< 0.0001		1.504425
I_p^2	0.0030	1	0.0030	294.68	< 0.0001		2.654867
T_{on}^2	0.0423	1	0.0423	4133.39	< 0.0001		37.43363
T_R^2	0.0076	1	0.0076	744.16	< 0.0001		6.725664
Residual	0.0001	10	0.0000				0.088496
Lack of Fit	0.0001	5	0.0000				
Pure Error	0.0000	5	0.0000				
Cor Total	0.0928	19					
R^2	0.9187	Adjusted R^2		0.9075	Predicted R^2		0.8989

Table 6.3 ANOVA fitted model for R_a on EN31 Steel-Electrolyte copper tool

Source	**SS**	**df**	**MS**	**FV**	**PV**		**% contribution**
Model	205.03	9	22.78	7544.48	< 0.0001	significant	
I_p-Current	64.09	1	64.09	21225.78	< 0.0001		49.72719
T_{on}-Pulse-on Time	9.68	1	9.68	3206.58	< 0.0001		7.510676
T_R-Tool Rotation	0.0048	1	0.0048	1.60	0.2352		0.003724
I_p T_{on}	1.20	1	1.20	397.25	< 0.0001		0.931076
I_p T_R	1.96	1	1.96	649.16	< 0.0001		1.520757
T_{on} T_R	0.0073	1	0.0073	2.41	0.1515		0.005664
I_p^2	46.52	1	46.52	15407.66	< 0.0001		36.0947
T_{on}^2	4.91	1	4.91	1625.32	< 0.0001		3.809651
T_R^2	0.4809	1	0.4809	159.25	< 0.0001		0.373129
Residual	0.0302	10	0.0030				0.023432
Lack of Fit	0.0302	5	0.0060				
Pure Error	0.0000	5	0.0000				
Cor Total	205.06	19					
R^2	0.9586	Adjusted R^2		0.9373	Predicted R^2		0.9298

*** SS=Sum of Squares, MS= Mean Square, FV= F-value, PV= p-value**

6.2 Mathematical Model and Diagnostics

6.2.1 The Mathematical model expressing the response variables and process parameters which were developed for minimizing the number of experiments of tool rotation EDM. The developed mathematical model for EN-31 Steel responses through analysis of regression using Design Expert CCD are given below:

$$\begin{aligned} MRR = {} & 1.22923 + (0.066155 \ast \mathrm{Ip}) - (0.000935 \ast \mathrm{Ton}) - (0.000895 \ast \mathrm{TR}) \\ & + \{(2.93297 \ast 10^{-6}) \ast Ip \ast Ton\} + (0.000029 \ast Ip \ast TR) \\ & + \{(3.39970 \ast 10^{-7}) \ast Ton \ast TR\} - (0.003041 \ast Ip^{2}) \\ & + \{(8.97306 \ast 10^{-8}) \ast Ton^{2}\} - \{(1.66162 \ast 10^{-8}) \ast TR^{2}\} \end{aligned} \tag{6.1}$$

$$\begin{aligned} TWR = {} & -0.446646 + (0.040690 \ast Ip) - (0.000896 \ast Ton) + (0.000437 \ast TR) \\ & - \{(5.65700 \ast 10^{-6}) \ast \mathrm{Ip} \ast \mathrm{Ton}\} + \{(1.04167 \ast 10^{-6}) \ast \mathrm{Ip} \ast \mathrm{TR}\} \\ & + \{(5.29710 \ast 10^{-8}) \ast Ton \ast TR\} - (0.000919 \ast Ip^{2}) \\ & + \{(6.99148 \ast 10^{-7}) \ast Ton^{2}\} - \{(1.46111 \ast 10^{-7}) \ast TR^{2}\} \end{aligned} \tag{6.2}$$

$$\begin{aligned} Ra = {} & 54.63071 - (4.70574 \ast Ip) - (0.008120 \ast Ton) - (0.006754 \ast TR) \\ & - (0.000142 \ast Ip \ast Ton) + (0.000138 \ast Ip \ast TR) \\ & + \{(1.10507 \ast 10^{-7}) \ast Ton \ast TR)\} + (0.114255 \ast Ip^{2}) \\ & + \{(7.53424 \ast 10^{-6}) \ast Ton^{2}\} + \{(1.16157 \ast 10^{-6}) \ast TR^{2}\} \end{aligned} \tag{6.3}$$

6.2.2 Diagnostics of Predicted and Actual Parameters

The predicted and actual values have been diagnosed through the regression analysis. The residual of predicted and actual values are in good agreement. The predicted and actual values are given in the table 6.4

Table 6.4 Predicted and actual values of EN-31 Steel for MRR, TWR and R_a

Run No.	**MRR**		**TWR**		**R_a**	
	Actual Value	**Predicted Value**	**Actual Value**	**Predicted Value**	**Actual Value**	**Predicted Value**
1	0.7800	0.7815	0.064	0.0628	0.5000	0.4729
2	0.4330	0.4396	0.01	0.0097	6.45	6.55
3	0.5100	0.5163	0.06	0.0627	2.15	2.18
4	0.6064	0.6062	0.0847	0.0861	0.0234	0.0228
5	0.4736	0.4710	0.1847	0.1843	4.85	4.85
6	0.6064	0.6062	0.0847	0.0861	0.0234	0.0228
7	0.6064	0.6062	0.0847	0.0861	0.0234	0.0228
8	0.6064	0.6062	0.0847	0.0861	0.0234	0.0228
9	0.1785	0.1742	0.009	0.0095	7.08	7.03
10	0.4200	0.4190	0.004	0.0041	0.3800	0.4090
11	0.4950	0.4988	0.0358	0.0376	8.00	8.01
12	0.6064	0.6062	0.0847	0.0861	0.0234	0.0228
13	0.5229	0.5197	0.132	0.1321	0.0500	0.0669
14	0.6064	0.6062	0.0847	0.0861	0.0234	0.0228
15	0.6700	0.6738	0.256	0.2518	2.05	2.03
16	0.8600	0.8523	0.1575	0.1554	9.31	9.27
17	0.4300	0.4274	0.078	0.0758	1.18	1.17
18	0.1590	0.1606	0.067	0.07	8.19	8.17
19	0.7443	0.7493	0.251	0.2547	3.90	3.97
20	0.5600	0.5539	0.1	0.0962	1.82	1.73

6.3 ANOVA Significant Factors on Responses

The ANOVA significant factors on MRR, TWR and Ra have been analysed as:

6.3.1 Material Removal Rate

Table 4.4 (in last chapter) represents the CCD as well as performance measures for every experiment. The collection and analysis of experimental data to set up significance for several parametric responses using statistical analysis ANOVA at the significant level of 0.05 performed. Table 6.1 represents statistical analysis for MRR having %age of participation of every variable along with their dominance. The parameters such as I_p, T_{on} and T_R, their square terms and interrelationship terms: $I_p \times T_{on}$, $I_p \times T_R$ and $T_{on} \times T_R$ are significant parameters. The ANOVA table signifies, T_R is valuable parameter for MRR having highest %age of participation of 44.32 % succeeded by T_{on} and I_p with participation percentage of 11.65 % and 7 % respectively. The Model F-value (2230.97) indicates the model is significant. The P-values (Values of "Prob> F") lower than 0.0500 indicates that model values are prominent. The $I_{p,}$ T_{on}, T_R, I_p $T_{R,}$ T_{on} T_R, and $I_p^2$are important model terms. The model terms are not significant if values greater than 0.1000. The determination coefficient (R^2), adjusted (R^2) and Predicted (R^2) values are identified as 93.67 %, 92.90 % and 92.10 % respectively.

6.3.2 Tool Wear Rate

The ANOVA table 6.2 for TWR having participation percentage for every variable and their relationship. The I_p, T_{on} and T_R, square terms of I_p, T_{on} and T_R and interaction terms: $I_p \times T_{on}$, $I_p \times T_R$ and $T_{on} \times T_R$ are important parameters. Table signify that T_{on} is considered to the most significant parameter for TWR having percentage of participation of 31.68 % followed by I_p and T_R with percentage contribution of 12.831 %, 5.3 % respectively. The Model F-value of 1007.74 suggests, the model is significant. The P-values (Values of "Prob> F") lower than 0.0500 represents that model values having significance. The I_p, T_{on}, T_R, I_p T_{on}, T_{on} T_R, I_p^2, T_{on}^2 and T_R^2 are relevant to model terms. The model terms are not significant if Values greater than 0.1000. The determination coefficient (R^2), adjusted (R^2) and Predicted (R^2) values are identified as 91.87 %, 90.75 % and 89.89 % respectively.

6.3.3 Surface Roughness

The ANOVA table 6.3 for R_a having the participation of each variable and their relationship. The I_p, T_{on} and T_R, square terms of I_p, T_{on} and T_R and interaction terms: $I_p \times T_{on}$, $I_p \times T_R$ and $T_{on} \times T_R$ are important parameters. Table signify that I_p is considered to most significant parameter for R_a having a percentage of participation 49.72 % succeeded by T_{on} having percentage contribution of 7.51 %. The Model F-value of 7544.48 indicates the model is significant. The P-values (Values of "Prob> F") less than 0.0500 indicate model terms are significant. In this case, I_p, T_{on}, I_p T_R, I_p^2, T_{on}^2 are significant model terms. Values greater than 0.1000 indicate the model terms are not significant. The determination coefficient (R^2) adjusted (R^2) and Predicted (R^2) values are identified as 95.86 %, 93.73 % and 92.98 % respectively.

6.4 Effect of Factors on Responses

The impact of input variables on MRR, TWR and R_a are as:

6.4.1 Effect of Tool Rotation

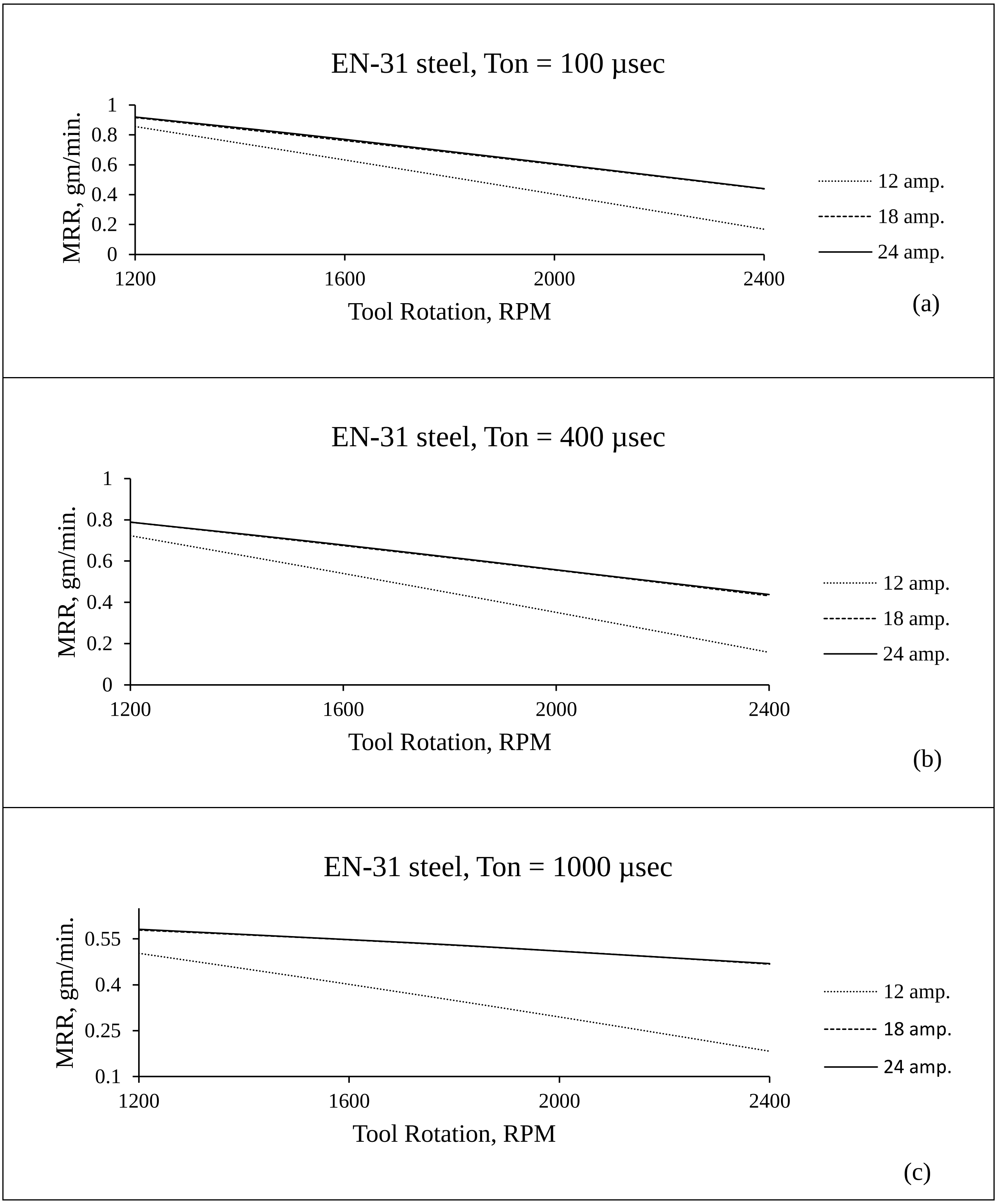

Figure 6.1: Effect of tool rotation on MRR at T_{on} 100, 400 and 1000 µsec

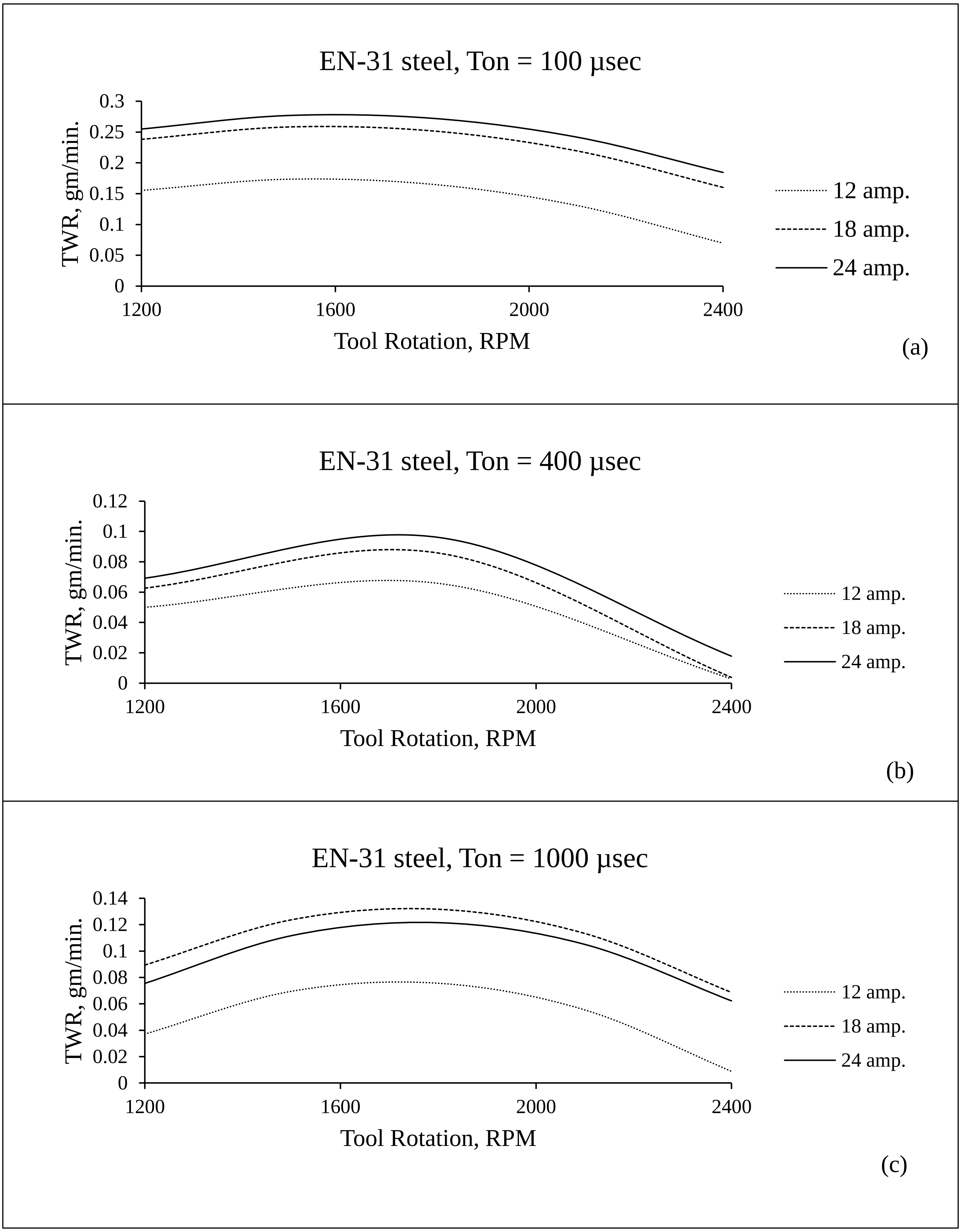

Figure 6.2: Effect of tool rotation on TWR at T_{on} 100, 400 and 1000 µsec

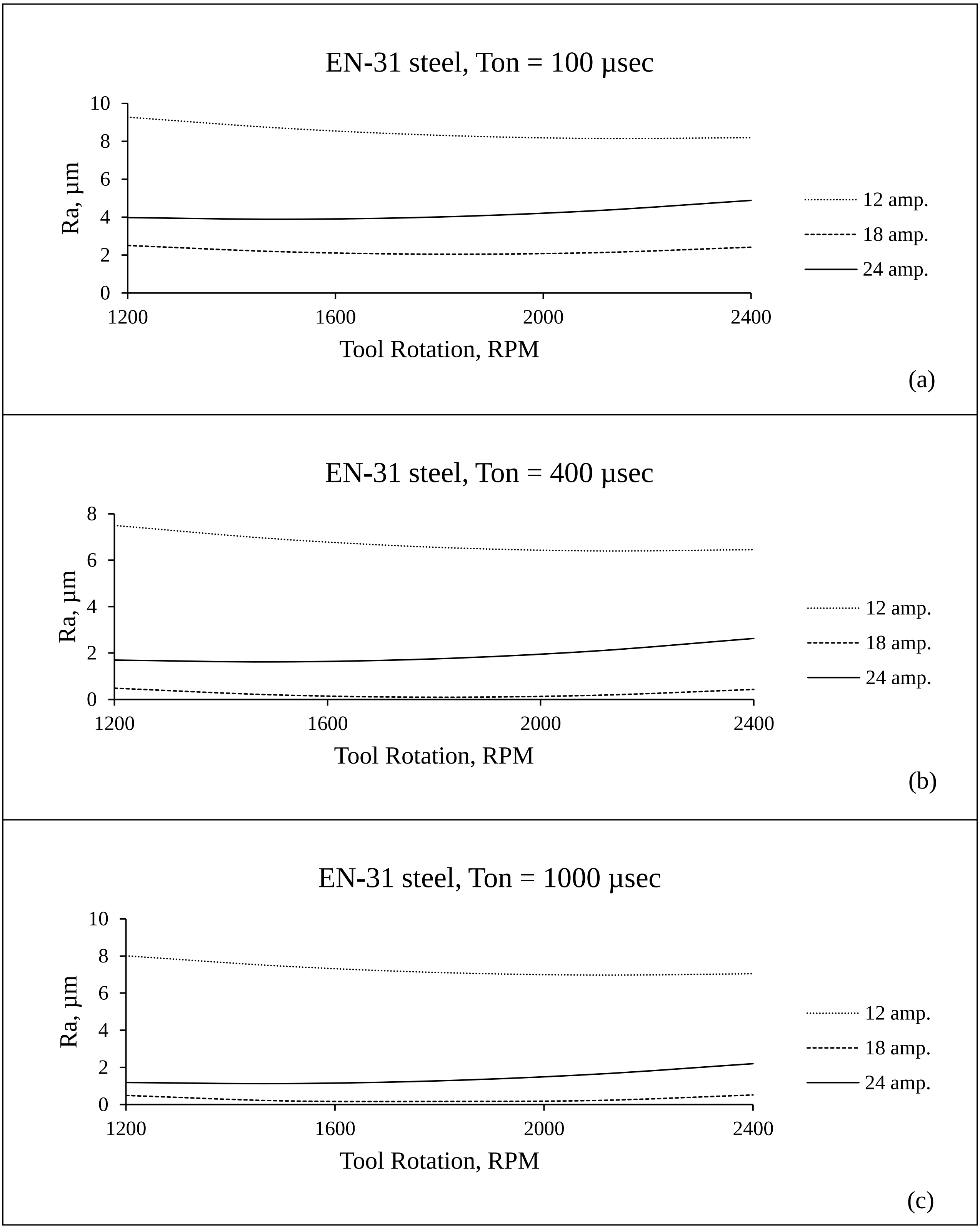

Figure 6.3: Effect of tool rotation on R_a at T_{on} 100, 400 and 1000 µsec

Figure 6.1 (a-c) shows plot between MRR and T_R for 100, 400 and 1000 μsec T_{on}. It shows that MRR is decreases as T_R increases from 1200 to 2400 rpm for all values of T_{on}. The MRR decreases as T_R increases for all values of I_p, but there is negligible change in MRR for 18 and 24 amp. I_p.

Figure 6.2 (a-c) shows plot between TWR and T_R on 100, 400 and 1000 T_{on}. It shows that TWR increases as T_R increases from 1200 rpm to 1800 rpm and than it starts decreasing from 1800 to 2400 rpm for all value of currents. At the highest T_R the TWR is 0.184 gm/min. at 100 μsec. The TWR is higher for high value of currents.

Figure 6.3 (a-c) shows plot between R_a and T_R on 100, 400 and 1000 T_{on}. It shows that the value of R_a decreases as T_R increases upto a certain value and than it starts increasing for all value of currents. The lower value of R_a noticed at 18 amp. I_p.

The T_R reduces R_a mainly due to the uniform distribution of thermal energy. It reveals reduction in R_a. The heating, melting and vapourisation of material takes place due to formation of plasma in IEG. The effectiveness of spark on the workpiece decreases due to enhancement in T_R.

The eventually distribution of pulse discharge energy reduces the value of R_a. The dielectric fluid flow also act as a coolant and perform heat treatment during machining. The T_R increases flushing efficiency between workpiece and tool, but at higher rpm thermal effect decrease.

6.4.2 Effect of Current

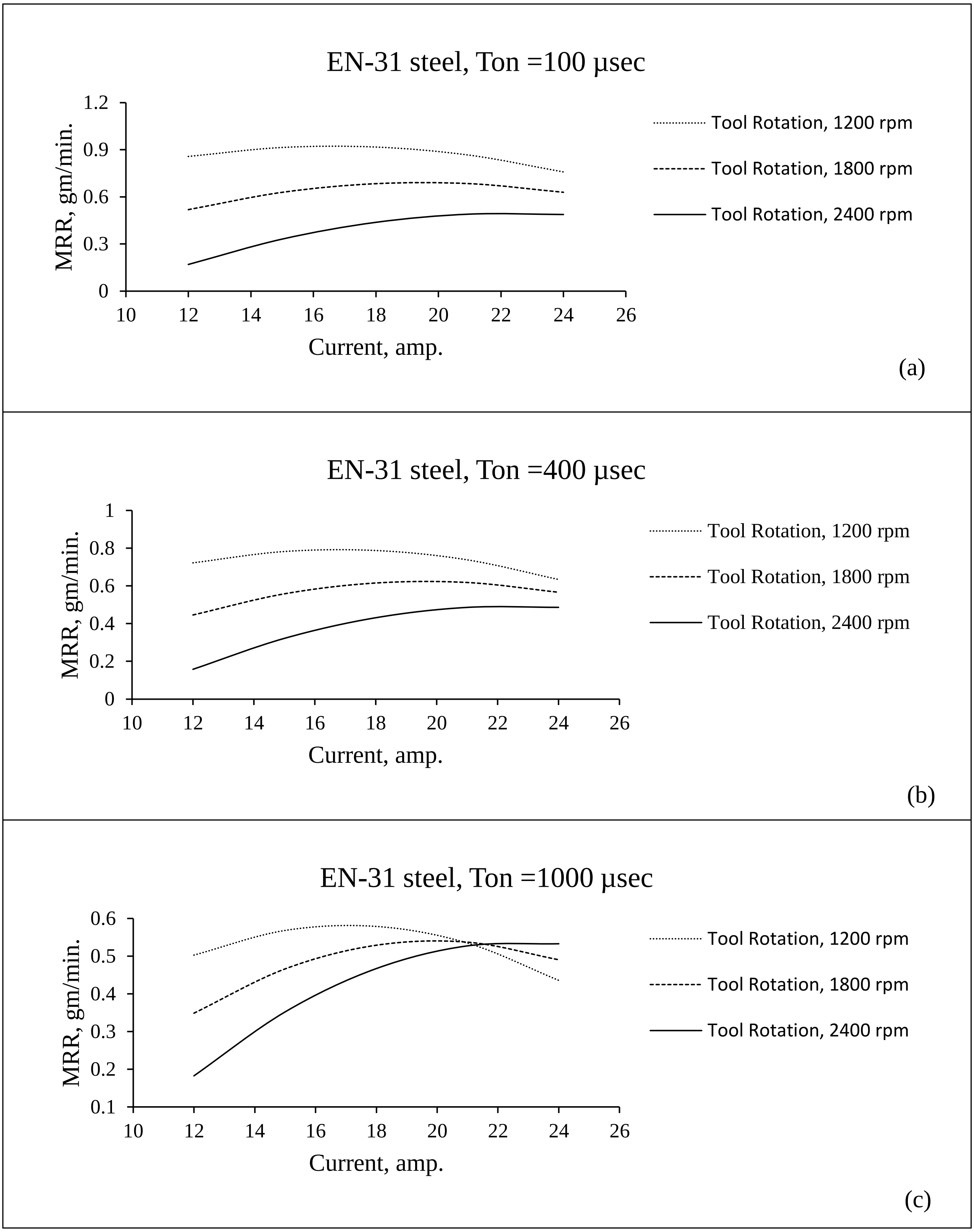

Figure 6.4: Effect of current on MRR at T_{on} 100, 400 and 1000 µsec

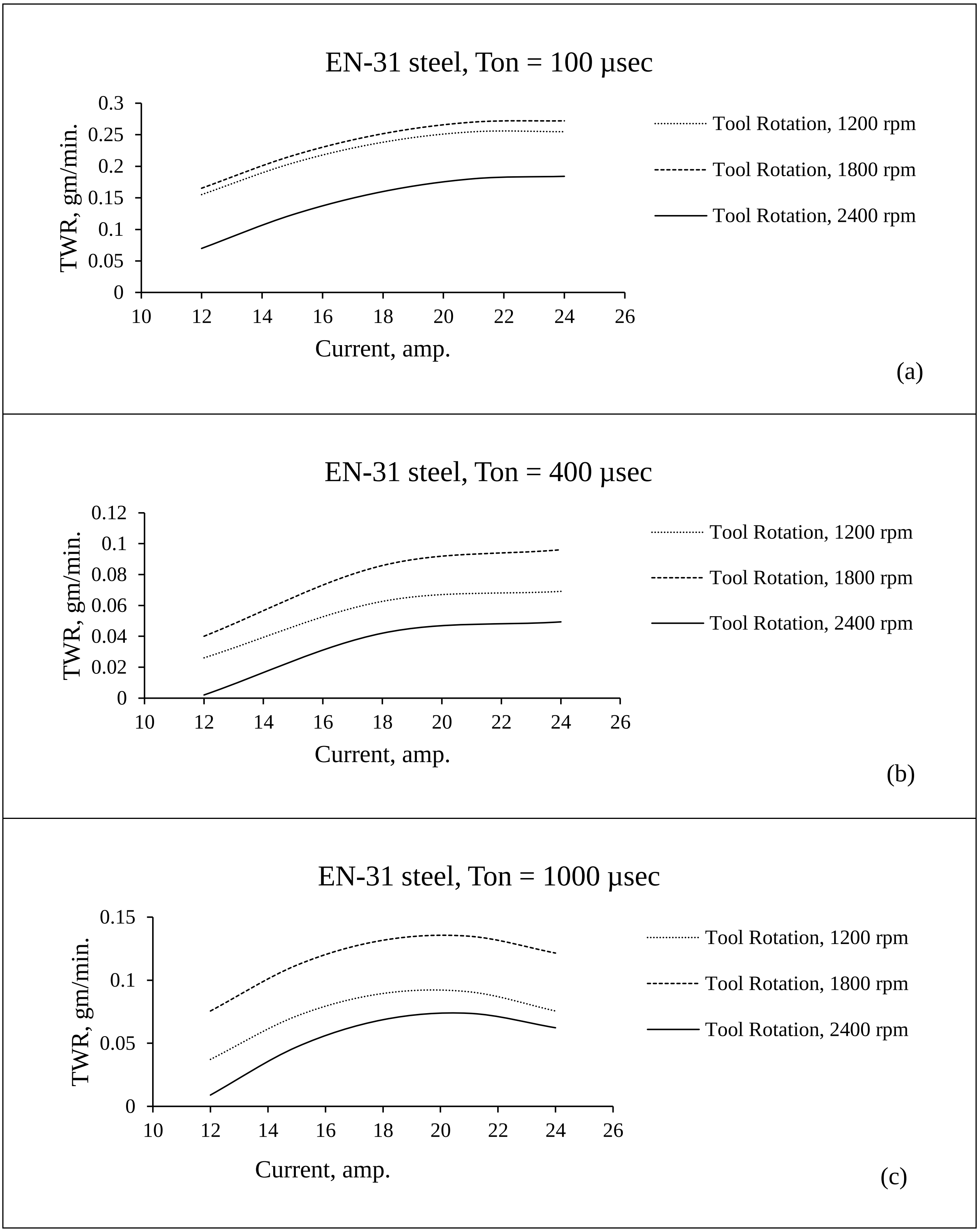

Figure 6.5: Effect of current on TWR at T_{on} 100, 400 and 1000 µsec

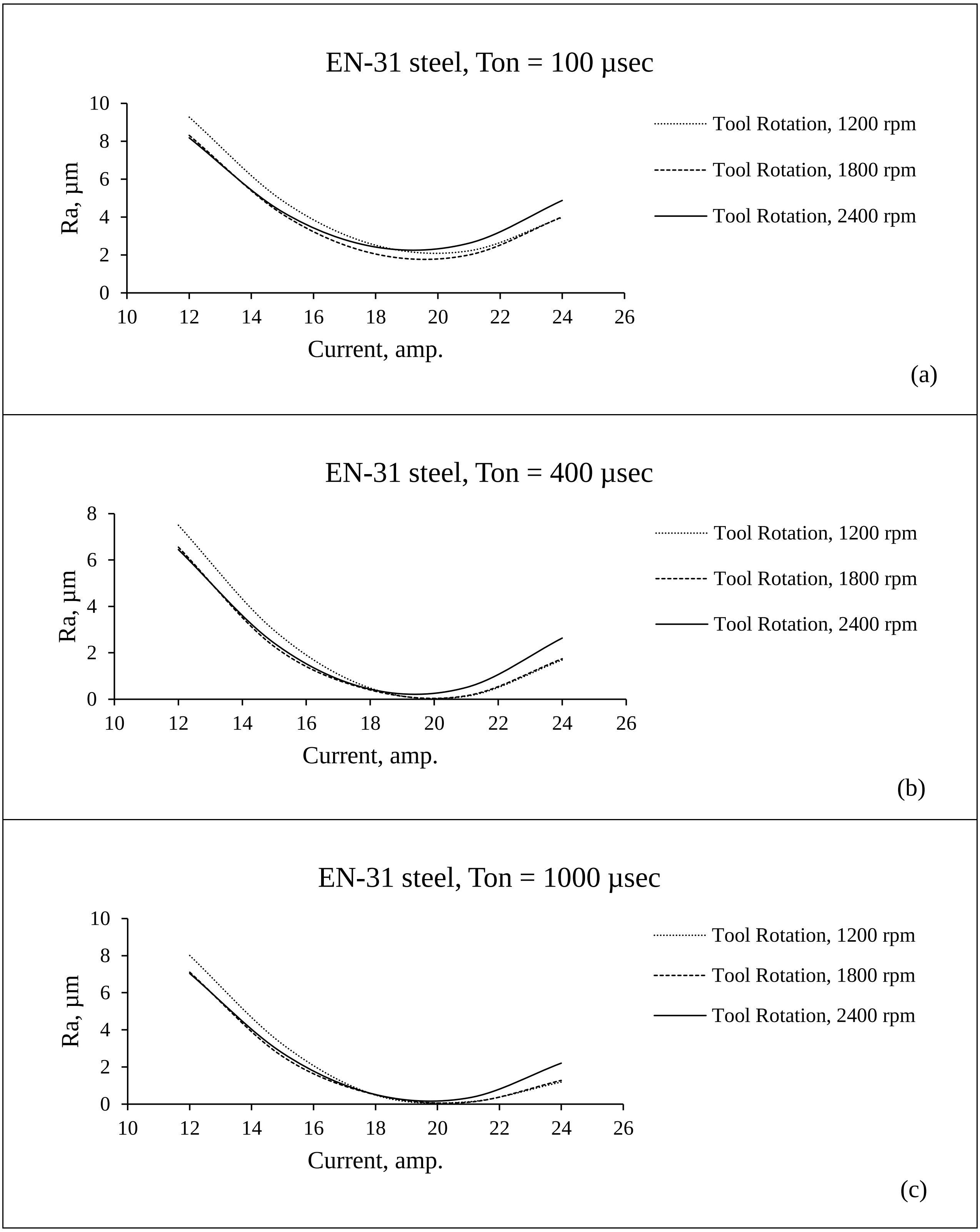

Figure 6.6: Effect of current on R_a at T_{on} 100, 400 and 1000 µsec

Figure 6.4 (a-c) shows the plot between MRR and I_p on 100, 400 and 1000 T_{on}. It shows that MRR increases as I_p increases (12 amp. to 24 amp.). The figure clearly shows that MRR decreases as tool rotation increases.

Figure 6.5 (a-c) shows the plot between TWR and I_p on 100, 400 and 1000 µsec T_{on}. It shows that TWR increase as T_{on} increases form 100 µsec to 1000 µsec for all value of currents. TWR is higher for 1800 rpm value of T_R. The TWR is significantly less (approximately 60%) as T_R increased from 1200 to 2400 rpm. Due to efficient flushing of debris from IEG.

Figure 6.6 (a-c) shows plot between R_a and I_p on 100, 400 and 1000 T_{on}. . It shows that the value of R_a decreases as T_R increases upto a certain value and than it starts increasing for all value of currents. Figure clearly indicates R_a decreases as T_{on} increase.

The temperature released by plasma is decreased by increase in T_R w.r.t. I_p. The generation of spark is forced to move in circular path due to T_R, which enhances the removal of debris produced during machining.

6.4.3 Effect of Pulse-on-Time

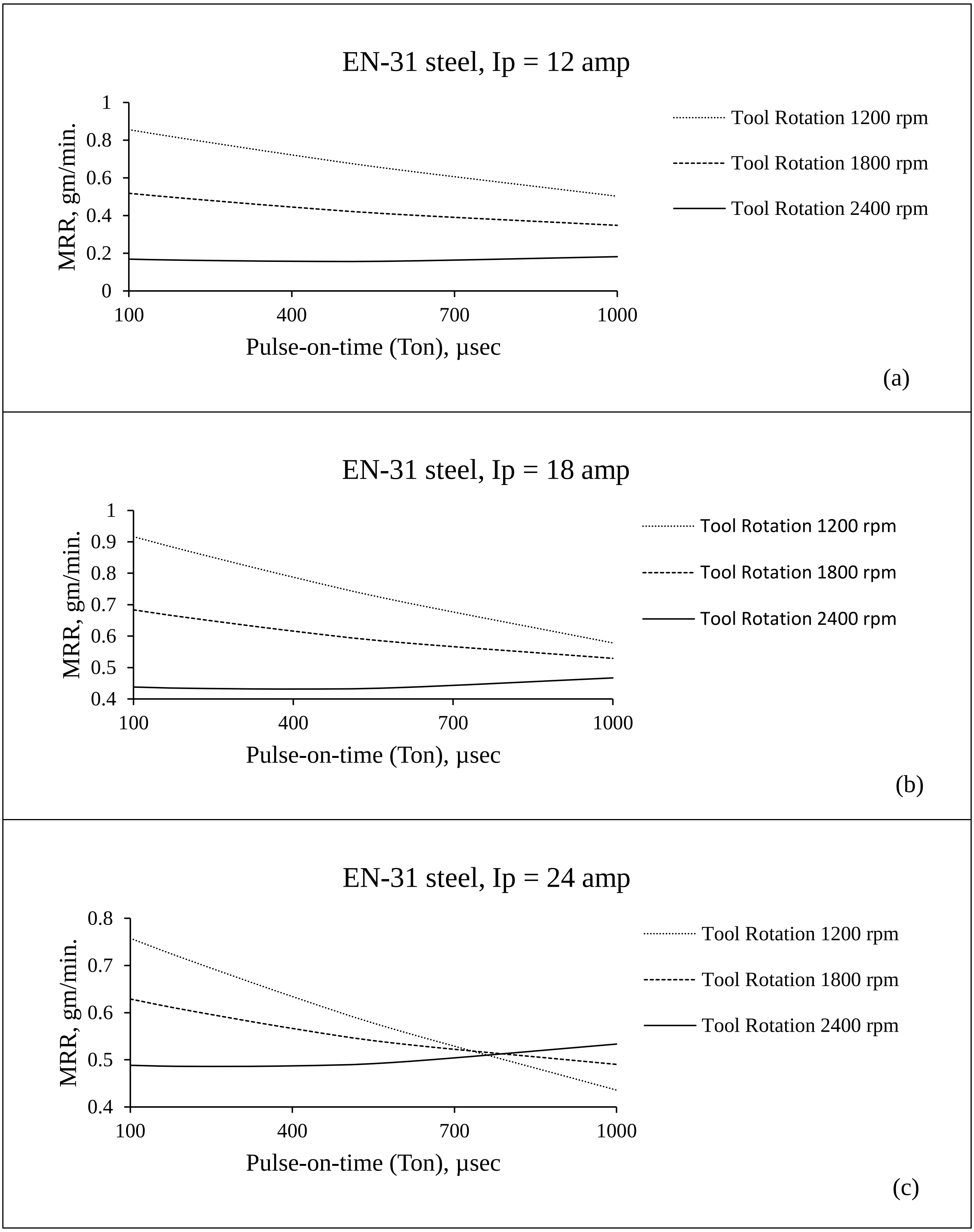

Figure 6.7: Effect of pulse-on-time on MRR at 12, 18 and 25 amp.

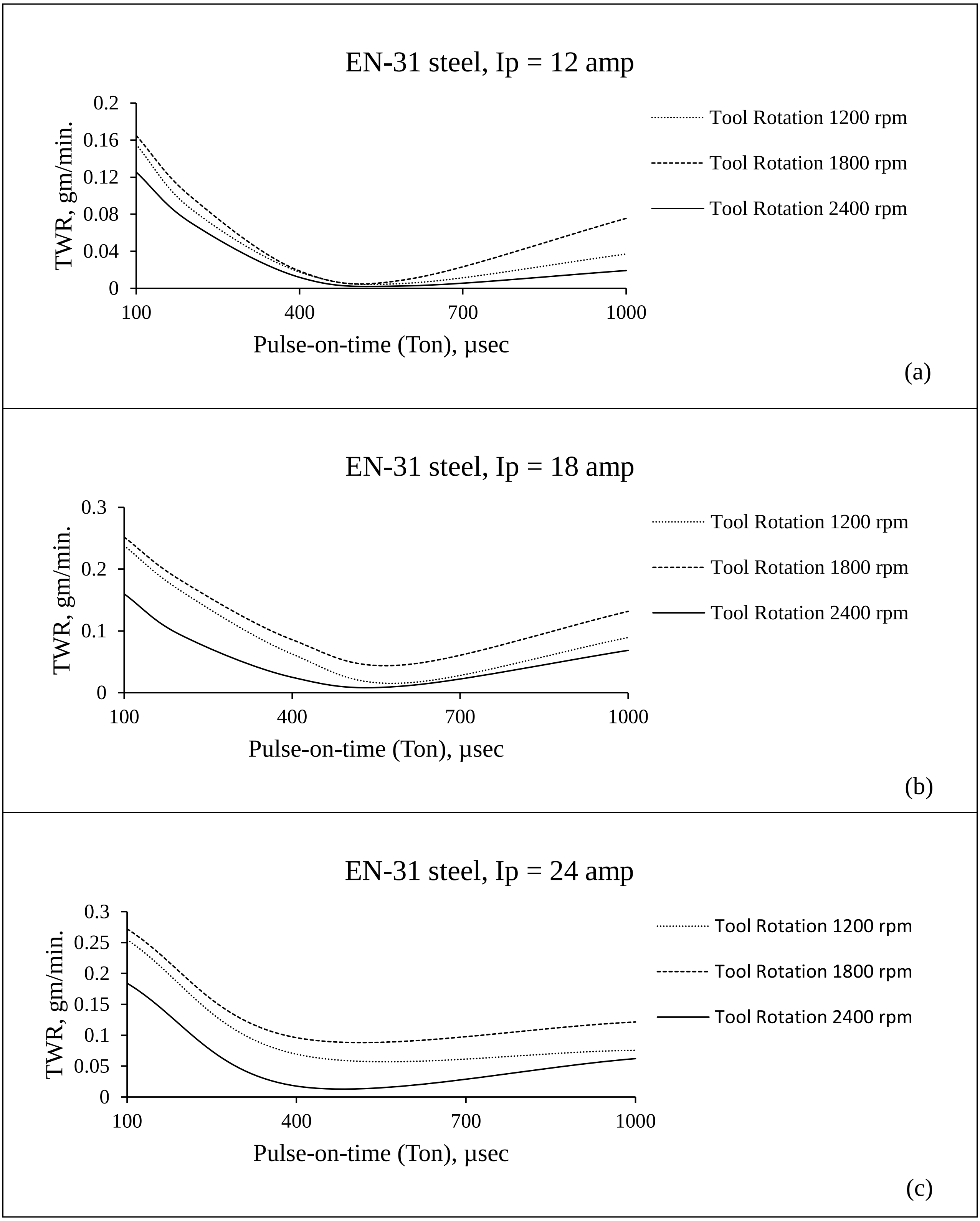

Figure 6.8: Effect of pulse-on-time on TWR at 12, 18 and 25 amp.

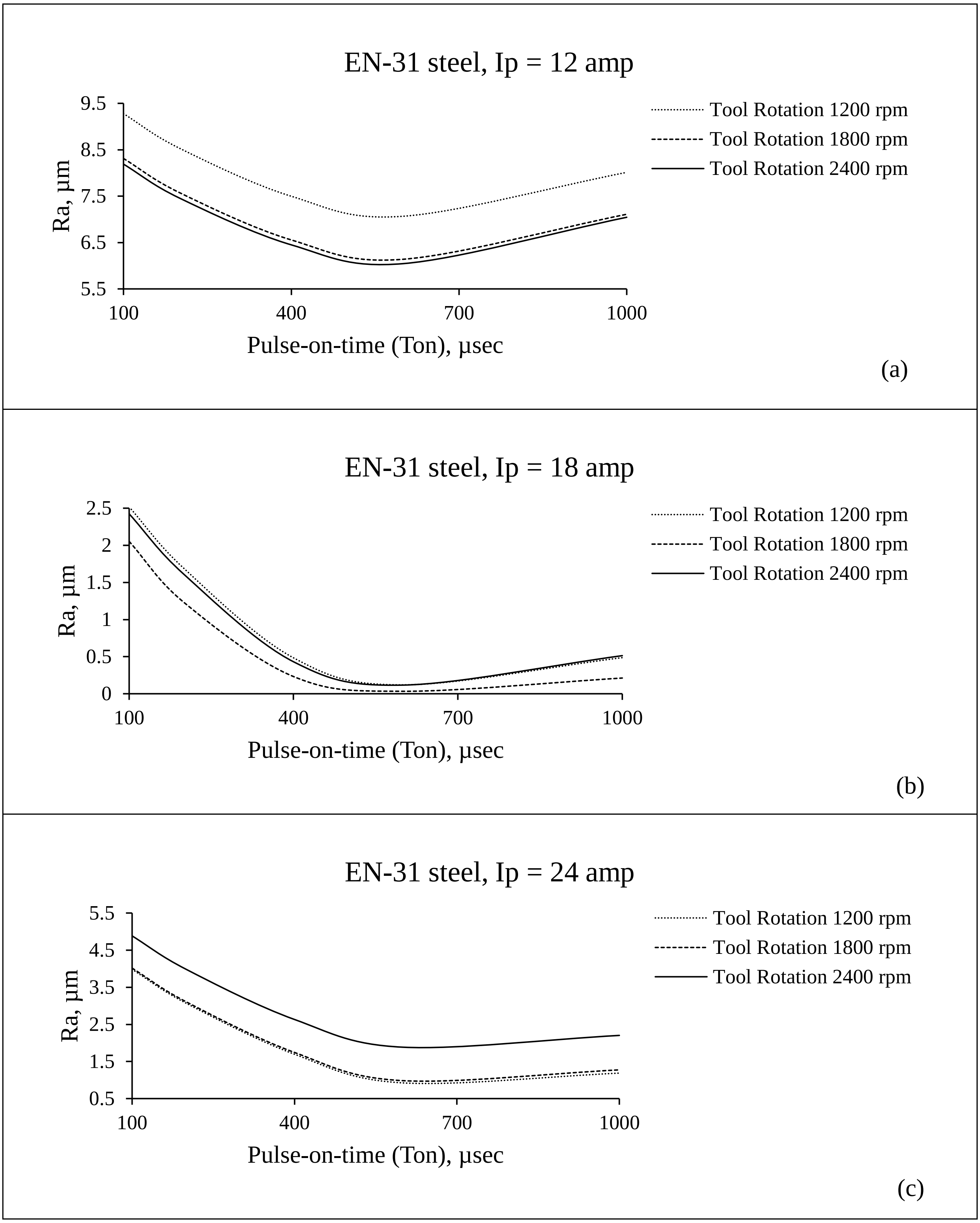

Figure 6.9: Effect of pulse-on-time on R_a at 12, 18 and 25 amp.

Figure 6.7 (a-c) shows an interaction plot between MRR and T_{on} for 12, 18 and 24 amp I_p. It shows that MRR increases as I_p increases from 12 amp. to 24 amp. MRR decreases as T_{on} increases upto to a particular value.

Figure 6.8 (a-c) shows a plot between TWR and T_{on} for 12, 18 and 24 amp I_p. It shows that TWR decreases as T_{on} increases for all value of currents. This can be easily identified form figures of TWR lower for higher values of T_R.

Figure 6.9 (a-c) shows interaction plot between R_a and T_{on} for 12, 18 and 24 amp I_p. It represents, the term R_a decreases for certain value of T_{on} and then increases for all values of T_R.

The value of R_a is lower due to spread of discharge energy in the form of spark. The whirling effect plays a significant role in lowering the R_a. It facilitate efficiently removal of tiny particles during the machining. Hence, every new spark strikes the workpiece material rather than striking with tiny particles available in between electrodes.

6.5 Interaction Plots Analysis

The interaction plot for MRR, TWR and R_a of EN-31 steel is as:

(i) Material Removal Rate

Figure 6.10 (a) shows interaction plot for MRR with interaction I_p (12 amp. to 24 amp.), T_{on} (100 µsec to 1000 µsec) and T_R (1200 to 2400 rpm) indicated in red to black colour lines respectively. The figure clearly represents MRR enhanced as the increase in I_p for all values of current, at current 12 amp., the MRR is 0.43 gm/min., but as current increase from 12 amp. to 24 amp. The maximum MRR at 18 amp. and then fallen down. The rate of MRR slightly higher, due to increase in T_{on} and I_p duration that reveals high amount of discharge energy. The parametric optimal MRR obtained at current 18 amp. Figure 6.10 (b) indicates that the MRR increased from 12 to 18 amp. In a significant rate but after that it falls and the value lies in narrow zone of T_{on}. Figure 6.10 (c) shows that MRR initially high at 100 µsec but after that T_{on} was insignificant. The optimal value lies at T_{on} 400 µsec. The parametric value of MRR at I_p = 18 amp., T_{on} = 400 µsec and T_R = 1800 rpm is 0.6064 gm/min.

(ii) Tool Wear Rate

Figure 6.11 (a) represents the interaction plot for TWR with interaction I_p (12 amp. to 24 amp.), T_{on} (100 µsec to 1000 µsec) and T_R (1200 to 2400 rpm). The figure shows that tool wear rate increases in a wider region. The maximum wear rate at 18 amp. and parametric value of TWR is 0.847 gm/min. Figure 6.11 (b) indicates TWR increases with small rate in high current region but in low current wear rate was significantly low, this effect minimize due to T_R. The rotation of tool decreases the effectiveness of discharge energy, due to spreading of spark. Figure 6.11 (c), shows that TWR significantly decreased upto T_{on} 400 µsec.

(iii) Surface Roughness

Figure 6.12 represents that R_a decreased upto 18 amp. as well the region more broader for R_a. The T_R plays an important role in R_a as shown in Figure 6.12 (b) and (c). R_a decreases as T_R increases, while at high amount of I_p also. The T_{on} and T_R have great impact at low value due to the uniform distribution of produced discharge energy continuously and having more concentric effect as compared to high rotation. At high discharge energy, the high T_R reduces the amount of R_a. The parametric value of R_a is 0.0234 µm.

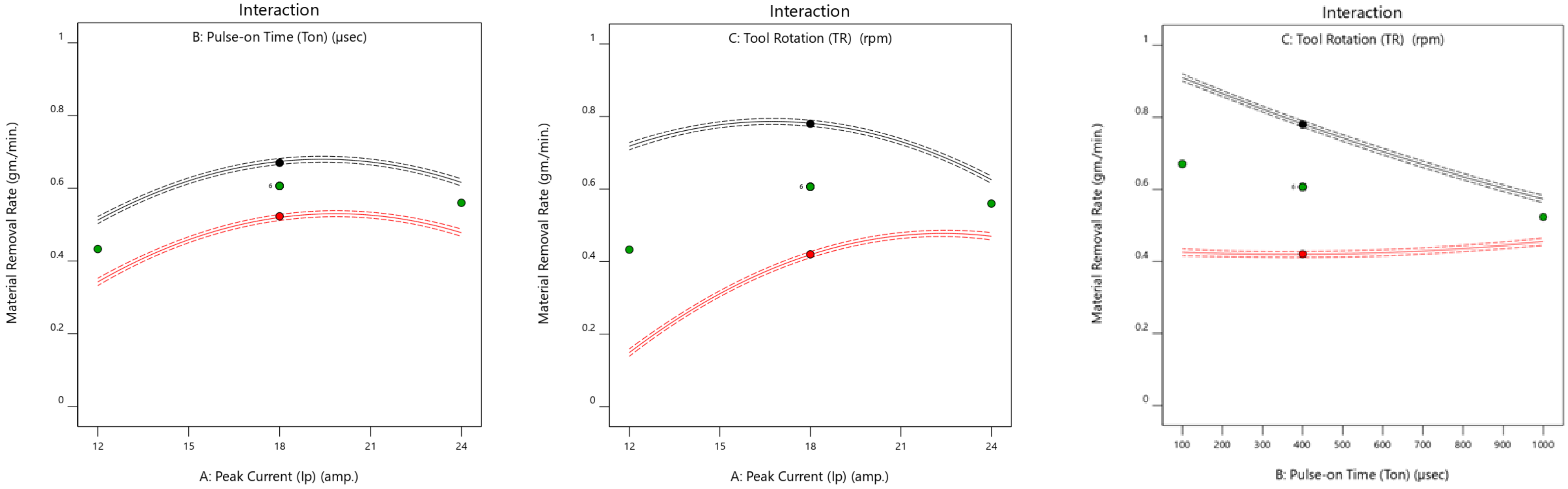

(a) Interaction plot of AB, (b) Interaction plot of AC (c) Interaction plot of BC

Figure 6.10: Interaction plot of AB, AC and BC for MRR. The actual factor A: I_p = 18 amp., B: T_{on} = 400 µsec and C: T_R = 1800 rpm

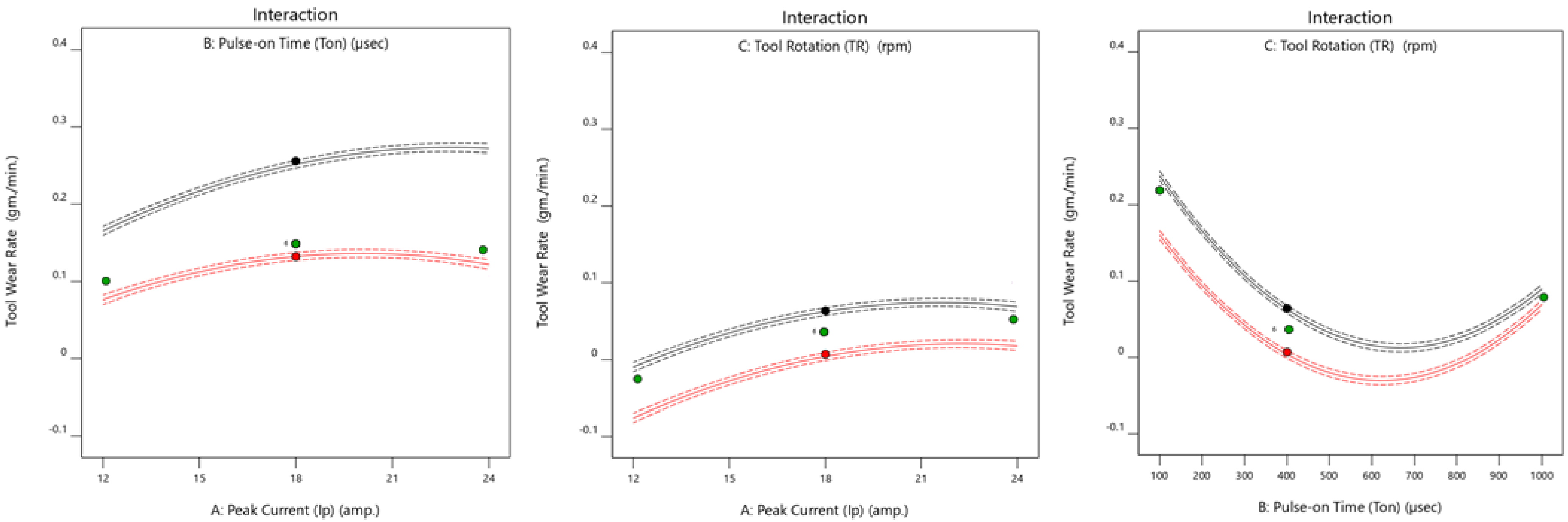

a) Interaction plot of AB

(b) Interaction plot of AC

(c) Interaction plot of BC

Figure 6.11: Interaction plot of AB, AC and BC for TWR. The actual factor A: I_p = 18 amp., B: T_{on} = 400 µsec and C: T_R = 1800 rpm

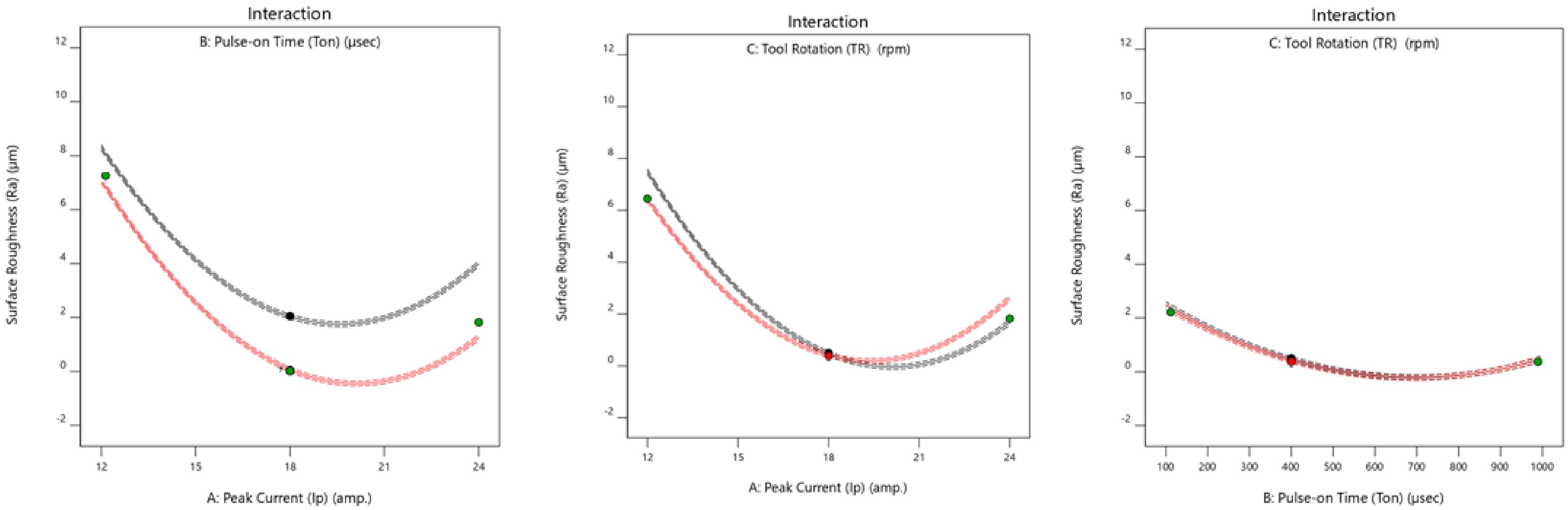

(a) Interaction plot of AB

(b) Interaction plot of AC

(c) Interaction plot of BC

Figure 6.12: Interaction plot of AB, AC and BC for Surface Roughness (R_a.). The actual factor A: I_p = 18 amp., T_{on} = 400 µsec and T_R = 1800 rpm

6.6 Influence of Input Parameters on Responses by 2D Contour and 3D Surface Interaction Plot

The Input Parameters Influence on Responses by 3D surface interaction plot is as:

(i) Material Removal Rate

Figure 6.13 (a-b) represents the 2D contour and 3D-surface plot for varying of MRR along I_p and T_{on}. It represents that MRR increases along with I_p. The discharge energy gets affected linearly by I_p along with T_{on} duration which results in more crater dimension i.e. high MRR. The 3D plot also represents that MRR increases as I_p. The design points and predicted points are laying on the 3D-surface plot between blue to red colour. The blue, green and red colour represents the low, optimum and high value of material removal rate. Figure 6.13 (c-d) indicated the 2D contour-plot and 3D-surface-plot for varying MRR along with I_p and T_R. The figure indicates that the increase in MRR along with the increase in I_p for all values of current. It represents MRR increases as an increase of I_p. The design points and predicted points are laying on the 3D-surface plot between blue to orange colour. Figure 6.13 (e-f) indicates the 2D contour-plot and 3D-surface-plot for varying MRR as T_{on} and T_R. The parametric value of MRR found at I_p, T_{on} and T_R values were 18 amp, 400 µsec and 1800 rpm. was 0.6064 gm/min.

(ii) Tool Wear Rate

TWR is a vital parameter in EDM with T_R. This affects the cost of machining. While machining work piece material using the copper tool, it is subjected to wear. The carbon particles from the di-electric fluid may get deposited on the tool tip, which protects further erosion of the tool. If the I_p increased, the TWR also increased but relatively

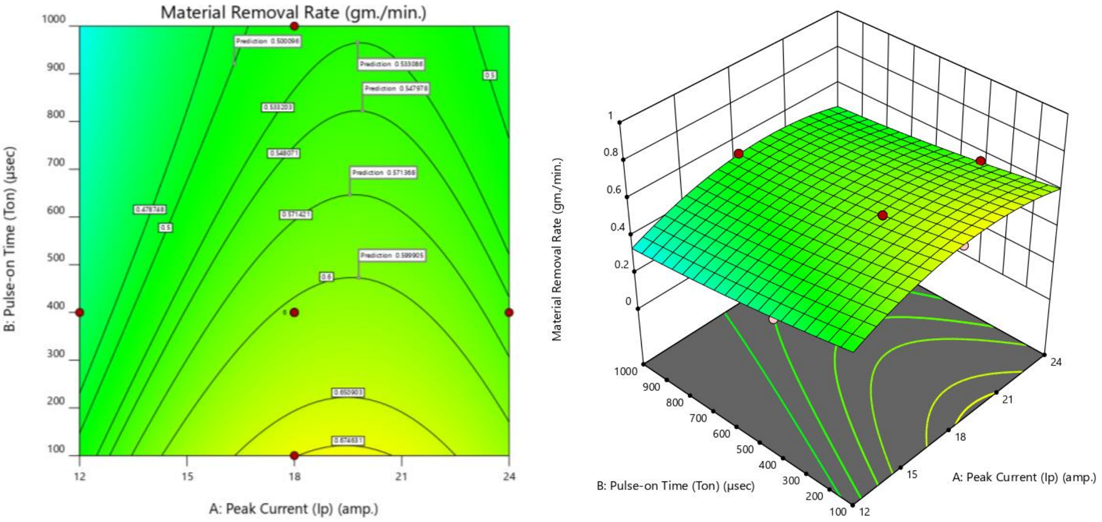

(a) 2-D Contour Plot of AB (b) 3-D Surface interaction Plot of AB

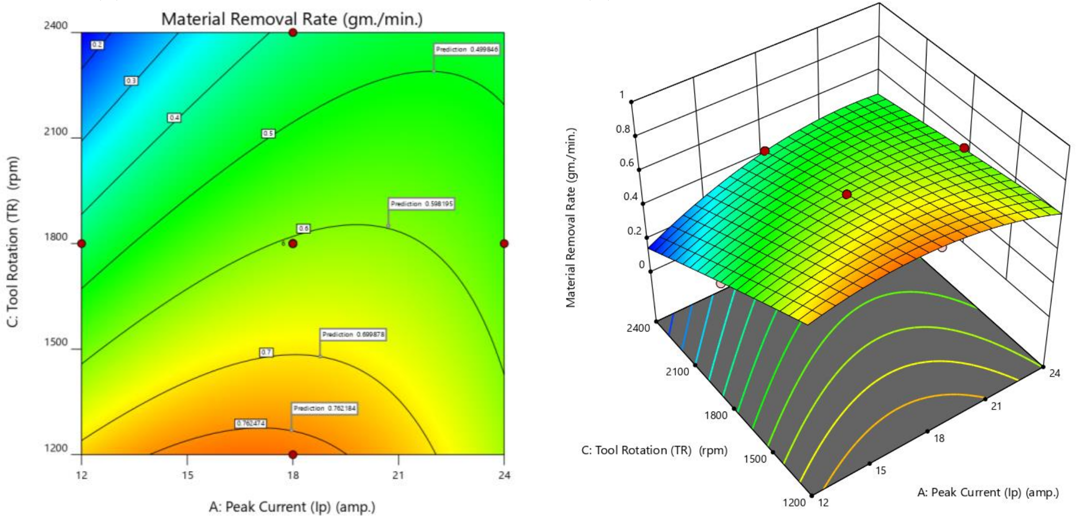

(c) 2-D Contour Plot of AC (d) 3-D Surface interaction Plot of AC

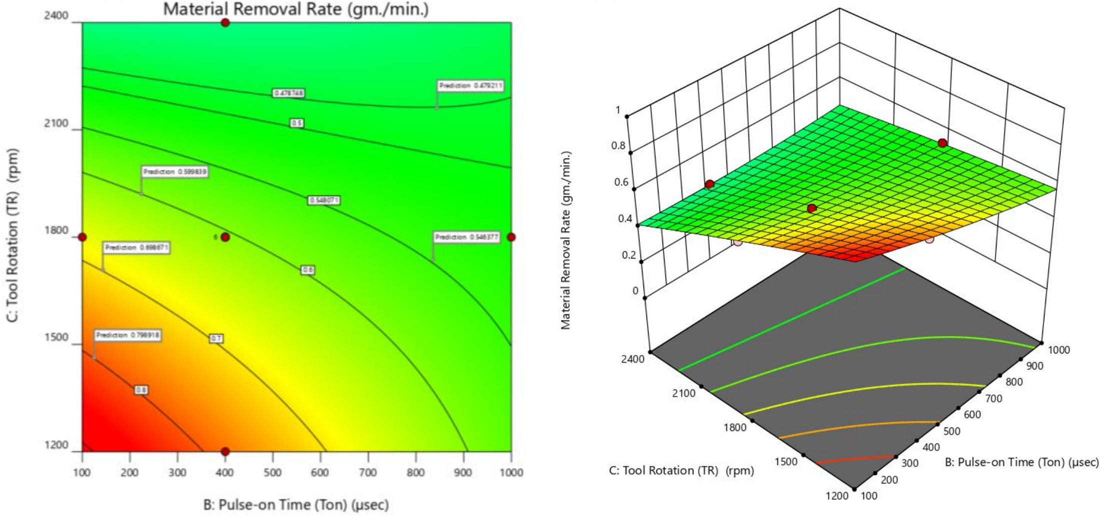

(e) 2-D Contour Plot of BC (f) 3-D Surface interaction Plot of BC

Figure 6.13: 3-D Surface plot with interaction AB, AC and BC of MRR. The actual factor A: I_p = 18 amp., B: T_{on} = 400 µsec and C: T_R = 1800 rpm

small with high speed T_R, due to uniform distribution of discharge energy. The response graph for TWR with interaction of I_p, T_{on} and T_R are represented in figure 6.14.

Figure 6.14 (a-b) represents the 2D contour and 3D surface plot for I_p and T_{on}. It proves that TWR increase along with I_p. It is clear that increase in I_p results in high amount of spark energy, hence liquid metal from both the ends i.e. rises in TWR. The TWR also depends on T_{on}, i.e. increase in T_{on} results in high TWR. This can be minimized by T_R. The T_R decreases in spark release density in the inter electrode gap. The area of plasma channel developed as increase in T_{on}, this expansion is enhanced by T_R. Another cause for less wear rate at T_{on} is the formation of carbon layer on tool end resulting rise in wear resistance of tool and decreasing TWR. Figure 6.14 (c-d) the TWR plot of I_p and T_R, it is noted that increase in TWR is less as increase in I_p by virtue of the uniform distribution of discharge energy by T_R. Similarly, Figure 6.14 (e-f) the 2D contour and 3D surface plot of TWR with T_{on} and T_R. It is considered that TWR decreased slightly upto 400 µsec and further that it increased as pulse-on-time T_{on} as a consequence of expansion in plasma channel.

(iii) Surface Roughness

Figure 6.15 represents the R_a is varying as I_p, T_{on} and T_R. The surface quality deteriorates by an increase in I_p and T_{on}. The spark discharge energy increase along with I_p. Therefore, high amount of heat is generated, resulting in more material removal from the workpiece area. This degrades surface quality of the machining surface. The recasting of melted material taken place if flushing is not efficient, surface cracks, carbon deposition and pitting may also take place.

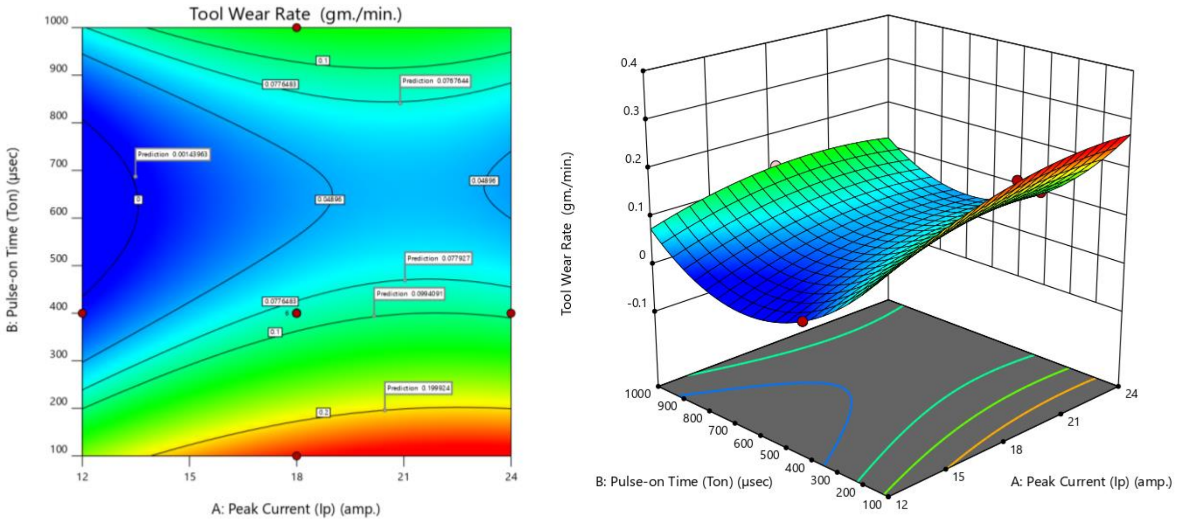

(a) 2-D Contour Plot of AB (b) 3-D Surface interaction Plot of AB

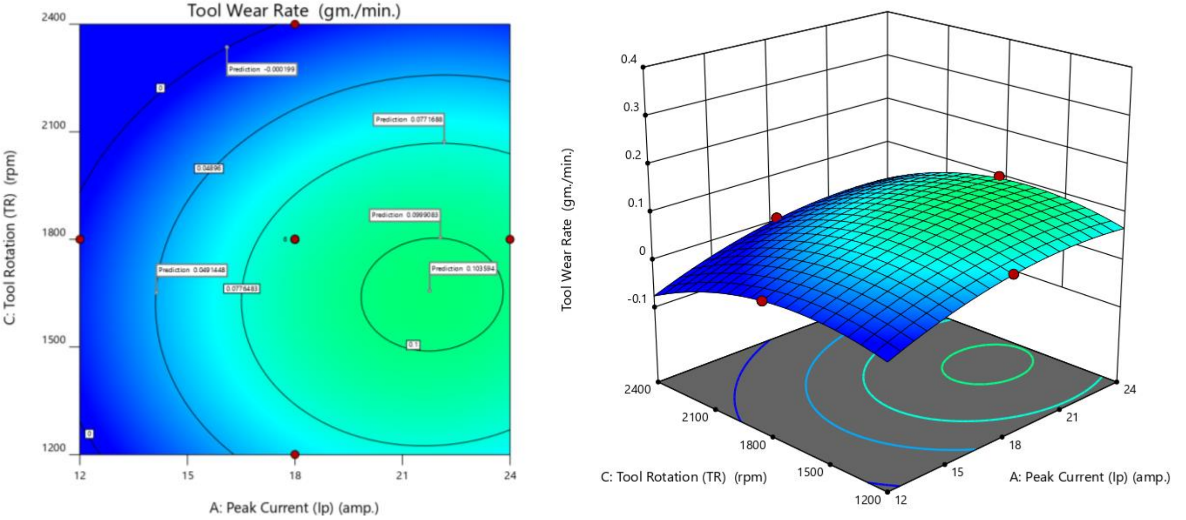

(c) 2-D Contour Plot of AC (d) 3-D Surface interaction Plot of AC

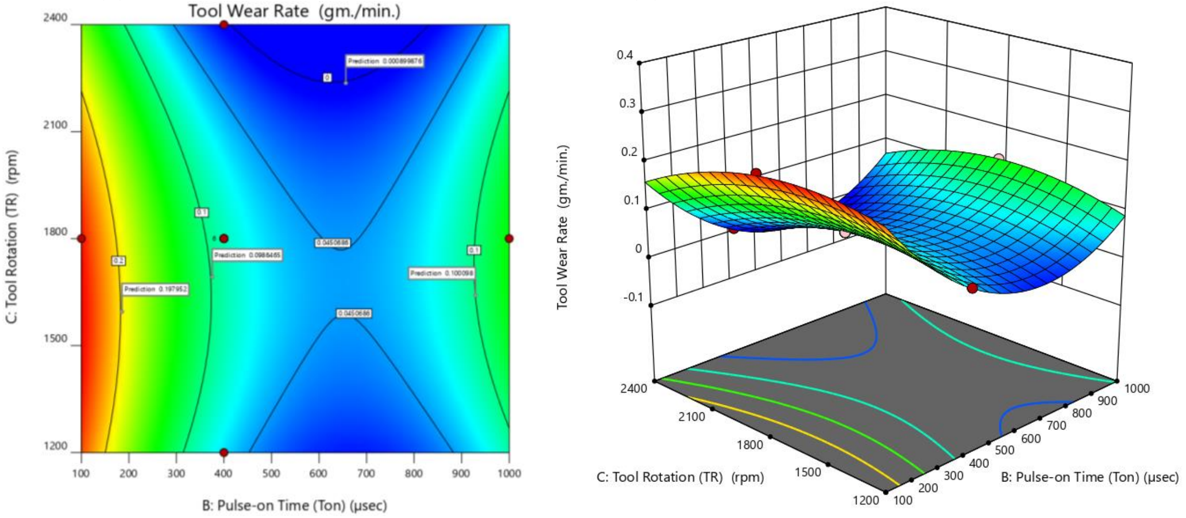

(e) 2-D Contour Plot of BC (f) 3-D Surface interaction Plot of BC

Figure 6.14: 3-D Surface plot with interaction AB, AC and BC of TWR. The actual factor A: I_p = 18 amp., B: T_{on} = 400 μsec and C: T_R = 1800 rpm

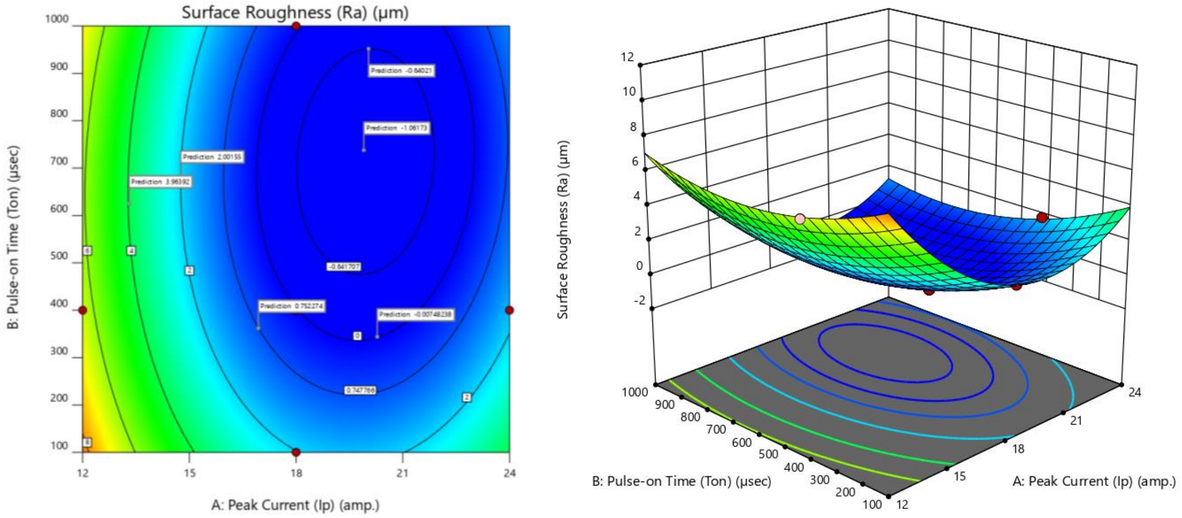

(a) 2-D Contour Plot of AB (b) 3-D Surface interaction Plot of AB

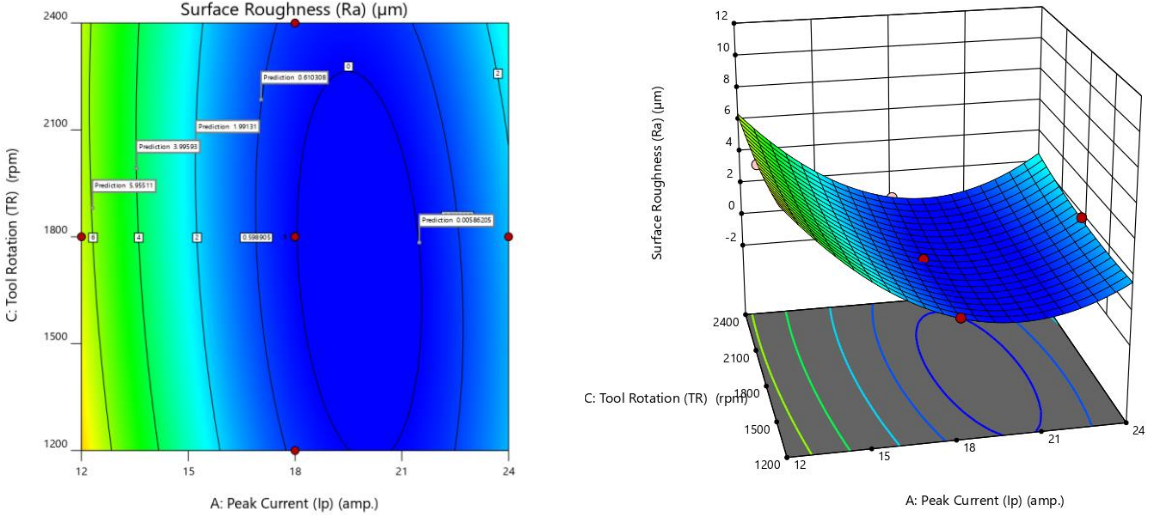

(c) 2-D Contour Plot of AC (d) 3-D Surface interaction Plot of AC

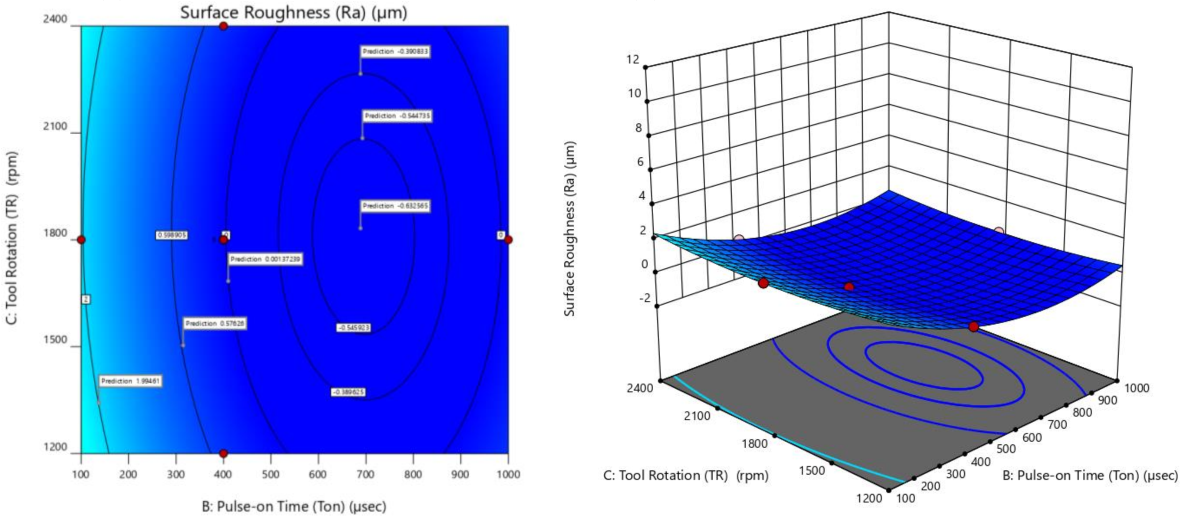

(e) 2-D Contour Plot of BC (f) 3-D Surface interaction Plot of BC

Figure 6.15: 3-D Surface plot with interaction AB, AC and BC of Surface Roughness (R_a). The actual factor A: I_p = 18 amp., B: T_{on} = 400 µsec and C: T_R = 1800 rpm

Figure 6.15 (a-b) represents the R_a increases with T_{on}. The increment in T_{on} to maximum R_a value even at the minimum value of I_p. Furthermore, whenever the T_{on} is at a minimum level with low value of I_p, the R_a value is still high. Figure 6.15 (c-d) R_a increases with I_p due to high energy is produced, leaves craters on the machined surface leads to poor surface finish. Similarly, figure 6.15 (e-f) R_a increases with T_{on}, which results in high surface roughness.

6.7 Stylus Based Surface Roughness Analysis

Roughness (R_a) was assessed to evaluate the varying surface peak and trough characteristics. The aim of surface roughness analysis is to improve the properties of the surface using tool rotation EDM. The effect of process variables on the response of R_a was analysed.

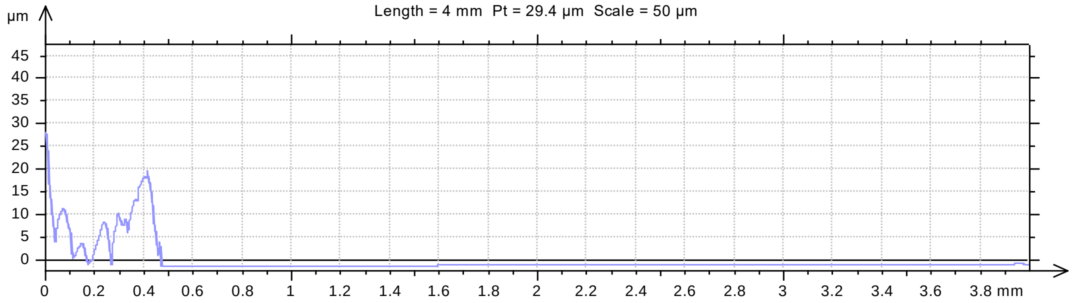

Figure 6.16: Peak and valley profile for surface after EDM machining, $R_a = 0.5$ µm

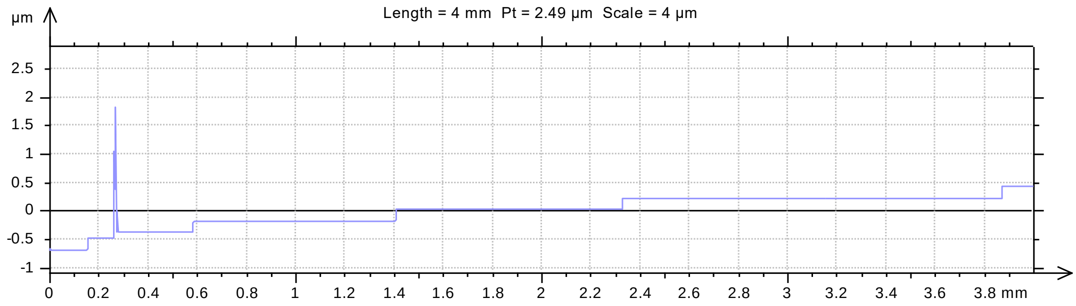

Figure 6.17: Peak and valley profile for surface after EDM machining, $R_a = 0.0234$ µm

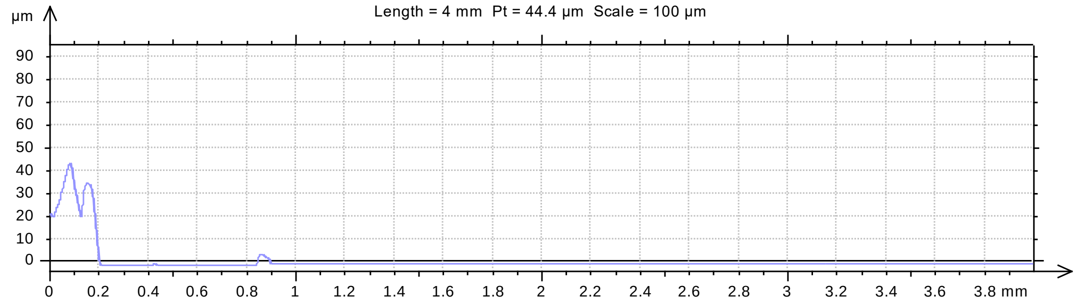

Figure 6.18: Peak and valley profile for surface after EDM machining, $R_a = 0.38$ µm

Figure 6.16 to 6.18 represents the profiles of machined surfaces for T_{on} 400 µsec. The machining area has high frequency and the peaks and troughs of less magnitude as compared to 1000 µsec machined surface. Figure 6.16 represents the R_a average value is 0.5 µm from 0 to 0.43 mm region and rest surface is uniform. The more peak and valley from 0 to 0.43 mm due to the formation of recast layer on the surface. Figure 6.17 and 6.18 also shows the peak and valleys, the average value of R_a is 0.0234 µm, due to the high rotation of T_R, the amount of melting is flushed away at high rate. This was the indication of reduction in R_a parameter from 0.5 µm mean to 0.0234 µm i.e. 95 % reduction in R_a by T_R. The enhancement in R_a has been noticed on further increment in

T_R. It facilitates the removal of debris or tiny particles from the inter-electrode gap, due to the presence of whirling effect. That prevents solidification of the recast layer.

6.8 Morphology of EN-31 Steel

Scanning Electron Micro graphs are used to analyse the closed spaced specimen at higher magnification since electromagnets are used instead of lenses. The plasma channel causes from high I_p causes the temperature or cool surface to rise above the liquid temp, which lead to vaporize.

The T_R and I_p are considered to be vital either as a parameter or in correlation with other variables for all the responding; it is determined to inspect the effect of T_R and I_p microscopically.

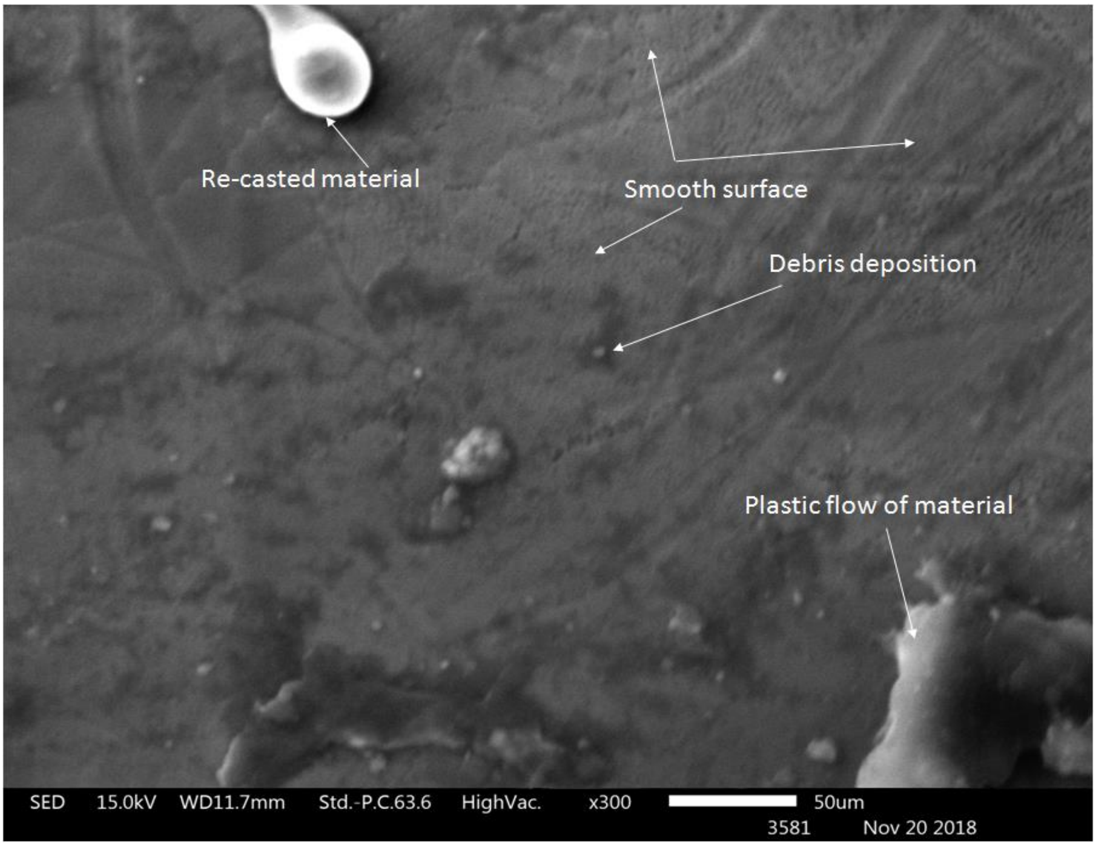

Figure 6.19 (a) SEM Micrograph indicating smooth surface, plastic flow of material

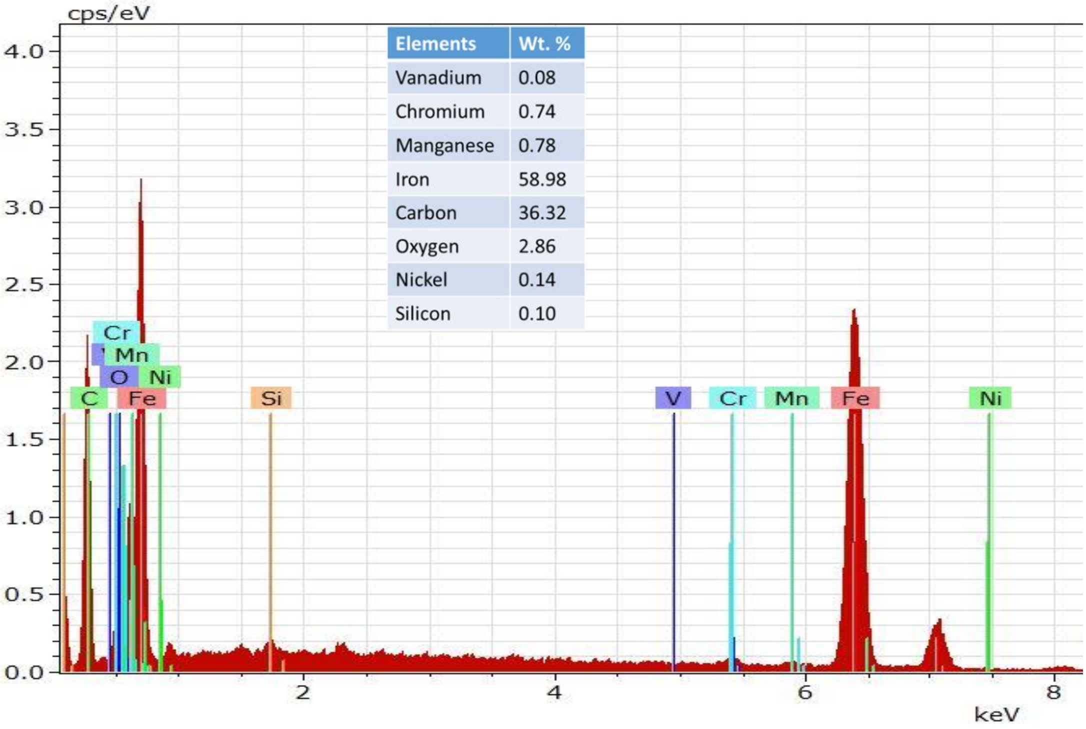

Elements	Wt. %
Vanadium	0.08
Chromium	0.74
Manganese	0.78
Iron	58.98
Carbon	36.32
Oxygen	2.86
Nickel	0.14
Silicon	0.10

Figure 6.19 (b) SEM EDS

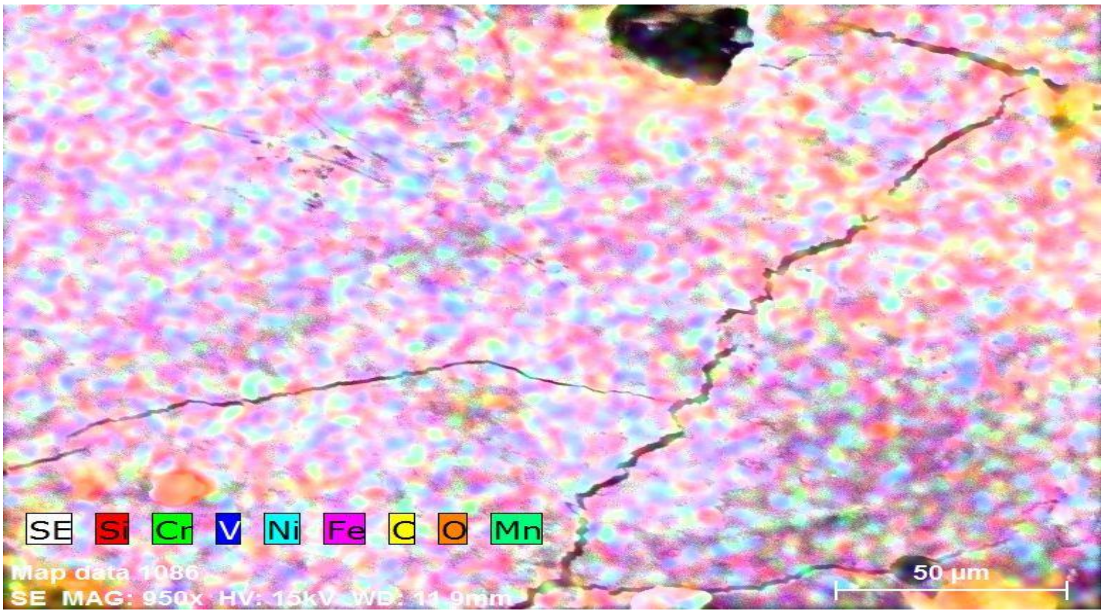

Figure 6.19 (c) EDS Mapping

Figure 6.19: SEM, EDS, EDS Mapping. At I_p = 18 amp, T_{on} = 400 µsec, T_R = 1800 rpm

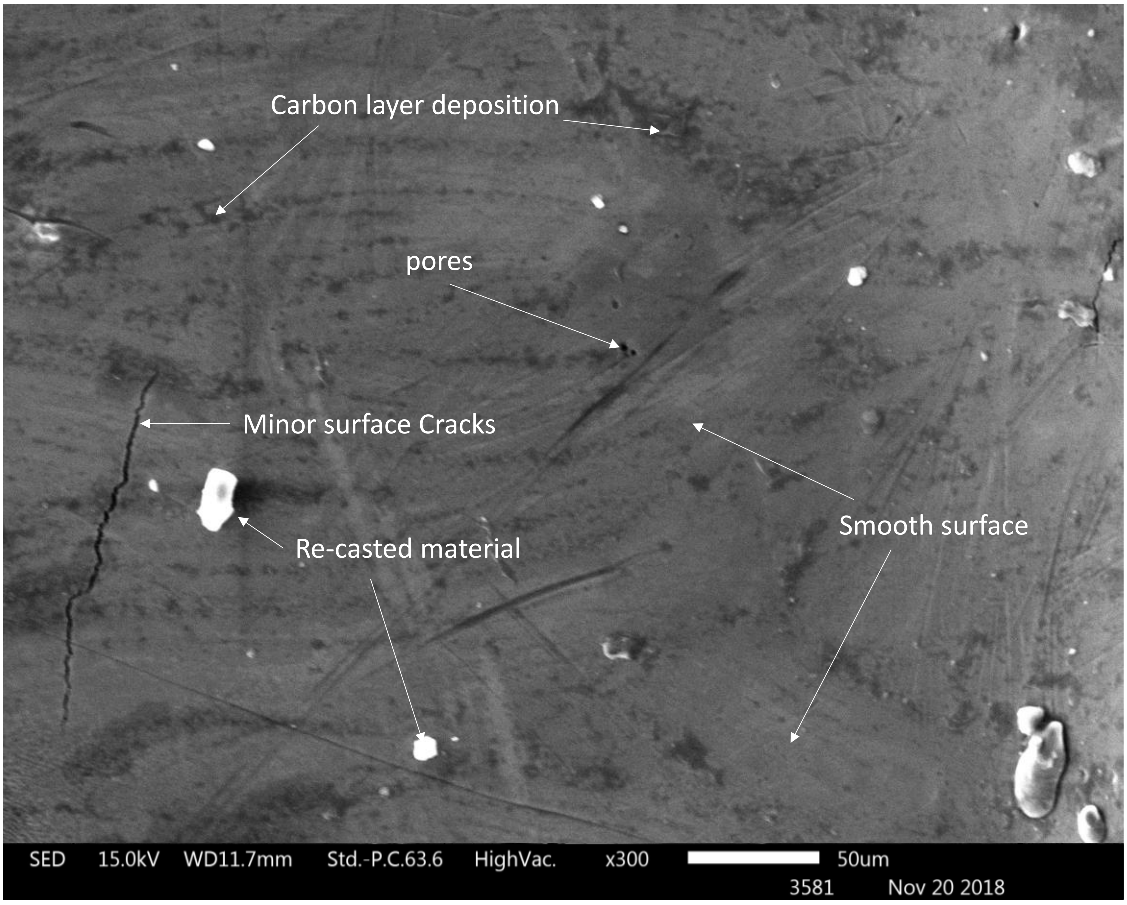

Figure 6.20 (a) SEM Micrograph indicating smooth surface, minor recast layer

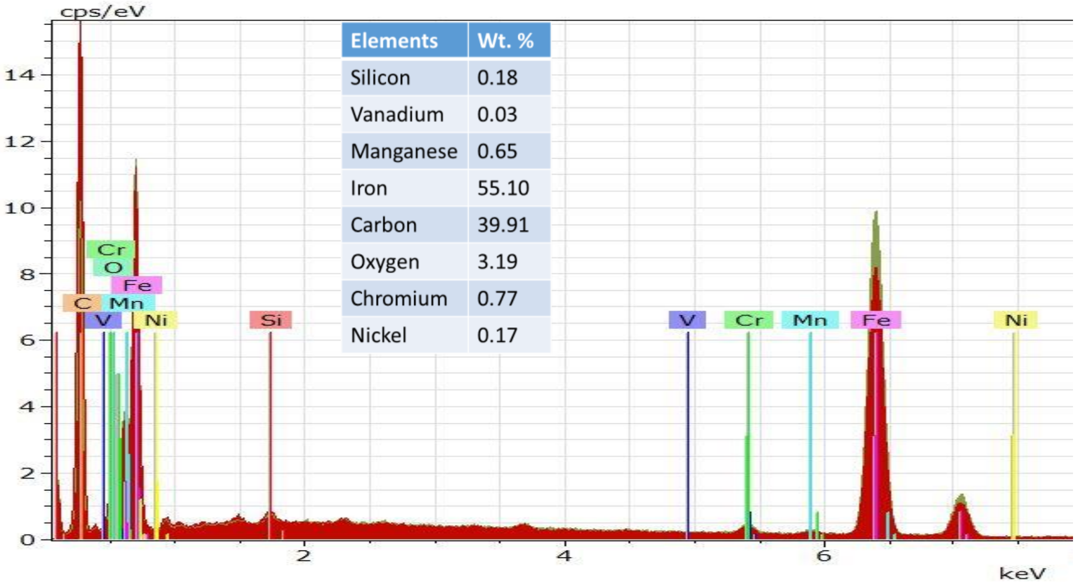

Elements	Wt. %
Silicon	0.18
Vanadium	0.03
Manganese	0.65
Iron	55.10
Carbon	39.91
Oxygen	3.19
Chromium	0.77
Nickel	0.17

Figure 6.20 (b) SEM EDS

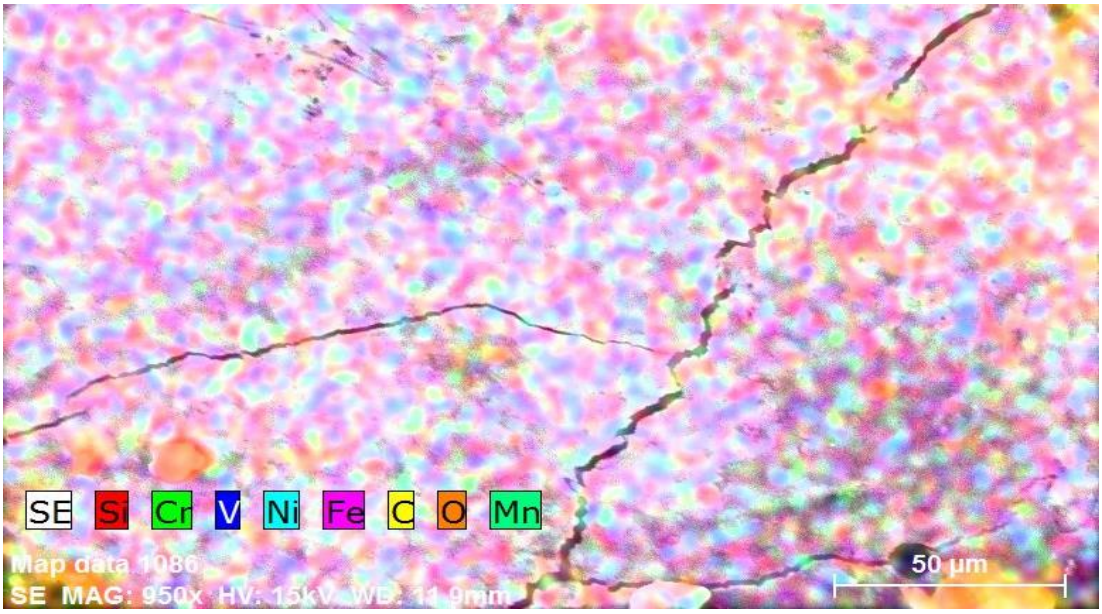

Figure 6.20 (c) EDS Mapping

Figure 6.20: SEM, EDS, EDS Mapping. At I_p = 18 amp, T_{on} = 400 µsec, T_R = 2400 rpm

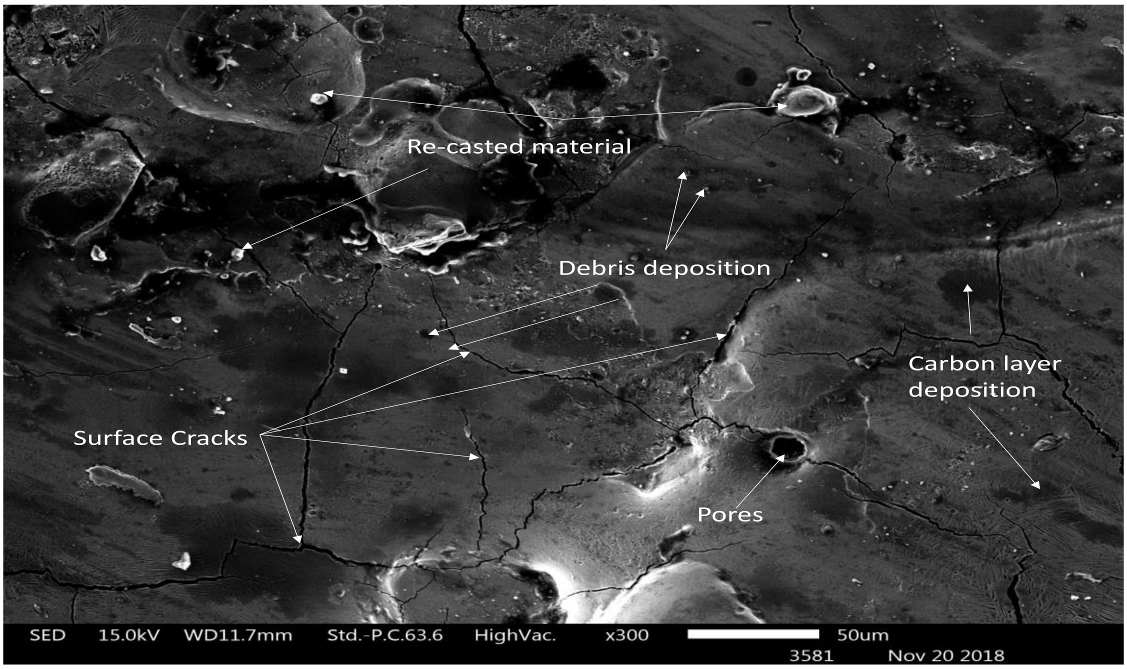

Figure 6.21 (a) SEM Micrograph indicating minor cracks and recast layer on the machining area

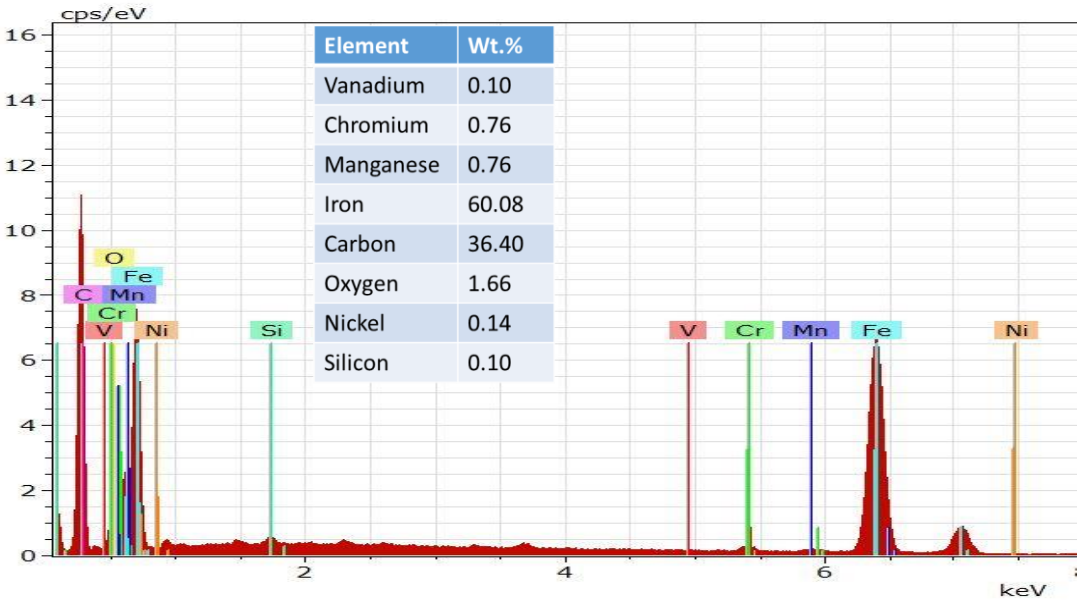

Element	Wt.%
Vanadium	0.10
Chromium	0.76
Manganese	0.76
Iron	60.08
Carbon	36.40
Oxygen	1.66
Nickel	0.14
Silicon	0.10

Figure 6.21 (b) SEM EDS

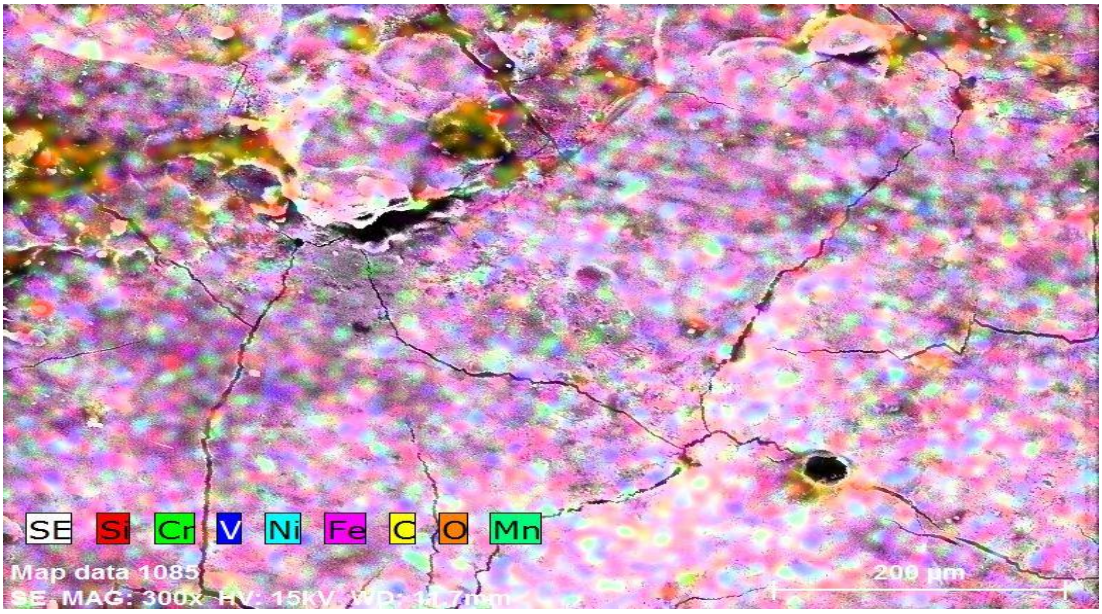

Figure 6.21 (c) EDS Mapping

Figure 6.21: SEM, EDS, EDS Mapping. At I_p = 18 amp., T_{on} = 400 µsec, T_R = 1200 rpm

Figure 6.19 (a), 6.20 (a) and 6.21 (a) represents the SEM micrographs at parametric condition I_p = 18 amp, T_{on} = 400 µsec, T_R = 1800 rpm (MRR = 0.6064 gm/min., TWR

= 0.0847 gm/min., R_a = 0.0234 µm); I_p = 18 amp, T_{on} = 400 µsec, T_R = 2400 rpm (MRR = 0.42 gm/min., TWR = 0.004 gm/min., R_a = 0.38 µm); I_p = 18 amp, T_{on} = 400 µsec, T_R = 1200 rpm (MRR = 0.78 gm/min., TWR = 0.064 gm/min., R_a = 0.5 µm) with copper tool for R_a, MRR and TWR accordingly. EDS is a systematic approach used for the description of elementals or chemical characterization of work material. It depends on excitation of correlation between X-ray and workpiece. Its characterization capabilities are due in large part to the fundamental principle that each constituent atom has a unique atomic structure allowing an unusual set of peak on its electromagnetic emission spectrum.

Figure 6.19 (b), 6.20 (b), 6.21 (b) and 6.19 (c), 6.20 (c), 6.21 (c) represents the energy dispersive analysis of EDS. Figure 6.19 (b), 6.20 (b) and 6.21 (b) represents constituent elements by wt. % i.e. major composition of Fe i.e. 58.98, 55.10, 60.08; C i.e. 36.32, 39.91, 36.40 and O 2.86 and 3.19 respectively. 6.19 (c), 6.20 (c), 6.21 (c) shows its elemental distribution.

6.9 Residual Stress Analysis

X-ray diffraction method is used to determine the residual stresses on the surfaces i.e. transverse stresses and longitudinal stress. It is a non-destructive testing method of the specimen. The µ- X360 portable residual stress analyser is very useful for analysis of stress. The pitch for measurement was 50 µm for measuring each point.

Figure 6.22 (a–f) illustrates the Debye ring (2D and 3D), distortion, surface extract (2D and 3D) and profile of samples. Residual stress can be accurately measured by the position of the Debye rings. The distortion images obtained during the process indicates that no or less damage i.e. no or less residual stresses are present in the machined sample. The base sample already having stress 241 MPa (tensile) and shear stress (Tau) 6 MPa (compressive) but stresses are uniformly distributed shown in figure 6.22 (c). The stress peak is available at alpha 157.1^o.

Figure 6.23 to 6.26 (a-f) represents that I_p having effect on the average residual stress profile in the subsurface. When I_p varies from 12 amp. to 24 amp. The discharge energy per pulse will increase. The maximum of average residual stress value in tensile stress vary from 207 MPa to 380 MPa on the same T_{on} and T_R i.e. 100 µsec and 1800 rpm. When I_p increased from 12 amp. to 24 amp. The effect of I_p results in the distortion intensity of peak laying on the 156.7^o, 157^o, 157^o and 172.7^o to 144.9^o respectively. The residual stress ring distorted on these points and the average value of residual stresses is 207, 308, 380 and 2008 MPa (compressive). This is because of the long duration of the pulse at discharge energy that leads to more heat generation and results in more melting of material and higher R_a. Therefore, less discharge energy is preferred in EDM to achieve a lower tensile and compressive residual stress by decreasing surface roughness.

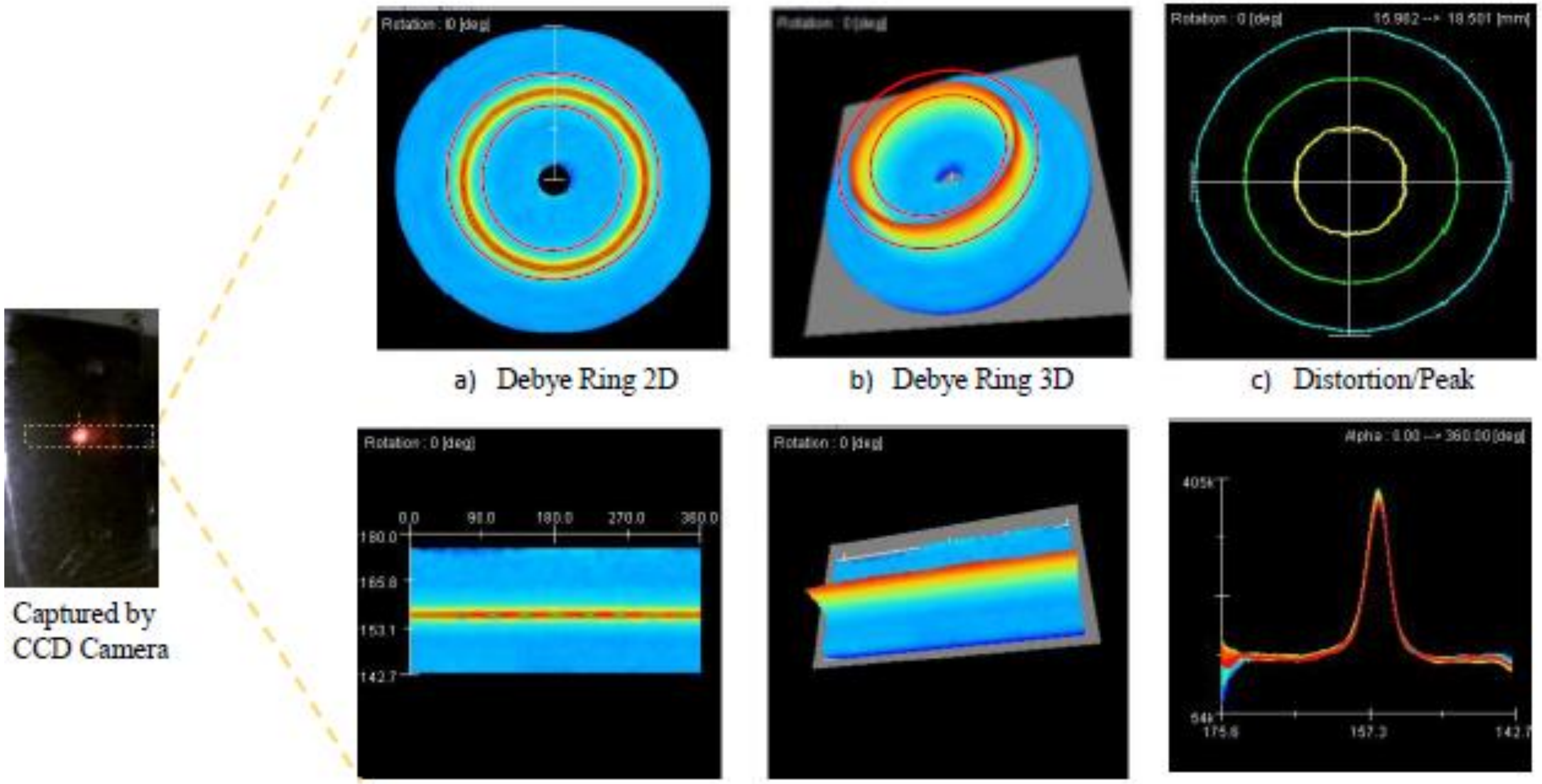

Captured by
CCD Camera

a) Debye Ring 2D

b) Debye Ring 3D

c) Distortion/Peak

d) Extract 2D

e) Extract 3D

F) Profile ($\alpha = 0\text{-}360^{\circ}$)

Figure 6.22: Residual Stress Mapping of base material, σ (x) = 241 MPa, Tau (xy) = -6 MPa, Sigma (y) = -78 MPa

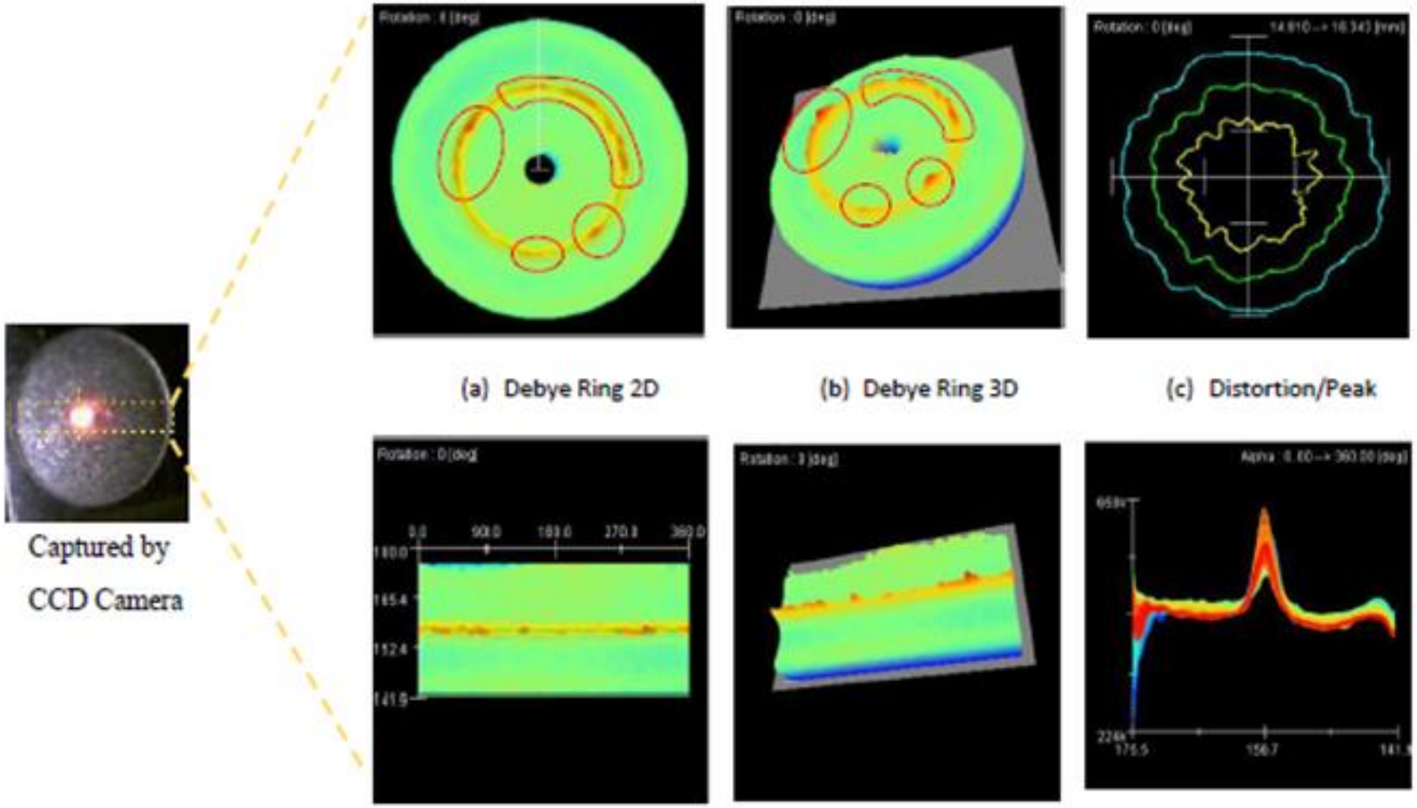

(a) Debye Ring 2D (b) Debye Ring 3D (c) Distortion/Peak

(d) Extract 2D (e) Extract 3D (f) Profile (α = 0-360°)

Figure 6.23: Residual Stress Mapping, I_p = 12 amp., T_{on} = 100 µsec, T_R = 1800 rpm, σ = 207 MPa, Tau (xy) = 31 MPa

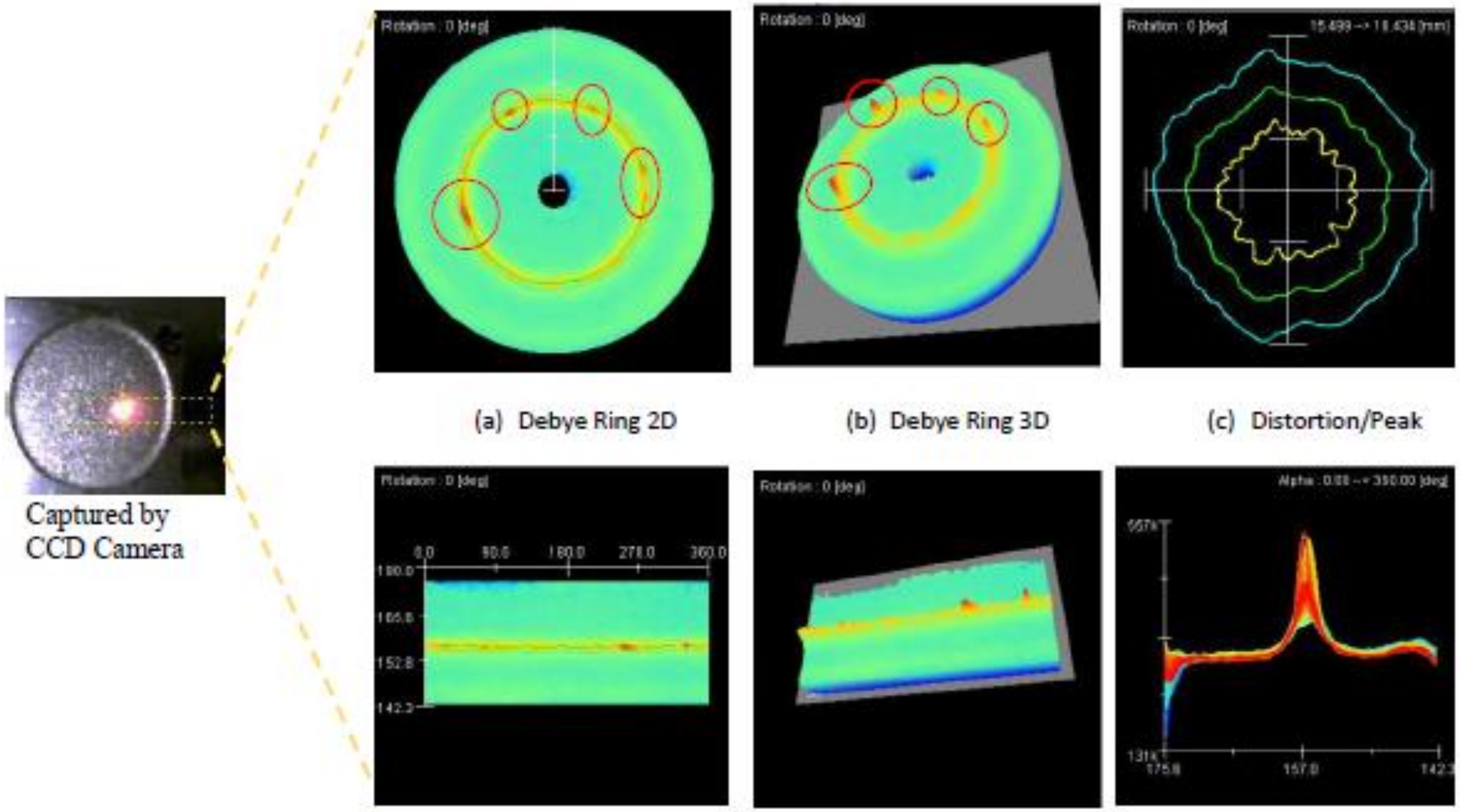

(a) Debye Ring 2D (b) Debye Ring 3D (c) Distortion/Peak

(d) Extract 2D (e) Extract 3D (f) Profile ($\alpha = 0\text{-}360^{\circ}$)

Figure 6.24: Residual Stress Mapping, $I_p = 18$ amp, $T_{on} = 100$ µsec, $T_R = 1800$ rpm, σ (x) = 308 MPa, Tau (xy) = 3MPa

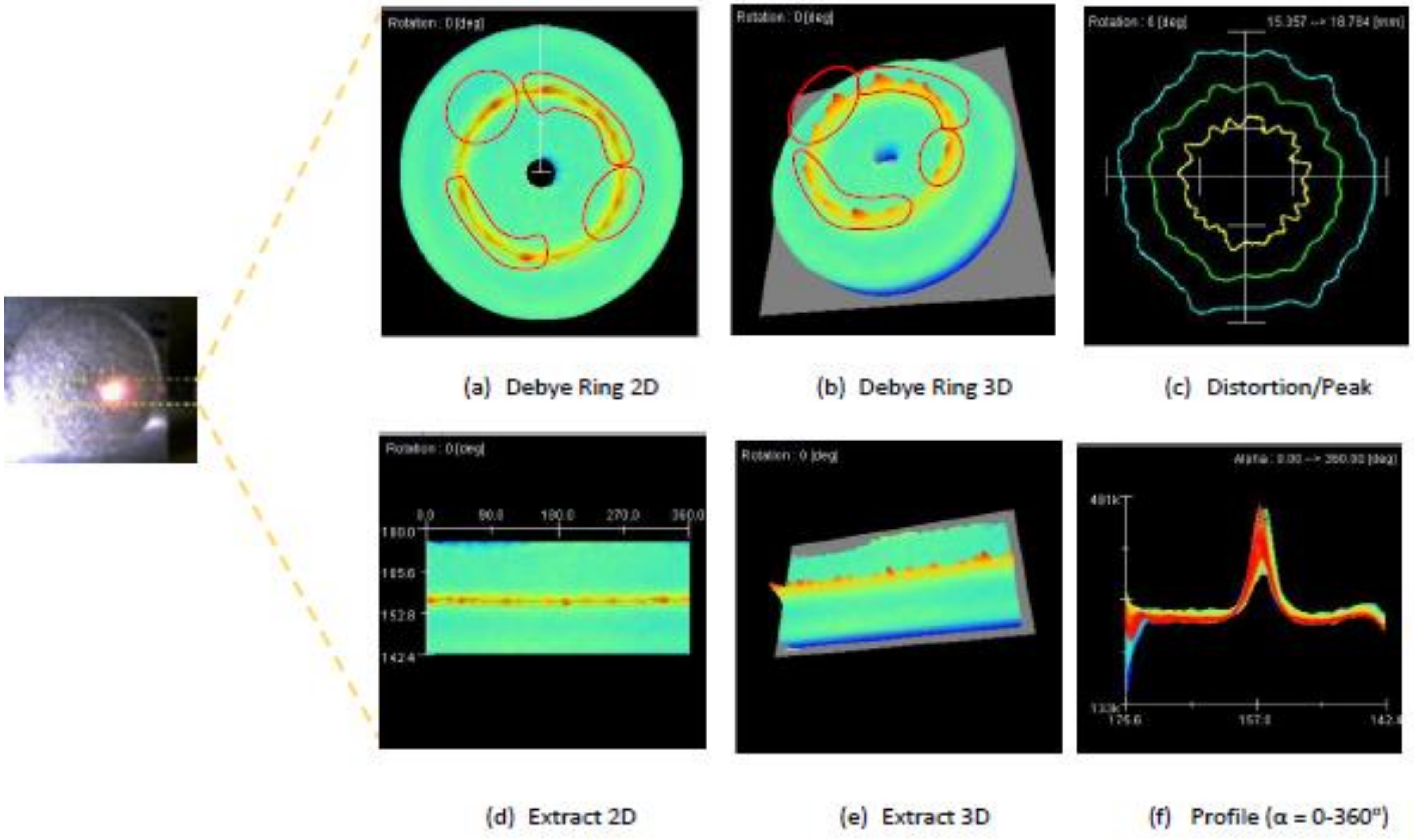

(a) Debye Ring 2D (b) Debye Ring 3D (c) Distortion/Peak

(d) Extract 2D (e) Extract 3D (f) Profile (α = 0-360°)

Figure 6.25: Residual Stress Mapping, I_p = 24 amp, T_{on} = 100 µsec, T_R = 1800 rpm, σ (x) = 380 MPa, Tau (xy) = -27 MPa

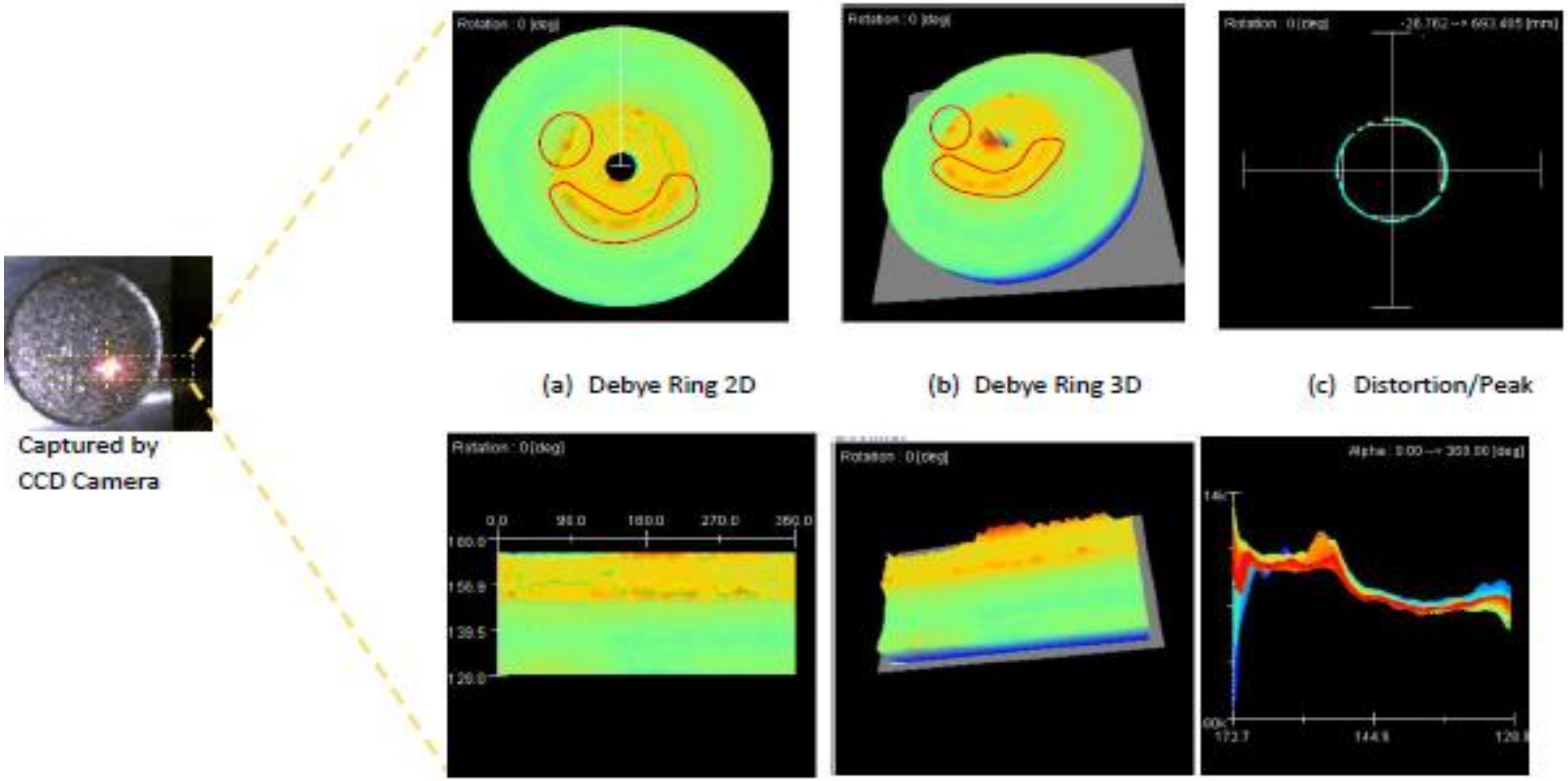

Captured by CCD Camera

(a) Debye Ring 2D

(b) Debye Ring 3D

(c) Distortion/Peak

(d) Extract 2D

(e) Extract 3D

(f) Profile (α = 0-360°)

Figure 6.26: Residual Stress Mapping, I_p = 24 amp, T_{on} = 1000 µsec, T_R = 1800 rpm, σ (x) = -2008 MPa, Tau (xy) = -1055 MPa

6.10 Pulse Discharge Energy Analysis

Pulse discharge energy analysis was done with the digital oscilloscope. Oscilloscope attached to tool and workpiece terminal of EDM with electronic circuit for pulse discharge energy waveform. The current flow from the tool (positive) to work material (negative) through the dielectric fluid. The discharge of energy between the tool and work material transferred in the form of pulses. This transferred energy converted into heat energy and builds up the workpiece temperature and melts the area on its surface.

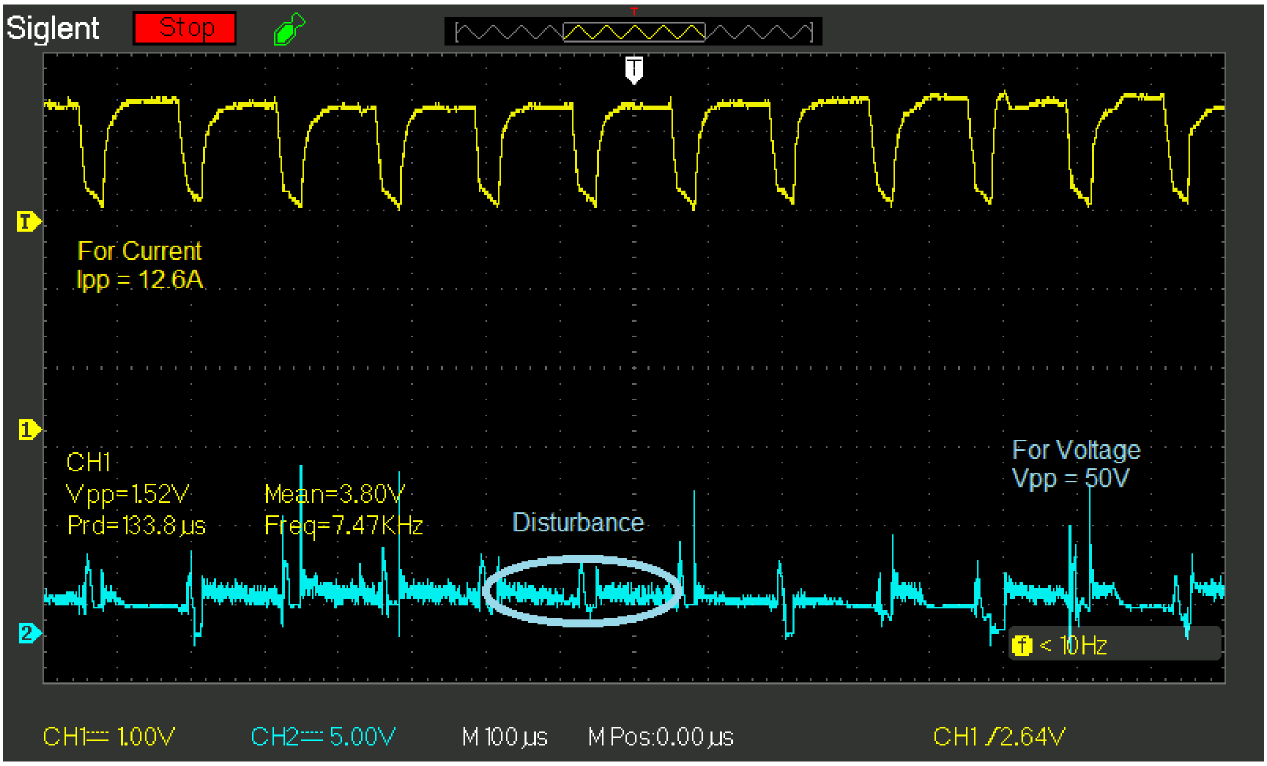

Figure 6.27: Current and Voltage Waveform, I_p = 12 amp., T_{on} = 100 µsec and T_R = 1200 rpm

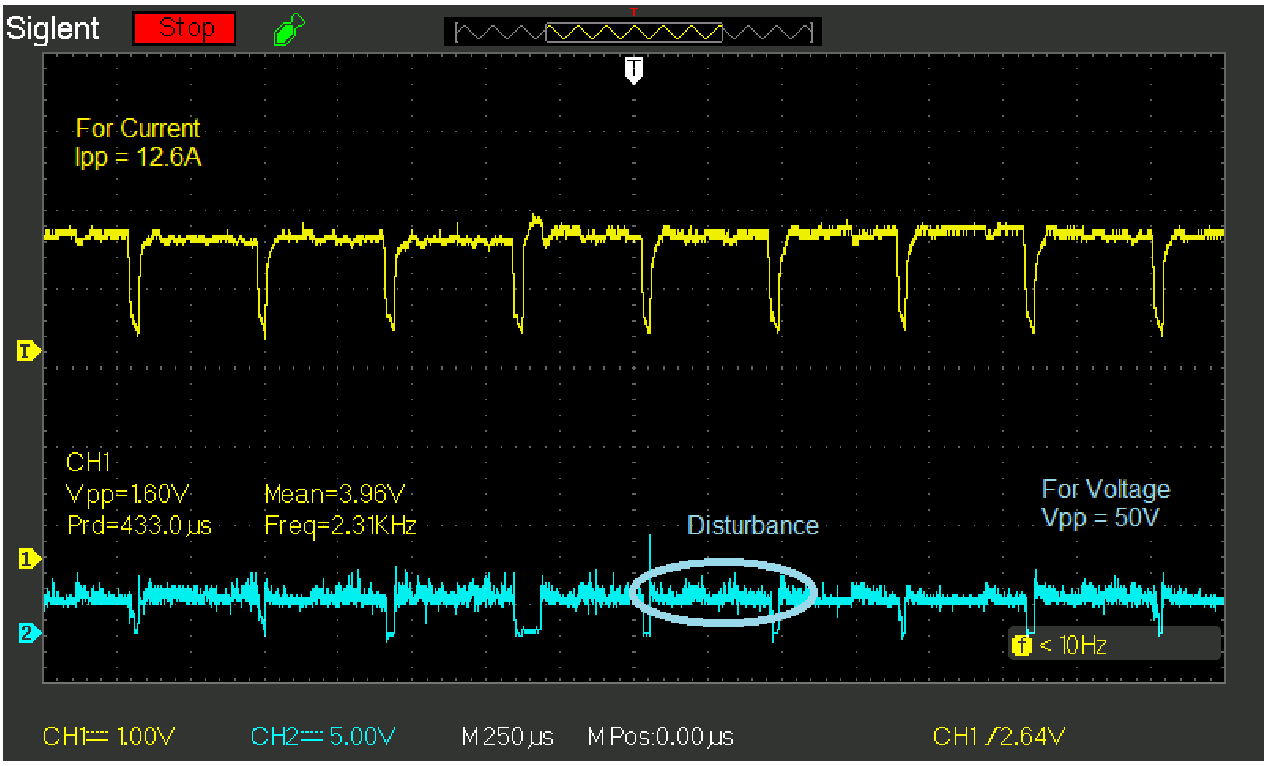

Figure 6.28: Current and Voltage Waveform, I_p = 12 amp., T_{on} = 400 µsec and T_R = 1200 rpm

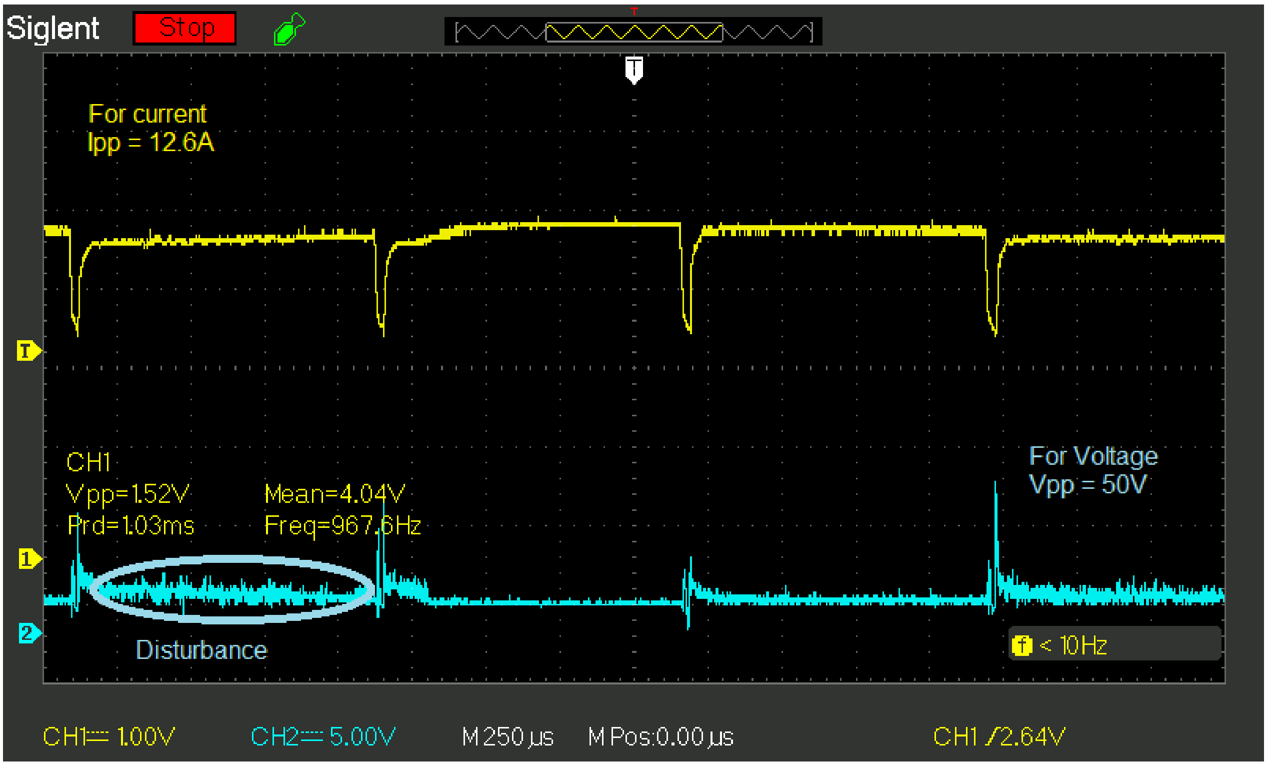

Figure 6.29: Current and Voltage Waveform, I_p = 12 amp., T_{on} = 1000 µsec and T_R = 1200 rpm

Figure 6.27 to 6.29: Shows the actual waveform of current (CH1) and voltage (CH2). One block in y-axis represents 1 volt and 2.5 volts at 0 amp. For channel 1 and 5 volts for channel 2. On x-axis time is 100, 250 and 250 µsec respectively. The peak-to-peak current for channel 1 is 12.6, amp and voltage of 50 volt for channel 2.

Figure 6.30 to 6.32: shows the actual waveform of current (CH1) and voltage (CH2). One block in y-axis represents 1 volt. At 0 amp. 2.5 volt for channel 1and 5 volt for channel 2. On the x-axis, time is 100, 100 and 250 µsec respectively. The peak-to-peak current for channel 1 is 17.8, 18.1 and 18.3 amp and voltage of 50, 55 and 50 volts form channel 2 respectively.

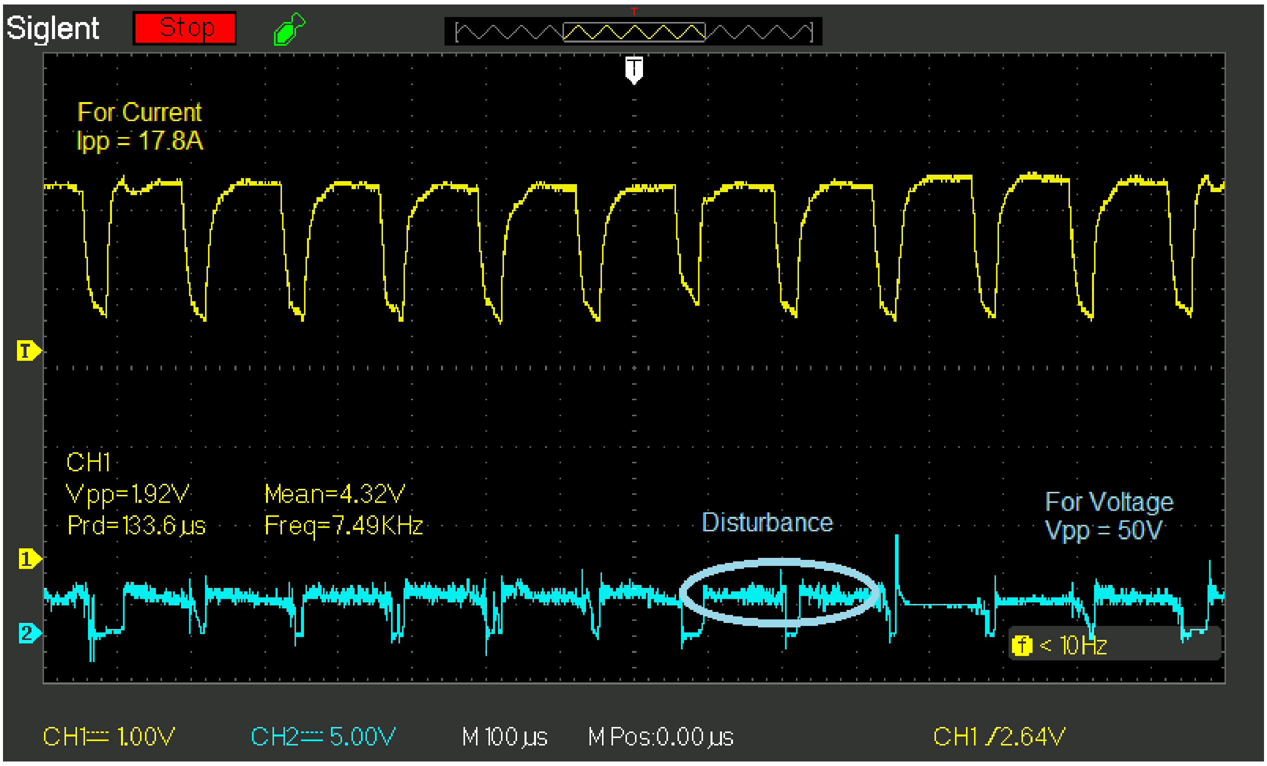

Figure 6.30: Current and Voltage Waveform, I_p = 18 amp., T_{on} = 100 µsec and T_R = 1800 rpm

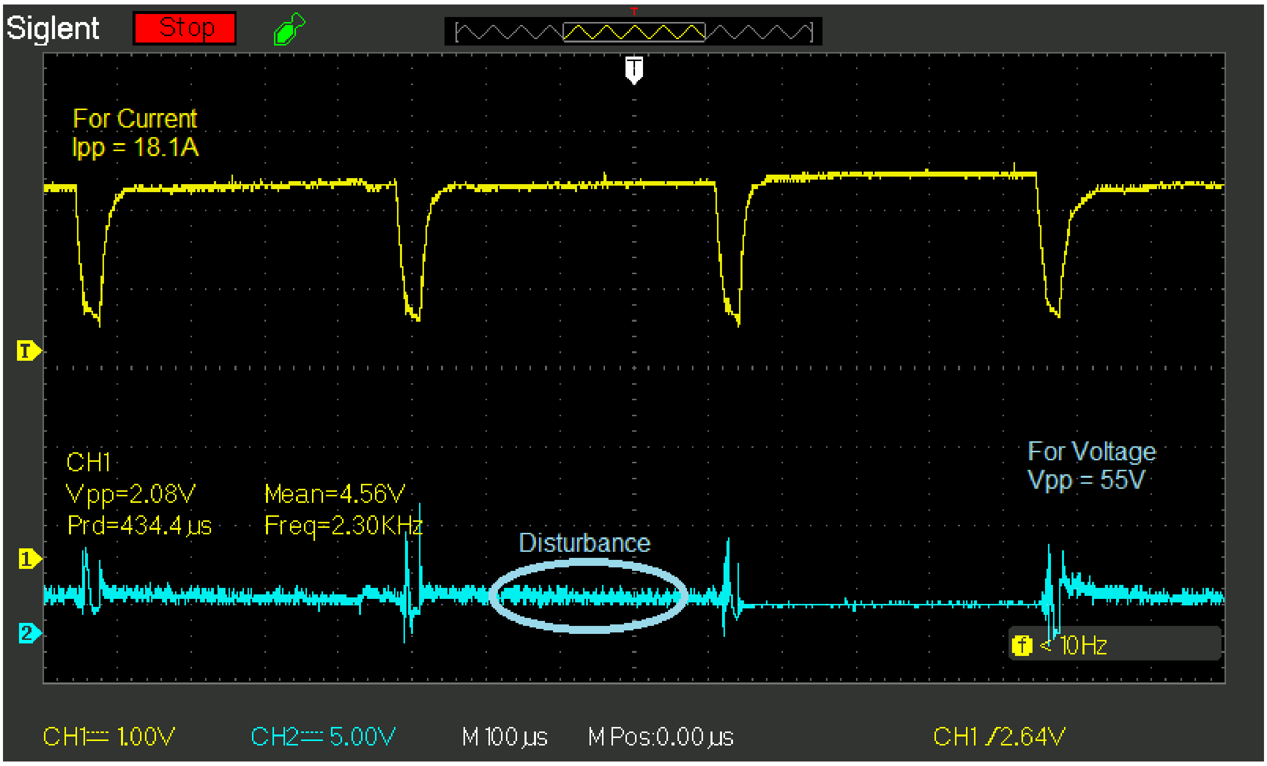

Figure 6.31: Current and Voltage Waveform, I_p = 18 amp., T_{on} = 400 µsec and T_R = 1800 rpm

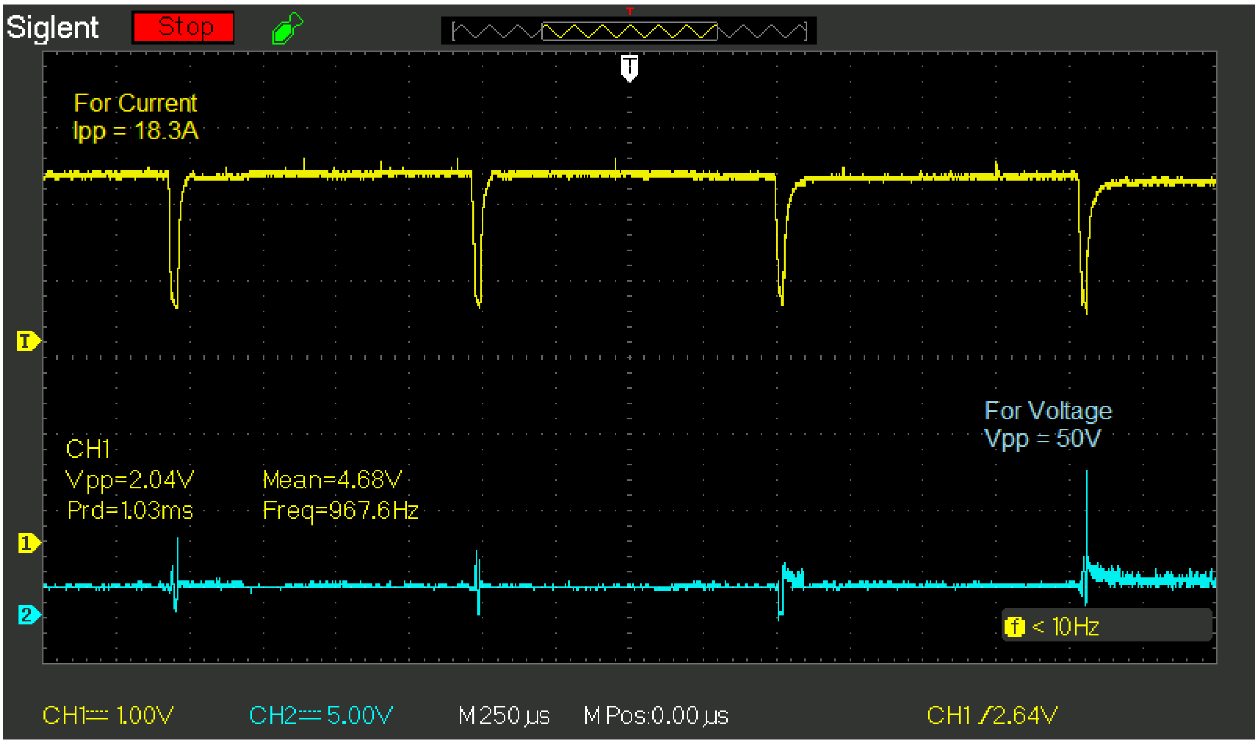

Figure 6.32: Current and Voltage Waveform, I_p = 18 amp., T_{on} = 1000 µsec and T_R = 1800 rpm

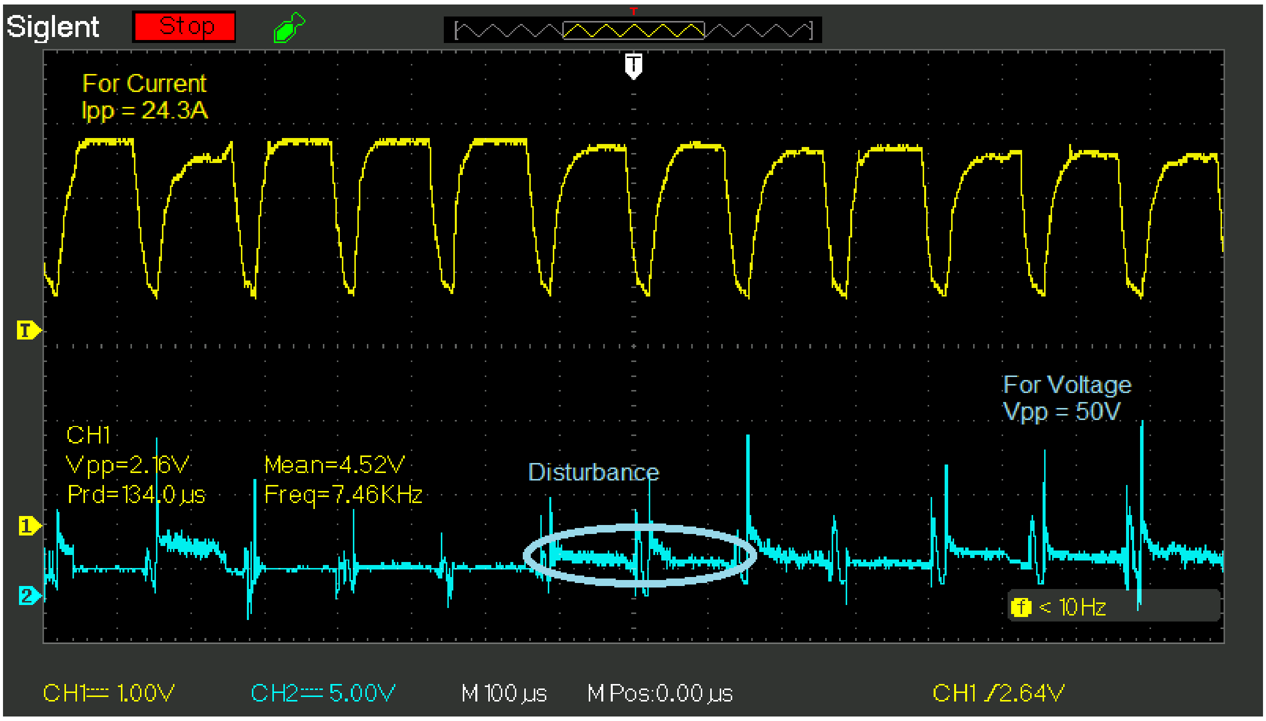

Figure 6.33: Current and Voltage Waveform, I_p = 24 amp., T_{on} = 100 µsec and T_R = 2400 rpm

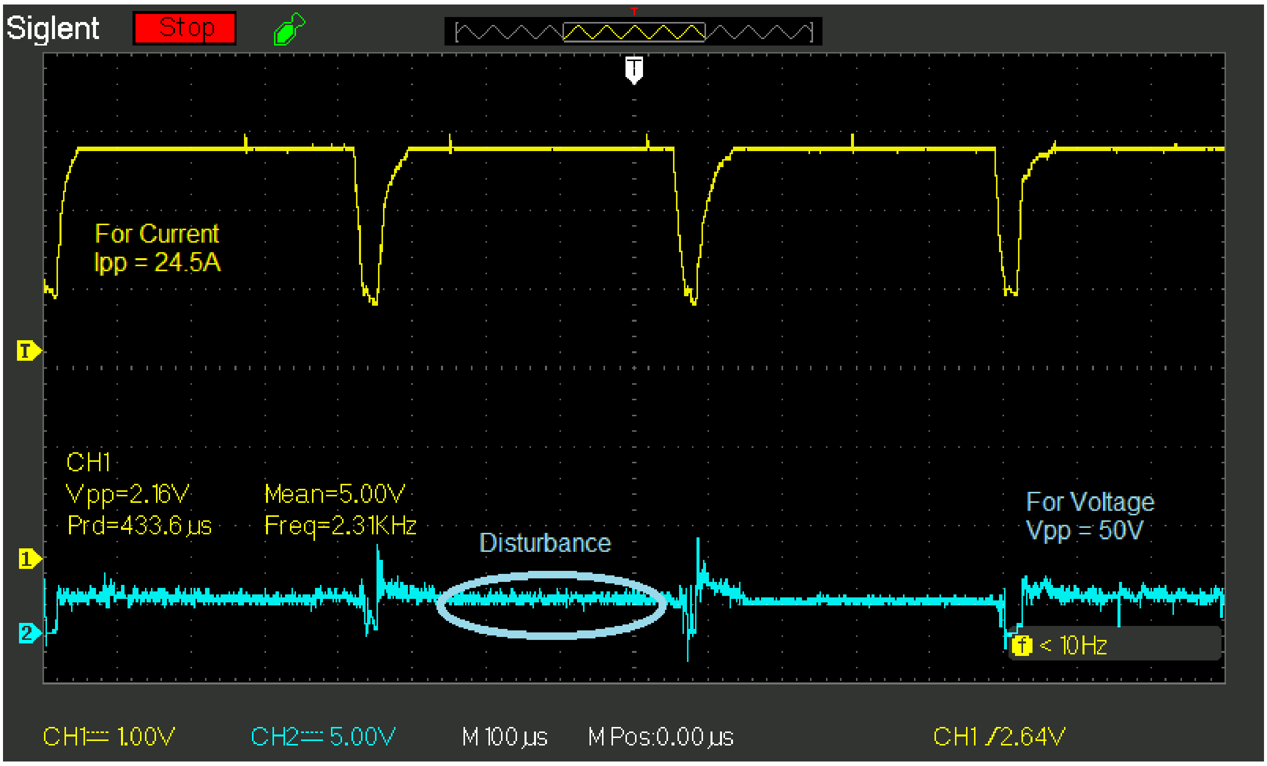

Figure 6.34: Current and Voltage Waveform, I_p = 24 amp., T_{on} = 400 µsec and T_R = 2400 rpm

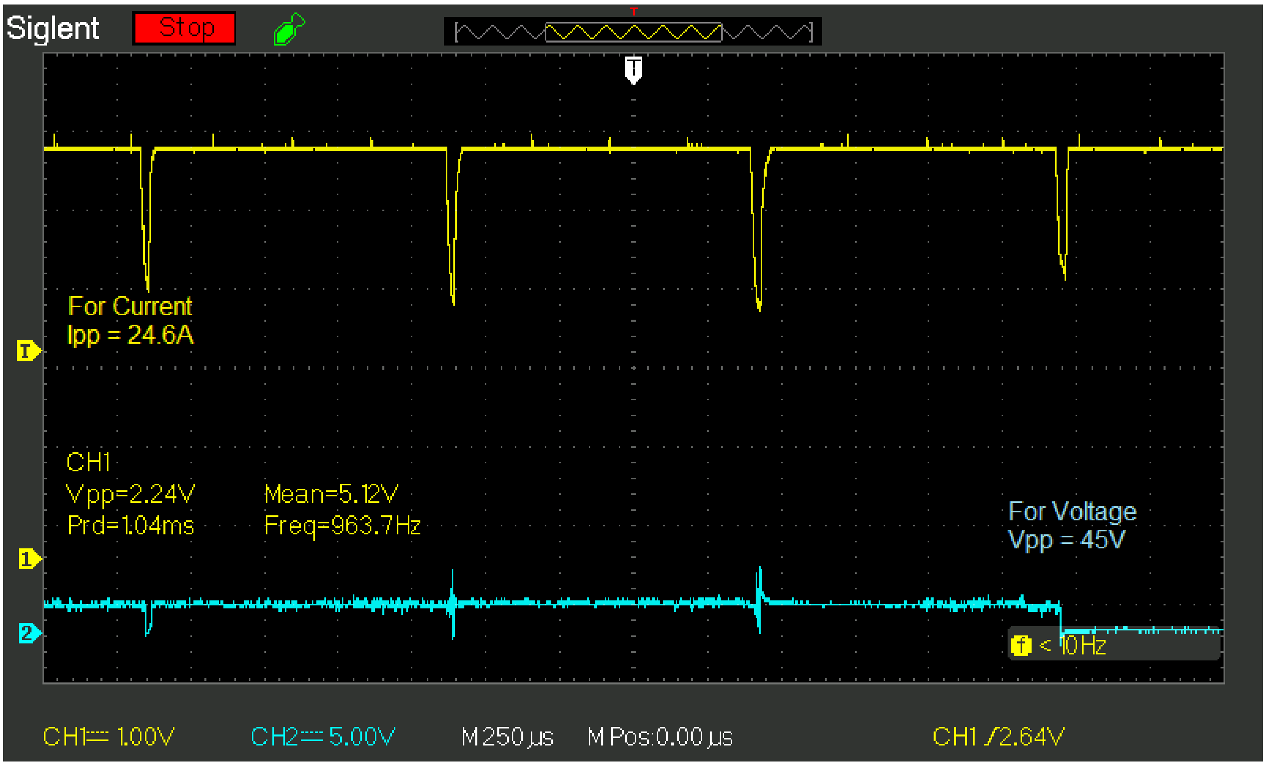

Figure 6.35: Current and Voltage Waveform, I_p = 24 amp., T_{on} = 1000 µsec and T_R = 2400 rpm

Figure 6.33 to 6.35: shows the actual waveform of current (CH1) and voltage (CH2). One block in y-axis represents 1 volt at 0 amp. 2.5 volt for channel 1and 5 volt for channel 2. On the x-axis, time is 100, 100 and 250 µsec respectively. The peak-to-peak current for channel 1 is 24.3, 24.5 and 24.6 amp. and voltage of 50, 50 and 45 volts form channel 2 respectively.

6.11 XRD Analysis

XRD analysis was performed on the samples machined with EDM using T_{on} 100, 400 and 1000 µsec T_{on} on Bruker D8 Advance and subject to 40 kV cathode voltage and 40 mA current to observed metallurgical changes.

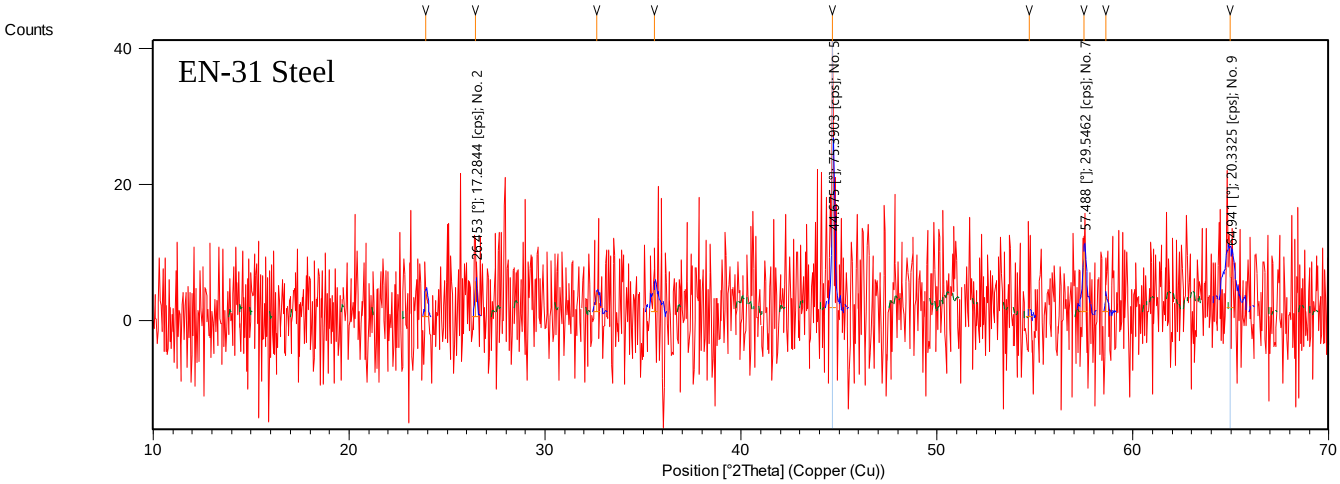

(a)

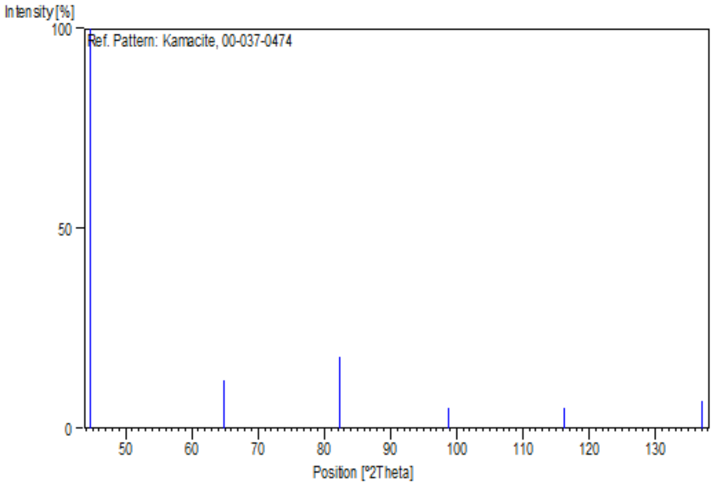

(b)

Figure 6.36: XRD investigation (a) XRD Spectra at T_{on} 100 µsec, (b) Stick Pattern of Peak no. 5

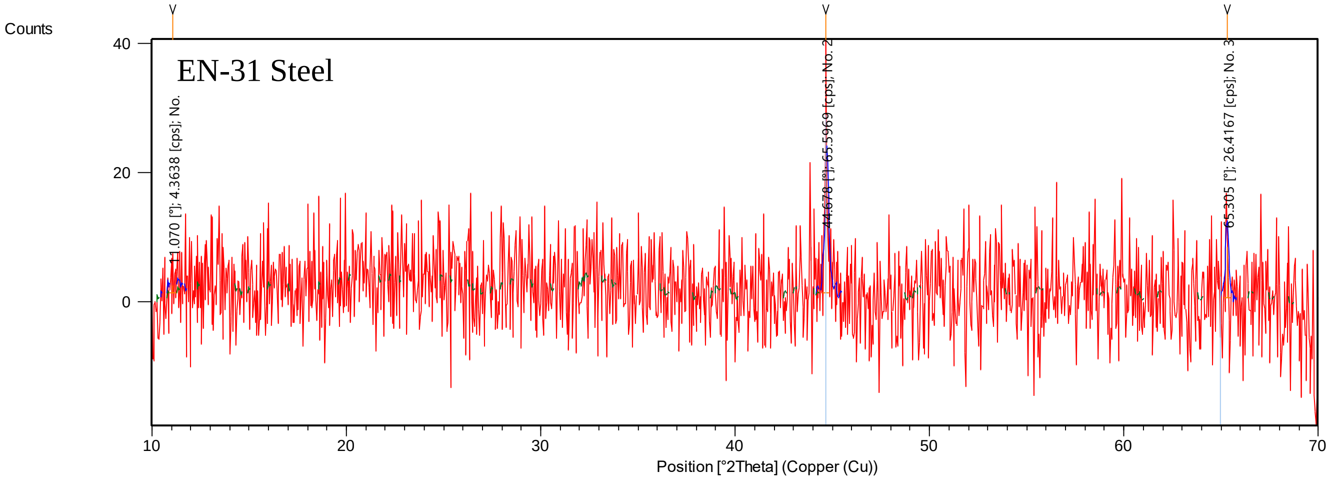

(a)

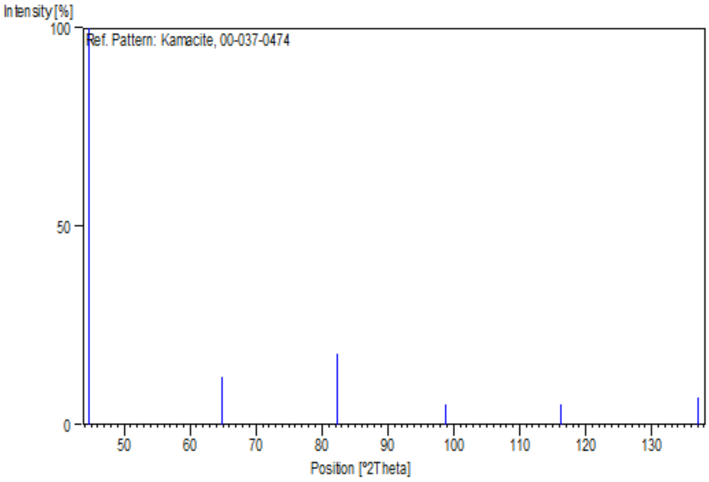

(b)

Figure 6.37: XRD investigation (a) XRD Spectra at T_{on} 400 µsec, (b) Stick Pattern of Peak no. 2

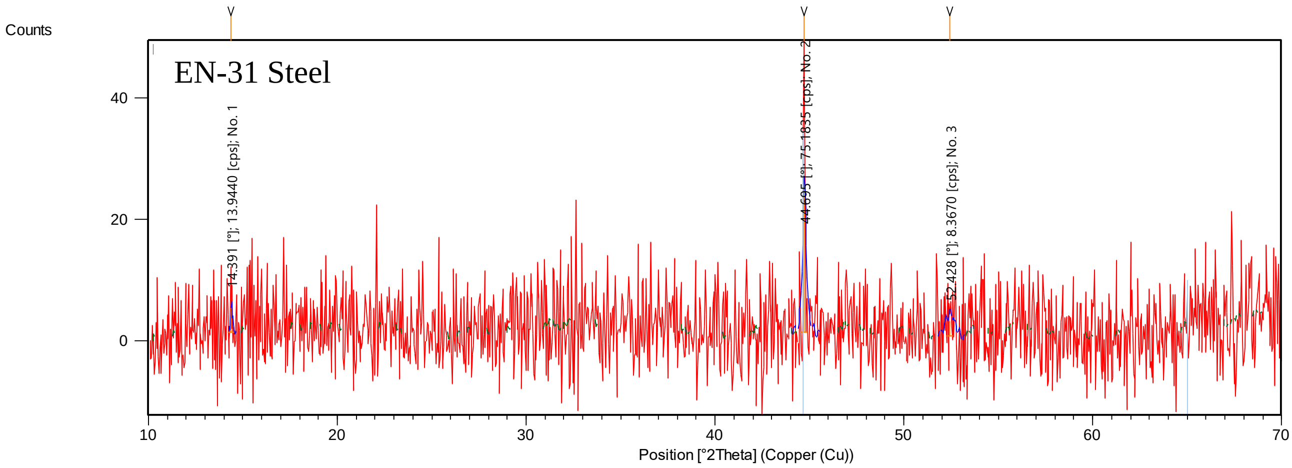

(a)

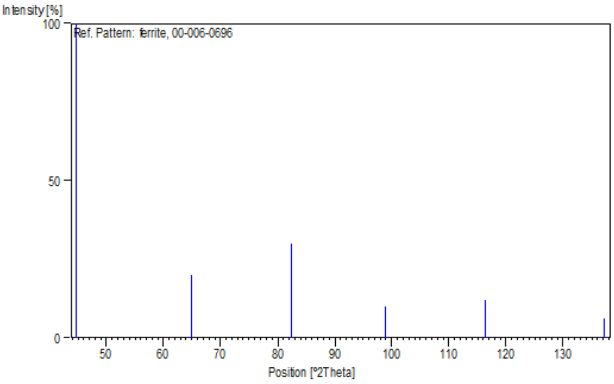

(b) Stick Pattern of Peak no. 2

Figure 6.38: XRD investigation (a)XRD Spectra at T_{on} 1000 µsec, (b)Stick Pattern of Peak no.2

Figure 6.36 (a), the maximum intensity of peak at position 44.675°, peak height 75.3903 [cps] at peak no. 5 at 100 µsec T_{on}. The stick pattern figure 6.36 (b) at peak no. 1 for Iron Nickel ($Fe_{0.94}$ $Ni_{0.06}$)); d [A] is 2.02800; 2 Theta at 44.647; I (Intensity %) is 100.0.

Figure 6.37 (a) the maximum intensity of peak at position 44.678°, peak height 65.5969 [cps] at peak no. 2 at 400 µsec T_{on}. The stick pattern figure 6.37 (b) at peak no. 1 for Nickel, Chromium, Iron (NiCrFe); h, l, k are 1, 1, 0; d [A] is 2.02800; 2 Theta at 44.647; I (Intensity %) is 100.0.

Figure 6.38 (a) the maximum intensity of peak at position 44.695°, peak height 75.1835 [cps] at peak no.2 at 1000 µsec T_{on}. The stick pattern figure 6.38 (b) at peak no.1 for Iron also; h, l, k are 1, 1, 0; d [A] is 2.02800; 2 Theta at 44.647; I (Intensity %) is 100.0. The Diffraction data was collected and the pressure-induced phase was produced due to quenching.

X-ray diffraction method is attempted to determine the change in location of material structure. Figure 6.36 to figure 6.38 represents the XRD results of machined surface that the crystallographic structure of the composite is not significantly changing. When the T_{on} is 1000 µsec shown in XRD spectra, then the peak is sharp, corresponding 2 Theta 44.647 and intensity is 44.695°; When the T_{on} is 100 µsec shown in XRD spectra, then the diffraction peak reduced, corresponding 2 Theta 44.647 and intensity is 44.647° somewhat low peaks are broaden. This shows when T_{on} has not a significant effect. As Ni existing in the compound and it forms the FeNi. The presence of FeNi enhances the property of steel strength, toughness to temperature, resistance to oxidation, density and hardness.

6.12 Correlation of Actual and Predicted Terms

The correlation of predicted and actual terms of the MRR, TWR and the R_a are illustrated in figure 6.39. The predicted models are satisfactory and the respective terms are in excellent accordance with the corresponding terms.

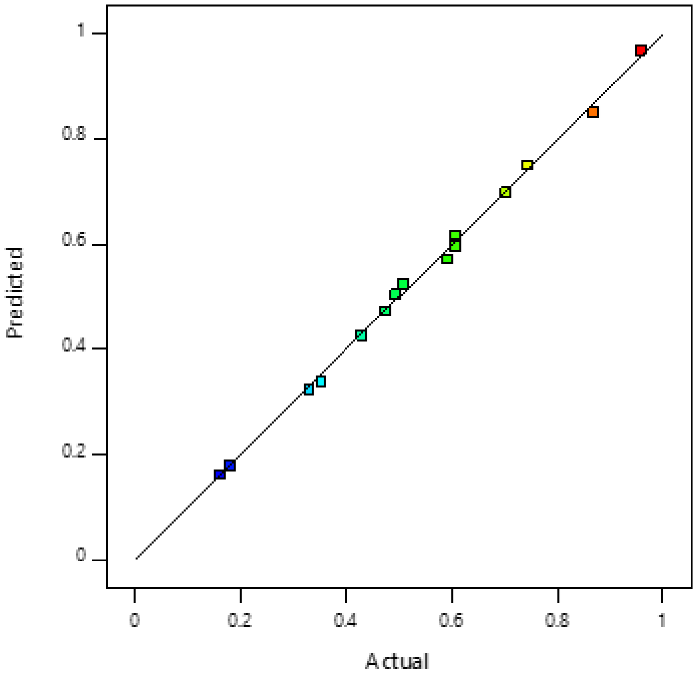

(a)

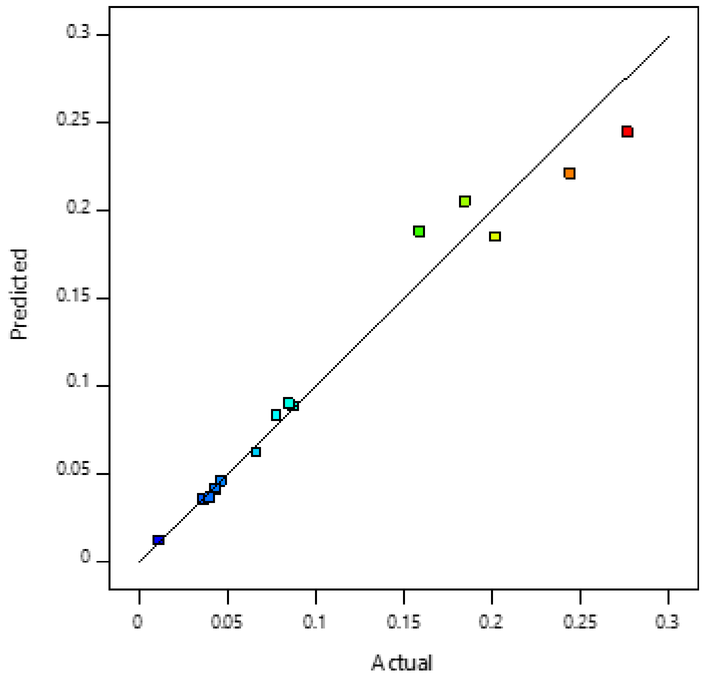

(b)

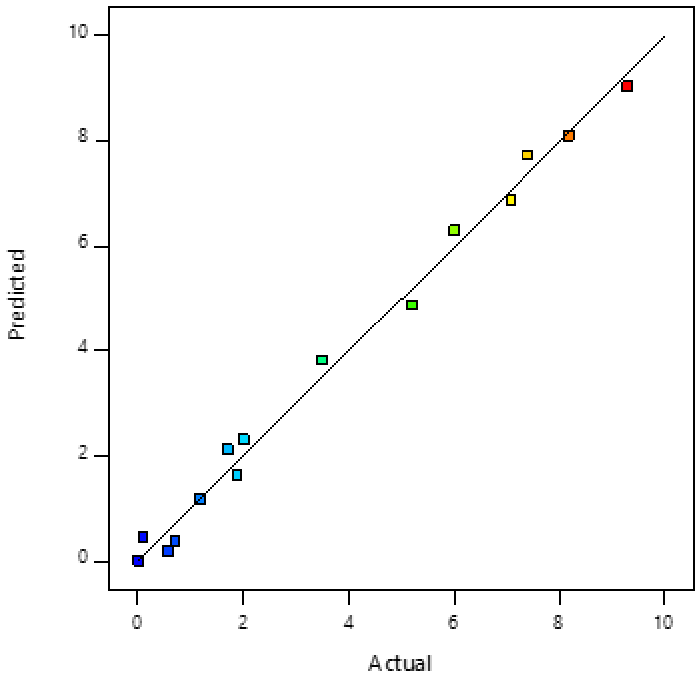

(c)

Figure 6.39: Correlation of predicted and exemplification values

(a) MRR (b) TWR and (c) R_a

CHAPTER 7

Conclusions and Future Work

Conclusions and Future Work

7.1 Conclusions

This work explores the extensive experimentation and process parameters analysis of tool rotation EDM on AISI D3 and EN-31 steel with electrolyte copper tool. The collection of data for the study is based on Central Composite Design, a famous Response Surface Methodology method. Statistics are performed to correlate the machining variables on the performance responses. The parametric model has been prepared to forecast the Material Removal Rate, Tool Wear Rate and Surface Roughness (R_a). The characterization of surface, residual stress and discharge pulse are carried out and the following conclusions/findings are drawn:

- Current and pulse-on-time are found prominent process variables for all the measures of AISI D3 steel. The current succeeded pulse-on-time and tool rotation are responsible variables for MRR of AISI D3 steel. The tool rotation is the dominant variable for MRR succeeded by current and pulse-on-time for EN-31 steel.

- Pulse-on-time is a substantial variable for tool wear rate succeeded by current and tool rotation respectively.

- Tool rotation is the most important variables for surface roughness succeeded by current and pulse-on-time variables.

- AISI D3 and EN-31 steel morphology rivals that at low discharge energy, less pulse-on-time and tool rotation results in recast layer, carbon deposition and surface roughness is minimized

- Residual tensile and compressive stresses increased as the rate of heating and cooling increase along with high pulse duration, due to the high rate of thermal contraction of AISI D3 steel and EN-31 steel.

- Increase of pulse-on-time and current rivals more fluctuation/disturbance in pulse wave due to the high frequency of charging-discharging the capacitor that results in discharge energy.

- XRD pattern was confirmed that the elements and its forms (FeCr, C60, CV_2, SiC) were present in AISI D3 and (FeNi, NiCrFe, FeNi) in EN-31 steel through the different peak intensity. As carbides and nickel-chromium existing in the compound form and enhances the mechanical properties.

- Surface roughness is linearly related to discharge energy and inversely related to tool rotation. Surface roughness decreased by an increase in tool rotation due to the whirling effect and minimum recast layer.

- Developed model having good correlation obtained by Response Surface Methodology. The plot developed was used for comparison the effect of all the process parameters.

7. 2 Future Work

The current work enables a broad opportunity for the subsequent researcher to investigate several features of tool rotation EDM process. Some proposal for forthcoming research:

- The process parameters effect on surface crack penetration, recast layer density, HAZ and circularity of the machining may be studied.
- The impact of composite tool material on responses may be studied.
- Hybrid non-conventional response optimization techniques may be used for obtaining optimal parametric setting.
- The investigation may be carried out for efficient use of pulse discharge energy and can be verified by DSO.

References

Bahgat, M.M., Shash, A.Y., Abd-Rabou, M. and El-Mahallawi, I.S., (2019), Influence of process parameters in electrical discharge machining on H13 die steel, Heliyon 5, e01813

Beri, N., Maheswari, S., Sharma, C. and Kumar, A., (2014), Surface quality modification using powder metallurgy processed CuW electrode during electrical discharge machining of Inconel 718, Procedia Materials Science, 5, 2629-2634

Boothroyd, G. and Winston A., (1989), A review of: Fundamentals of machining and machine tools, Knight Marcel Dekker, Inc., New York Second edition, 542

Bulent, E., Erman, T. and Abdulkadir, E., (2006), A semi-empirical approach for residual stresses in electric discharge machining (EDM), International Journal of Machine Tools and Manufacture, 46, 858–868

Carlo, F., Atanas, I. and Antoine, P., (2008), Electrical measurements in Micro-EDM, Journal of Micromechanics and Microengineering, 18, 1–13

Chattopadhyay, K.D., Verma, S., Satsangi, P.S. and Sharma, P.C., (2009), Development of empirical model for different process parameters during rotary electrical discharge machining of copper–steel (EN-8) system, Journal of Materials Processing Technology, 209, 1454–1465

Cogun, C. and Akaslan, S., (2002), The effect of machining parameters on tool electrode edge wear and machining performance in Electrical Discharge Machining (EDM), Korean Society of Mechanical Engineering International Journal, 1(16), 46-50

Dewangan, S., Gangopadhyay, S., and Biswas, C.K., (2015), Multi-response optimization of surface integrity characteristics of EDM process using grey-fuzzy logic-based hybrid approach, Engineering Science and Technology, an International Journal, 18(3), 361-368

Dhar, S., Purohit, R., Saini, N., Sharma, A. and Kumar, G.H., (2007), Mathematical modeling of electric discharge machining of cast Al-4Cu-6Si alloy-10 wt.% sicp composites, Journal of Materials Processing Technology, 193(1-3), 24-29

Donald, B.M., (2013), Wire EDM: The fundamentals, Tec Rep., EDM network, Sugar Grove, IL, 1- 22

Dwivedi, A.P. and Choudhury, S.K., (2016a), Effect of tool rotation on MRR, TWR, and Surface Integrity of AISI-D3 Steel using the rotary EDM process, Materials and Manufacturing Processes, 31(14), 1844–1852

Dwivedi, A.P. and Choudhry, S.K., (2016b), Increasing the performance of EDM process using tool rotation methodology for machining AISI D3 Steel, 7th HPC 2016 –CIRP Conference on High Performance Cutting, Procedia CIRP, 46, 131 –134

Dwivedi, A.P. and Choudhury, S.K., (2017), Estimation of recast layer thickness in rotary tool EDM process for machining AISI D3 tool steel, Materials Today: Proceedings, 4(10), 10816–10822

Fujun, R., Dechen, H. and Dianjun, W., (2004), Analysis of motion laws of machining non-sphere by EDM with rotary electrode, Journal of Materials Processing Technology, 149, 323–327

Gopalakannan, S., Senthilvelan, T. and Renganathan, S., (2013), Statistical optimisation of EDM parameters on machining of aluminium hybrid metal matrix composites by applying taguchi based grey analysis, Journal of Scientific and Industrial Research, 72, 358-365

Habib, S.S., (2009), Study of the parameters in electrical discharge machining through response surface methodology approach, Applied Mathematical Modelling, 33(12), 4397-4407

Han, F., Wang, Y. and Zhou, M., (2009), High-speed EDM milling with moving electric arcs, International Journal of Machine Tools & Manufacture, 49, 20–24

Hasan, E.H., (2014), Fundamentals of machining processes: Conventional and nonconventional processes, ISBN 13: 9781466577022, CRC Press, 2

Heuvelman, C.J. and Horn, B.L., (1974), Review of Co-operative work on EDM in STCE of CIRP, Annals of the CIRP, 23(2), 213

Hewidy, M.S., El-Taweel, T.A. and El-Safty, M.F., (2005), Modelling and machining parameters of wire Electrical Discharge Machining of Inconel 600 using RSM, Journal of Material Processing Technology, 169, 328-336

Izquierdo, B., Sanchez, J.A., Plaza, S., Pombo, I. and Ortega, N., (2009), A numerical model of the EDM process considering the effect of multiple discharges, International Journal of Machine Tools and Manufacture, 49(3-4), 220-229

Jin, W., Fuzhu, H., Gang, C. and Fuling, Z., (2012), Debris and bubble movements during electrical discharge machining, International Journal of Machine Tools and Manufacture, 58, 11–18

Kao, C.C., Jia, T. and Albert, J.S., (2007), Near dry electrical discharge machining, International Journal of Machine Tools and Manufacture, 47, 2273–2281

Karthikeyan, R., Narayanan, L. and Naagarazan, R.S., (1999), Mathematical modeling for electric discharge machining of aluminium-silicon carbide particulate composites, Journal of Materials Processing Technology, 87(1-3), 59-63

Koshy, P., Jain, V.K. and Lal, G.K., (1993), Experimental investigations into electrical discharge machining with a rotating disk electrode, Precision Engineering, 15(1), 6–15

Kumar, N.M., Kumaran, S.S. and Kumaraswamidhas, L.A., (2015), An investigation of mechanical properties and material removal rate, tool wear rate in EDM machining process of

AL2618 alloy reinforced with Si3N 4 , AlN and ZrB 2 composites, Journal of Alloys and Compounds, 650, 318–327

Kun, L.W., Biing, H.Y., Fuang, Y.H. and Shin, C.C., (2005), Improvement of surface finish on SKD steel using electro-discharge machining with aluminum and surfactant added dielectric, International Journal of Machine Tools and Manufacture, 45, 1195–1201

Kung, K., Horng, J. and Chiang, K., (2009), Material removal rate and electrode wear ratio study on the powder mixed electrical discharge machining of cobalt-bonded tungsten carbide, International Journal of Advanced Manufacturing Technology, 40, 95-104

Kunieda, M. and Kameyama, A., (2010), Study on decreasing tool wear in EDM due to arc spots sliding on electrodes, Precision Engineering, 34, 546–553

Kuruvila, N. and V., R.H., (2011), Parametric influence and optimization of Wire EDM of hot die steel, Machining Science and Technology, 15(1), 47–75

Lazarenko, B.R. and Lazarenko, N.I., (1964), Technological characteristics of electro-spark machining of current conducting materials, Electro-spark Machining of Metals Consultants Bureau, N. Y., 2, 1

Lee, S.H. and Li, X.P., (2001), Study of the effect of machining parameters on the machining characteristics in electrical discharge machining of tungsten carbide, Journal of Materials Processing Technology, 115(3), 344-358

Li, C.P., Kim, M.Y., Islam, M.M. and Ko, T.J., (2016), Mechanism analysis of hybrid machining process comprising EDM and end milling, Journal of Materials Processing Technology, 237, 309–319

Lin, Y., Cheng. and Hwang, L., (2006), Machining characteristics and optimization of machining parameters of SKH 57 high-speed steel using electrical-discharge machining based on Taguchi method, Materials and Manufacturing Processes, 21(8), 922-929

Lin, Y.C., Yuan., Lin, C. and Hsinn, T., (2008), Feasibility study of rotary electrical discharge machining with ball burnishing for Al2O3/6061Al composite, 23, 391–399

Mahardika, M., and Mitsui., K., (2008), A new method for monitoring micro-electric discharge machining processes, International Journal of Machine Tools and Manufacture, 48(3-4), 446–458

Mandaloi, G., Singh, S., Kumar, P. and Pal, K., (2016), Effect on crystalline structure of AISI M2 steel using tungsten–thorium electrode through MRR, EWR, Measurement, 90, 74–84

McGeough, J.A., and Rasmussen, H., (1997), A theoretical model of electrodischarge texturing, Journal of Materials Processing Technology, 68(2), 172–178

Minhat, A.E., Yahya, A., Khamis, N.H., Samion, S., Bakar, Z.A. and Andromeda, T., (2014), Power generator of Electrical Discharge Machining (EDM) system, Applied Mechanics and Materials, 554, 638-642

Mohan, B., Rajadurai, A. and Satyanarayana, K.G., (2002), Effect of SiC and rotation of electrode on electric discharge machining of Al-SiC composite, Journal of Materials Processing Technology, 124(3), 297-304

Montgomery, D.C., (2005), Design and analysis of experiments, 6th Edition, John Wiley and Sons, New York

Muthuramalingam, T., Mohan, B., and Saravanakumar, D., (2015), Evaluation of surface finish of Electrical Discharge Machined AISI 304 Stainless Steel with various pulse generators, Applied Mechanics and Materials, 772, 279–283

Nakagawaa, T., Yuzawab, T. and Sampeic, M., (2017), Improvement in machining speed with working gap control in EDM milling, Precision Engineering, 47, 303–310

Nizar, B.S., Farhat, G. and Kais, B.A., (2006), Numerical study of thermal aspects of electric discharge machining process, International Journal of Machine Tools and Manufacture, 46, 908–911

Panda, D.K., and Bhoi, R.K., (2006), Electro-Discharge Machining–a qualitative approach, Materials and Manufacturing Processes, 21(8), 853–862

Payal, H.S., Choudhry, R. and Singh, S., (2008), Analysis of Electro Discharge Machined Surfaces of EN-31 Tool Steel, Journal of Scientific and Industrial Research, 67, 1072-1077

Prabhu, S. and Vinayagam, B.K., (2011), Development of empirical model for surface roughness during electrical discharge machining using single wall carbon nanotubes, International Journal of Computational Materials Science and Surface Engineering, 4(1), 23-36

Pradhan, M.K., (2010), Experimental investigation and modelling of surface integrity, accuracy and productivity aspects in EDM of AISI D2 steel, Doctoral dissertation, National Institute of Technology, Rourkela (India)

Puertas, I. and Luis, C.J., (2004), A study of optimization of machining parameters for electrical discharge machining of boron carbide, Materials and Manufacturing Processes, 19(6), 1041-1070

Rahman, M.M., Khan, M.A.R., Kadirgama, K., Noor, M.M. and Bakar, R.A., (2011), Experimental Investigation into Electrical Discharge Machining of Stainless Steel 304, Journal of Applied Sciences, 11(3), 549-554

Rajesha, S., Sharma A.K. and Kumar, P., (2012), Some aspects of integrity study of electro discharge machined Inconel 718, Proceedings of the 36th International MATADOR Conference, 439-443

Robert, H., Dell, K. and Leo, A., (1994), Manufacturing processes reference guide, Industrial Press Inc.

Sarand, J. and Shabgard, M.R., (2015), Investigation of the effect of thermal diffusivity coefficient of tool material on electrode-tool wear in the EDM process, Archives of Civil and Mechanical Engineering,15(4), 806-821

Shabgard, M.R., Seyedzavvar, M. and Nadimi, B.O., (2006), Influence of input parameters on characteristics of EDM process, Journal of Mechanical Engineering, 2, 123–135

Simao, J., Lee, H.G., Aspinwall, D.K., Dewes, R.C. and Aspinwall, E.M., (2003), Workpiece surface modification using electrical discharge machining, International Journal of Machine Tools and Manufacture, 43(2), 121-128

Singh, P.N., Raghukandan, K., Rathinasabapathi, M. and Pai, B.C., (2004), Electric discharge machining of Al-10% SiCP as cast metal matrix composites, Journal of Materials Processing Technology, 155-156(1-3), 1653-1657

Sohani, M.S., Gaitonde, V. N., Siddeswarappa, B. and Deshpande, A.S., (2009), Investigations into the effect of tool shapes with size factor consideration in sink electrical discharge machining (EDM) process, International Journal of Advanced Manufacturing Technology, 1-15

Soundhar, A., Zubar, H.A., Sultan, M.T.B.H.H. and Kandasamy, J., (2019), Dataset on optimization of EDM machining parameters by using central composite design, Data in Brief, 23, 103671

Sourabh, K.S., (2009), Experimental investigation of the dry electric discharge machining (dry edm) process, Master's thesis, Indian Institute of Technology Kanpur

Soveja, A., Cicala, E., Grevey, D. and Jouvard, J.M., (2008), Optimisation of TA6V alloy surface laser texturing using an experimental design approach, Optics and Lasers in Engineering, 46(9), 671-678

Takahisa, M., (1997), A quarterly survey of new products, systems and technology, Tech. Rep., Mitsubishi Electric Advance, 81

Tanjilul, M., Ahmed, A., Kumar, A.S. and Rahman, M., (2018), A study on EDM debris particle size and flushing mechanism for efficient debris removal in EDM-drilling of Inconel 718, Journal of Materials Processing Technology, 255, 263–274

Tarng, Y.S., Tseng, C.M. and Chung, L.K., (1997), A fuzzy pulse discriminating system for electrical discharge machining, International Journal of Machine Tools and Manufacture, 37, 511–522

Teimouri, R. and Baseri, B., (2012), Effects of magnetic field and rotary tool on EDM performance, Journal of Manufacturing Processes, 14, 316–322

Tsai, H.C., Yan, B.H. and Huang, F.Y., (2003), EDM performance of Cr/Cu-based composite electrodes, International Journal of Machine Tools and Manufacture, 43(3), 245-252

Tsai, Y. and Lu, C., (2007), Influence of current impulse on machining characteristics in EDM, Journal of Mechanical Science and Technology, 21, 1617-1621

Vishwakarma , U. K., Dvivedi, A. and Kumar, P., (2012), FEA modeling of material removal rate in Electrical Discharge Machining of Al6063/SiC composites, World Academy of Science, Engineering and Technology, International Journal of Mechanical, Aerospace, Industrial, Mechatronic and Manufacturing Engineering, 6(3), 2012, 586-591

Wang, C. and Lin, Y.C., (2009), Feasibility study of electrical discharge machining for W/Cu composite, International Journal of Refractory Metals and Hard Materials, 27(5), 872-882

Wei, B. and Lee, M.K., (2002), Apparatus and method for electrical discharge machining multiple holes, United States Patent 6,373,018, et al.

Yahya, A., Minhat, A.E., Rachim, T.A.A., Khamis, N.H.H., Khalil, K. and Arif, M., (2011), Communication within hardware of Electrical Discharge Machining (EDM) system, Jurnal Teknologi (Special Edition) Sciences & Engineering, 55 (1), 201-212

Yan, B.H., Wang, C.C., Chow, H.M. and Lin, Y.C., (2000), Feasibility study of rotary electrical discharge machining with ball burnishing for Al2O3/6061Al composite, International Journal of Machine Tools and Manufacture, 40(10), 1403-1421

Yang, X., Han, X., Zhou, F. and Kunieda, M., (2013), Molecular dynamics simulation of residual stress generated in EDM, Procedia CIRP, 6, 432–437

Younis, A., Abbas, S., Gouda, A., Mahmoud, H. and Abd-Allah, A., (2015), Effect of electrode material on electrical discharge machining of tool steel surface, Ain Shams Engineering Journal, 6(3), 977-986

Zhang, Q.H., Du, R., Zhang, J.H. and Zhang, Q.B., (2006), An investigation of ultrasonic-assisted electrical discharge machining in gas, International Journal of Machine Tools and Manufacture, 46, 1582–1588

Zhou, M. and Han, F., (2009), Adaptive control for EDM process with a self-tuning regulator, International Journal of Machine Tools and Manufacture, 49(6), 462-469